

**UNIVERSITÀ DEGLI STUDI DI CAMERINO**

**School of Advanced Studies**

**DOCTORAL COURSE IN  
CHEMICAL AND PHARMACEUTICAL SCIENCES AND  
BIOTECHNOLOGY**

**CHEMICAL SCIENCES**

**XXXIII cycle**

**CHROMITES IN ORDINARY CHONDRITE  
FUSION CRUSTS**

**PhD Student**

**Dr. Manlio Bellesi**

**Supervisors**

**Prof. Carlo Santini**

**Prof. Gabriele Giuli**

**Academic Years 2017/2018 – 2019/2020**

# ***CONTENTS***

<b>Foreword .....</b>	<b>page 1</b>
-----------------------	---------------

## **Chapter One – Meteorites: An Overview**

1.1 – Meteorites and their classification .....	page 2
1.2 – Chromites .....	page 17
1.3 – Fusion crusts .....	page 22
1.4 – Scope and aim of this work .....	page 34

## **Chapter Two – samples and experimental**

2.1 – Samples .....	page 35
2.2 – Optical microscopy .....	page 35
2.3 – Field Emission Scanning Electron Microscopy .....	page 35
2.4 – Aba Panu (Nigeria) .....	page 39
2.5 – Bassikounou (Mauritania) .....	page 44
2.6 – Chelyabinsk (Russia) .....	page 50
2.7 – Chergach (Mali) .....	page 55
2.8 – Kobo (Nigeria) .....	page 62
2.9 – Kilabo (Nigeria) .....	page 66
2.10 – NWA 869 (Northwestern Africa) .....	page 70
2.11 – Tamdakht (Morocco) .....	page 73
2.12 – Viñales (Cuba) .....	page 81
2.13 – El Hammami (Mauritania) .....	page 86
2.14 – Discussion and conclusions .....	page 95

<b>Cited references .....</b>	<b>page 99</b>
-------------------------------	----------------

<b>Appendix – Experimental data for chromites .....</b>	<b>page 105</b>
---	-----------------

<b>Summary .....</b>	<b>page 115</b>
----------------------	-----------------

## ***FOREWORD***

Meteorites are several orders of magnitude older than *homo sapiens* – or any other *homo* genus, for that matter. Their origin dates back to the formation of the solar system (4.56 billion years ago), whereas our species traces its roots back to two hundred thousand years in the past. Even though anthropologists are expected to push this estimate further back in the past, humankind is bound to remain a latecomer in the history of Universe. Considering that the beginning of our Universe is currently placed at 13.8 billion years ago, it is correct to say that the solar system itself is very young.

The time when humankind began to guess the true nature of the space rocks is far more recent than 200,000 years – we should drop three zeros and write 200 years. The term ‘origin’ thus applies to two very different contexts: the epoch when meteorites formed and the time when people started to regard them as celestial remnants of a very remote past, when our Sun and the planets came to life.

Meteorites are the falling debris of a vast class of solar system objects – the minor bodies, which include asteroids and comets as well as a host of objects discovered in the last decades: trans-Neptunian objects (TNOs), plutinos, Centaurs, Kuiper Belt and scattered disk objects (KBOs), Oort Cloud members etc.. Prior to the Apollo missions, meteorites were the only extraterrestrial material available on Earth and thus an extremely valuable source of information about the origin of the solar system.

Minor bodies, planets and satellites all share a common origin. However, the building blocks of the larger bodies have been heavily altered by gravity, pressure and heat – a process which has erased previous traces of their history. On the other hand, small solar system objects preserve a record of their birth; this fact, only recently recognized by researchers, confers on them the very special status of time capsules from a very remote past. But these capsules have had their own evolution, though less destructive with respect to their larger siblings. Evidence of aqueous alteration and/or thermal metamorphism is very common among meteorites; they have a complex history, of which the formation of a fusion crust on entering Earth’s atmosphere is only the final chapter.

Crusts have always received less attention than the inner part (*bulk*) of meteorites: however, interest has been constantly increasing, mainly sparked by the desire to build a detailed theoretical model of the atmospheric flight. Due to the scarcity of reliable data, current knowledge of physical mechanisms leading to the formation of a fusion crust is very crude and inadequate. Alternative approaches aiming at collecting more information have been tried, ranging from plasmatron experiments (in an attempt to create synthetic analogs of real crusts) to chemical analysis of the minerals formed inside the crust.

This study focuses upon some minerals forming within the crust during atmospheric flight – chromites, a class of spinels. Although secondary in meteorites (because not present from the start), once they are formed spinels are remarkably resistant to alteration and can be found in the sample even after a very long time. In search of quantitative results, various authors have tried to take advantage of this stability.

We have studied ten samples of meteorites – H, L and LL ordinary chondrites – searching for bulk as well as crust chromites. Almost 300 chromites were found, from bulk and crust in equal proportions; SEM analyses confirm significant differences in size, shape and chemical composition between crust and bulk. Results may help shed light upon the processes operating during atmospheric flight, as well as make a comparison with chromites found in layers of terrestrial remnants of impact craters. Such chromites have often been cited as samples of extraterrestrial matter and considered reliable markers of asteroid (or comet) impacts.

The issue is very complex and still actively debated: we hope to give a little, but valuable contribution with the present work.

# Chapter One – Meteorites: an overview

## 1.1 – Meteorites and their classification

Stones from space are a common occurrence: a fair estimate of the total mass of meteorites falling on Earth is estimated at more than 50,000 tons per year (e.g., Zolensky *et al.*, 2006; Bland *et al.*, 1996). Making sense of the various typologies is a daunting task; nowadays, however, scientists have reached a general consensus upon a comprehensive classification scheme for meteorites. Changes may always occur in the future, though a revolution in the field looks unlikely.

As a preliminary step we turn our attention to the use of terminology (following Mc Sween's book, *Meteorites and their Parent Planets*, 1999).

*Meteoroids* are (natural) space objects of up to ~100 m in diameter; *meteors* are the visual phenomena associated with a meteoroid passing through the atmosphere. *Meteorites* are the fragments of meteoroids which survive the passage and reach the surface of Earth.

The sizes of meteorites range from microns to kilometers. Fortunately for us, the biggest ones visit Earth very rarely – about once in a hundred million years – whereas their number grows exponentially as their size decreases (fig. 1.1.1)

Objects exceeding the ~100 m limit are *asteroids* or *comets*, depending on their provenience – usually the main belt for the asteroids and the outer Solar System for the comets. At the other end of the size spectrum sit the *interplanetary dust particles*, or IDPs – micron-sized, light enough to float in air and be collected in the lower stratosphere or into polar ices.

Most meteorites and IDPs are fragments of asteroids, with the following exceptions:

- some IDPs may be of cometary origin;
- more than 100 meteorites (nakhlites, shergottites, chassignites, orthopyroxenites) arrived from Mars;
- about 400 meteorites are known to come from the Moon;
- eucrites are very likely chunks of the asteroid Vesta.

*Falls* are the meteorites recovered just after their arrival. They represent only a minority; the rest are called *finds*. Chemical interaction with the environment can significantly alter the original composition of finds, which for this reason are less dependable as chemical indicators.

There have been many attempts at classifying meteorites in the past (Brezina, 1904; Prior, 1916 among others). The older schemes just defined a distinction between stony, stony-iron and iron meteorites, focusing on their metal content but at the same time ignoring other clues to their formation process. A more modern approach distinguishes between *differentiated* and *undifferentiated* meteorites. The former have undergone (at least to some extent) the same process which formed planets like Earth, with a denser, metallic core and a lighter silicate crust. The latter are more primitive – in the sense that they were never exposed to a gravitational field strong enough to start a chemical differentiation. It is important to point out that the distinction differentiated/ undifferentiated

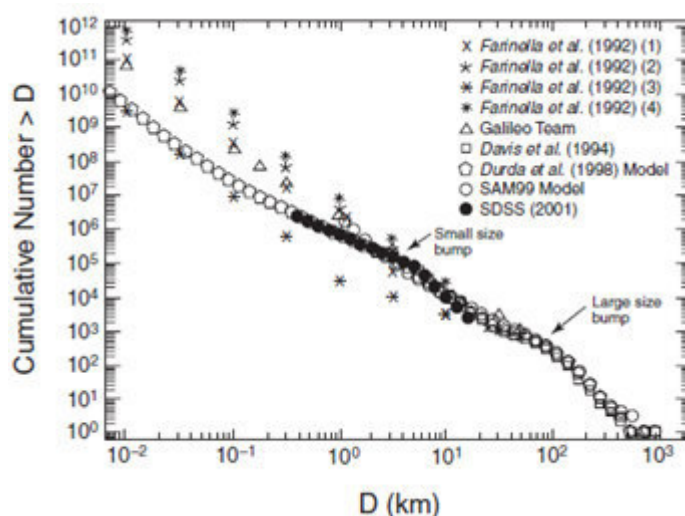


Fig. 1.1.1 – Some estimates of the main-belt asteroids size distribution. A 'broken' power law ( $N \sim D^{-p}$ ) generally fits the data, with  $p$  varying from -2.3 (for  $0.4 \text{ km} < D < 5 \text{ km}$ ) to -4 (for  $5 \text{ km} < D < 40 \text{ km}$ ) (data from Ivezić *et al.*, 2001). From Hughes *et al.*, 1993



does not by any means rule out that the accreted starting materials of the parent bodies were similar – it only implies that the evolution of the body was different (Bischoff *et al.*, 2006).

The current classification scheme (Van Schmus and Wood, 1967; Krot *et al.*, 2003); Weisberg *et al.*, 2006) divides meteorites in two broad categories, *chondrites* and *nonchondritic meteorites*. The term ‘chondrite’ comes from the Greek *χόνδρος* via the Latin *chondrula*; the meaning is ‘salt/wheat grain’, and is used for the spherical, sub-spherical or even ellipsoidal structures (ranging in size from 0.1 to 4 mm) commonly found in chondrites – with a percentage in volume varying from a few percent up to 70%.

Chondrules are considered the remnant of the coalescing and aggregating processes that took place at the very first stages of the formation of our planetary system; details of these processes, however, are still poorly known and understood.

Chondrites are by far the most common type of space rock, summing up to 84% of the total of meteorites – a figure rising up 90%, or even more, when only the falls are considered. These objects are far more susceptible to terrestrial alteration than iron meteorites and therefore harder to collect as finds, because they are often no longer recognizable as extraterrestrial rocks.

Classification of chondrites makes extensive use of a hierarchy of terms. They are, in decreasing order: *class*, *clan*, *group*, and *subgroup*.

A chondrite class consists of two or more groups sharing primary whole-rock chemical and O-isotopic properties (see, for instance, Hutchison, 2004). Chondrites belonging to the same class share broadly similar refractory lithophile-element abundances – be them enriched, depleted, or equal to solar abundances (Fig. 1.1.6), with CI chondrites defining our best estimate of solar composition (e.g., Anders and Grevesse, 1989), and their O-isotopic compositions plot in the same general region (above, on, or below the terrestrial fractionation line, TF) on a three-isotope diagram.

Chondrites are divided into three major classes – *carbonaceous* (C), *ordinary* (O), and *enstatite* (E). However, the terms ‘carbonaceous’ and ‘ordinary’ are more historical than meaningful; ‘ordinary’ originally applied because these are the most common meteorites, but the name fatally tends to underestimate their importance. ‘Carbonaceous’, on the other hand, is somewhat of a misnomer, for today we know that the carbon content of some C chondrites is very low.

*Clan*, the last term to arrive in chondrite classification, is used as a higher order of classification than group, though less inclusive than class. It was originally meant for those chondrites – having chemical, mineralogical, and isotopic similarities – which were thought to have formed within a narrow range of heliocentric distances in the solar nebula (Kallemeyn and Wasson, 1981; Kallemeyn *et al.*, 1996). Some authors (Weisberg *et al.*, 1995) used the term clan for a limited number of chondrites within a class that have chemical, mineralogical, and isotopic similarities suggesting a petrogenetic kinship, but with petrologic and/or bulk chemical characteristics incompatible with a group relationship. A clan consists of chondrite groups that may have closely similar refractory lithophile element abundances (Fig. 1.1.6), plot on the same O-isotopic mixing line, share an isotopic anomaly, or have some similarities in petrologic characteristics (e.g., chondrule size or primary mineral compositions).

So far, four C-chondrite clans have been recognized: the CR clan, which includes the CR, CH, CB, and ungrouped chondrite Lewis Cliff (LEW) 85332; the CM-CO clan; the CV-CK clan; and the CI clan (Weisberg *et al.*, 1995a; Kallemeyn *et al.*, 1996).

To summarize, the significance of chondrite clans is still debated, requiring further research and evaluation; a single clan may include materials from the same local nebular reservoir that were sorted according to size, or materials that experienced different secondary histories such as brecciation, impact events, oxidation or reduction, and/or hydrothermal alteration.

Group is arguably the most basic and significant unit used in meteorite taxonomy; it is usually interpreted to indicate that the meteorites are from the same parent body. The term *group* is defined as a minimum of five unpaired chondrites of closely similar petrologic (chondrule size, modal abundances, and mineral compositions), whole-rock chemical and O-isotopic characteristics (Table 1, fig 1.1.6).

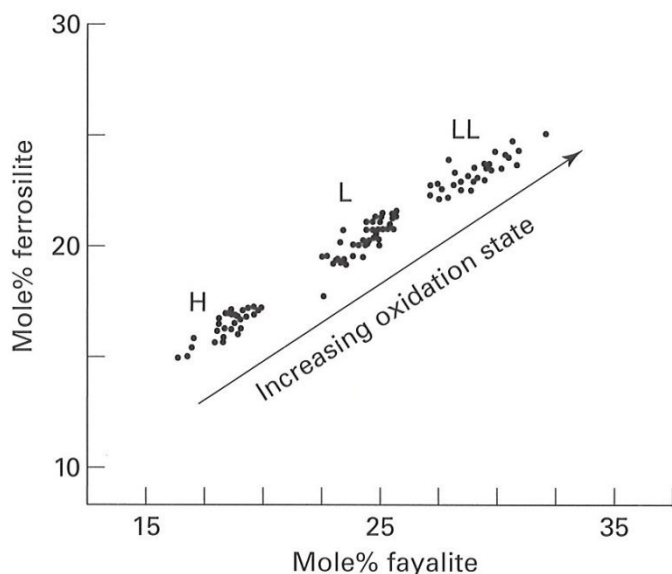


Fig. 1.1.2 – A plot of fayalite (Fa) of olivine versus ferrosilite (Fs) content of orthopyroxene in equilibrated ordinary chondrites shows three oxidation groups, clearly identifiable (H/L/LL). From Weisberg *et al.*, 2006; adapted from Fredriksson and Keil, 1964)

Fe and the ratio of metallic Fe ( $\text{Fe}^0$ ) to oxidized Fe ( $\text{FeO}$ ). Ordinary chondrites are the most common type of chondrites – which, in turn, are the most abundant meteorites found on Earth.

Letters stand for *High Iron* (H), *Low Iron* (L) and *Low Iron-Low Metal* (LL), depending on the  $\text{FeO}/(\text{MgO}+\text{FeO})$  ratio, or the atomic abundances in their most common femic minerals – olivines and pyroxenes. H chondrites have the highest Fe and highest  $\text{Fe}^0/\text{FeO}$  ratios (H, 0.58; L, 0.29; LL, 0.11), LL chondrites the lowest. In the equilibrated O chondrites (petrologic types 4–6), this is also reflected in their olivine [(in mol% Fa): H, 16–20; L, 23–26; LL, 27–32] and low-Ca pyroxene compositions.

Usually considered as a single entity, olivine is actually a set of minerals – all orthorhombic in

The larger differences can be found among the stony meteorites, which may be differentiated rocks from asteroids or even chunks from planet-sized parent bodies (Lunar and Martian meteorites), along with 15 recognized chondrite groups. Within the C-chondrite class (*carbonaceous* – they are the richest in organic compounds) eight groups are identifiable, designated with the letter C and a second letter that is usually the first initial of the type specimen for that group: CI (Ivuna-like – the most ancient, with chemical abundances closest to solar photosphere composition), CM (Mighei-like), CO (Ornans-like), CV (Vigarano-like), CK (Karoonda-like), CR (Renazzo-like), CH (high Fe), CB (Bencubbin-like).

Two groups are *enstatite* (EH and EL, depending on their high/low Fe-content), and other two are the R (Rumuruti) and K (Kakangari) chondrites.

Groups within the O- (ordinary) chondrite class are H, L, and LL – based on the abundance of

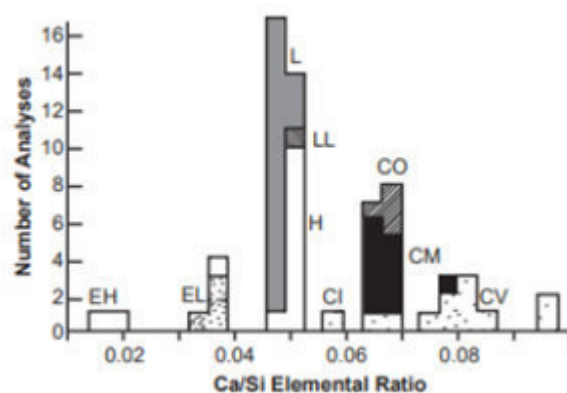
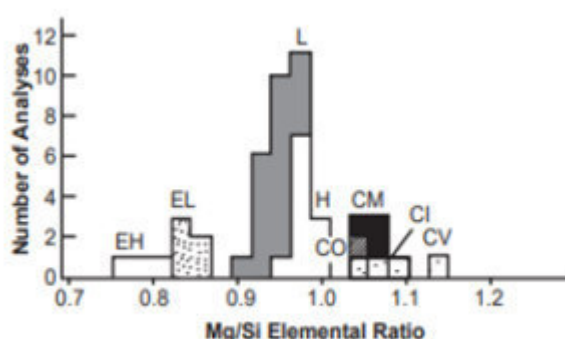


Fig. 1.1.3 – Mg/Si and Ca/Si ratios as indicators of chondrite clans (from von Michaelis *et al.*, 1969, in O. Norton, *The Cambridge Encyclopedia of Meteorites*, 2002, p. 83)

structure, but with a variable composition. The general formula is  $(\text{Mg,Fe})_2\text{SiO}_4$ ; both Fe and Mg have similar atomic radii, so that they can easily replace each other inside the lattice structure.

Distinguishing between the various chondrite clans is possible by determining the elemental ratios of the lithophiles – in particular, Mg/Si and Ca/Si; these elements bind with Si and O and form silicates.

The highest values are found in carbonaceous chondrites. Enstatite chondrites display the lowest: ordinary chondrites lie in between.

TABLE 1. Average petrologic characteristics of the major chondrite groups. *From: Weisberg et al., 2006*

	CI	CM	CO	CV	CK	CR	CH	CB	H	L	LL	EH	EL	R	K
Chondrule abundance (vol%)*	≪1	20 <sup>†</sup>	48	45	45	50–60	70	20–40	60–80	60–80	60–80	60–80	60–80	>40	27
Matrix abundance (vol%)	>99	70 <sup>†</sup>	34	40	40	30–50	5	≪1	10–15	10–15	10–15	2–15 <sup>‡</sup>	2–15 <sup>‡</sup>	36	73
CAI – AOA abundance (vol%)	≪1	5	13	10	10	0.5	0.1	≪1	≪1	≪1	≪1	≪1	≪1	0	≪1
Metal abundance (vol%)	0	0.1	1–5	0–5	0–5	5–8	20	60–80	8	4	2	10	10	0.1	7
Average chondrule diameter (mm)	NA	0.3	0.15	1.0	1.0	0.7	0.02	(0.2–1 cm)	0.3	0.7	0.9	0.2	0.6	0.4	0.6
Olivine composition (mol% Fa)	††	††	††	††	(<1–47) <sup>§</sup> 29–33	1–3 <sup>¶</sup>	(<1–36) <sup>§</sup> 2 <sup>¶</sup>	(2–3) <sup>§</sup> 3 <sup>¶</sup>	(16–20) <sup>§</sup> 19.3 <sup>**</sup>	(23–26) <sup>§</sup> 25.2 <sup>**</sup>	(27–32) <sup>§</sup> 31.3 <sup>**</sup>	0.4	0.4	38.0 <sup>**</sup>	2.2

\*Chondrule abundance includes lithic and mineral fragments.

<sup>†</sup> Highly variable.

<sup>‡</sup> The amount of matrix, if any, is not well established in E chondrites.

<sup>§</sup> Range of compositions.

<sup>¶</sup> Mode.

<sup>\*\*</sup> Data for equilibrated varieties.

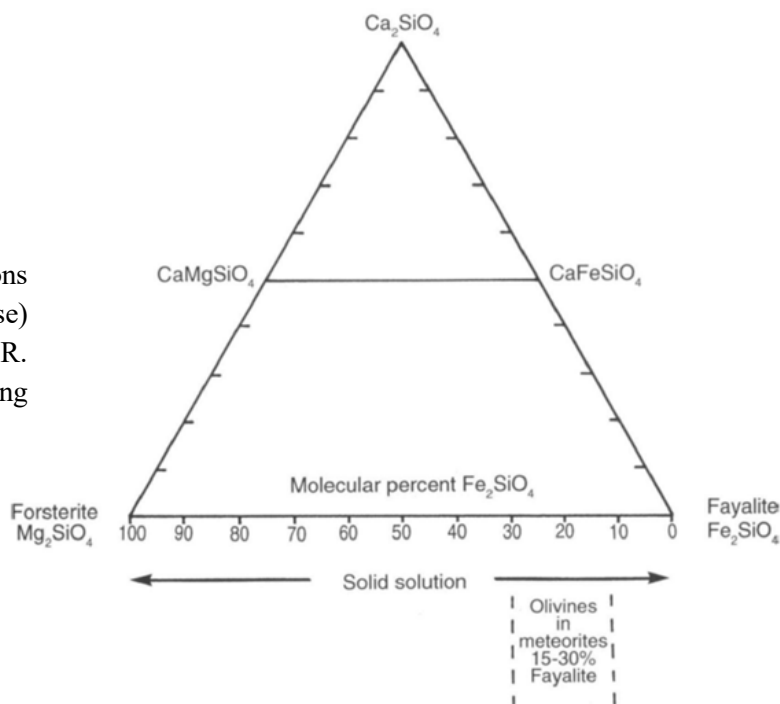
<sup>††</sup> Highly variable, unequilibrated.

NA = not applicable.

Systematic petrologic differences have been recognized in members of some chondrite groups, which led to division of these groups into *subgroups*. For example, the CV chondrites can be divided into the oxidized and reduced subgroups, based on matrix/chondrule ratios, metal/magnetite ratios, and Ni content of metal and sulfides. Some chondrites are mineralogically and/or chemically unique and defy classification into the existing chondrite groups; these are commonly called *ungrouped* chondrites. Among the most significant of these are Acfer 094, which appears to have largely escaped parent-body processing, and the unusual breccia Kaidun, which contains clasts of a variety of chondrite classes mixed on a millimeter scale. Meteorites within a group that have an atypical feature are often referred to as *anomalous*.

Graphs of figures 1.1.4 and 1.1.5 show the series of solid solutions for olivines, with all the possible proportions for the end members – forsterite (Mg<sub>2</sub>SiO<sub>4</sub>, 100% Mg, 0% Fe) and fayalite (Fe<sub>2</sub>SiO<sub>4</sub>, 0% Mg, 100% Fe). Olivine composition in meteorites is usually reported as fayalite mole %, i.e. a measure of iron oxidation state. For meteorites this percentage typically ranges from 15% to 30% (Norton, 2002, p. 84).

Fig. 1.1.4 – Diagram showing possible compositions for olivine. The forsterite/fayalite ratio (or its inverse) is crucial in meteorite classification (from O. R. Norton, *Rocks from Space*, Mountain Press Publishing Company, 1994)



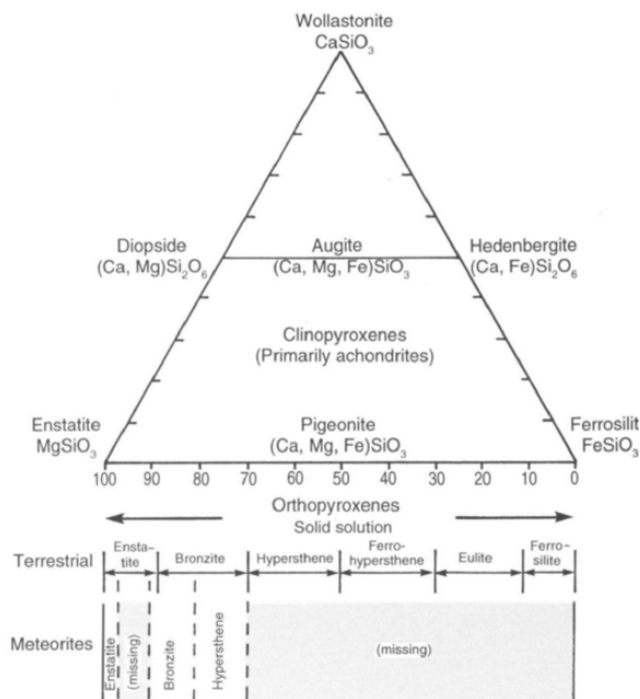


Fig. 1.1.5 – Diagram showing possible compositions for pyroxene. In meteorites, the last members of the sequence (from hypersthene onward) are missing. The forsterite/fayalite ratio (or the inverse) is crucial in meteorite classification (from O. R. Norton, *Rocks from Space*, Mountain Press Publishing Company (1994))

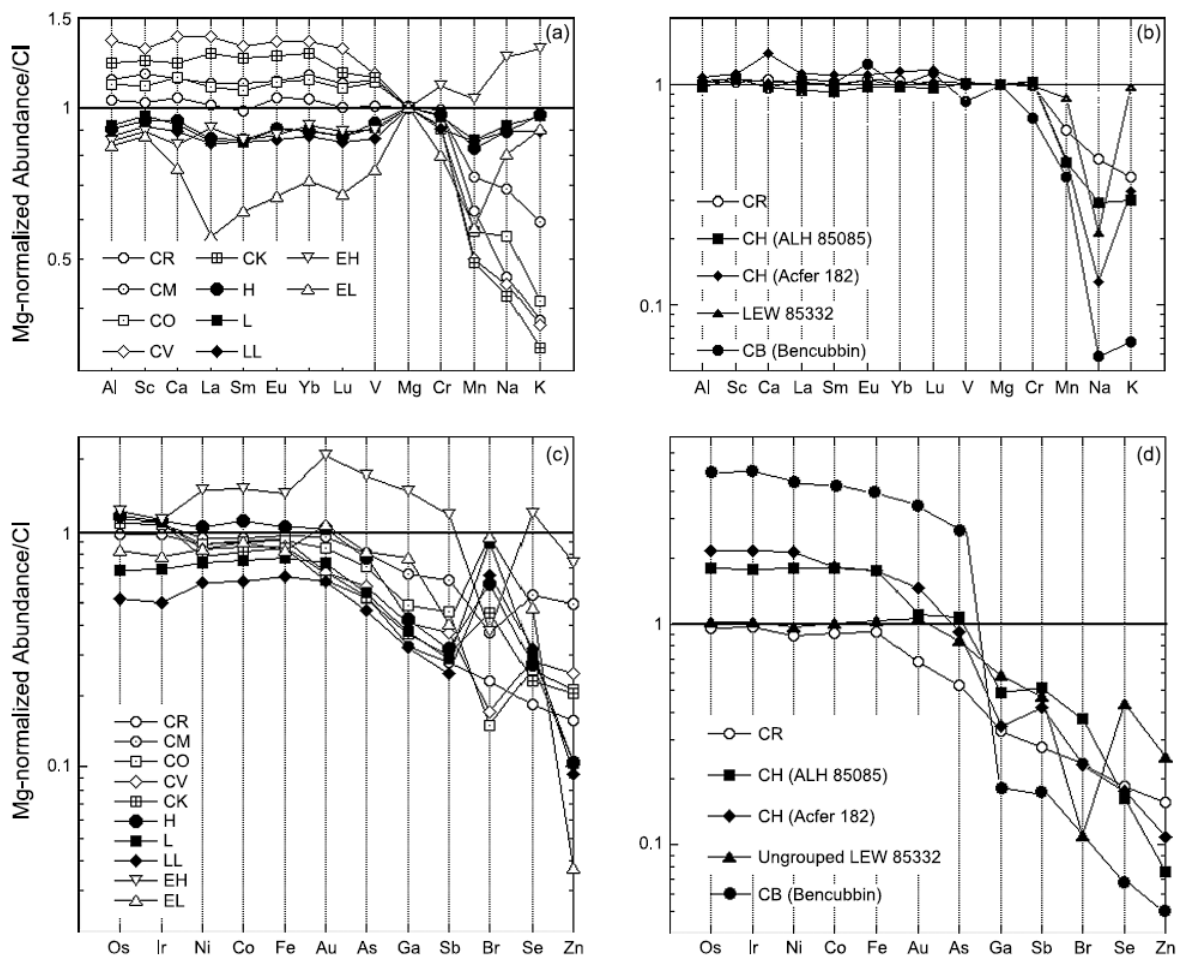


Fig. 1.1.6 – Chemical differences among the various chondrite groups. Shown in this diagram are average whole-chondrite lithophile-element abundances in (a) various chondrite groups and (b) chondrite groups in the CR clan and siderophile-element abundances in (c) various chondrite groups and (d) chondrite groups in the CR clan. All data are normalized to Mg and CI chondrites. Elements are arranged according to their volatility. Data are from Kallemeyn and Wasson (1981, 1982, 1985), Kallemeyn *et al.* (1978, 1989, 1991, 1994, 1996), Sears *et al.* (1982), and Wasson and Kallemeyn (1988).

The nonchondritic meteorites include the primitive *achondrites* and the igneously differentiated meteorites. The textures of primitive achondrites suggest that they were molten, partially molten, melt residues, or extensively recrystallized, but their petrologic characteristics, whole-rock chemical compositions, or O-isotopic compositions display a close affinity to the chondrites from which they formed (e.g., Prinz *et al.*, 1983). Their nomenclature tends to follow the terminology first established by the German mineralogist Gustav Rose (1798-1873) for achondrites, applying the *-ite* suffix to a particularly well-known or well characterized member of the groups (e.g., *acapulcoite* for Acapulco), although it can also include the terminology of iron meteorites.

TABLE 2. Average petrologic characteristics of the major (asteroidal) achondrite and primitive achondrite groups. From: Weisberg *et al.*, 2006

	URE	ACA	LOD	ANG	AUB	BRA	WIN	HED	MES	PAL
Texture	coarse, some mosaized	fine	coarse	medium to coarse	coarse/ brecciated	equigranular, with triple junctures	fine to medium	fine to coarse equigranular brecciated	breccias/ impact melt	coarse
Olivine composition Fa (mol%)	2–26*	4–13	3–13	11–66 (La 0.1–48)	<0.1	30–35	1–8	27–44	8–37	8–30
Low-Ca pyroxene Fs (mol%)	13–25	1–9	1–9		0.1–1.2	trace	1–9	14–79	23–59	—
Ca-pyroxene Fs (mol%)	13–32	46–50	46–50	12–50	0–0.2	10–13	2–4			
Wo (mol%)	2–16	43–46	43–46	50–55	40–46	38.7–47 (up to 5% TiO <sub>2</sub> ) (up to 12% Al <sub>2</sub> O <sub>3</sub> )	44–45	—	—	
Plagioclase An (mol%)	rare to absent	12–31	12–31	86–99.7	2–23	22–32	11–22	73–96	91–93	—
Metal	rare	present	present	rare	rare	minor†	present	rare	(stony-iron)	(stony-iron)
Other minerals present	augite graphite	troilite phosphates spinel graphite	troilite phosphates spinel graphite	spinel troilite phosphates oxides	variety of cubic sulfides	sulfide oxides	troilite daubreelite schreibersite graphite	pigeonite silica chromite	pigeonite silica phosphates	phosphates troilite

\* Olivine has reduction rims with near-end-member compositions. La-Ca end member.

URE = ureilites, ACA = acapulcoite, LOD = lodranite, ANG = angrites, AUB = aubrite,

† Tafassasset is a metal-rich (8 vol%) brachinite.

BRA = brachinite, WIN = winonaites, HED = howardite = eucrite = diogenite, MES = mesosiderite, PAL = pallasite.

The identification of primitive achondrites is one of the major classification developments in the past several years; the definition of Prinz *et al.* (1983) is useful for their recognition. The idea is that primitive achondrites are generally meteorites that exceeded their solidus temperature on the parent body – thus experiencing partial melting – but did not crystallize from a melt; alternatively, if they were molten, they are derived from parent bodies in which planetary differentiation did not achieve isotopic equilibrium.

Achondrites include irons, stony irons, and stones that are from differentiated asteroids, Mars, and the Moon. Historically the term achondrite referred to stony meteorites only, and irons and stony irons have been considered separately; however, most iron meteorites are thought to be the cores of differentiated asteroids. Some stony irons have been interpreted to be mixtures of core and mantle materials, core and crustal materials, or products of impact from differentiated asteroids. Therefore, they are considered here as achondrites.

Terms like ‘class’ or ‘clan’ have not been used systematically to achondrites, while the term ‘group’ has been applied with different meaning compared to its use for the chondrites. It is generally implied that members in a chondrite group are fragments of the same or similar asteroid, but this need not to be the case within the achondrites; some groups (e.g., howardites) fit this definition, whereas other groups (e.g., pallasites) include materials from multiple parent bodies. It would be desirable to standardize the naming conventions, although it’s likely that historical reasons would make acceptance of any new system very difficult.

The classification scheme currently used is largely based upon knowledge of a meteorite’s petrologic characteristics, which include:

- its texture, mineralogy, and mineral compositions;
- whole-rock chemical composition;

– O-isotopic composition (Tables 1-2, Figs. 1.1.6 and 1.1.7).

The vast majority of meteorites are characterized by their petrology alone, although knowledge of all three is a virtual prerequisite for defining a new group; other characteristics can occasionally provide supporting data. Nitrogen and C abundances and isotopes, for example, have been used to distinguish between chondrite groups (Kung and Clayton, 1978; Kerridge, 1985). Similar cosmic-ray-exposure ages for meteorites that are petrologically, chemically, or isotopically similar may suggest a single ejection event from a common parent body, thus reinforcing evidence of a genetic linkage.

Whole-rock chemical composition is the oldest of the three classification methods; it relies upon the ability of geologists to determine chemical composition without using additional tools like a polarizing microscope. Chondrite compositions are usually expressed as Mg- or Si-normalized abundances relative to CI chondrites; one of their defining chemical characteristics is that their whole-rock chemical compositions are not fractionated relative to the solar photosphere, with the exception of the moderately volatile to highly volatile elements (fig. 1.1.6). CI chondrites are considered the best match to solar abundances; the other chondrite groups are characterized by a narrow range of uniform enrichments or depletions in refractory elements, as well as volatility controlled depletions in the (moderately volatile) lithophile and siderophile elements relative to CI chondrites (fig. 1.1.6). Other bulk compositional criteria useful for characterizing the chondrite groups involve plotting reduced Fe (metallic Fe and Fe as FeS) versus oxidized Fe (Fe in silicate and oxide phases). Other compositional diagrams of elements of different volatility are also used: Sb/Ni vs. Ir/Ni, Sc/Mg vs. Ir/Ni, and Al/Mn vs. Zn/Mn (Kallemeyn *et al.*, 1996).

Bulk chemical composition is less used as a classification criterion for stony achondrites, although it has helped to pinpoint different igneous trends in the eucrites.

For iron meteorites, the trace elements Ga, Ge, Ir, and Ni help classifying chemical groups; bulk chemical studies have been replaced as the primary method by petrologic investigation – including both textural and mineralogical studies in the polarizing microscope as well as mineralogical and mineral chemical studies using the electron microprobe or scanning electron microscope.

A fundamental distinction between chondrites and achondrites is texture; chondrites generally have characteristic aggregational textures that sharply distinguish them from the igneous or recrystallized textured achondrites (fig. 1.1.7, 1.1.8). Most meteorites have unique textural and mineralogical properties that allow their classification by petrologic thin section analysis; in chondrites, these properties include chondrule size, chondrule to matrix ratios, abundance of metal, and mineral compositions (Table 1, fig. 1.1.6, 1.1.7, 1.1.8).



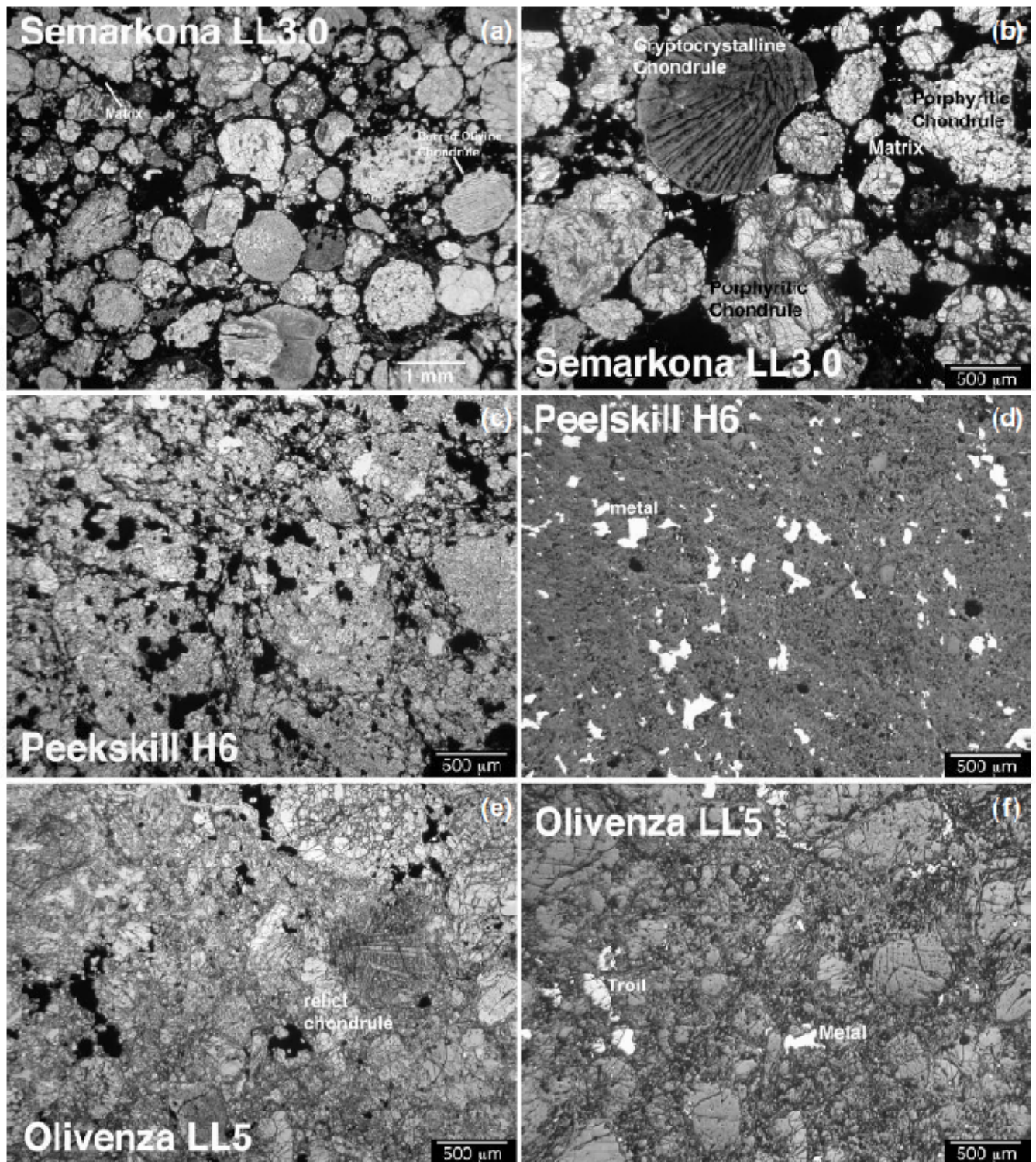


*Fig. 1.1.7. Thin section, plane-polarized light (PL) and reflected light (RF) photomicrographs of representative examples of chondrites showing petrographic variations among chondrite groups. (a) The Semarkona L3.0 ordinary chondrite in PL showing a high density of chondrules with different textures (textural types) including barred and porphyritic chondrules, surrounded by opaque matrix. (b) The Semarkona chondrite in PL showing a large indented cryptocrystalline chondrule, porphyritic chondrules, and matrix. (c) The Peekskill H6 chondrite in PL showing a recrystallized ordinary chondrite in which the primary texture has been essentially destroyed and chondrule boundaries are not easily discernible. (d) Peekskill shown in RF showing about 7% metal. (e) The Olivenza LL5 ordinary chondrite in PL showing the texture of a recrystallized LL chondrite in which some relict chondrule are discernible, but chondrule boundaries are not as sharp as in Semarkona [(a),(b)]. (f) Olivenza in RF showing a lower abundance of metal (~2 vol%) than in the Peekskill H6 chondrite. From Weisberg *et al.*, 2006*



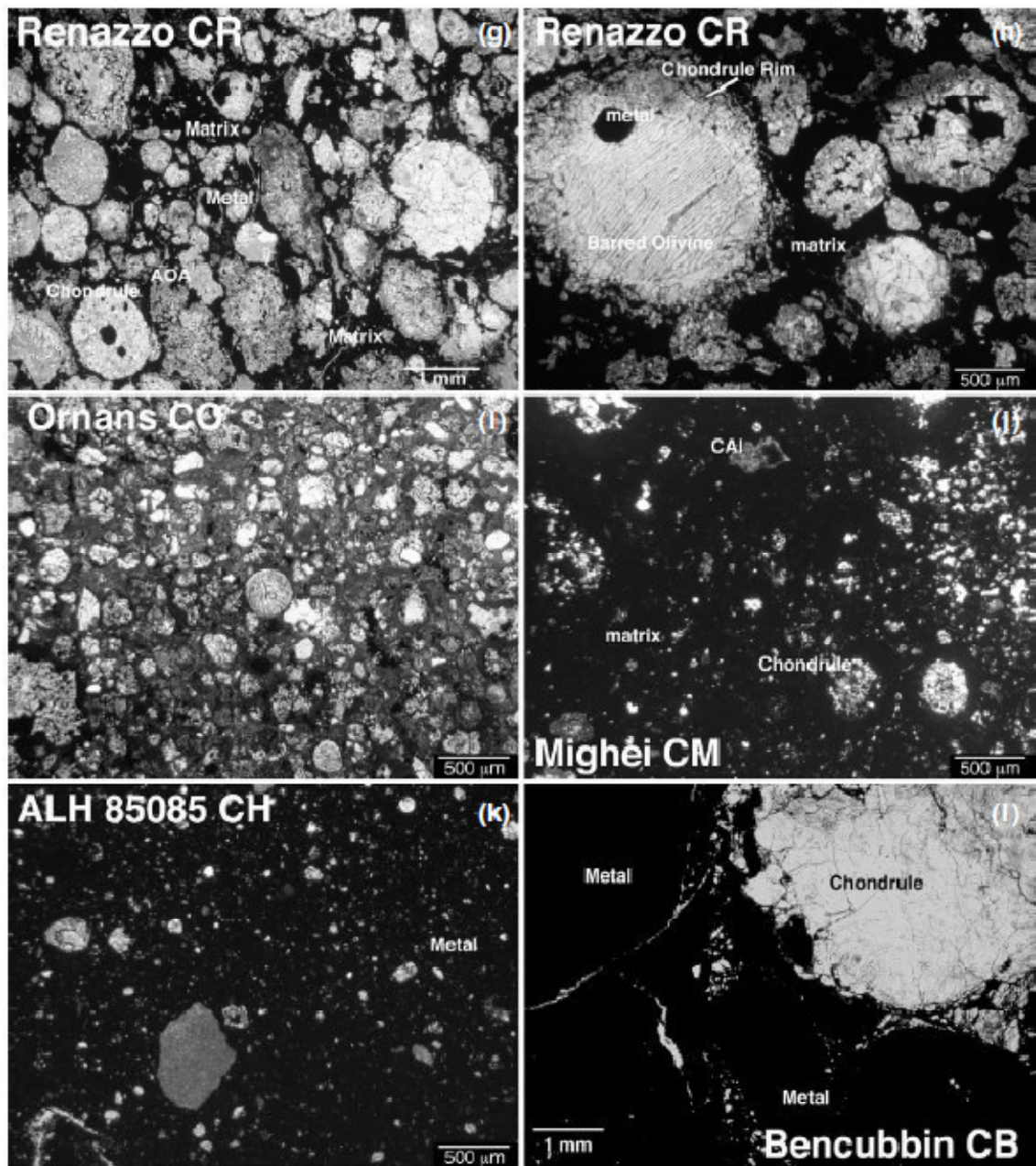


*Fig. 1.1.8. (continued). (g)* The Renazzo CR carbonaceous chondrite showing chondrules, opaque matrix, an amoeboid olivine aggregate (AOA) and a variety of other irregular-shaped objects. *(h)* Renazzo PL image showing a large (2 mm) barred olivine chondrule containing a metal bleb and a silicate rim. *(i)* The Ornans CO chondrite in PL showing the small (~200  $\mu\text{m}$ ) chondrules typical of CO chondrites and about 30% matrix. *(j)* PL photo of the Mighei CM chondrite showing the very high matrix abundance (up to 70 vol%) and small chondrules (100–200  $\mu\text{m}$ ) typical of CM chondrites. *(k)* The ALH 85085 CH chondrite in PL showing its micro-chondrules (most less than 100  $\mu\text{m}$  in diameter) and fragments surrounded by Fe,Ni metal (~20 vol%). Most of the opaque areas are metal. *(l)* The Bencubbin CB chondrite in PL showing a large chondrule that is near 1 cm in diameter and opaque large Fe,Ni metal spheres. From Weisberg *et al.*, 2006

Achondrites are identified from their thin section, which show characteristic textures (e.g., igneous vs. granoblastic), modal abundances of minerals, and mineral compositions (e.g., Table 2). Petrologic studies and whole-rock chemical compositions are generally in fair agreement, as the chemical composition tends to reflect the composition and abundance of the individual minerals and the bulk chemical composition controls mineral crystallization (at least, this holds for achondrites).



Seminal work by R. Clayton and colleagues at the University of Chicago (Clayton *et al.*, 1996; 1999) has shown that small anomalies in  $^{17}\text{O}$  isotope abundance can reveal details about the nebular or parent-body origin of a meteorite, shedding light upon relationships among meteorites which couldn't be inferred from petrology or whole-rock chemical composition. However, more than 98% of the world's known meteorites have been adequately classified from petrologic studies alone, although that number is dominated by equilibrated O chondrites from hot and cold deserts.

For the sake of fairness, it must be remembered that petrologic studies alone have produced some spectacular misclassifications in the past. For instance, the lunar meteorite Elephant Moraine (EET) 87251 was originally thought to be a eucrite (asteroidal basalt) and the ALH 84001 pyroxenite (a martian meteorite) was classified as a diogenite (asteroidal orthopyroxenite). In the latter case, the misclassification stemmed from a lack of appreciation of the petrologic diversity existing on Mars.

TABLE 3. Summary of the criteria for classifying chondrites according to petrologic type, based on *Van Schmus and Wood* (1967). From: *Weisberg et al.*, 2006

Criterion	1	2	3	4	5	6	7
Homogeneity of olivine compositions	—	>5% mean deviations		≤5%	Homogeneous		
Structural state of low-Ca pyroxene	—	Predominantly monoclinic		>20% monoclinic	≤20% monoclinic	Orthorhombic	
Feldspar	—	Minor primary grains		Secondary <2-μm grains	Secondary 2–50-μm grains	Secondary >50-μm grains	
Chondrule glass	Altered or absent	Mostly altered, some preserved	Clear, isotropic	Devitrified	Absent		
Metal: Maximum Ni (wt%)	—	<20 taenite minor or absent	>20 kamacite and taenite in exsolution relationship				
Sulfides: Mean Ni (wt%)	—	>0.5	<0.5				
Matrix	Fine grained opaque	Mostly fine-grained opaque	Opaque to transparent	Transparent, recrystallized			
Chondrule-matrix integration	No chondrules	Sharp chondrule boundaries		Some chondrules can be discerned, fewer sharp edges		Chondrules poorly delineated	Primary textures destroyed
Carbon (wt%)	3–5	0.8–2.6	0.2–1	<0.2			
Water (wt%)	18–22	2–16	0.3–3	<1.5			

After *Van Schmus and Wood* (1967) with modifications by *Sears and Dodd* (1988), *Brearley and Jones* (1998), and this work.

Even today, some of the best-studied meteorites in the world cannot be confidently placed into the existing scheme, suggesting either transitional properties between groups or sampling of a previously unknown type of meteorite.

Other parameters for classification criteria are in use. Chondrites are assigned a number according to petrologic type (*Van Schmus and Wood*, 1967; Table 3). Type 3.0 is believed to represent the most pristine materials, 3.1 to 6 indicate increasing degree of petrologic equilibration and recrystallization, and 2 to 1 represent increasing degree of hydrous alteration in chondrites. Type 7 is reserved to chondrites that have been completely recrystallized or melted; however, some (or most) of these meteorites may be impact melted.

Types are determined through petrologic observation, mineral composition (Table 3), and thermoluminescence properties of the meteorite. However, the mineral criteria in Table 3 do not work equally well for all chondrite groups (Huss *et al.*, 2006); for instance, heterogeneity of olivine composition - which is used to distinguish between type 3 and 4 - is difficult to apply to E chondrites because of their low olivine abundance. Also - due to the reducing conditions under which meteorites formed - the amount of Fe in silicates is low and this is not related to the degree of metamorphic equilibration. In some cases, the petrologic type is reflected in whole-rock O-isotopic compositions - which in equilibrated chondrites (type 4–6), for instance, become increasingly homogeneous.

Figure 1.1.9 shows the petrologic types represented in each chondrite group. Some, like H, L, LL, EH, and EL do not have heavily hydrated (petrologic types 2 and 1) members, whereas others (e.g., CI, CM, CR) lack less altered (type 3) members – which for CI chondrites is an unfortunate circumstance, being among the most primitive solar system materials.

The technique of thermoluminescence (TL) is useful to subdivide the petrologic type 3 chondrites into 3.0 to 3.9 subtypes (Sears *et al.*, 1980); it has been extensively applied to ordinary chondrites, and its sensitivity depends on the degree of crystallization of the chondrule mesostasis. Thus, we can recognize meteorites such as Semarkona (LL3.0) and Krymka (LL3.1), which are believed to be examples of the most pristine ordinary chondrites. The TL data are supported by the high degree of disequilibrium in the mineral assemblage of chondrules and matrix and the abundance of glassy mesostasis in the chondrules of the low petrologic type (<3.5) chondrites (Huss *et al.*, 2006).

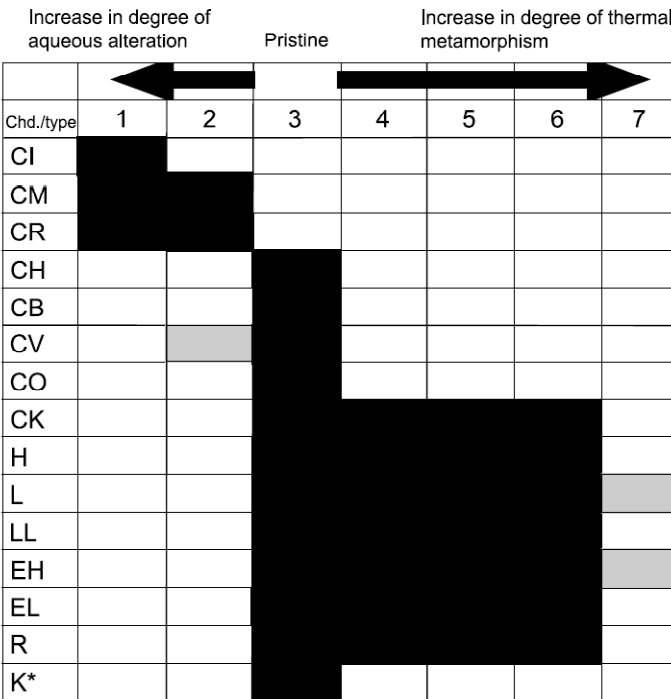
The classification of petrologic types still needs improvement. Some meteorites have been hydrously altered and later reheated during thermal metamorphism; such cases don't fit in the current scheme. One solution may be to have separate schemes for denoting degree of hydrous alteration and degree of metamorphism.

Chondrites are also assigned values describing the degree of shock pressure they experienced; these values range from S1 (unshocked, pressure <5 GPa) to S6 (very strongly shocked, pressures up to 90 GPa), depending on petrographic features of the silicate minerals olivine, pyroxene, and plagioclase – also including undulatory extinction, fracturing, and mosaicism, as well as transformation of plagioclase into maskelynite (e.g., Stöffler *et al.*, 1991; Rubin *et al.*, 1997). Other indicators of high degrees of shock in chondrites are the presence of high-pressure minerals, such as majorite garnet and wadsleyite (a high-pressure form of olivine; e.g., Kimura *et al.*, 2003); it should be remarked, however, that shock degree can vary within a meteorite on the scale of centimeters.

Last but not least, meteorites have undergone 4.6 billion years of impact processing, which produced myriad breccias. Chondrite breccias usually consist of clasts belonging to the same chondrite group (genomict), with a few exceptions containing clasts from different meteorite groups (polymict); this observation has led to the conclusion that each chondrite group may represent a single parent body. Some chondrites are termed genomict breccias (Bischoff *et al.*, 2006) to indicate that they contain fragments of the same chondrite group, but different petrologic types. Many achondrites are brecciated; most notable among them are the howardites – breccias composed of eucrite and diogenite.

As for iron meteorites, true breccias – i.e., recemented fragments of previously formed and fragmented iron meteorites – are completely absent.

Figure 1.1.10 displays a general classification of meteorites, taken from the article by Weisberg *et al.* (2006). To the left stand all chondrite classes and clans, whereas the right side of the diagram shows achondrites and iron meteorites.



\*Grouplet.  
Chd. = chondrite group.  
Fig. 1.1.9. Diagram showing the petrologic types for each chondrite group. From Weisberg *et al.*, 2006.



Chondrites are among the most primitive solar system materials available for study; within them we found submillimeter- to centimeter-sized components, including chondrules, Ca-Al-rich inclusions (CAIs), amoeboid olivine aggregates (AOAs), Fe, Ni-metal, and fine-grained matrix (Fig. 1.1.7). These components are thought to have formed as independent objects in the protoplanetary disk by high-temperature processes that included condensation and evaporation (e.g., Ebel, 2006; Fedkin and Grossman, 2006). As a result, chondritic components of primitive (unaltered and unmetamorphosed) chondrites preserved records of the physical-chemical properties of the protoplanetary disk region where they formed, and are ground truth for astrophysical models of nebular evolution.

Chondrules are spherical to semi-spherical objects, generally composed of mafic minerals and interpreted to have formed as molten or partly melted droplets from transient heating event(s) in the solar nebula. Calcium-aluminum-rich (CAIs) inclusions and AOAs are irregular to spherical objects having primary minerals that are composed of more refractory elements than those found in the chondrules; the mineralogy of CAIs is discussed by Beckett *et al.* (2006). Surrounding the chondrules and inclusions is a fine-grained (generally <5  $\mu\text{m}$ ) silicate-rich matrix. Chondrite matrix is a separate component, and not made of pulverized chondrules and CAIs; its relationship to chondrules and CAIs is not well understood.

Additionally, chondrites contain small (<5–10  $\mu\text{m}$ ) presolar grains of diamond, silicon carbide, graphite, silicon nitride, and oxides (e.g., Anders and Zinner, 1993; Bernatowicz and Zinner, 1997).

The achondrites include meteorites from asteroids, Mars, and the Moon. Primitive achondrites may represent melts, partial melts, or melt residues from local heating events on planetary bodies during the earliest stages of differentiation – or possibly from local impact events. Further discussions of achondrites are given by McCoy *et al.* (2006), while Chabot and Haack (2006) provide a description of irons.

We won't get involved in a thorough discussion of carbonaceous chondrites, which are not the focus of this study. They display an O-isotopic composition plotting near or below the terrestrial fractionation (TF) line, and exhibit a wide range of chondrule sizes, from the large rimmed chondrules in CV and CR chondrites to the small chondrules in CH chondrites (Table 1, Fig. 1.1.8).

CI (Ivuna-type) chondrites are often considered the most primitive solar system materials, with bulk compositions close to that of the solar photosphere. They are altered, brecciated rocks devoid of chondrules and CAIs, of petrologic type 1 – heavily hydrated meteorites, hydrothermally altered, brecciated chondrites with their primary mineralogy entirely erased during extensive aqueous alteration. It's not easy to reconcile their history with their primitive composition.

Ordinary chondrites are characterized by a high abundance of large (millimeter-sized) chondrules with various textures and mineral compositions. Matrix abundances (10–15 vol%) are generally lower than in carbonaceous chondrites; CAIs and AOAs are very rare (Table 1). Petrologic types range from 3 to 6 (Fig. 1.1.7), with several less-altered (petrologic types 3.0–3.1) members. Some of the least-metamorphosed (e.g., Semarkona and Bishunpur) show evidence for aqueous alteration (e.g., Hutchison *et al.*, 1987; Alexander *et al.*, 1989; Sears and Weeks, 1991; Sears *et al.*, 1980, 1991), mainly in the matrix and (in some cases) chondrule mesostases (Hutchison *et al.*, 1987). Their O-isotopic compositions plot above the TF line, sharply distinguishing them from the carbonaceous chondrites. H, L, and LL chondrites have similar, overlapping petrologic characteristics and O-isotopic compositions indicating they are closely related members of a clan.

A number of parameters are used to resolve the H, L, and LL groups. Small, systematic differences are observed for metal abundances and chondrule size (Table 1, Fig. 1.1.7); a plot of Co concentration in kamacite vs. fayalite content in olivine will show a hiatus between H and L, but no hiatus between L and LL chondrites (Rubin, 1990). Olivine composition is not a reliable indicator of

group for unequilibrated O chondrites of low petrologic type ( $<3.5$ ), although it is successfully used for distinguishing the equilibrated varieties (Table 1).

Siderophile element abundances can also be used to distinguish H, L, and LL (Kallemeyn *et al.*, 1989; Sears *et al.*, 1991). Several ordinary chondrites (Bjurböle, Cynthiana, Knyahinya, Qidong, Xi Ujimgin) are intermediate between L and LL groups, possibly indicating formation on a separate parent body (Kallemeyn *et al.*, 1989). Based on their siderophile-element abundances and olivine and kamacite compositions, two chondrites (Tieschitz and Bremervörde) are intermediate between H and L and have been classified as H/L chondrites (Kallemeyn *et al.*, 1989).

Enstatite chondrites formed under highly reducing nebular conditions, as recorded by their mineralogy and mineral chemistry (e.g., Keil, 1968). They contain Fe-poor silicates and Si-bearing metal, and elements that are generally lithophile in most meteorite groups (Mn, Mg, Ca, Na, K) can behave as chalcophile elements. Enstatite ( $\text{MgSiO}_3$ ) is the major silicate mineral in the chondrules.

Chondrule olivine rarely occurs in chondrites of low petrologic types (EH3 and EL3), and is essentially absent in the higher petrologic types.

Enstatite chondrites are the only ones with O-isotopic compositions plotting on the TF line and close to the O composition of Earth and the Moon (Clayton *et al.*, 1984). They are divided into EH and EL groups, clearly distinguished by the composition of the (Mg,Mn,Fe)S phase – EH chondrites are more reduced than the EL chondrites and contain niningerite and various alkali sulfides. In addition, EH chondrites have higher Si (2–3 wt%) in the Fe,Ni-metal, whereas EL chondrites generally have less than 1.0 wt% Si in the metal.

The Rumuruti chondrites have refractory-lithophile-element abundances and O-isotopic compositions that are consistent with placing within the ordinary chondrite class, but this has not yet been established. They are quite different from the H, L, and LL chondrites. They are highly oxidized meteorites characterized by NiO-bearing, FeO-rich olivine ( $\text{Fa}_{37-40}$ ) and nearly complete absence of Fe,Ni-metal.

A number of chondrites do not fit into any of the existing groups, so that they are referred to as ungrouped. In many cases, they have characteristics that are intermediate between chondrite groups. They may be anomalous members of chondrite groups – or the first representatives of new groups.

Comparison of the mineralogical-petrological properties with O-isotopic compositions of meteorites has revealed a number of interesting relationships. Some meteorites with differing petrologic and whole-chondrite chemical compositions display similar O-isotopic compositions; this has been interpreted to indicate derivation of these groups (or their components), which have grossly different petrographic features from the same local nebular reservoir or parent asteroid.

The disagreement between O-isotopic compositions and petrologic-chemical studies — both in terms of pointing to differences between petrologically similar materials and possibly between petrologically disparate materials — has sparked an active debate about the classificational structure over the last few decades. The classification scheme illustrated here stems largely from chemical-petrological studies, and perhaps only in the case of C chondrites and a few groups of achondrites (e.g., acapulcoite-lodranites vs. winonaites) do the O isotopes play a prominent role. It is possible to develop an entirely different classification scheme, which is illustrated in Fig. 1.1.11.

In such a scheme, meteorites are grouped to point out origins from common parent bodies or derivation from common nebular reservoirs or precursor materials. In this sense, we find groupings between chondrites and irons (e.g., IVA-LL, IIEH), between achondrites and irons (e.g., angrites-IVB), and between chondrites and achondrites (CV-ureilites, EH-EL-aubrites).

The problem with such a scheme is that it is highly interpretive. In some cases, links are based on petrology, chemistry, and O-isotopic compositions (e.g., E chondrites and aubrites), while in other cases the link rests almost completely on O isotopes (e.g., IVA irons and LL chondrites). In addition, it is unclear what, if anything, these links actually represent. In some cases, a common parent body may be

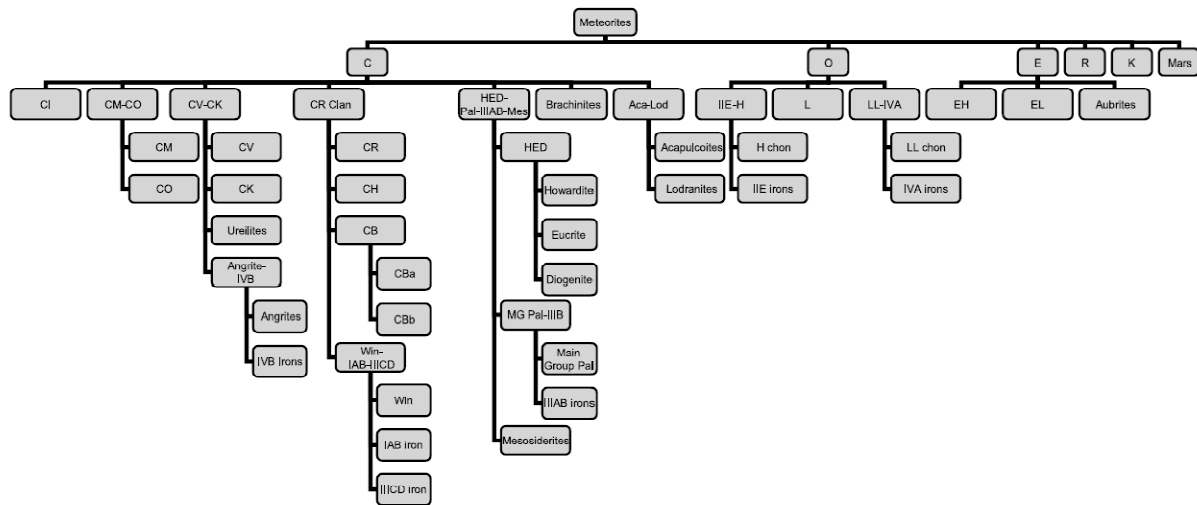


*Fig. 1.1.11.* Alternative classification scheme in which meteorites are linked by origins from common parent bodies or derivation from common nebular reservoirs. Some links are based on petrology, chemistry, and O-isotopic compositions (e.g., enstatite chondrites and aubrites), while in other cases, the link is based almost completely on O isotopes (e.g., IVA irons and LL chondrites). We note that this scheme is highly interpretive and is just one of a number of possibilities.

indicated (e.g., angrites-IVB irons), while in others, the link may only reflect derivation of a particular achondrite or iron from a precursor similar, but not identical, to the known chondrite (e.g., EH-EL-aubrites). Such a diagram can provide some interesting insights, such as the apparent paucity of achondrites and irons apparently derived from the abundant O chondrites, while most achondrites and irons appear linked to C chondrites. Even in this case, care must be applied, since this may be essentially an artifact of defining meteorites below the terrestrial fractionation line as C chondrites. If such a simplistic link were applied to the terrestrial planets, Earth would be linked to E chondrites and aubrites, while Mars would derive from a yet-undiscovered chondrite more akin to O chondrites. Neither of these conclusions appears valid at this time. Given these uncertainties, and the ongoing debate about meteorite origins reflected in the remainder of this book, we find it unlikely that such a classification scheme will supplant the more traditional version (Fig. 1) in the foreseeable future, although knowledge of the possible links is a key piece of information for any worker new to the field.

The evolution of meteorite classification needs a constant influx of new samples and continuing efforts to determine their petrologic characteristics and bulk chemical and O-isotopic compositions. While classification schemes will continue to evolve, in both the groups of meteorites and the techniques used for classification, one of the ultimate goals is to put meteorites into geologic context.

In many respects, classification is simply an effort to deduce the kind of information that the terrestrial field geologists know when they collect their samples – where the samples came from and what their spatial relationship was to the rocks around it. It seems likely that in the next few decades missions to asteroids, Mars, the Moon, and comets will allow us to place meteorites in geologic context; for any meteorite, the final goal will be to identify parent type, parent asteroid or family of asteroids.



## 1.2 - Chromites

Compounds with a spinel-type structure include mineral species with the general formula  $AB_2\phi_4$ , where  $\phi$  can be  $O^{2-}$ ,  $S^{2-}$ , or  $Se^{2-}$ . Space group symmetry is  $Fd\bar{3}m$ , even though lower symmetries are reported owing to the off-center displacement of metal ions. In oxide spinels ( $\phi = O^{2-}$ ),  $A$  and  $B$  cations can be divalent and trivalent (“2–3 spinels”) or, more rarely, tetravalent and divalent (“4–2 spinels”). From a chemical point of view, oxide spinels belong to the chemical classes of oxides, germanates, and silicates. So far, 25 mineral species have been approved: ahrensite, brunogeierite, chromite, cochromite, coulsonite, cuprospinel, dellagiustaitite, filipstadite, franklinite, gahnite, gahnite, jacobsite, magnesiocromite, magnesiocoulsonite, magnesioferrite, magnetite, manganochromite, qandilite, ringwoodite, spinel, trevorite, ülvospinel, vuorelainenite, and zincochromite.

Thiospinels ( $\phi = S^{2-}$ ) and selenospinel ( $\phi = Se^{2-}$ ) are isostructural with oxide spinels. 23 different mineral species have been approved so far for thiospinels and only three for selenospinel (bornhardtite, trüstedtite, and tyrrellite). (Biagioni and Pasero, 2014).



Fig.1.2.1 – Terrestrial chromite (Pic du Champ-de-Bataille, Mont-Dore Commune, Southern Province, New Caledonia).

From: [www.mindat.org](http://www.mindat.org)

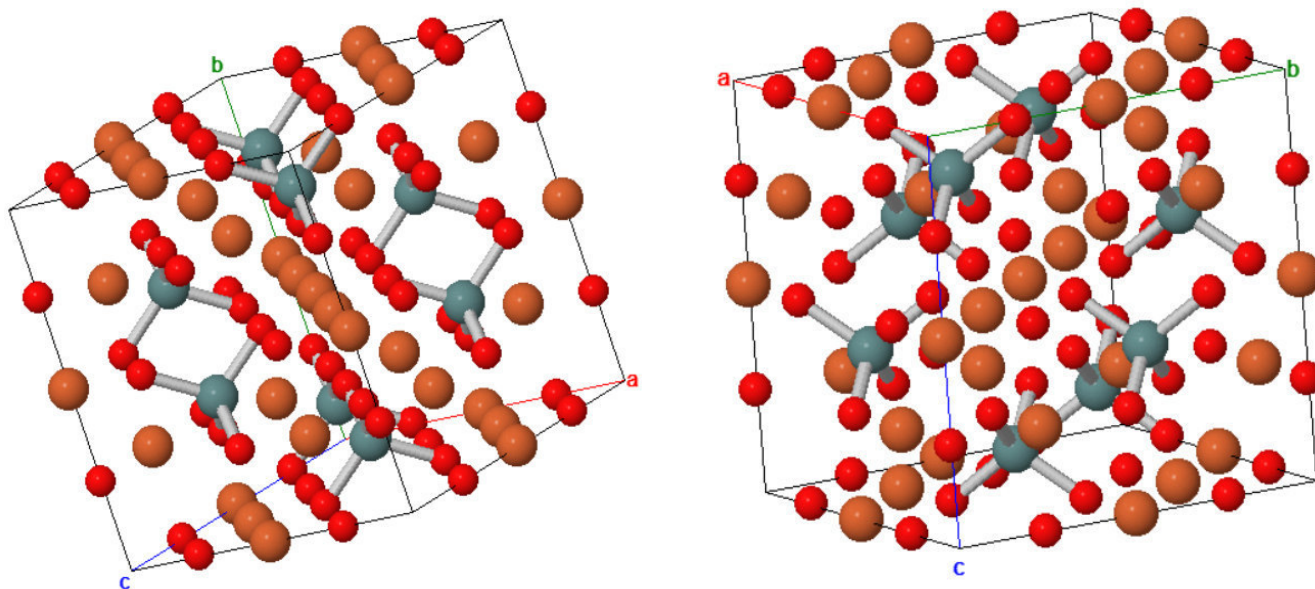


Fig.1.2.2 – The unit cell of spinel  $AB_2\phi_4$ , shown from two different viewpoints. Red spheres are anions ( $O^{2-}$ ,  $S^{2-}$ , or  $Se^{2-}$ ); brown and grey spheres represent  $A$  and  $B$  cations, respectively. From: [www.mindat.org](http://www.mindat.org)

### Spinel structure

The spinel class of oxides,  $AB_2O_4$  – where  $A$  and  $B$  represent differing cations and  $O$  is oxygen – belongs to space group  $Fd\bar{3}m$  (Oh), a cubic lattice consisting of 8 molecules within the unit cell, for a total of 56 atom positions. This space group belongs to the Oh point group. The unit cell of spinel is shown in Figure 1.2.2.

Because of the large number of atoms within the spinel unit cell, it is common practice to identify sub-units within the spinel unit cell, also displayed in figure 1.2.2. A tetrahedral unit,  $AO_4$  is composed of a cation at the center of a cube and four oxygen atoms in the nonadjacent corners. The

octahedral unit consists of a cation surrounded by six oxygen atoms, two along each dimensional axis, to form a  $\text{BO}_6$  octahedron.

The tetrahedra within the spinel lattice are isolated from one another. No sides of a tetrahedron are in contact with other tetrahedra. The octahedral units, on the other hand, do share a single edge. Two oxygen atoms are shared between adjacent octahedra.

Atoms other than oxygen can occupy the anion position of the spinel lattice. Sulfur and selenium belong to the same periodic group as oxygen and many spinels are composed of these elements. A class of compounds known as the “cyanospinel” with formula,  $\text{A}_2 \text{M}(\text{CN})_4$ , also exist. Spinel containing oxygen are exclusively examined in the present work, though work on spinels composed of sulfur and selenium will be referenced.

In a normal spinel, shown in figure 1.2.2, the  $\text{A}^{2+}$  cations occupy the tetrahedral positions, and the  $\text{B}^{3+}$  cations occupy the octahedral positions. A completely inverse spinel places one half of the  $\text{B}^{3+}$  cations onto all of the tetrahedral positions and the remaining half on the octahedral sites, while the  $\text{A}^{2+}$  cations fill up the remaining half of the octahedral positions. Spinel systems may exist in a state between completely normal and inverse, and thus an inversion parameter ( $\xi$ ) is defined, which indicates the fraction of  $\text{A}^{2+}$  cations occupying octahedral positions.

Spinel often have cations with valences other than +2 or +3. Different classes of spinels are often defined by the valences of the spinel’s cations. The spinels dealt with in the present all belong to the normal and inverse class of II-III spinels, as they contain cations with valences of +2 and +3.

### **Spinel group minerals in meteorites**

Chromite is the dominant oxide in ordinary chondrites; ilmenite and rutile occur as rare phases. Some highly oxidized Type-3 chondrites also contain magnetite (e.g., Taylor *et al.*, 1981; Krot *et al.*, 1997). Chromian spinel is the dominant oxide phase in K chondrites, whereas magnetite and ilmenite are rare. Ferroan chromian spinel and isolated grains of spinel occur in CH chondrites.

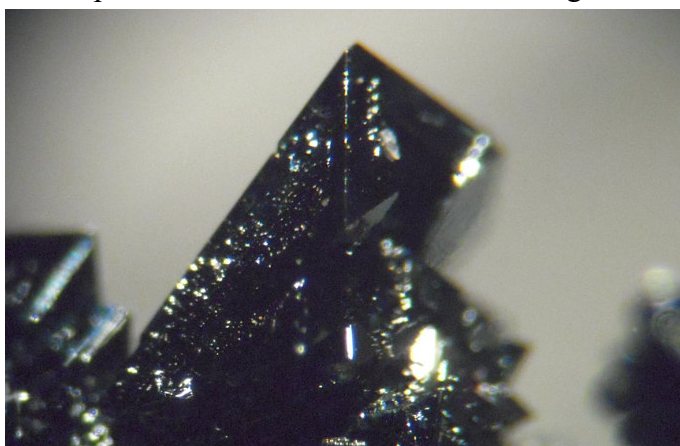


Fig.1.2.4 – Terrestrial magnesioferrite (Napoli, Mt. Somma-Vesuvius, Italy). Source: [www.mindat.org](http://www.mindat.org)



Fig.1.2.3 – Terrestrial magnetite (Tre Croci, Vetralla (VT), Italy). Source: [www.mindat.org](http://www.mindat.org)

Magnetite is the principal oxide phase on CK chondrites; many of the large magnetite grains contain ilmenite and spinel lamellae formed during oxidation and exsolution (Geiger and Bischoff, 1990, 1995). Among CO chondrites, oxide phases are essentially absent except for spinel, perovskite, hibonite and rare grossite inside refractory inclusions (Rubin, 1997).

Chromites in meteorites usually are solid solutions between chromite ( $\text{FeCr}_2\text{O}_4$ ), magnesiochromite ( $\text{MgCr}_2\text{O}_4$ ), spinel ( $\text{MgAl}_2\text{O}_4$ ) and also hercynite ( $\text{FeAl}_2\text{O}_4$ ); minor amounts of V and Ti

usually substitute for Cr and Al, whereas minor amounts of Mn and Zn may substitute for Fe and Mg. Their composition is expressed as  $\text{Mg\#} = \text{Mg}/(\text{Mg} + \text{Fe})$  and  $\text{Al\#} = \text{Al}/(\text{Al} + \text{Cr})$ .



A systematic study of chromite composition in ordinary chondrite meteorites has been carried out by Wlotzka (2005), Ramdohr (1967), and Bunch et al. (1967). All these authors find Al# close to 0.14, and Mg# varying in a range between 0.09 (LL samples) and 0.17 (H samples), with an average value of 0.13 for the L samples (Wlotzka, 2005). In particular, the Mg# seems to correlate with ordinary chondrite class, with LL group having usually lower Mg# than L and H groups; however, this systematic variation has seldom been used to deduce meteorite class from chromites residues found in fossil meteorites (this term refers to the recognizable remnants of meteorites fallen in the past history of Earth – of which only a handful of specimens have been identified – see, for instance, Schmitz and Tassinari, 2001), because chances of fossilization for meteorites are comparable to those of living organisms.

Chromites in ordinary chondrites have been further classified by Rubin (2003) and interpreted in terms of shock indicators, in order to facilitate determination of shock degree of meteorites; the table below summarizes the main features of the scheme he devised.

<i>Major petrographic varieties of chromite in ordinary chondrites</i>	<i>Description</i>
1	Unmelted, unfractured chromite grains
2	Unmelted, impact-fractured chromite grains
3	Chromite grains transected by opaque veins
4	Chromite-plagioclase assemblages
5	Veinlets containing chromite needles and blebs
6	Chromite-rich chondrules

Rubin updated and generalized an already existing classification scheme (Ramdohr, 1967), by taking into account the effect of shock processes.

**Variety 1** – Unmelted, unfractured chromite grains. Equilibrated ordinary chondrites with a low shock stage exhibit chromite grains surrounded by mafic silicates (sometimes with plagioclase nearby), frequently with intergrowth of metallic Fe-Ni or troilite (fig. 1.2.5). The size of these chromite grains ranges between 10 and 200  $\mu\text{m}$  (50-100  $\mu\text{m}$ , more often), with morphologies that can be blocky, equant, anhedral, subhedral or even rounded. They have been called ‘coarse chromites’ in literature (Ramdohr, 1967; 1973). An enrichment in FeO, MnO and  $\text{Al}_2\text{O}_3$  can be observed with increasing petrology (Bunch et al., 1967).

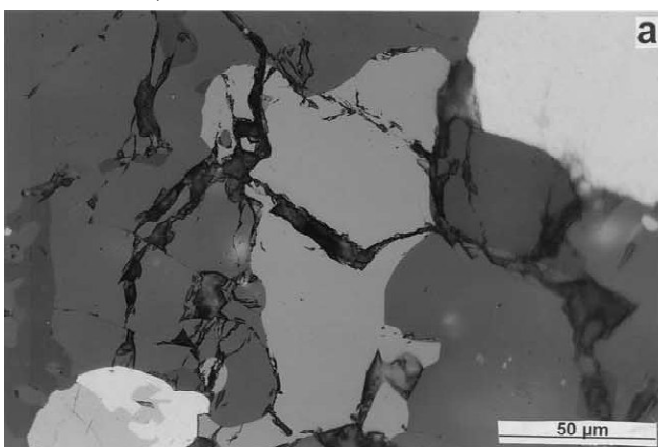


*Fig.1.2.5 – Variety 1. Unmelted chromite grain in Kernouvé (H6, S1), surrounded by silicate (dark grey) and adjacent to metallic Fe-Ni (white) and troilite (bottom left). (from Rubin, 2003)*

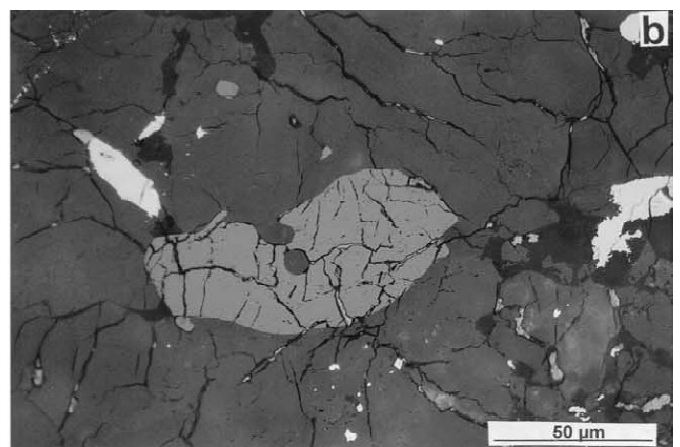


*Fig.1.2.6 – Variety 2. Unmelted, but fractured chromite grain (medium gray) in Jartai (L6, S4). Similar fractures (narrow black lines) occur in the surrounding silicate grains. (from Rubin, 2003)*

**Variety 2** – Unmelted, fractured chromite grains. Several ordinary chondrites with a shock degree ranging from weak to moderate display chromite grains which, though still unmelted, have been fractured or even crushed by impact processes (fig. 1.2.6). Adjacent silicates also display similar fractures.

**Variety 3** – Chromite grains transected by opaque veins. Albeit still unmelted, chromite grains of some ordinary chondrites are transected or incised by 1-10  $\mu\text{m}$ -thick veins of metallic Fe-Ni or troilite. Some of these chromites display an intergrowth of coarse grains of metallic Fe-Ni or troilite; others are surrounded by mafic silicates, themselves crossed by opaque veins (fig. 1.2.7, 1.2.8).

As a thumb rule, veins can occupy from 1% to 25% of the overall chromite volume.

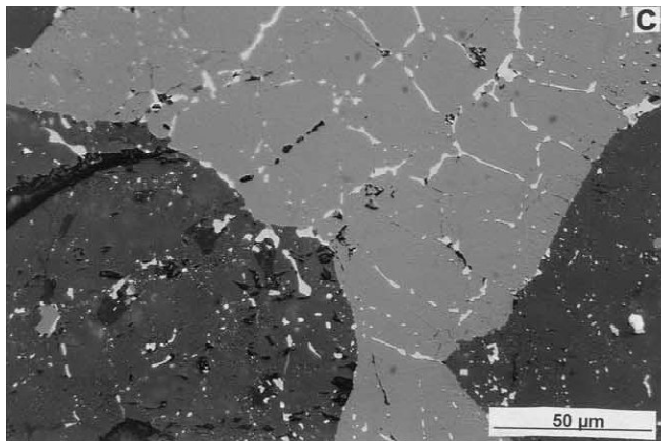


*Fig.1.2.7 – Variety 3. Unmelted chromite crossed by white thin troilite veins (Rose City, H-chondrite impact-melt breccia, S6). The troilite veins also occur in the surrounding silicate (from Rubin, 2003)*

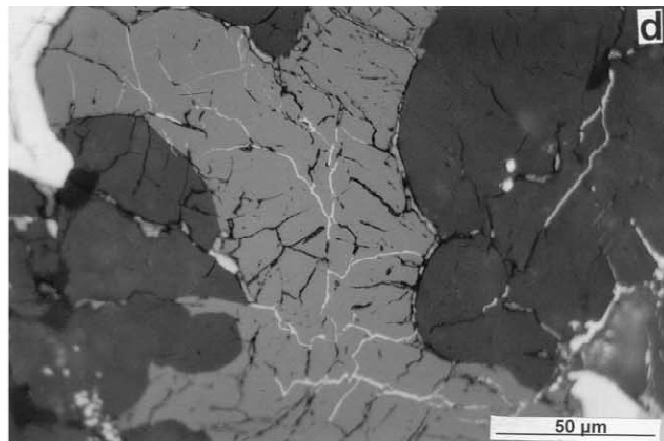


*Fig.1.2.8 – Variety 3. Unmelted chromite with very thin veins of troilite (white) (Jartai, L6-chondrite, S4). A few troilite veins also occur in the surrounding silicate (from Rubin, 2003)*

**Variety 4** – Chromite-plagioclase assemblages. Equilibrated, shocked ordinary chondrites exhibit features which have been termed ‘chromite-plagioclase assemblages’ by Rubin (and “clusters of chromite aggregates” by Ramdohr, 1967, 1973). Such features, which have been reported in many ordinary chondrites, vary widely in size, texture, grain size as well as chromite/plagioclase proportion (fig. 1.2.11). Usually 20-300  $\mu\text{m}$  across, they are formed by 0.2-20  $\mu\text{m}$ -size chromite grains (euhedral subhedral, anhedral or even rounded) surrounded by plagioclase; volume occupied by chromite grains ranges from 10% to 75% of the assemblages.

**Variety 5** – Chromite veinlets. Mafic silicate grains of many shocked ordinary chondrites are transected by irregular trails or veinlets of chromite needles and small rounded chromite blebs.

Typical thickness is 0.5-2  $\mu\text{m}$ , while length varies from ~10 to 300  $\mu\text{m}$ . Veinlets are often found

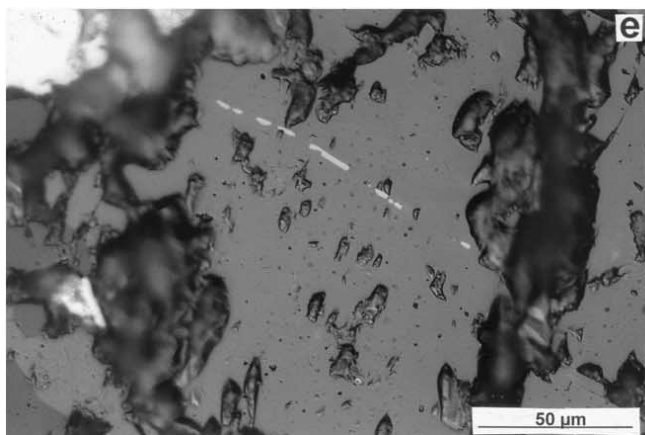


*Fig.1.2.9 – Variety 5. Chromite needles forming a veinlet transecting silicate grains in Portales Valley (H6-chondrite, S1). From Rubin, 2003*

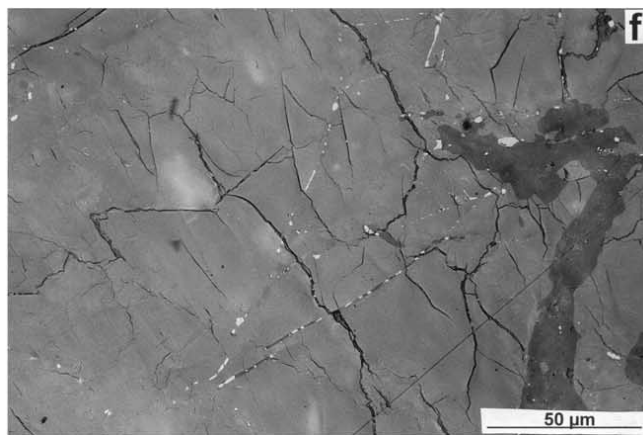


*Fig.1.2.10 – Variety 5. Chromite veinlets, some with glass of plagioclase composition (dark grey), within silicate grains in Jartai (L6-chondrite, S4). From Rubin, 2003*



near – i.e., within a few hundred micrometers – chromite-plagioclase assemblages.

Most veinlets consist only of chromite (fig. 1.2.9); a few also include plagioclase or glass of plagioclase composition (fig. 1.2.10).

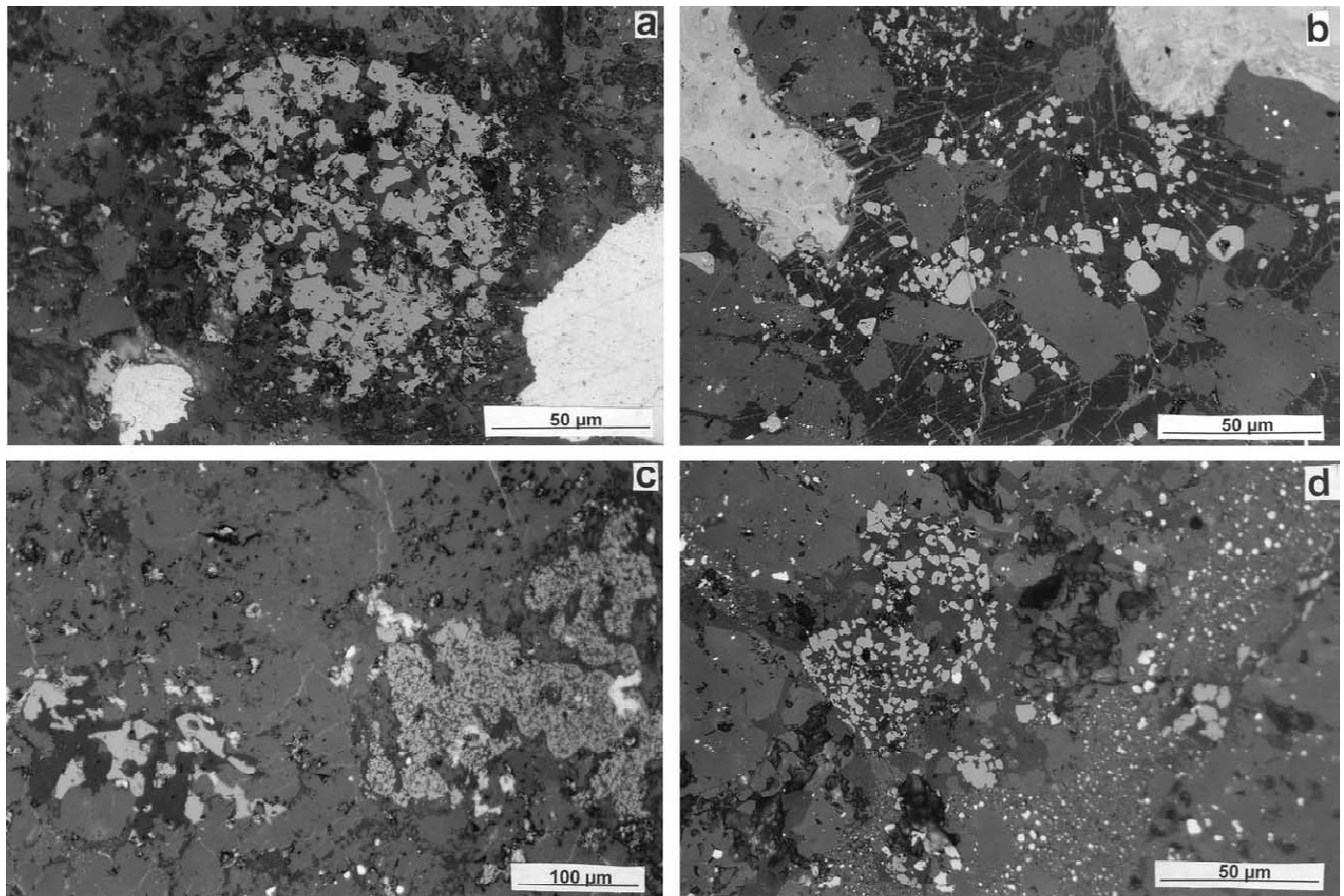


*Fig.1.2.11 – Chromite-plagioclase assemblages in ordinary chondrites. a) Round assemblage containing much more chromite than plagioclase (Rose City, H-chondrite impact-melt breccia). b) Situation reversed (Chico, L-chondrite impact breccia), with much more plagioclase than chromite in a network of interconnected assemblages; grey lines crossing the plagioclase are limonite veins. c) Fine-grained (right) and coarse-grained (left) assemblage (Hualapai Wash). They have very different plagioclase/chromite modal abundance ratios, i.e., 0.3 and 2, respectively. The coarse chromite grains may be unmelted grain fragments. (d) Medium-grained assemblage (left of center) near a thick silicate-rich shock vein (right of center) with numerous small Fe-Ni blebs (Farmington). All images in reflected light. From Rubin, 2003*

**Variety 6 – Chromite-rich chondrules.** Shocked, equilibrated ordinary chondrites (and regolith breccias) display rare chondrules consisting of silicate (85-95% in volume) – mainly olivine and plagioclase-normative mesostasis – and chromite (5-15% in volume) (fig. 1.2.12).

Such chondrules can have cryptocrystalline, radial, barred or porphyritic textures; they are known from literature as ‘chromite chondrules’ (Ramdohr, 1967) or ‘chromite-bearing silicate chondrules’ (Krot and Rubin, 1993). Krot and Rubin found 50 chromite-rich chondrules in 43 H, L and LL ordinary chondrites, as well as 17 chromite-rich chondrules in 10 solar gas-rich ordinary chondrite regolith breccias.

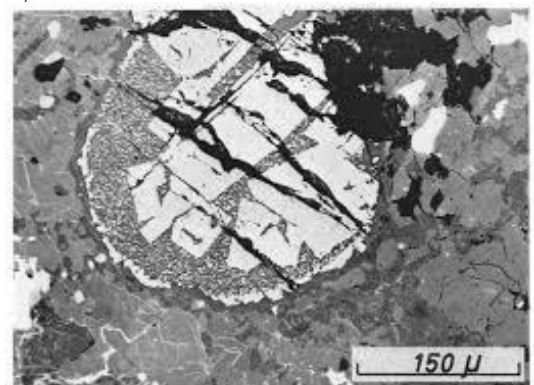


*Fig.1.2.12 – Chromite chondrule with plagioclase rim; intermediate zone with fine chromite dust and chromite crystals in the nucleus (Plainview meteorite). From Ramdohr, 1967*

### 1.3 – Fusion crusts

All meteoroids form a fusion crust while crossing Earth's atmosphere, as a by-product of the intense heating generated by their hypervelocity (tens of kilometers per second) interaction with air molecules. Details of the process are very poorly understood (to be optimistic), the outcome depending on the typology of meteoroid; the resulting crust is very thin – often less than 1 mm-thick, and also very prone to terrestrial alteration. Some examples are shown in the pictures below:

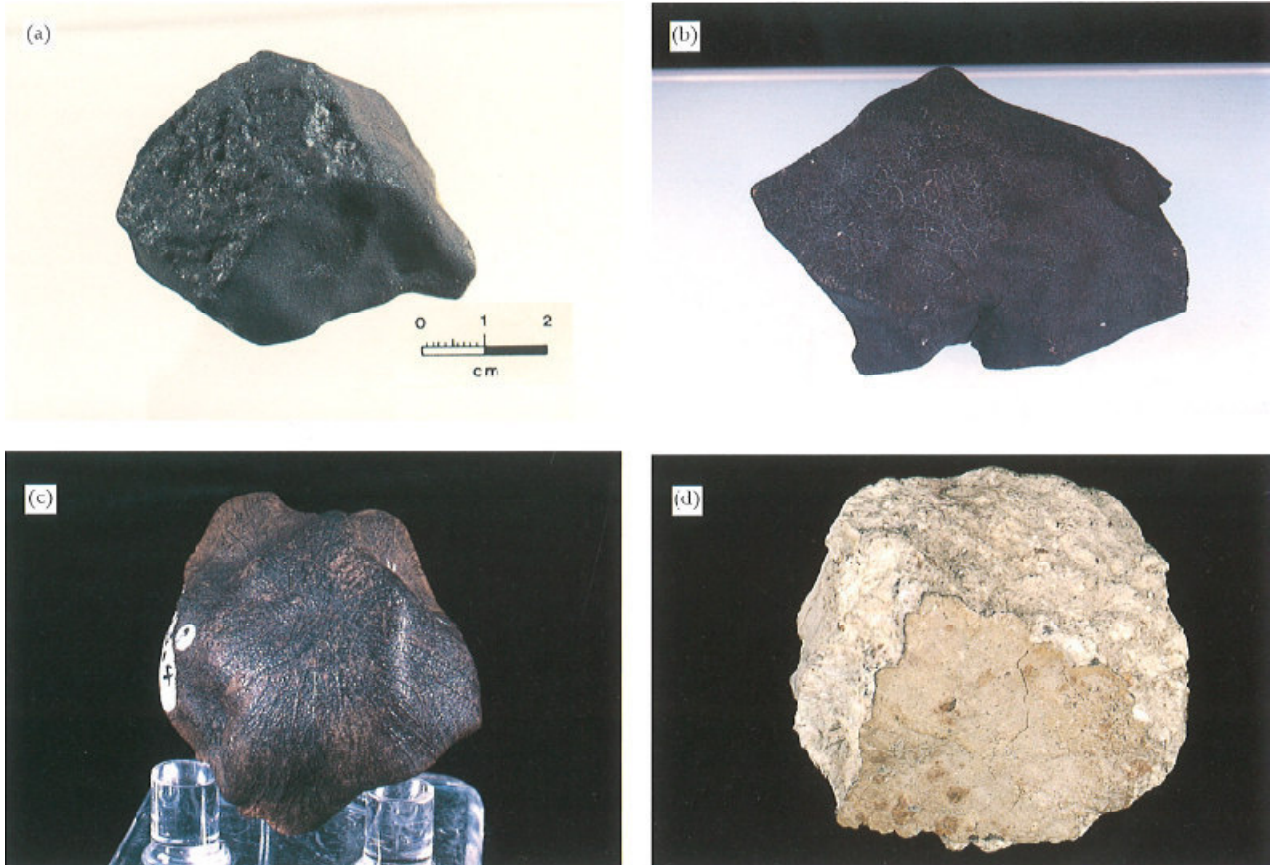


Fig. 1.3.1 – Examples of fusion crusts. (a) L6 ordinary chondrite (Kirchener) (b) CM2 carbonaceous chondrite (Murchison). This specimen is about 11.4 cm largest dimension (c) eucrite (Millbillillie). Horizontal dimension is approximately 35 mm (d) iron-poor achondrite (Norton County). The specimen is 102 mm largest dimension across the fusion crust area (from O. R. Norton, *The Cambridge Encyclopedia of Meteorites*, p. 54).

There are comparatively few studies available on the subject – especially upon outer fusion crusts, which are completely melted and form a continuous covering around the meteoroid; the most important contribute was perhaps Genge and Grady's (1999), from which we have taken most of the main ideas (and the data) illustrated in this paragraph.

On entering the atmosphere, the meteoroid is heated up by friction and starts melting its outer surface; drops of molten liquid slip away from the main body, in a process called *ablation*. No crust forms at this stage, while the trail becomes visible and sometimes can be very bright ( $M = -8$  or even brighter). Only later, when the would-be meteorite slows down and cools, the molten material solidifies and forms a coating on the meteoroid. Ablation stops and the path is no longer visible: so the *dark phase* of the atmospheric flight begins.

Iron meteorites have (almost) no silicate inclusions, so that the crust they form – up to 2 mm thick – has no glass. Its upper part is just oxidized iron, i.e. magnetite and wüstite, and beneath it there is a complex mixture of iron minerals with different melting points – in decreasing order, kamacite,



(usually be converted to martensite), taenite, troilite, schreibersite. Troilite is found as sub-spherical inclusions, frequently emptied by ablation and later refilled with recrystallized troilite – often with a coating of magnetite-wüstite; schreibersite is even more affected by ablation and can be melted away entirely.

The outer crust (~50 µm thick) is very fragile and can be altered and destroyed after some months of permanence in humid environment (leaving a rusty coating of limonite).

Stony meteorites develop a different type of crust. Chondrites are mainly composed of iron and magnesium silicates; Si and O are arranged in a tetrahedron-shaped structure, where Fe, Mg (and even other metals) can enter the configuration. When temperature reaches the melting point the crystalline structures vanish and all their elements become part of the melt, partially mixing with the elemental iron already present within the bulk. The crust forms when the meteoroid cools, during the dark phase; iron and magnesium silicates – olivine and the orthopyroxene called bronzite – form a light brown glass, whereas the elemental molten iron reacts with oxygen in the high-temperature environment, producing magnetite (black). Iron sulfide along with iron oxide enter the crust, whose final colour ranges from brown to black.

Most stony meteorites are composed of refractory material with a high melting point, which usually produces a black and porous fusion crust – occasionally displaying thicker zones resembling a foam of bubbles; often small silicate crystals, along with spinel (also chromite), Fe-Ni particles and iron sulfide are present.

The study of fusion crusts can shed light upon the processes taking place during the heating phase, as well as the nature of the material carried away during the ablation stage. In this sense, fusion crusts are regarded as a suitable analogue of melted micrometeorites, which continuously enter our atmosphere as extraterrestrial dust particles. Both species are thought to contain asteroid debris, and for this reason they are likely to share common precursor materials, mineralogies and compositions – which in the case of fusion crusts are the same as the meteoroid bulk's, whereas they still remain unknown for micrometeorites.

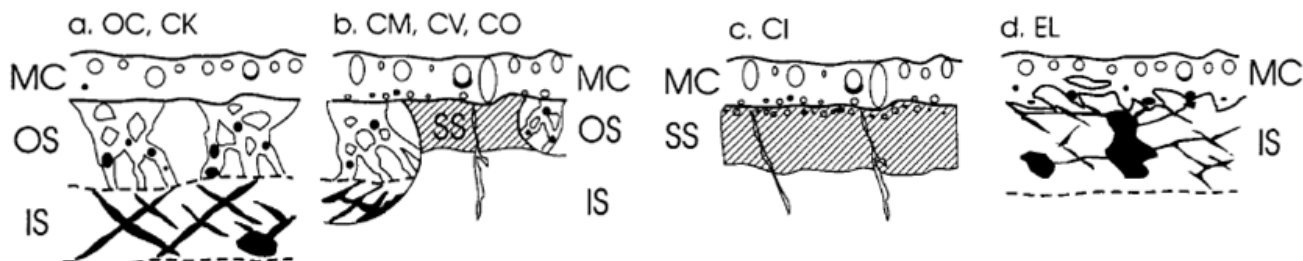


Fig. 1.3.2 – Fusion crust of chondritic meteorites. a) Ordinary and CK chondrites: an outer melted crust (MC) sits upon an outer substrate (OS) full of silicate glass veins with droplets of sulfide and metal, beneath which an inner substrate (IS) contain veins of sulfide and metal. b) CM, CV and CO chondrites show the same zones, even within individual chondrules. A sulfide-enriched substrate (SS) appears. c) In CI chondrites SS can expand into a layer beneath the MC d) Enstatite chondrites (EL) lack an OS with silicate glass. From Genge and Grady (1999).

Also related to fusion crusts are the so-called meteorite ablation spherules (MAS), which solidify from droplets of molten material separating from the meteoroid during the ablation phase. Distinct from melted micrometeorites (from which cosmic spherules form), they seem to be far less common (Love and Brownlee, 1993) and their mineralogical and compositional properties can be inferred – to some extent, at least – from those of the fusion crusts.

Fusion crust is not a single uniform layer; instead, it displays an outer zone and an inner region. Genge and Grady (1999) distinguish four different crustal zones in stony meteorites: 1) *quench* phases,

formed during cooling of the silicate melt 2) *refractory* phases, which didn't melt during heating and therefore are composed by relics 3) Fe-rich droplets crystallized from liquid metals 4) vesicles. The occurrence of these components varies with the meteorite typology. These zones deserve to be described in some detail.

1) *Porphyritic quench textures* characterize the melted crusts of chondritic meteorites, which display olivine phenocrysts (zoned, euhedral to subhedral), magnetite and wüstite in a glassy mesostasis

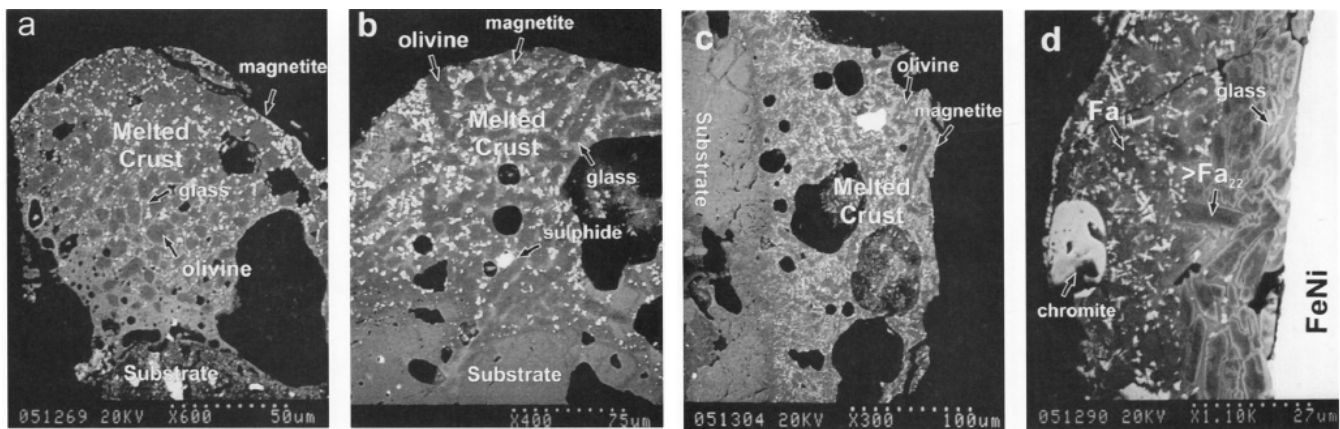


Fig. 1.3.3 – a) Orgueil (CO): porphyritic structure, with glassy mesostasis, zoned olivine and magnetite dendrites. b) Cherokee Springs (LL6): olivine in equant crystals or laths. c) ALH76001 (L6): magnetite in cruciform-like or lattice-like dendrites d) Alessandria (H): inner crust with metal nearby, no magnetite, fayalite-rich olivine (from Genge and Grady, 1999).

Olivines can vary widely in composition ( $\text{Fa}_{7-45}$ ) and can have high-Ni contents (up to 2% in weight), suggesting a crystallization process taking place in a relatively oxidising environment. Wüstite can be found in the innermost zone of the melted crusts, often forming the cores of the magnetite grains (Ramdohr (1967)), and the mesostasis of the melted crust is mainly Na- and Ca- bearing aluminosilicate glass.

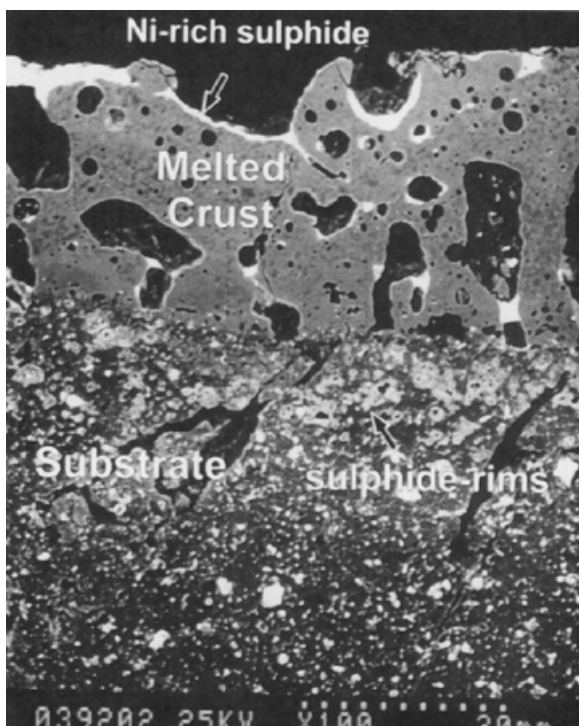


Fig. 1.3.4 – Sulfides in a melted crust (Alais, CI), are found as isolated droplets or menisci on vesicles. This sample lacks magnetite. From Genge and Grady, 1999.

As the meteorite group changes, so does its quench texture. The crusts of carbonaceous and enstatite chondrites are finer-grained and display less magnetite or wüstite; by contrast, no variation in olivine grain size or magnetite abundance has been observed in the crusts of ordinary chondrites – save for the case of H equilibrated chondrites, which often exhibit fayalite-rich olivine laths and lack magnetite/wüstite (fig. 1.3.3d).

Finally, achondrite fusion crusts have their own specific features; diogenites exhibit a porphyritic crust dominated by pyroxene, phenocrysts and a glassy mesostasis. Howardites, eucrites and ureilites have a fusion crust almost entirely consisting of glass.

2) Refractory phases are composed by unmelted grains left as relics in the melted crust. They are quite common in ordinary chondrites, with some differences.

Rounded grains of forsterite ( $\text{Fa} < 5\%$ , with overgrowths of more fayalitic olivine) and fractured enstatite grains ( $\text{Fs} < 5\%$ , rimmed by more ferrosilic pyroxene) are the most common relic grains in the melted crusts of carbonaceous chondrites; enstatite grains are also common occurrence in the melted crusts of enstatite chondrites, but only unequilibrated ordinary chondrites

exhibit them – whereas crusts of equilibrated chondrites display only relics of more Fe-rich olivine and pyroxene, with a composition similar to that of the original object. It's not unusual to find around these Fe-rich olivines complex reaction rims of Mg-rich olivine, iron oxide inclusions and silica-rich glass veins (*fig. 1.3.4*).

The sizes of iron oxide inclusions suggest growth by Ostwald ripening (dissolution of smaller features to form bigger ones – in this case, thermodynamically favoured); often the outermost layer is an overgrowth of Mg-rich olivine (Fa<sub>11</sub>). Forsterite grains, iron oxide and glass are common, and they may be relic olivines transformed by the reaction described above.

Other relic phases are more difficult to find; chromite can occur as relic grains in the melted crust of some carbonaceous and LL ordinary chondrites, often with rims of surrounding magnetite. The crusts of some ordinary chondrites also display albite.

Fusion crusts of achondrites seldom display relic grains; magnesiocromite grains are quite common in the crusts of diogenites.

3) Sulfide and metal are found in the melted crust of chondrites as subspherical droplets or menisci on vesicles, up to a few percent in volume (*fig. 1.3.4*). Sulfides – the most abundant chemical species – are usually Ni-rich (55-73% in weight), with a stoichiometry close to heazlewoodite (Ni<sub>3</sub>S<sub>2</sub>) and Fe replacing some Ni. Droplets with a higher Ni-content (74-83% in weight) display nonstoichiometric compositions and may result from the assemblage of sulfide and (high-Ni) metal.

The crusts of CI, CM2, ordinary and enstatite chondrites show a certain amount of pentlandite ((Fe,Ni)<sub>9</sub>S<sub>8</sub>, ~20 wt% Ni) and pyrrhotite (1-4 wt% Ni); sulfide droplets in enstatite chondrites display a trend of (roughly) increasing Ni content across the melted crust going towards the surface.

Metal blebs are less frequently observed than sulfides, and are usually Ni-rich.

4) Vesicles are most common in the melted crusts of carbonaceous chondrites (CC) and eucrites, summing up to ~50% of the overall crust volume. Two distinct morphologies are present in CCs: a) subspherical vesicles dispersed within the melted crust, with the smaller ones (<10 µm) concentrated at the bottom, and b) large, irregular or elongated vesicles, more or less aligned – either parallel or perpendicular to the boundary between substrate and crust. This last feature hints at formation by degassing from the substrate.

Among meteorites, ordinary chondrites display the most developed substrate, which forms two zones – approximately, the same as those classified by Ramdohr (1967):

Zone a: it's an outer substrate, characterised by irregular veins of ferromagnesian aluminosilicate glass containing embayed olivine and pyroxene relics (*fig. 1.3.6b*).

In equilibrated ordinary chondrites, sulfide and metal grains are found as sub-spherical droplets or large,

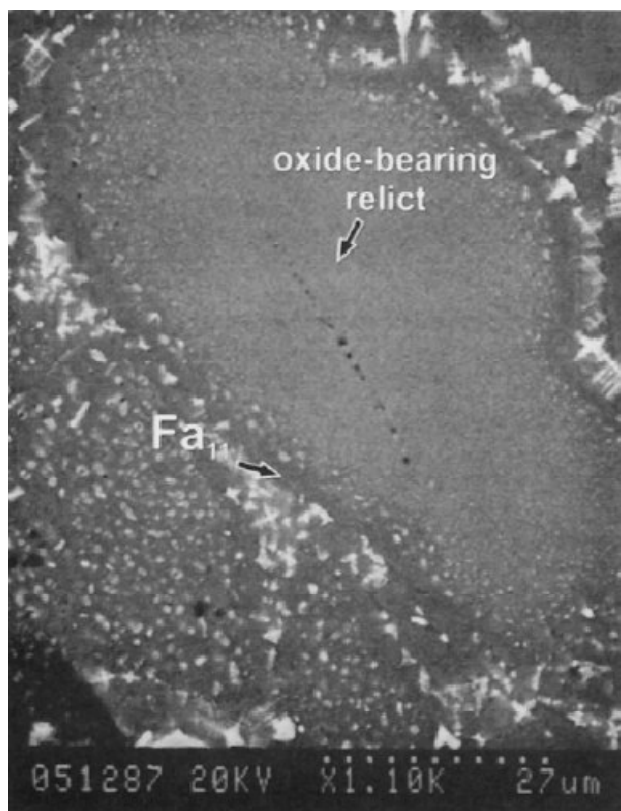


*Fig.1.3.5* – An unmelted Fe-rich olivine in Allegan (H5) shows many µm-sized Fe-oxide inclusions in Fe-poor olivine and a silica-rich phase (glass?). The size of Fe-oxide inclusions increases towards the margins of relics as abundances decrease. The outer layer is often an oxide-free overgrowth of Fe-poor olivine (~ Fa<sub>11</sub>). From Genge and Grady,(1999).

rounded concentrations within the silicate melt veins; they form interconnected networks in the outer substrate of H chondrites. Metal-rich areas usually display metal and sulfide together – a likely result of coexistence between immiscible liquids within the surrounding silicate melt (*fig. 1.3.6c*). Assemblages of Fe-Ni metal and sulfide are frequently found in H and L chondrites; though their composition varies, they are usually Ni-rich compared to the sulfide nearby. The general trend is of Ni enrichment for smaller droplets, also when moving towards the external part of the meteorite.

In LL chondrites, assemblages of sulfide and Fe-Cr oxide are common occurrence in the outer substrate; their textures suggest that these two-phase features formed as coexisting liquids (*fig. 1.3.6a*). Oxide composition shows a higher Cr content (35-41 wt%) compared to Ni, with Mg (1-2 wt%) and Al (2-3.5 wt%) also present. Oxides may even occur as isolated subspherical droplets in the substrate as well as in the melted crust.

The outer substrates of enstatite chondrites are far less developed than those of ordinary chondrites; a likely explanation is that the abundance of enstatite in the bulk of meteorite prevents general silicate melting.

Zone b: it's an inner substrate, featuring metal and sulfide interconnected veins (*fig. 1.3.6a*), especially in the H chondrites; they may be the result of formation by melting of pre-existing phases.

The stoichiometry of sulfides is similar to troilite (FeS) and pentlandite, with less than 5 wt% Ni; occasionally, Ni-poor sulfides stoichiometrically similar to heazlewoodite (albeit poorer in Fe-Ni) are observed. They may consist of crypto-crystalline mixtures of metal and pentlandite.

The inner substrate commonly shows two-phase assemblages of Fe-Ni and sulfide, which probably formed (as in the outer substrate) as non-miscible liquids.

a) In carbonaceous chondrites (Genge and Grady, 1999 – with data on 14 meteorites), with the sole exception of CK (Karoonda), proper inner/outer substrates can only be found within individual chondrules in proximity of the melted crust. In the matrix, the substrate consists of a sulfide-rich layer, even more enriched in S near the vesicles (*fig. 1.3.6d*). A likely cause for such trend is the reaction between matrix and a S-rich gas generated by devolatilization processes. The enriched matrix may undergo partial melting near the melted crust, thereby forming sulfide droplets.

The composition of melted crusts shares many similarities with those of the bulk meteorite (*fig. 1.3.7*), even though they show high depletion in S (suggesting loss after degassing – Greshake et al., 1998; Genge et al., 1997) and also, in many cases, depletions in Fe/Si and Ni/Si ratio relative to whole rock, as a result of loss of siderophile elements during the heating phase.

Other departures from whole rock composition depend on the meteorite type.

a) For carbonaceous chondrites (Genge and Grady, 1999 – data on 4 meteorites) the melted crusts display overall Mg/Si, Cr/Si and Mn/Si ratios similar to bulk composition, suggesting that they have undergone little fractionation during their flight through the atmosphere. However, the higher absolute abundance of these elements (and other non-volatiles) with respect to the bulk may be attributed to a loss of volatiles (C, H and S, for instance) by degassing. Such loss matches the volatile content of the bulk meteorite, so that they are largest for the CI group.

b) Melted crusts of enstatite chondrites (Genge and Grady, 1999 – data on 4 meteorites) show larger values of Cr/Si (1.4-3.3 times), Mn/Si (1.8-3.3 times), Ti/Si (2.1 times) and Ca/Si (1.8 times) ratios with respect to the bulk meteorite. If Ca/Si ratios lie within the range of ordinary chondrites, Cr/Si and Mn/Si are higher than in any other meteorite group. Fe-sulfides at the base of melted crust display traces of Cr, Mn, Ti and Ni, whereas those within the crust only display Ni; therefore, it may be inferred that Cr, Mn and Ti can easily migrate from sulfides to the silicate melt. The observed enrichments, then, may result from the reaction of sulfides (originally in the substrate) with the liquid silicate forming the melted crust.



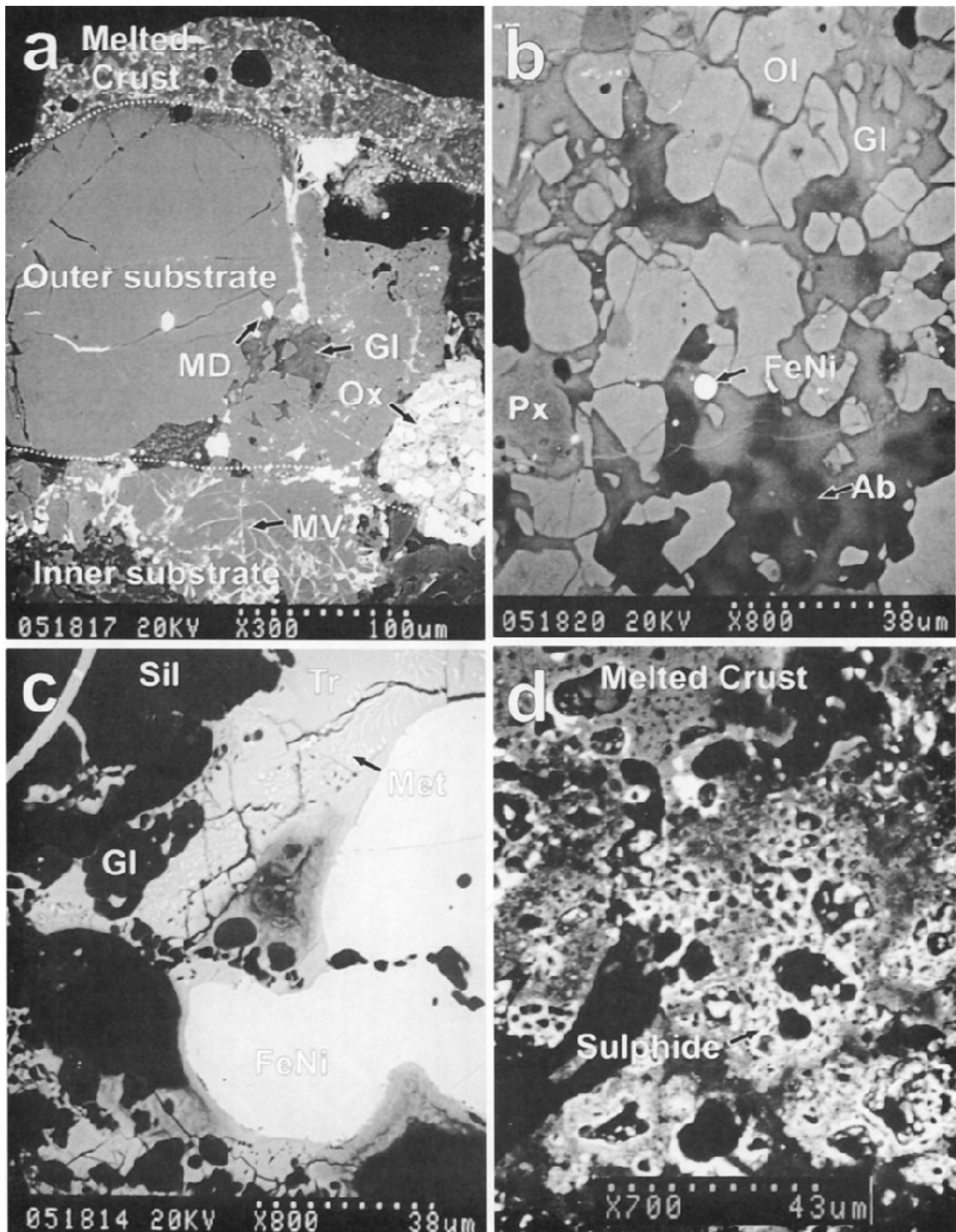


*Fig. 1.3.6 – Partially melted substrates of chondrites. (a) Olivenza (LL5). The inner substrate shows veins of metal and sulfide (MV) but also droplets of metal-sulfide (MD) or sulfide-oxide (Ox). The outer substrate displays irregular veins of ferromagnesian glass (GI), formed by partial melting. Metal and sulfide are less common than in the inner substrate and mainly occur as isolated droplets. The silicate partial melt is compositionally heterogeneous, showing in (b) Tuxtuac (LL5) embayed and rounded olivine and pyroxene relics and partially melted albite. With increased melting, albite enters the liquid, producing Na- and Al-rich zones. Outer substrate may also have two-phase, Fe-rich assemblages that formed as coexisting immiscible liquids. In (c) Borkut (L5), droplets of metal and sulfide include droplets of silicate liquid preserved as glass. Sulfides have also Ni-rich metal. The substrate of carbonaceous chondrites is similar to the ordinary ones within individual chondrules. In matrix, a sulfide-enriched layer is developed, and sulfide-enrichment occurs adjacent to vesicles, as in (d) Alais). From Genge and Grady (1999).*

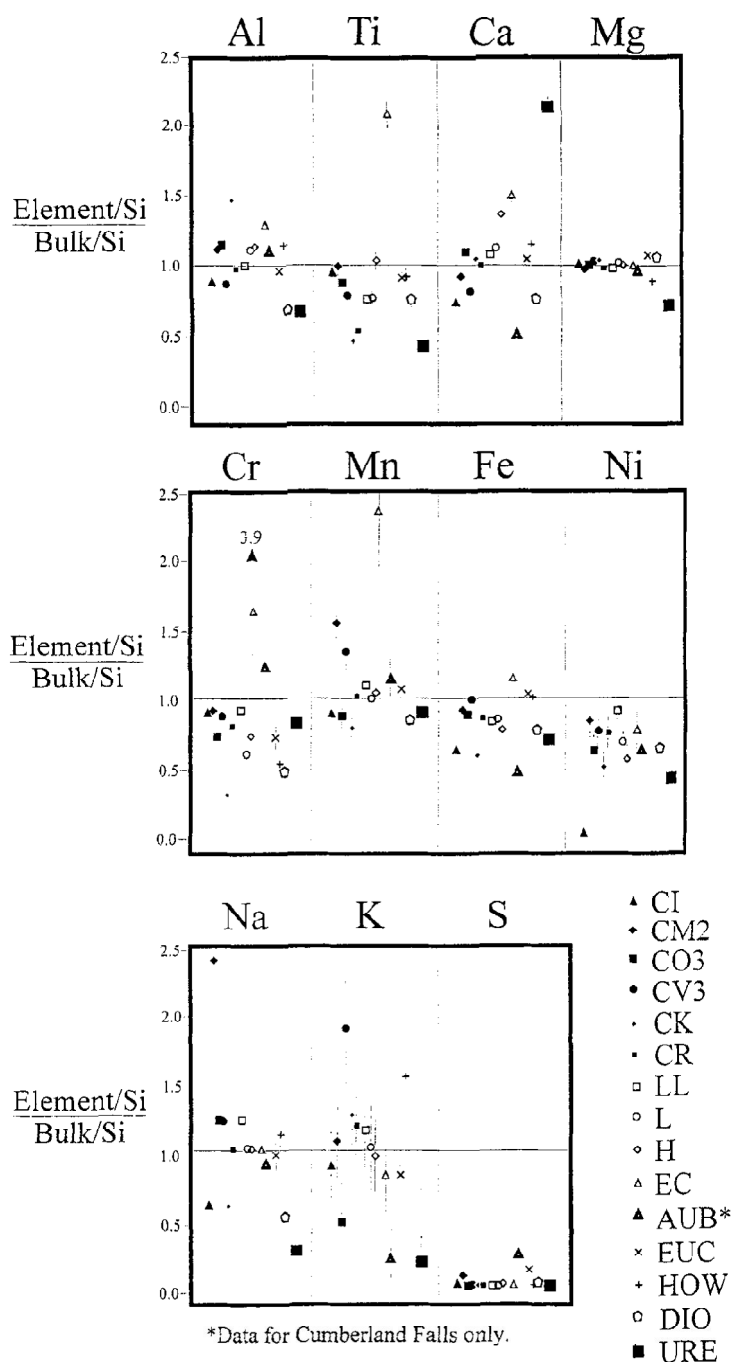


Fig.1.3.7 – Compositions of melted crusts, calculated as fractions of the Si abundance (in wt%) and normalized to those of bulk meteorite. The horizontal line marks bulk meteorite values. From Genge and Grady, 1999.

report data only about two samples. Both melted crusts have similar composition, which in both cases differs from the meteorite bulk: crusts are depleted in Mg/Si (55%-86% of the bulk) and Fe/Si (55%-85% of the bulk) ratios, but enriched in Ca/Si ratio (from 1.93 to 2.37 times the bulk abundance). Depletions may be at least partly explained with separation of metal and/or sulfide liquids formed by melting of original metallic phases; however, variations in Ca/Si e Mg/Si still lack a clear interpretation.

d) Ordinary chondrites of all groups (H-L-LL) consistently show divergence in composition between melted crust and bulk meteorite; therefore, they may have undergone similar heating processes during their atmospheric flight. Mg/Si ratios for these meteorites display a large variability range; they

Small depletions relative to bulk meteorite observed for Na/Si and K/Si can instead be attributed to evaporation.

c) The situation for achondrites (data on 13 meteorites – from Genge and Grady, 1999) is mixed. Unlike enstatite chondrites, Fe-sulfides containing Cr and Mn are not easily incorporated into the melted crust of enstatite achondrites; actually, Mg/Si, Fe/Si and Ca/Si ratios are lower when compared with their bulk values (94%, 46% and 51% of the bulk meteorite ratios, respectively). Small depletions for Mg/Si can be accounted for by incomplete melting of silicate phases, whereas reductions in Fe/Si and Ca/Si ratios may be the outcome of the loss of metal liquids and Ca-bearing Fe-sulfides.

Basaltic achondrites show a large variability in crust composition with the meteorite type. Values for crust and bulk meteorite are the same in eucrites, within analytical error – suggesting little or no element fractionation. Howardites and diogenites display significant variations between crust and bulk – however, similarities between individual meteorites are difficult to find, and uncertainties in bulk compositions don't make things any easier. All diogenite crust are poorer in Cr/Si (35%-67% of bulk values), possibly because of an incomplete melting of magnesiochromite; howardite crusts show Si and Fe abundances similar to bulk values, but they are poorer in Mg/Si (75%-94% of the bulk) and Cr/Si (38%-73% of the bulk). All other differences are less significant because of the heterogeneity of this group.

For ureilites, Genge and Grady (1999)

are generally (slightly) lower for the melted crusts compared to bulk meteorite, and similar to carbonaceous and enstatite chondrites (ordinary can be distinguished by carbonaceous by their lower Al/Si ratio); by contrast, the melted crusts of a few samples exhibit a large increase in Mg/Si over whole-rock composition. However, these crusts also show the highest abundance of olivine relics (Allegan is one example); this surely is a source of bias for compositional data.

Those meteorites depleted in Mg/Si also display higher values in Na/Si, Ca/Si and Al/Si over bulk meteorite. This suggests contamination by a feldspathic source, but relic feldspars are too scarce to account for the contamination; silicate partial melts (present as glass veins in the outer substrate) may represent a possible explanation, with their higher ratios of Na/Si, Ca/Si and Al/Si (and lower Mg/Si) (fig. 1.3.9).

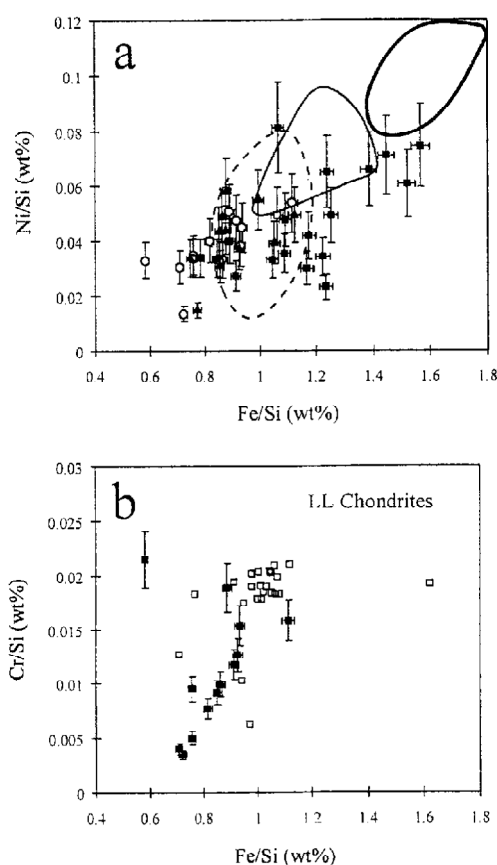
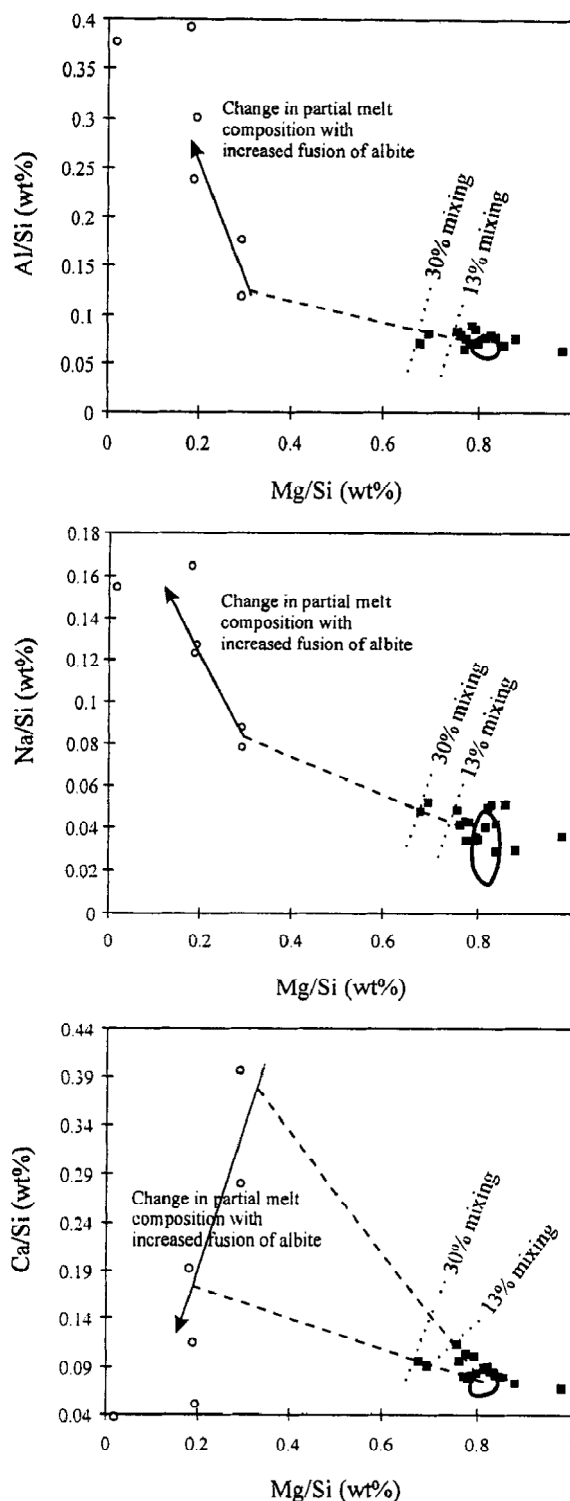


Fig. 1.3.8. (a) The Ni/Si and Fe/Si abundances of H, L, and LL group fusion crusts (solid squares = H, solid triangles = L, open circles = LL) and bulk meteorite (bold outline = H, solid outline = L, dashed outline = LL; data are derived from Jarosewich, 1990). (b) The Cr/Si and Fe/Si abundances for LL group; open symbols represent bulk meteorite data. From Genge and Grady, 1999.

Fig. 1.3.9. Variations in the Na/Si, Al/Si, Ca/Si and Mg/Si ratios of H-group ordinary chondrite fusion crusts. Some fusion crusts (solid symbols) show small enrichments in Na/Si, Ca/Si and Al/Si relative to bulk ordinary chondrite with decreasing Mg/Si. These can be explained by mixing between substrate partial melts (shown as open symbols) and a fusion crust melt of bulk meteorite composition (shown by the field outlined in bold). Most H-chondrites require <13% (by mass) partial melt to explain enrichments; however, some require up to 30%. The Mg/Si enriched crusts generally have abundant olivine relics. The substrate partial melt becomes locally enriched in Na, Al, and Ca by partial melting of albite (shown as the solid arrow). From Genge and Grady, 1999.



Melted crusts of ordinary chondrites generally contain lower abundances of Fe and Ni than whole-rock; the presence in crusts of sulfide and metal droplets suggests losses through separation of Fe-Ni immiscible liquids, and correlations in Ni/Si and Fe/Si ratios shows that Fe and Ni losses took place in all ordinary chondrites.

The data from Genge and Grady indicate that the separating liquids had average Ni/Fe ratios  $\sim 0.04$  (fig. 1.3.8a) – which is consistently less than sulfide droplets found within the melted crust ( $\sim 5.2$ ), but still within the range of droplets present in the outer substrate.

Depletions in Cr/Si aren't correlated with Ni/Si and Fe/Si, except in the crusts of the LL group (fig. 1.3.8b); the presence of Cr-rich and Fe-oxide liquids suggests losses occurring from their separation. Melted crusts of ordinary chondrites show unequal depletion in siderophile elements over whole-rock, which results in a general overlapping for all ordinary chondrites in crust composition (though only H chondrites display Fe/Si ratios higher than 1.1 for their crusts). It can thus be said that melted crusts of ordinary chondrites are chemically quite homogeneous.

During its passage through the atmosphere the meteoroid undergoes several processes that create its fusion crusts: (1) the separation and reaction of molten droplets (Fe-rich sulfides, metals or oxides), (2) the reaction with atmospheric oxygen, (3) the mixing occurring between partial melts from the substrate with bulk melted crust liquid, (4) the loss of volatile elements by evaporation and/or degassing.

(1) *Separation and reaction of Fe-rich liquids.* Metal, sulfide, Fe- and Cr- oxides are immiscible with the silicate partial melt generated during the heating of the meteoroid, so they must have crystallised independently. In the inner substrate (where no silicate melt existed), the same species are found in composite, interconnected veins, and their abundance is generally higher; they likely result from the melting of preexisting minerals, which afterwards became part of the silicate partial liquids. Sulfide and metal together should have formed as immiscible liquids – probably in non-equilibrium conditions (Naldrett, 1969).

Melted crusts of ordinary chondrites are generally depleted in siderophile and chalcophile elements with respect to bulk meteorite, though enriched relative to the silicate fraction of the unmelted rock; this means that metallic components must have dissolved into the silicate melt, at least in part. This proportion varies accordingly to the metal abundance in bulk meteorite ( $\text{Fe}^0/\text{Fe}_{\text{tot}}$ , for instance); it increases for LL-group with metal content, whereas the opposite holds for H-chondrites as shown in figure 1.3.10.

For  $\text{Fe}^0/\text{Fe}_{\text{TOT}} \sim 0.25$ , the Fe abundance of the melted crust matches that of the bulk meteorite, which implies a dissolution of most of the metallic component into the silicate melt. The dissolution of Fe-metal liquids into silicate melts requires the oxidation of  $\text{Fe}^0$  to  $\text{Fe}^{2+}$ , which in turn depends on the O fugacity  $f\text{O}_2$ .

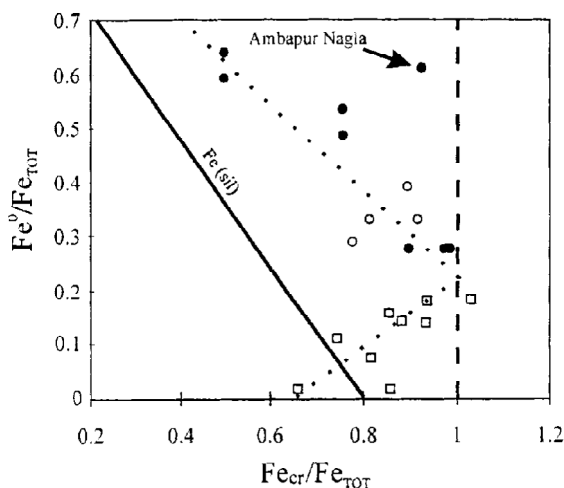


Fig.1.3.10. Abundance in Fe of the silicate portion of fusion crust compared to the metal content of the bulk meteorite (both normalized to total bulk Fe). The dashed line to the right gives the expected composition of melted crust if all metallic Fe dissolved in the silicate liquid. The bold line ( $\text{Fe}_{\text{SIL}}$ ) is the composition expected when no exchange of Fe occurs between metal and silicate liquids. The LL chondrites (open squares) are roughly positively correlated; the L chondrites (open circles) lie close to the maxima in crust Fe content (normalized to bulk Fe). Finally, the H-chondrites (solid circles) are depleted in normalized crust Fe content relative to bulk metal content. Values lying below  $\text{Fe}_{\text{SIL}}$  indicate a loss of Fe-oxide liquid. From Genge and Grady, 1999.

The partitioning of Fe from sulfide to silicate liquids also increases with  $fO_2$ , but for sulfide melts Fe is already present in a divalent state (e.g., Peach and Mathez, 1993), so that, whatever the value of  $fO_2$  sulfide liquids will partition more Fe into the silicate melt than Fe metal liquids. This means that the higher Fe-content of LL-chondrite crusts (which has the same trend of increasing metal content of the bulk meteorite) may imply increases in the metal/sulfide ratio.

On the other hand, decreases in Fe content for the melted crusts of H chondrites with respect to bulk meteorite with increasing whole-rock metal abundance are probably caused by larger-sized metal blebs in the fusion crust; larger metal bodies are less likely to equilibrate with the coexisting silicate liquid than smaller droplets. Moreover, redox reactions will affect the Ni-content of metallic liquids; Ni is harder to oxidize than Fe, which means it will preferably stay in the metallic melt during the oxidation process.

The observed increases of Ni (metal and sulfide) in ordinary and enstatite chondrite fusion crusts when moving from inner substrate to the outer margin of the melted crust seem thus generated by increasing oxidation; the reactions probably lead to the capture of some atmospheric oxygen. The same oxidation process may help explain the loss of Cr and Mn from sulfide melt coming from the substrate of enstatite chondrites, as well as the enrichment in the same elements (relative to whole rock) of their melted crusts.

Variations of Ni content of metallic droplets (i.e., the smaller ones display a higher Ni abundance) suggest that kinetic mechanisms must be operating on the partitioning process; small droplets would easier equilibrate with the surrounding silicate melt.

There is enough evidence that metallic liquids react with the silicate liquid – at least to some extent; however, most chondrites show in their melted crusts lower Fe and Ni abundances with respect to the bulk meteorite, while at the same time the occurrence of sulfide and metal droplets within the melted crust can't account (with only some exceptions) for the depletion observed in the silicate melt. Therefore, metals must have escaped from the crust and got lost; the observation that metallic droplets within the melted crust are frequently observed as menisci on vesicles suggests a possible separation process. Vesicles could have migrated toward the outer surface carrying metal with them, which could have been dragged away by ablation.

(2) *Reaction with atmospheric O.* Atmospheric oxygen can enter the crust by reacting with the silicate melt. While the similarity between the melted crusts of carbonaceous and enstatite chondrites is evident, with both olivine crystal size and magnetite abundance decreasing from the outside to the substrate boundary (which often leaves no magnetite near the substrate), ordinary chondrites, on the other hand, show little or no variation across their melted crusts.

The aforementioned increase of Ni content observed in the sulfide droplets when moving from the outer surface inwards suggests a corresponding  $fO_2$  decrease along the same path – which in turn tends to inhibit magnetite formation. The same holds for the growth of olivine crystals.

Since enstatite chondrites are highly reduced, an increase in  $fO_2$  when moving outward would be the natural outcome of atmospheric oxygen being incorporated in the silicate melt. In a similar way could be explained the lack of variation in olivine size and magnetite abundance observed in ordinary chondrites – which, being more oxidized than enstatite ones, are expected to show little variation in  $fO_2$  across their crusts (see for instance, Rubin *et al.*, 1988). By contrast, the behaviour of carbonaceous chondrites doesn't fit the same line of reasoning, for they are even more oxidized than ordinary chondrites but show a clear decrease in olivine crystal size and magnetite abundance across their melted crusts; however, reduction could arise via thermal decomposition (pyrolysis) of carbonaceous materials in the substrate, changing the  $fO_2$  value across the crust.

Even though  $fO_2$  shows little change across ordinary chondrite melted crusts, both the common occurrence of magnetite and the high Ni content of their olivine signal a higher oxidation degree with respect to bulk meteorite; however, the crusts of H chondrites may have experienced localized reduction, as testified by the presence of regions lacking magnetite and featuring Fe-rich, Ni-poor olivines. They are always in proximity of large concentrations of metal – suggesting that the reduction of the silicate melt and the oxidation of the metallic liquid may have taken place at the same time.

The presence of reduced region in H-chondrite crusts is a natural consequence of the unequilibrated nature of fusion crusts.

(3) *Partial melting of the substrate and mixing with the melted crust.* Some ordinary chondrites exhibit crusts enriched in Na/Si, Ca/Si, Al/Si, and depleted in Mg/Si relative to bulk meteorite; this can be the result of some feldspar incorporated into the melt. Evidence of mixing between partial melts from the substrate and the liquids of the melted crust are the Na-, Ca-, and Al-rich silicate glasses found in the outer substrate of ordinary chondrites, and extending well into the melted crust; this process can account for the observed enrichments.

Mixing processes of melts as the one described above have another interesting consequence; they enrich the melted crust in alkali metals, which otherwise would get depleted due to their high volatility.

The Na- and Al-enriching source may well be albite, whereas for Ca the situation is far less clear – mainly because of the higher melting temperature of most Ca-bearing minerals found in ordinary chondrites.

An alternative explanation for the divergences in composition between crust and whole-rock may be the partial (instead of bulk) melting; while this may have actually happened in crusts of CV3 chondrites (because of the observed depletion in Calcium-Aluminium Inclusions – or CAIs – components in their crusts), bulk melting of the outer melted crust is considered more likely, because with increasing abundance of relic silicates, the compositions diverge due to incorporation of solid fragments into the bulk-meteorite melt.

(4) *Loss of Volatile Components by Evaporation and Degassing* – A natural consequence of this process is the abundance increase of the nonvolatile elements. There exists a broad correlation with the abundance of carbonaceous materials within the bulk meteorite. Degassing of carbonaceous components and water, which occurs at temperatures lower than 700°C (see, for instance, Greshake *et al.*, 1998), is the likely source of the gas phase forming vesicles in the carbonaceous chondrites.

Another element present in the gas phase must be sulfur, as indicated by the deposition of sulfides around vesicles in the substrates of these chondrites; other volatile-rich minerals, such as carbonates and sulfates, are likely to dissociate because of the heating. The de-volatilization of carbonates, perhaps also of sulfates, is the simplest way to account for Ca/Si depletion in the melted crusts of C1 and CM2 chondrites – though Ca loss could only take place by removing solid CaO through CO<sub>2</sub> escape; this is possible, but very difficult to assess.

High temperatures of the silicate melt are expected to favour the evaporation of volatiles, though Na and K losses may be reversed in those crusts which undergo enrichments via the mixing processes described in (3) – or at least hampered by a vapour shell generated over the meteoroid surface (see, for instance, the book by Bronshten, *Physics of Meteoric Phenomena*, 1983).

In the wake of Genge and Grady's work, we must devote the last part of this paragraph to a discussion of the Meteorite Ablation Spheres (MAS); this term indicates melt droplets removed from the meteoroid by ablation during atmospheric flight. Droplets leaving the meteoroid in the last few seconds of its luminous path should have the same composition as the melt which cooled and formed the crust. These droplets could be the MAS generated at low altitude, which abound on the surface of Earth, at

least in specific areas (Taylor *et al.*, 1998); however, they must be safely distinguished from the so-called *cosmic spherules*, formed by the melting of extraterrestrial dust particles arriving on Earth. The overall composition of these objects points to the C-type (and also S-type) asteroids as their primary origin, with a minor fraction showing a non-chondritic elemental composition (Brownlee *et al.*, 1997); finally, a minor fraction of the spherules are melt products of precursor particles that did not have chondritic elemental composition.

Aerodynamic melting of small meteoroids (mm-sized, or less) takes place when the power dissipated by atmospheric friction exceeds the power thermally radiated by the object when it reaches its melting temperature; the physics of this process, though complex, is simplified by the small thermal inertia of these objects – which, being small, do not form gas shells during their passage in atmosphere (Öpik, 1958), further simplifying their study. In the following discussion we refer to the work of Brownlee *et al.* (1983).

The velocity required to heat a small meteoroid to a temperature  $T$  in a gas of density  $\rho$  can be expressed by the equation (in cgs units):

$$v = \left( \frac{8 \varepsilon \sigma}{\rho} \right)^{1/3} T^{4/3},$$

where  $\varepsilon$  is the emissivity and  $\sigma$  the Stefan-Boltzmann constant. Chondritic materials have melting temperatures around 1300 °C, so that the critical velocity  $v_c$  for melting (this time expressed in km/s) becomes:

$$v_c = 1.41 \cdot 10^{-2} \left( \frac{\varepsilon}{\rho} \right)^{1/3}$$

Typical values for Earth's atmosphere are 0.6 km/s (at 32 km altitude) and 9.4 km/s (at 90 km altitude), which are well within the range of extraterrestrial objects arriving on Earth. Meteoroid melting typically occurs at altitudes below 100 km, at pressures of  $10^{-6}$  atm or more. It's interesting to remark that – for a suitable range of velocities and entry angles – aerodynamic atmospheric melting can convert irregularly-shaped, mm-sized particles into spherules, and the process can be very effective (Brownlee *et al.*, 1983).

Cosmic spherules are routinely classified by composition into three general types: S (stony), I (iron), and FSN (iron-sulfur-nickel), with the S-type dominating the overall terrestrial influx.

An effective way to identify MAS is determining their isotopic ratio  $Al^{26}/Be^{10}$ ; these trace nuclides are (almost exclusively) produced by cosmic-ray-induced nuclear reactions, at a fairly constant rate with time. Production only occurs at the surface, for cosmic rays cannot penetrate deep into rock; therefore, MAS, formerly part of a larger meteoroid, must have been less exposed to cosmic rays than cosmic spherules (Harvey *et al.*, 1988).

Unfortunately, isotopic analyses are destructive and difficult to perform over large numbers of particles; it would be thus very useful to pinpoint reliable criteria – mineralogical, textural or chemical – for comparing the characteristics of cosmic spherules with those of the melted crusts of stony meteorites, helping identify MAS. Also, possible differences between MAS and melted crusts cannot be overlooked.

Cosmic spherules and melted crusts are both porphyritic – and either characterised by olivine phenocrysts and magnetite dendrites (like chondrites fusion crusts), or simply glassy (like most achondrites). To a closer look, however, olivine dendrites are seldom found in melted crusts, whereas many cosmic spherules display barred dendritic olivine (*barred-olivine spherules* in Blanchard *et al.*, 1978); pyroxene phenocrysts haven't been found in cosmic spherules, but they are present in diogenite crusts. The much faster cooling of cosmic spherules – which is due to their much higher surface

area/mass ratio when compared to that of typical meteoroids – is what prevents pyroxene crystallization (see, for instance, Taylor and Brownlee, 1991), at the same time favouring the formation of barred olivines. Since MAS likely crystallize after leaving their meteoroids, their cooling rate should be similar to that of cosmic spherules – and the same should hold for their mineralogy and morphology. However, low-altitude MAS (along with their parent meteoroids) might have been exposed to much higher  $fO_2$  values during heating with respect to cosmic spherules, which form at high altitude (Love and Brownlee, 1991) from liquids probably more reduced by the pyrolysis processes earlier described for the carbonaceous materials present in the original dust particles (see, for instance, Brownlee *et al.*, 1983; Genge and Grady, 1998), which in turn meant lower  $fO_2$  values. Consequently, olivines and magnetites contained in MAS and melted crusts might be recognized by their higher Ni content which, on the other hand, would be generally negligible for their counterparts in cosmic spherules.

Other minerals which are likely typical of MAS (because they are also common in melted crusts) are high-Ni sulfides like heazlewoodite. These minerals form from the oxidation of the sulfide melt leading to Fe loss, but lower values of  $fO_2$  inhibit this process in cosmic spherules, so that the only high-Ni sulfides eventually found there will be unmelted relics.

In general, melted crusts differ from the silicate-dominated cosmic spherules in three main crucial aspects, which should also identify MAS.

(I) The composition of melted crusts is very similar to that of bulk meteorites – whereas cosmic spherules display a much larger variety.

(II) Melted crusts exhibit higher Na, K and S abundances than S-type cosmic spherules – probably because of less evaporation and more enrichment (by melt mixing) in alkali metals. The reason for the reduced evaporation is, again, the lower surface area/mass ratio that comes with a larger size; by contrast, abundances of alkali metals (and also S) in S-type cosmic spherules are usually below detection limits (Brownlee *et al.*, 1997; Genge *et al.*, 1997).

(III) Chondritic melted crusts routinely show higher Ni abundances than cosmic spherules. Even though the depletion of siderophile and chalcophile occurs for both (Genge and Grady, 1998), the higher  $fO_2$  conditions in which melted crusts and MAS form (at lower altitudes) allow more Ni to enter the silicate portion of the melted crust.

Metallic liquids observed in chondrite melted crusts are usually (relatively) Ni-rich – in contrast with I-type cosmic spherules, which generally display Ni-poor magnetite and wüstite. It has been suggested (Brownlee *et al.*, 1983; Engrand *et al.*, 1998) that they may form by oxidation of metal in the atmosphere; metallic MAS oxidized after separation from their meteoroids may get depleted in Ni, thus becoming indistinguishable from I-type spherules. Sulfide droplets separated from meteoroids may also form Fe-rich MAS resembling the FSN spherules (Brownlee *et al.*, 1983; 1997), which abound in our atmosphere; these particles may derive from the separation of sulfide droplets from micrometeoroids. By comparison, high-Ni sulfide spherules are more likely to be produced by MAS, because oxidation processes (at lower altitudes) are responsible for large Ni enrichments. High Ni sulfide cosmic spherules larger than 50  $\mu\text{m}$  are uncommon, though found in Antarctic ice (Robin *et al.*, 1988).

In conclusion, the issue of the utility of MAS as *bona fide* analogues of chondrite melted crusts is still actively discussed; however, it seems clear that particles identified as low altitude MAS won't have compositions which may be truly diagnostic of their parent meteorites. Most low-altitude MAS formed from carbonaceous chondrites will have higher Al/Si ratios than MAS formed from the other chondrite groups and have higher Fe/Si than MAS derived from L, LL, and EL chondrites. Similarly, MAS derived from H chondrites may display higher Fe/Si than L, LL, and EL chondrites. MAS from enstatite chondrites may be recognized when they retain the high Cr/Si and Mn/Si ratios of the melted crusts from which they separate; MAS of CM2 chondrites, finally, can have higher Na/Si than those



from the other chondrite groups. This leaves only the MAS derived from achondrites as compositionally diagnostic of their source.

#### **1.4 – *Scope and aim of this work***

The study of fusion crusts of the ordinary chondrites is one of the main topics dealt with in this work. In particular, we have sought chromites in the crusts, in order to make a systematic comparison with chromites found in the bulk of meteorites. Samples must be very fresh and unaltered, to allow quantitative analyses of their fusion crusts; that's the reason why we have selected for our study only falls or well-preserved finds. Our goal was to pinpoint chemical and mineralogical differences – a study that (to our knowledge) hasn't been carried out before in literature.

The purpose of this work is to carry out a systematic comparison between chromites found in the bulk of ordinary chondrites and chromites forming within the fusion crust during the meteoroid passage through the Earth atmosphere. These data may help understand the outcomes of meteorite fusion experiments (by plasmatron), and may possibly lead to a deeper understanding of the formation and evolution of meteorite melt during the ablation stage, about which very little is known in the literature. We regard this thesis as a preliminary, tentative step towards a better analysis of meteoroid ablation during atmospheric entry, hoping to contribute to a deeper understanding of the genesis of ablation spherules and of the effects of atmospheric flight on melted micrometeorites.

## Chapter two – samples and experimental

### 2.1 Samples

This study is focused on the microchemical characterization of ten ordinary chondrites and their fusion crusts: two belong to the LL group (Chelyabinsk LL5, Kilabo LL6), three to the L group (Aba Panu L3.6, Viñales L6, NWA869 L3-6) and four to the H group (Bassikounou H5, Chergach H5, Kabo H4). We also analysed a H ordinary chondrite (El Hammami, H5) that has been experimentally melted (creating in laboratory a fusion crust) by a Plasmatron at the von Karman Institute in Brussels, operated at known plasma temperature and velocity; the surface temperature of the meteorite has been measured during the melting experiment.

All meteorite samples studied in the present work are falls, with the exceptions of El Hammami and NWA869. We chose *fall* meteorites whenever available, in order to take advantage of their much lower degree of terrestrial alteration compared to *find* meteorites. However, to further increase the number of studied chromite grains, we also examined a fine meteorite (NWA869) which displays a relatively minor degree of terrestrial alteration. Source for the meteorite data is the *Meteoritical Bulletin*.

### 2.2 Optical microscopy

Each sample has been previously examined by optical microscopy using transmitted light with parallel or crossed polarisers. This preliminary investigation allowed to characterise the chondrule types present in each sample (e.g. porphyritic olivine, porphyric pyroxene-olivine, Radial Pyroxene, cryptocrystalline), to detect the presence of Chromite-Plagioclase assemblages, and to ascertain the presence of fusion crust before attempting Scanning Electron Microscopy analysis. The preliminary optical analysis proved crucial in identifying reliable reference features on the samples, allowing us to retrace the position of any point analysed via SEM.

### 2.3 Field Emission Scanning Electron Microscopy

All the samples have been characterised by means of Field-emission Scanning Electron Microscopy. We used two FE-SEMs present at the School of Science and Technology of the University of Camerino and at the Physics-Geology Department of the University of Perugia. The two FE-SEM used in this study have the following characteristics:

#### *UniCam*

FE-SEM Sigma300 Zeiss equipped with 3 electron detectors: “In-lens” secondary electron detector, an Everhart-Thornley secondary electron detector, 4-sector High Definition Back-Scattered Electron Detector. X-rays emitted by the samples have been analysed by a Silicon Drift Detector (SDD) Bruker Qantax 200, with a 129 eV resolution at the Mn K $\alpha$  emission line. Samples have been covered with a 30 nm-thick carbon coating by means of a Quorum Q150T ES coater, able to use Cr, Au, or C for coating.

#### *UniPG*

FE-SEM LEO 1525 Zeiss, using a back-scattered electron detectors AsB (Angle selective back-scattered detector), a Inlens secondary electron detector, a EDX detector Bruker Quantax 200 (equipped with a X-Flash 410 detector). The SEM was operated at 15 kV voltage, in order to be able to

easily detect also the Fe, Co and Ni K $\alpha$  emission lines. EDX spectra have been processed by means of a Espirit 1.9 software using ZAF correction in order to derive elemental abundances.

Multiple analyses on the same samples performed with each instrument allowed us to ascertain the good agreement with instrumental resolution and analytical sensitivity of both facilities. Moreover, it also proved their ability to obtain compositional data not biased by neighbouring crystals – at least for chromite grains larger than 2-3 micrometers.

The two instruments used have similar performances in terms of magnification, EDX data collection, and reliability of the determined chemical composition. In particular, synthetic silicates and oxides composition have been determined at both facilities providing comparable results.

Compared to optical microscope, the SEM offers a higher magnification, a larger depth of field (allowing a large portion of the sample to be in focus at one time, and thus giving an image that is a good representation of the three-dimensional sample), and a greater resolution – as well as compositional and crystallographic data.

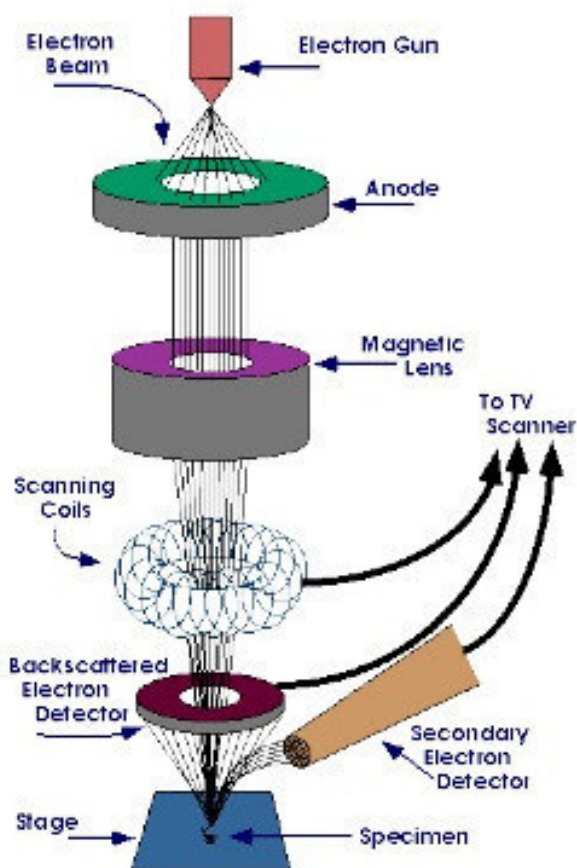


**Fig. 2.3.1** – Simplified scheme of a SEM

The scanning tool for SEM is a focused electron beam (working voltage: 2-50 keV) hitting the sample surface. Different types of signals are produced and detected as a function of position, with a spatial resolution that can be as high as 1 nm.

Each signal provides a specific information: secondary electrons (SE) probe the surface structure, as do back-scattered electrons (BSE) – which also provide average elemental information. X-rays and Auger electrons give elemental composition, with different thickness-sensitivity (fig. 2.3.1).

The electron beam increases its size as it penetrates deeper into the sample. The volume covered varies with the density of the material; secondary electrons, back-scattered electrons and X-rays all probe at different depths – a fact to be accounted for in data analysis and reduction (fig. 2.3.2)

SEM collects information from the entire beam volume – even from hidden features beneath the visible sample surface, so that a measure can be biased by the elemental imprint of the underlying minerals. Images produced by SEM display different hues of grey, depending on the Z (atomic number) of the surface material: the higher the Z, the brighter the area. Topographic contrast arises because the generation of secondary electrons depends on the angle between the incoming beam and the surface of the sample (fig. 2.3.3).

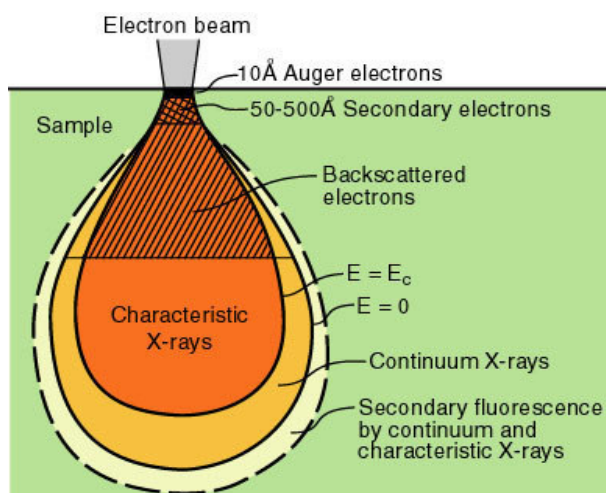


**Fig. 2.3.2** – Volume probed by SEM

A typical SEM image is shown in figure 2.3.4, along with minerals commonly associated to that specific shade of grey.

Our main goal was the morphological and chemical characterization of chromites – in particular, we searched any such pattern comparing chromites found in the bulk and those formed within the crust (mostly during their atmospheric flight).

Significant differences are consistently present in the samples we examined; on the other hand, no evidence of similar trend among bulk chromites from the various samples has been proved beyond any reasonable doubt, suggesting that to this purpose a more robust statistics will be required.

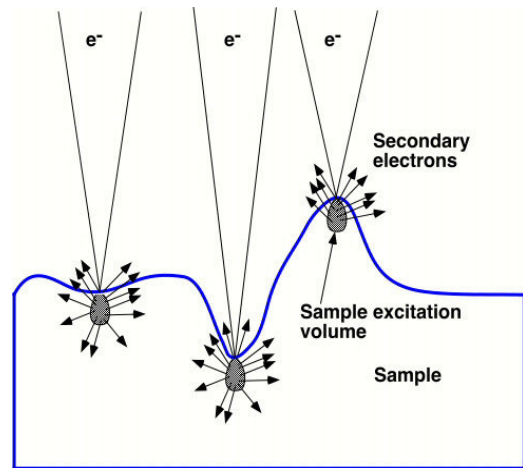


**Fig. 2.3.3** – Interaction between electrons and the surface of the sample

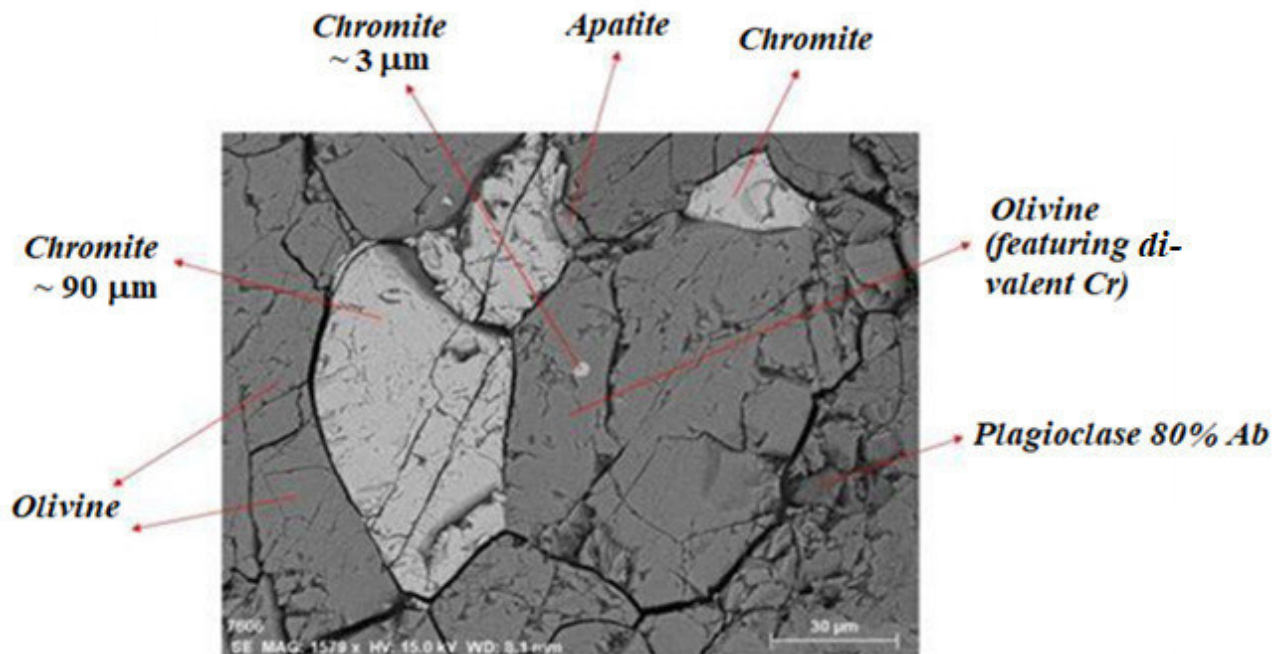


**Fig. 2.3.4** – Different hues of grey displayed by SEM, with some of their associated minerals (Kilabo meteorite, LL6)

## 2.4 Aba Panu (Nigeria)

**Fall. Ordinary chondrite, class L, petrologic type 3.6, shock stage S4, weathering grade W0.**

The following is a citation extracted from the *Meteoritical Bulletin* (MB107):

**“History:** On the afternoon of 19 April 2018, a large fireball detonated over the Nigerian state of Oyo. This fireball was recorded by NASA's Center for Near Earth Object Studies (CNEOS) as event 2018-04-19 14:02:27. The meteoroid entered at 20.9 km/s and detonated at an altitude of 30 km at 7.5°N, 3.6°E releasing a calculated total impact energy of 0.23 kt. Many stones fell between the villages of Ipapo (8°7'50.84"N, 3°30'34.58"E) and Tede to the north (8°33'21.49"N, 3°26'46.31"E). Stone were collected at multiple locations. The meteorite is named for the village of Aba Panu near the center of the strewn-field: multiple kg-sized stones were found in and around this village. Current total known weight is near 160 kg.

**Physical characteristics:** The stones are hard, range from 30 g to near 40 kg, rounded with broad poorly developed regmaglypts, and largely lacking fusion crust. Fusion crust is occasionally preserved within the shallow regmaglypts. Most stones are greyish green and show areas of rounded to angular light-colored clasts. Largest clast (5 × 2 cm) is angular, fine-grained, and achondritic. Observations from multiple slices show that clasts constitute roughly <10 areal%.

**Petrography:** Visually the cut surfaces are dominated by a gray matrix, studded with well-developed chondrules and chondrule fragments. Some chondrules to 4 mm but the majority are 0.1 to 1 mm across. Observations on an 8 × 7 cm slab shows the following clasts: L6 (3 × 1 cm); L5 (1.5 × 1 cm); and sub-rounded 1-cm dark clast with sparse 200 micron chondrules. Shock veins are rare. Metal and sulfide occurs as: fine grained spheres in the matrix; armoring chondrules; and, occasional lumps to 5 mm. Petrographic observations show a range of chondrule types dominated by PO, POP, RP, PP, and BO. Particularly evident in thin section are BO and PO chondrules with reddish purple (in plain polarized light) glass that is isotropic under crossed polars. The silicates are extensively shocked with olivine showing mosaicism and PDFs. SEM observations show that much of the metal/sulfide in the matrix occurs as fine-droplets, veins, and melt pods. Large Fe-Ni grains are polycrystalline with each crystal showing a kamacite core, dark-etched martensitic inner rim, and outer Ni-rich rim. Troilite is dominantly single crystal, and occasionally polycrystalline. Sparse chromite grains.

**Geochemistry:** (L. Garvie, ASU) Olivine  $Fa_{24.3\pm5.7}$ ,  $n=18$ , range  $Fa_{7.5-32.8}$ . Mean  $Cr_2O_3 = 0.08$ ,  $\sigma-Cr_2O_3 = 0.07$ , range 0.02 to 0.3.  $FeO/MnO=55.8\pm12.6$ . Low Ca, pyroxene  $Fs_{17.0\pm11.6}Wo_{2.0\pm1.9}$  range  $Fs_{2.4-49.2}Wo_{0.3-6.0}$ ,  $n=17$ . High Ca pyroxene  $Fs_{8.7}Wo_{49.2}$ ,  $n=1$ . Reddish purple, isotropic glass within BO and PO chondrules  $Or_{1.4\pm0.8}Ab_{87.6\pm4.8}$ ,  $n=6$ ,  $TiO_2$  to 1 wt%. Oxygen isotopes (K. Ziegler, UNM): analyses of three subsamples by laser fluorination gave, respectively,  $\delta^{17}O = 3.724$ , 3.625, 3.684;  $\delta^{18}O = 5.160$ , 4.980, 5.089;  $\Delta^{17}O = 1.000$ , 0.996, 0.997 per mil.

**Classification:** Geochemistry and oxygen isotopic data consistent with L chondrite. Estimated petrologic type 3.6 based on Fa and Fs spread, and  $Cr_2O_3$  content in olivine. L3, S4, W0.

**Specimens:** Michael Farmer and Moritz Karl - 50 kg, Eric Twelker 7.74 kg, and ASU 242 g. Based on photographic evidence, it is estimated that the Nigerian government collected on the order of 100 kg of stones, though this mass is uncertain. Given the size of the fall and area of the fall, the total mass is conservatively given as 160 kg.”

Studies about the meteorite strength (Cotto-Figueroa *et al.*, 2020) and its degassing products (Stennikov *et al.*, 2020) have been undertaken.



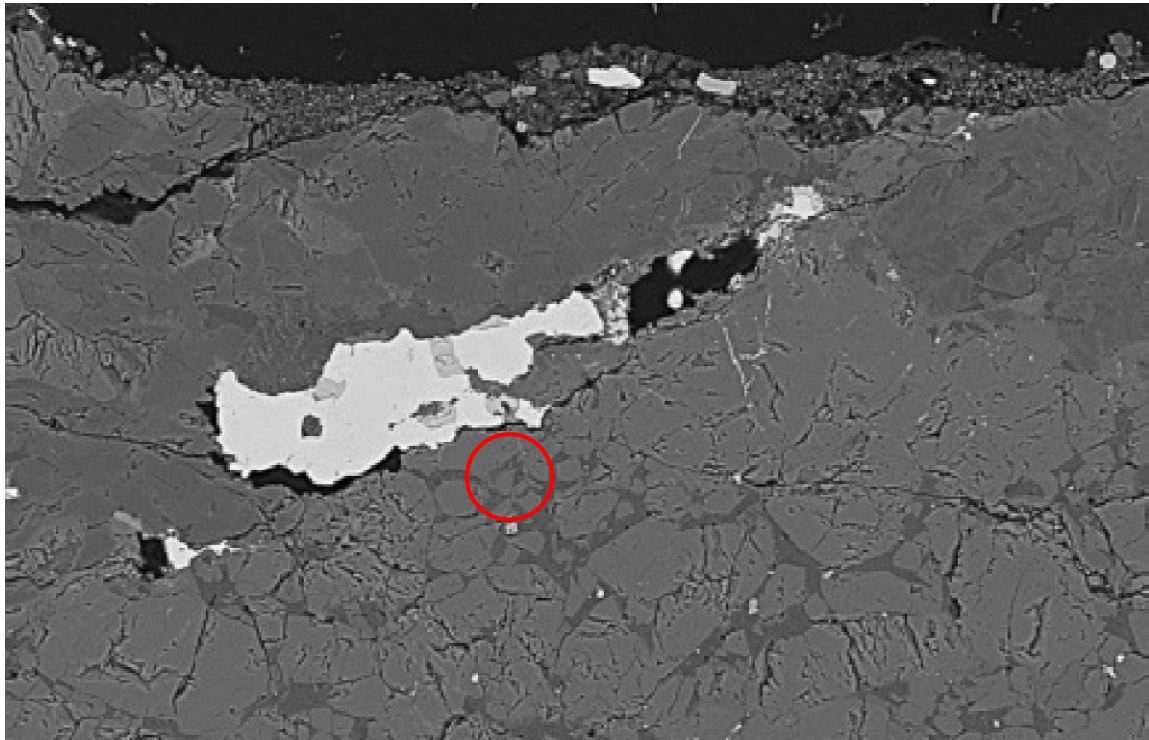


**Fig. 2.4.1.** – *Fe (90%)-Ni(10%) formation with small crust chromites.*

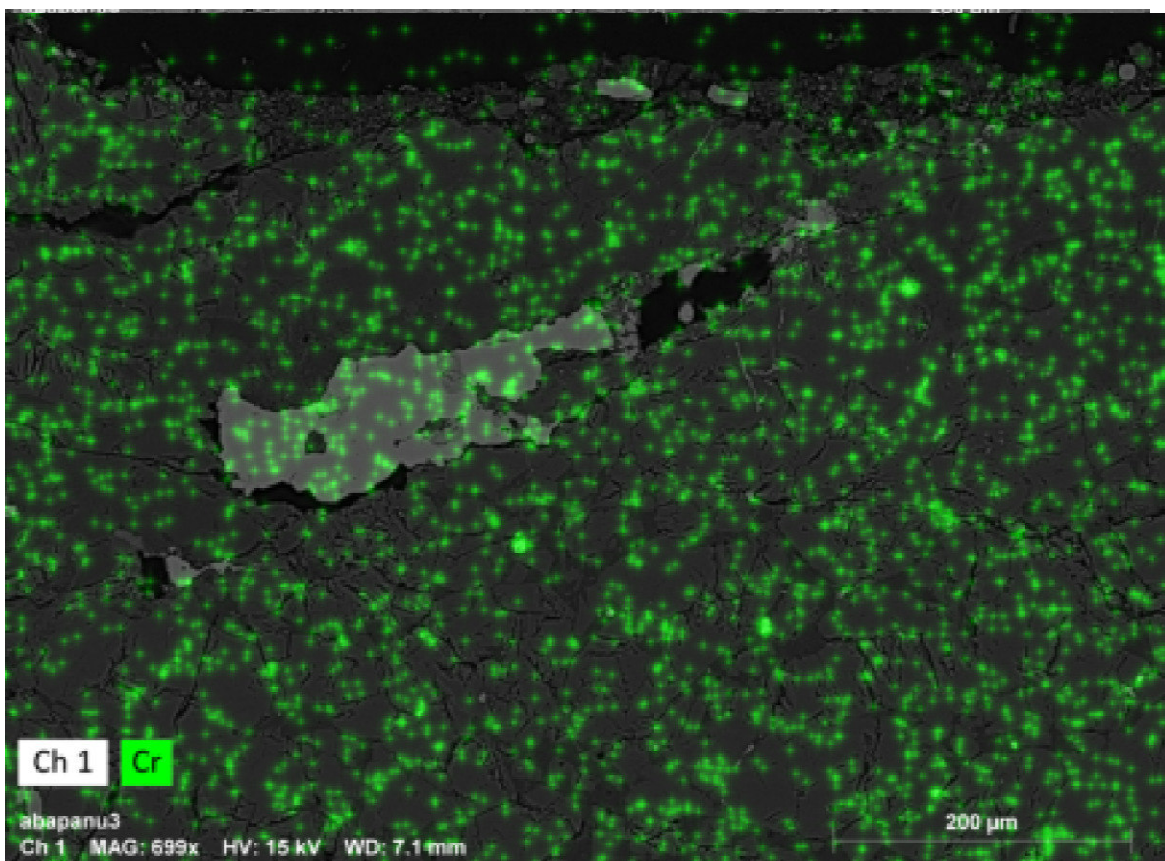


**Fig. 2.4.2.** – *Relative chromium abundance map superimposed on the previous image.*



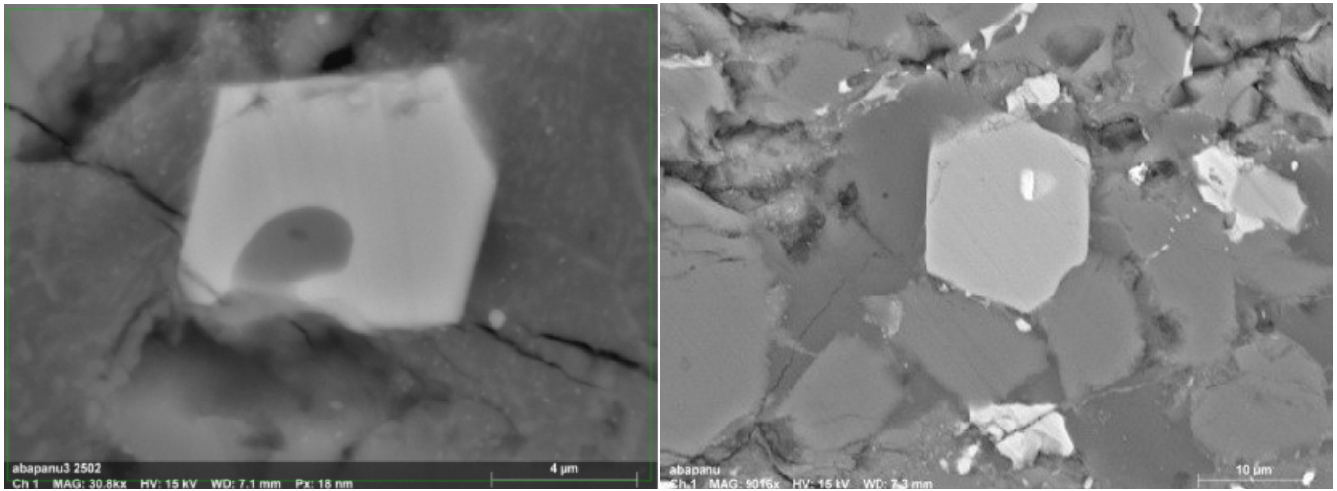


**Fig. 2.4.3.** – Euhedral chromites from the crust (about 10  $\mu\text{m}$  and 15  $\mu\text{m}$  across, respectively). The first image is a magnification of the object inside the red circle in figure 2.4.1.

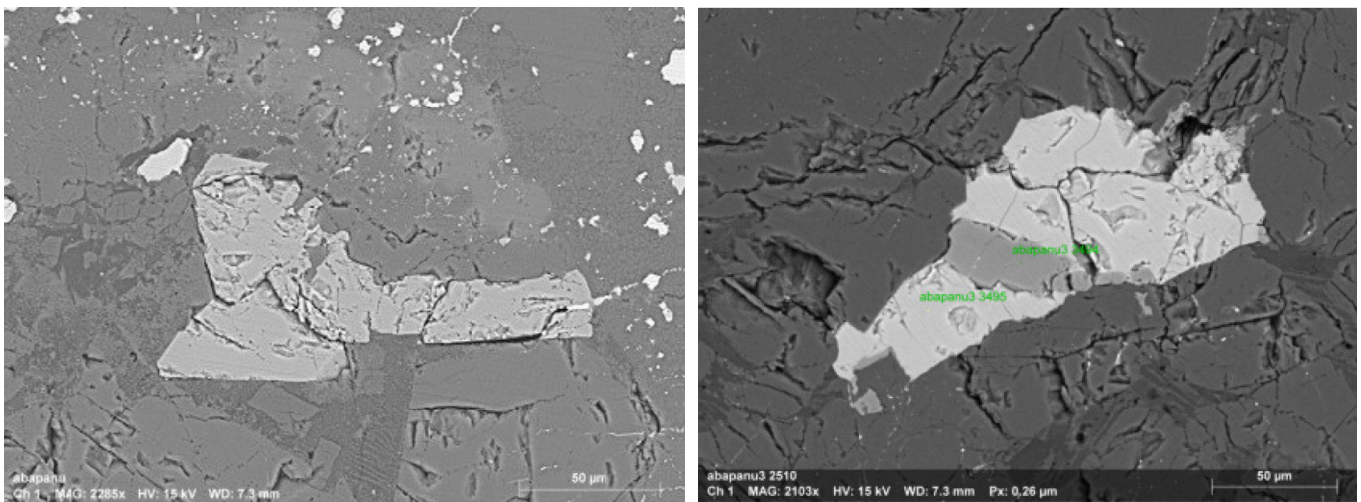


**Fig. 2.4.4.** – Two semi-euhedral, slightly fractured chromites from the bulk (about 100  $\mu\text{m}$  across)

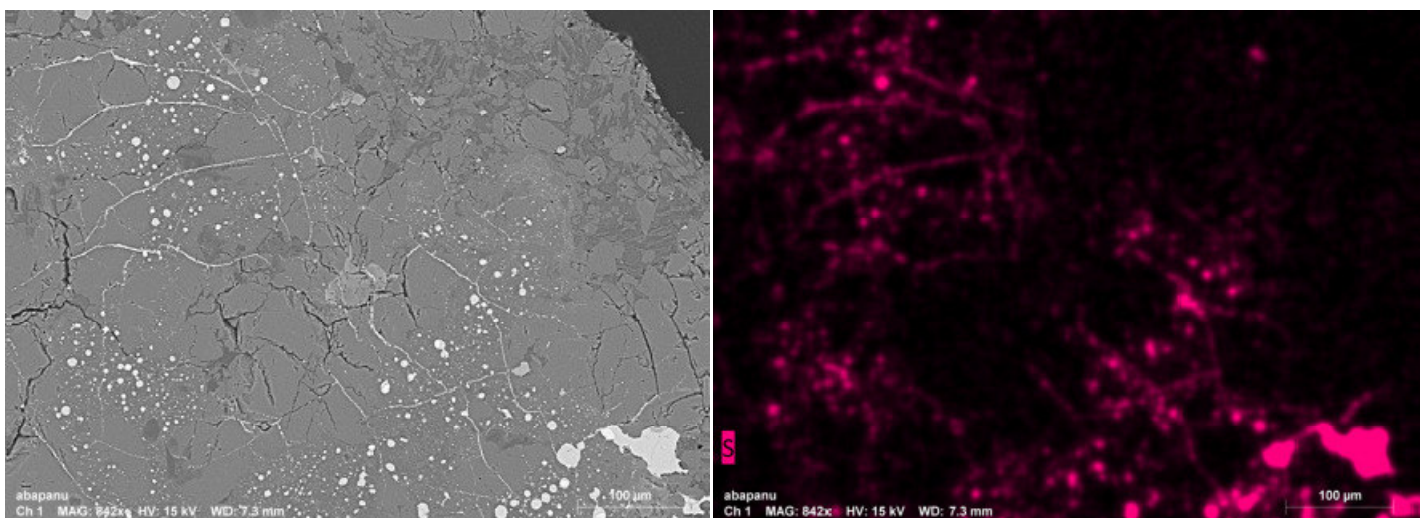


**Fig. 2.4.5.** – Inner substrate of Aba Panu's crust (SEM image and elemental map with sulfur relative abundances)

Like all other samples studied, bulk chromites found in Aba Panu are considerably larger than crust chromites (figures 2.4.1 to 2.4.4), consistently showing a less regular shape; bulk chromites also display on average a low shock stage. Also present are the sulfide veins typical of the inner substrate of the crust (figures 2.4.5 and 2.4.6).

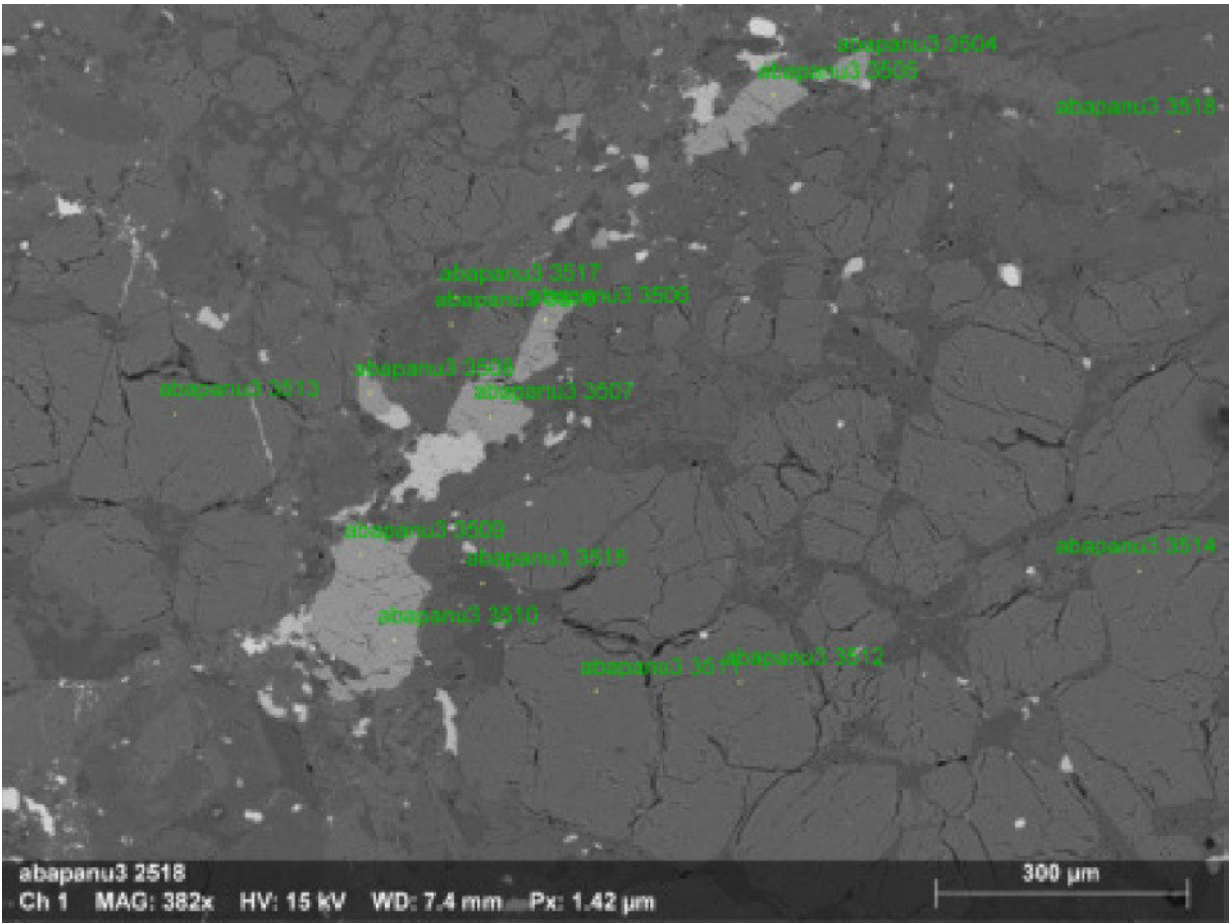


**Fig. 2.4.6.** – *String of bulk chromites, with olivines and pyroxenes nearby from a porphyritic chondrule.*

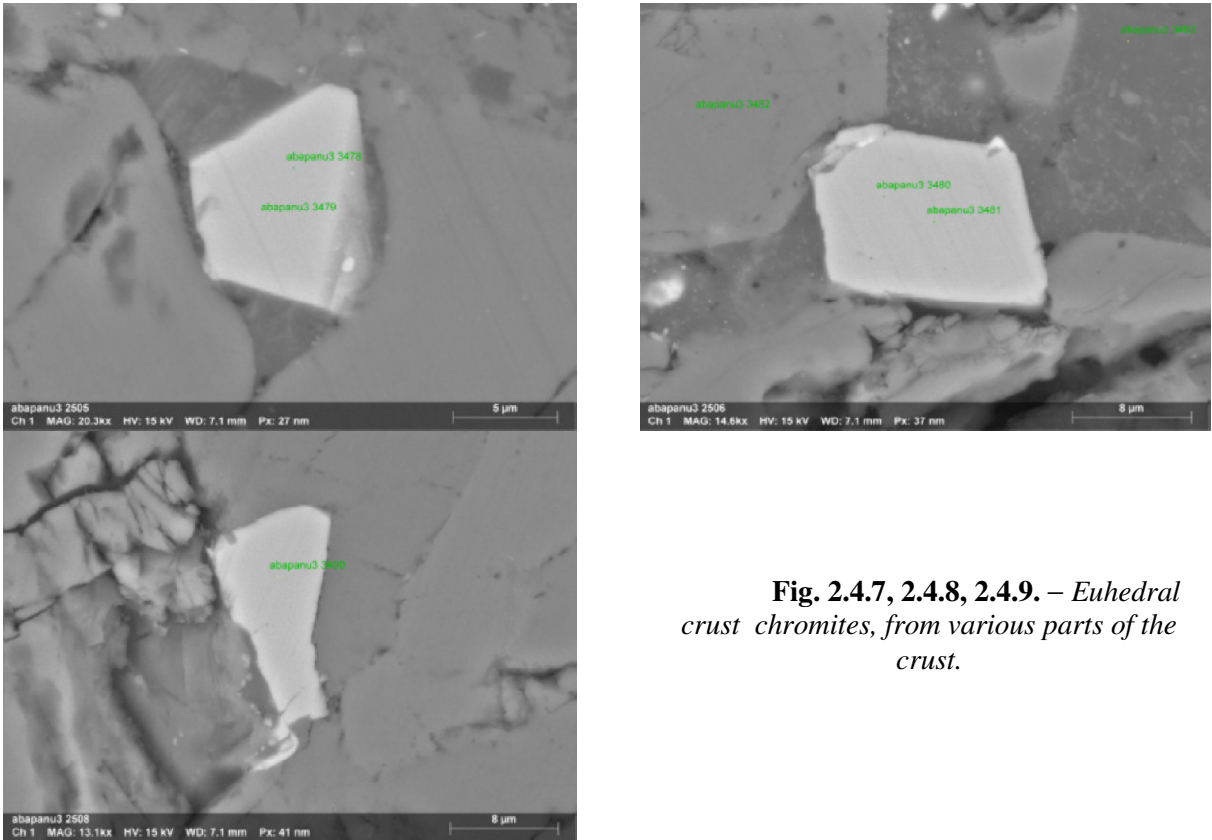


**Fig. 2.4.7, 2.4.8, 2.4.9.** – *Euhedral crust chromites, from various parts of the crust.*

For this sample we have found and classified 45 chromites – 20 from the bulk and 25 from the crust; the complete data record is available in the appendix. Below is shown the graph reporting Al# versus Mg# for the bulk chromites (blue squares) and the crust chromites (red squares). The error bars reported represent the standard deviation. Bulk and crust data are clearly distinguishable; moreover, bulk chromites are much more clustered around the average value than their crust counterparts. Compared to other meteorites, crust chromites of Aba Panu (figures 2.4.7 to 2.4.9) don't exhibit a significant enrichment in Mg# with respect to bulk chromites.

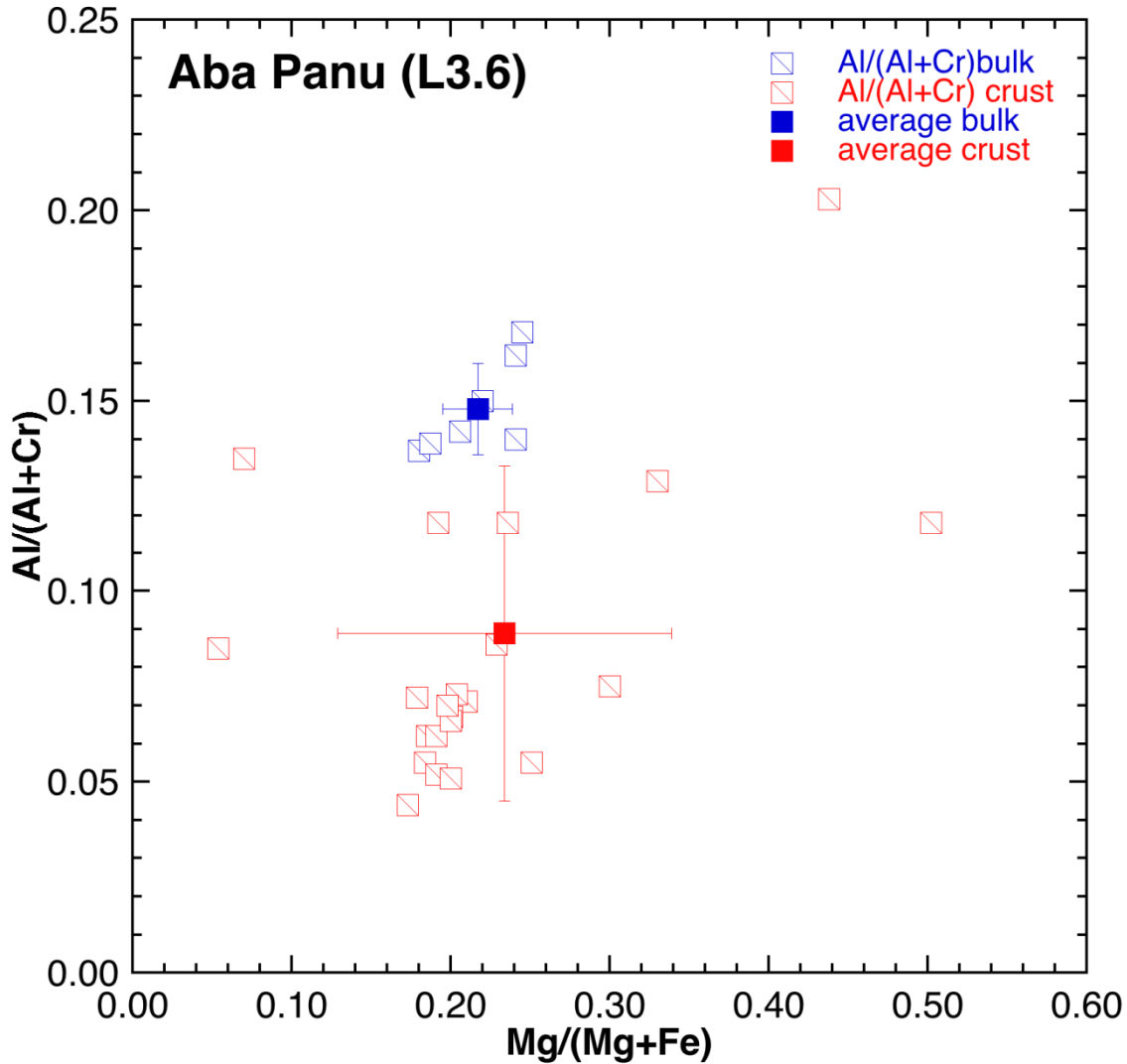


**Fig. 2.4.10.** – Plot of the Al# versus the Mg# for crust chromites (red) and bulk chromites (blue). The error bars represent the standard deviation.

## 2.5 Bassikounou (Mauritania)

**Fall. Ordinary chondrite, class H, petrologic type 5, shock stage S2, weathering grade W0.**

The following is a citation extracted from the *Meteoritical Bulletin* (MB92):

“: A fireball was witnessed in the area, but no records of the direction of movement were recorded. A single stone of 3165 g was found by A. Salem El Moichine, a local resident, on the same day at 13:00 hr local time, 11 km SE of Bassikounou. The sample for classification was provided to NMBE by M. Ould Mounir, Nouakchott, who obtained it from his cousin who recovered the meteorite. According to S. Buhl (Hamburg, Germany), more than 20 specimens were later recovered by locals and meteorite finders. These finds define a 8 km long strewnfield. The total recovered mass is 46.00 kg.

**Physical characteristics:** The 3165 g specimen is largely covered by black fusion crust. The interior is light gray. On the surface of the fusion crust there is some adherent soil material, some of which is bright red. Shortly after recovery, the stone was cut into two pieces of 1200 and 1950 g. The larger piece has a rectangular shape and shows indications of flow-lines in the fusion crust.

**Petrography:** (E. Gnos, MHNGE; B. Hofmann, NMBE, M. Eggimann, Bern/NMBE): Mean chondrule size 0.35 mm ( $n=53$ ). Metal abundance is 8 vol%, troilite 6.6 vol%. Mean plagioclase grain size is ~20  $\mu$ m. Troilite is polycrystalline, rich in silicate inclusions, and shows diffuse boundaries to metal. Metal is partly rich in silicate- and troilite inclusions. Rare metallic Cu (10  $\mu$ m) occurs at kamacite-taenite boundaries and in troilite. Some shock veins and no weathering products were observed.

**Mineral compositions:** Olivine ( $Fa_{18.6}$ ), pyroxene ( $Fs_{16.3} Wo_{1.1}$ ), plagioclase ( $An_{13.7}$ ).

**Cosmogenic radionuclides:** (P. Weber, PPGUN) Gamma-spectroscopy performed in December-January 2006 showed the presence of the following radionuclides:  $^{48}V$ ,  $^{46}Sc$ ,  $^{56}Co$ ,  $^{54}Mn$ ,  $^{58}Co$ ,  $^7Be$ ,  $^{51}Cr$ ,  $^{57}Co$ ,  $^{22}Na$ ,  $^{26}Al$  and  $^{60}Co$ . Recalculated to 12 October 2006  $^{22}Na$  was  $38.0 \pm 2.2$  and  $^{26}Al$   $31.5 \pm 2.1$  (both dpm/kg), the activity ratio of 1.21 is fully consistent with a fall on that date.

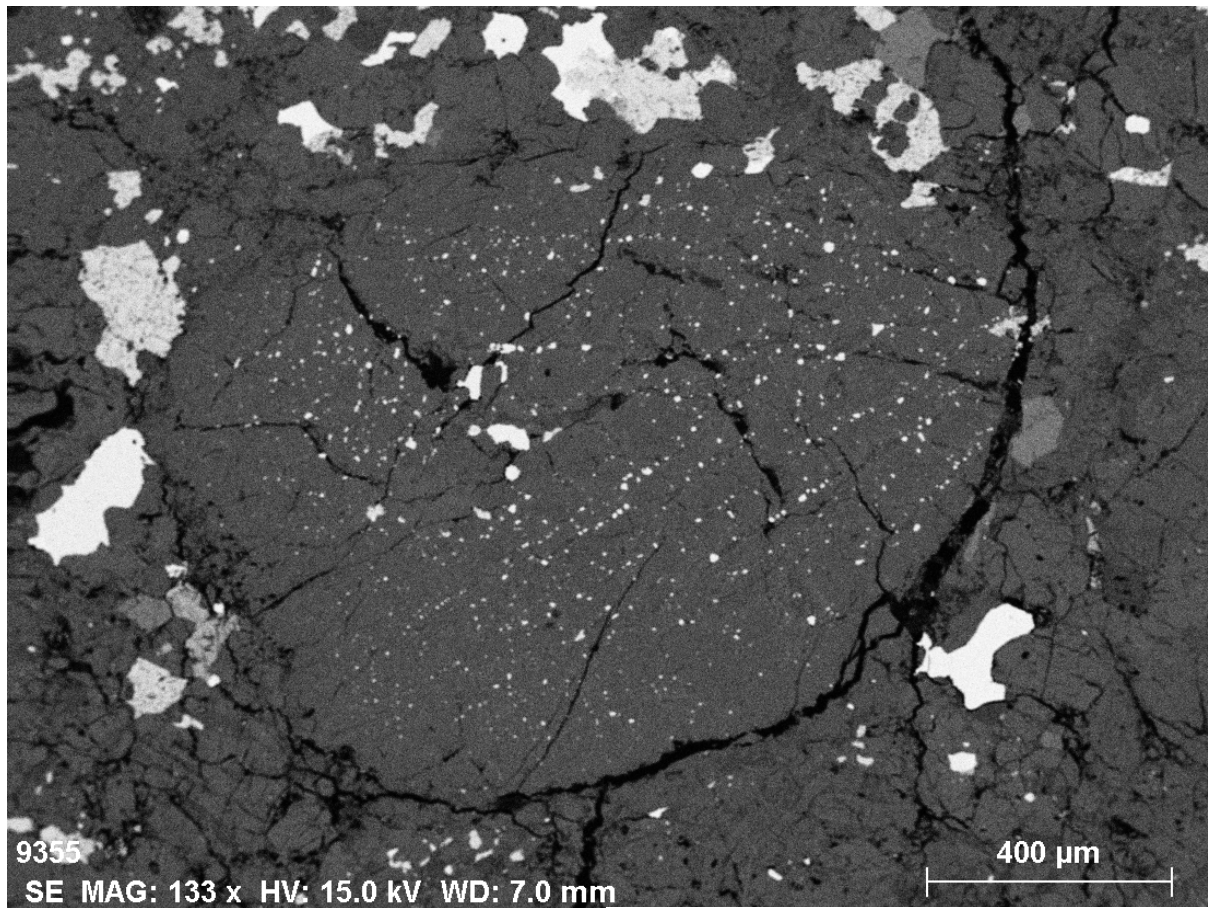
**Classification:** Ordinary chondrite (H5); S2, W0.

**Type s:** A total of 115 g are on deposit at NMBE. Boudreaux holds the main mass.”

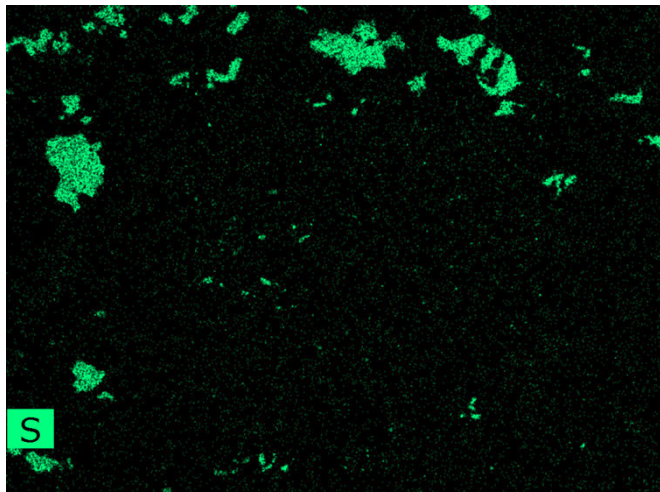
A tentative estimate of the original shape of the meteoroid can be found in Vinnikov *et al.* (2014).

Several porphyritic chondrules are visible in the meteorite bulk, often studded with sulfide and metal blebs (figures 2.5.1 to 2.5.4). It's not unusual to find fractured chromites, within the bulk (fig. 2.5.5) as well as in the crust (fig. 2.5.6). Like other samples examined in this work, various portions of the crust display dendritic magnetites with small euhedral crust chromites nearby – far too small to get reliable data from a SEM analysis (figure 2.5.9). Magnesiochromites are also frequent (figures 2.5.7 and 2.5.8); sometimes a chromite sheathed in magnetite overgrowth can be found (fig., 2.5.10), a feature observed in the crust of other meteorites.

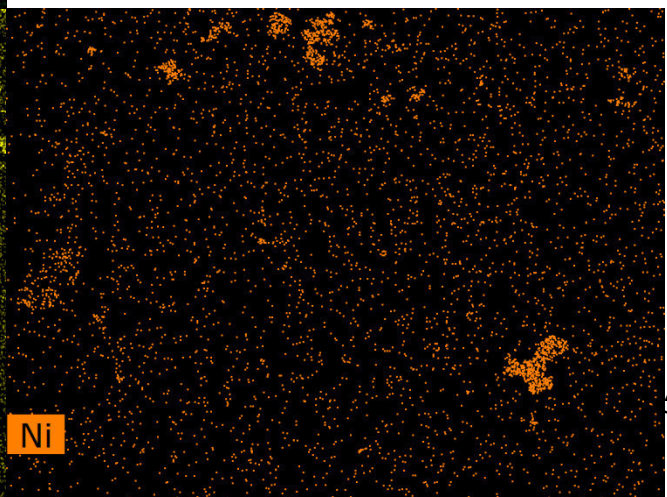
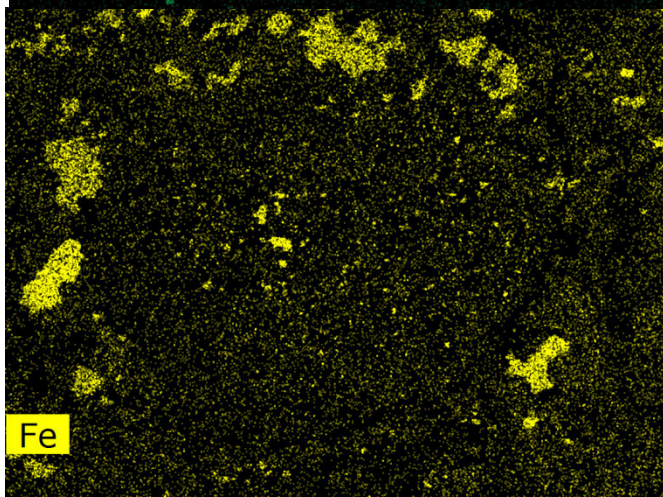




**Fig. 2.5.1.** – A barred olivine chondrule, studded with metal and sulfide blebs.



**Fig. 2.5.2., 2.5.3., 2.5.4.** – Relative abundances maps (Fe, Ni and S) around the porphyritic chondrule of figure 2.5.1.





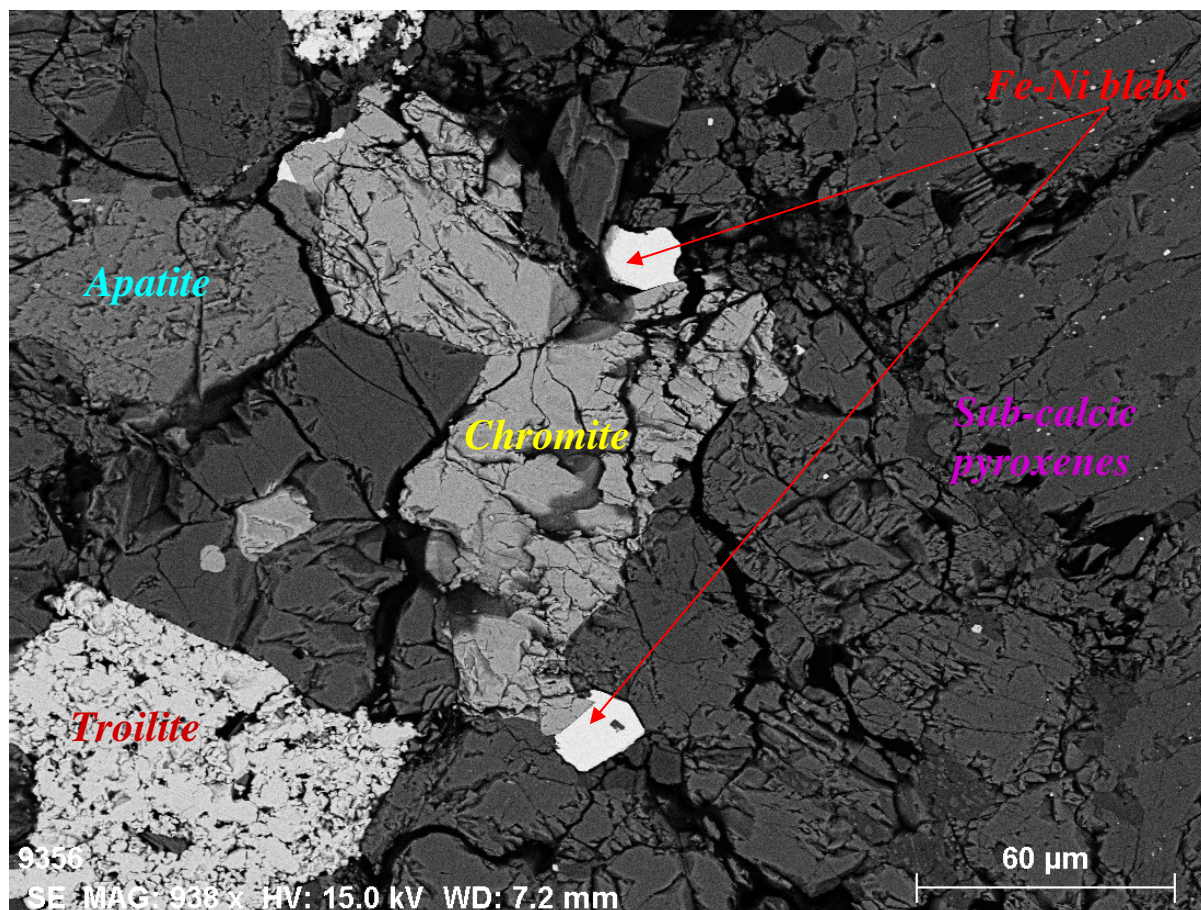


**Fig. 2.5.5.** – Fractured bulk chromites. The bright adjacent blebs are Fe (60%)-Ni(40%), the darker areas nearby are sub-calcic pyroxenes. An apatite (lighter grey) can be seen on the upper left. The brighter zone to the lower left is iron sulfide (troilite).

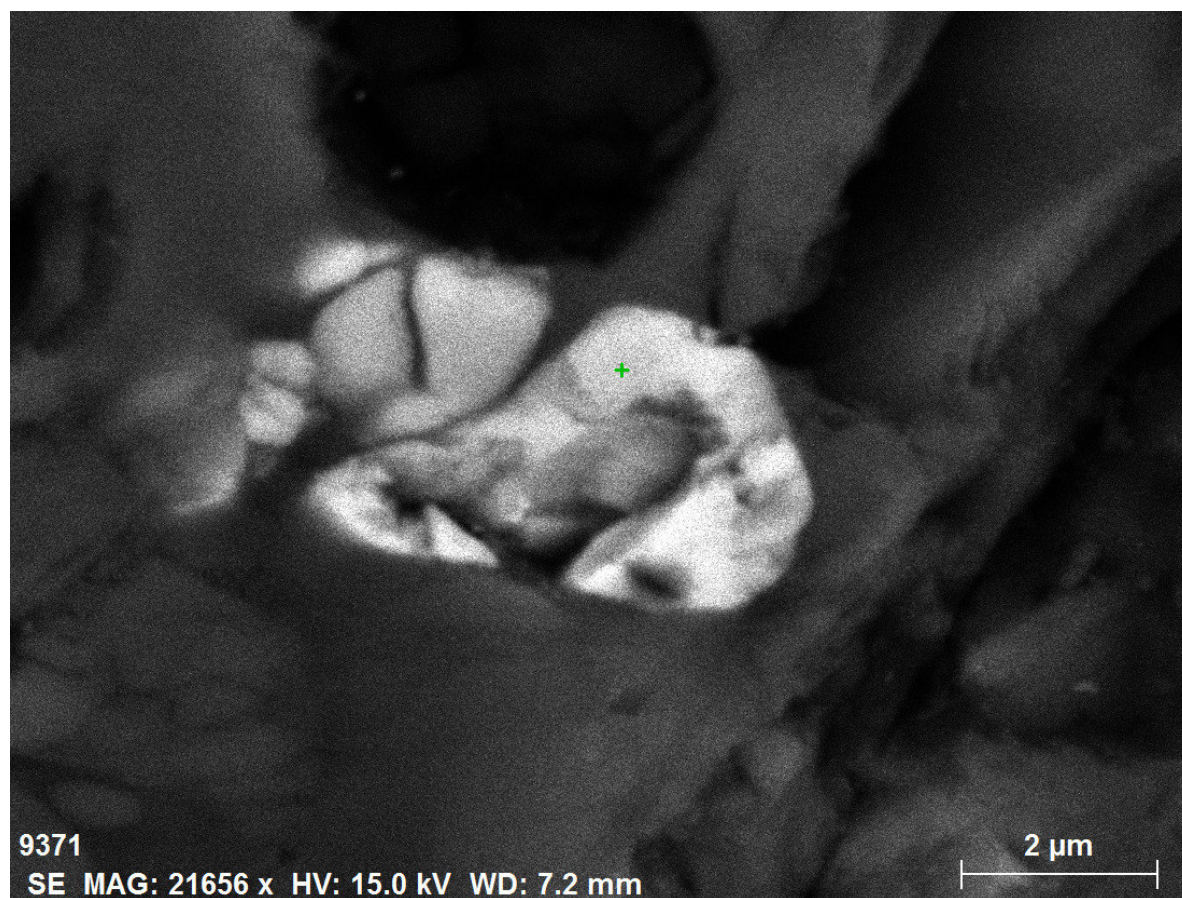


**Fig. 2.5.6.** – A crust chromite



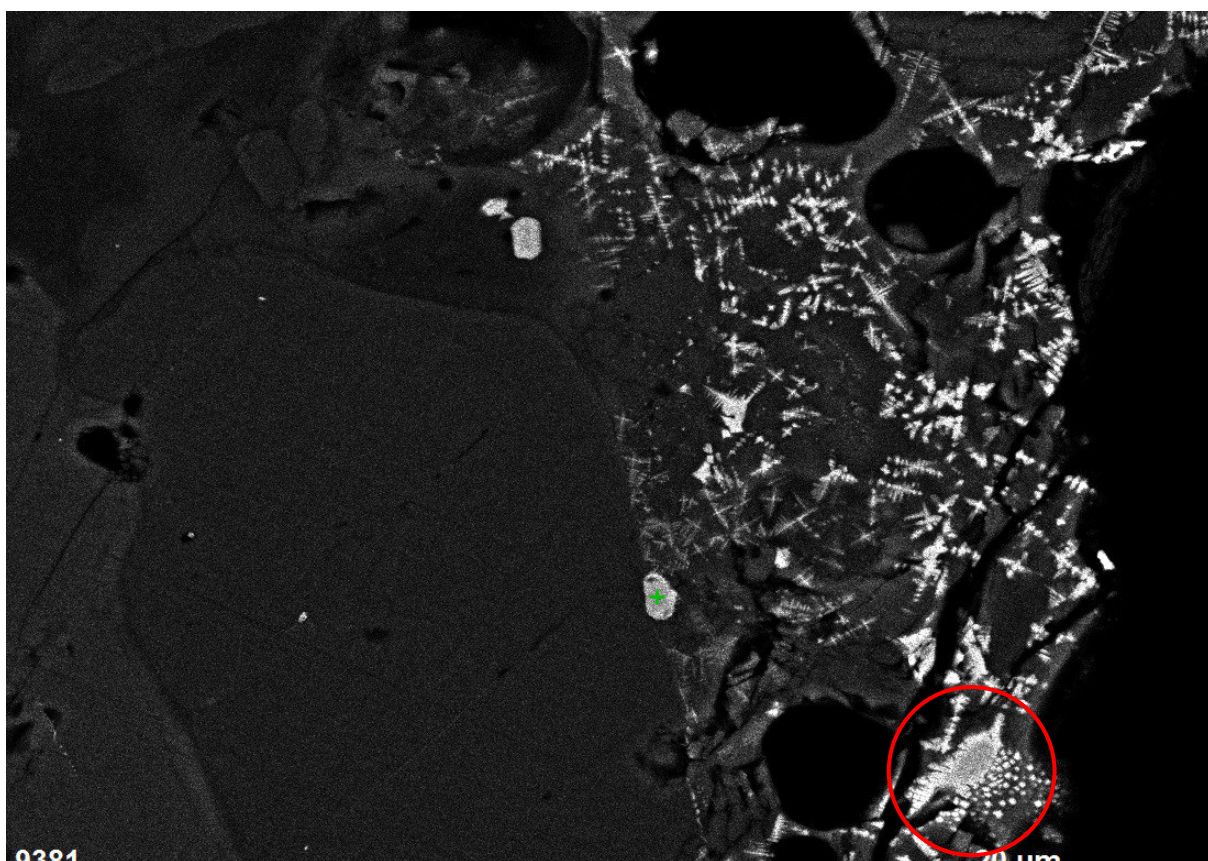


**Fig. 2.5.7.** – *Portion of the crust, with dendritic and euhedral magnetites.*

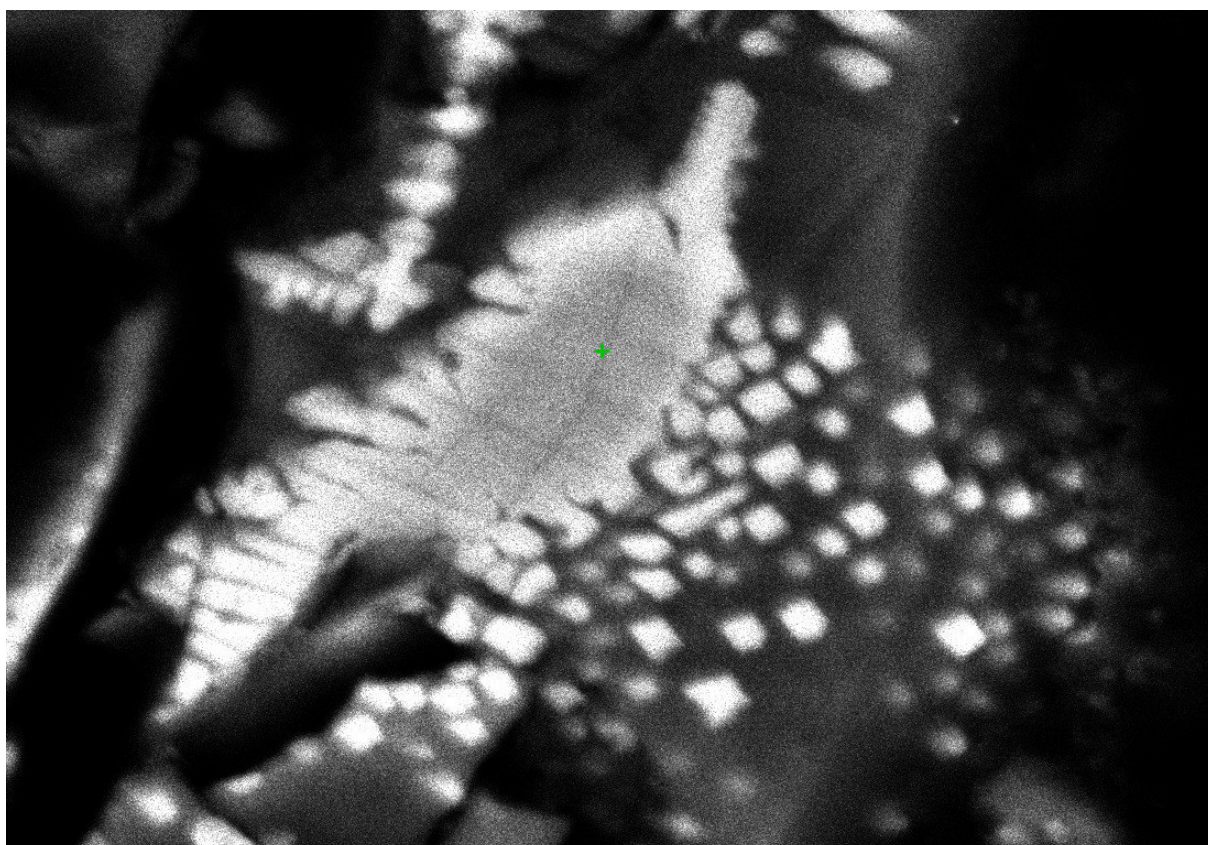


**Fig. 2.5.8.** – *Magnification of part of the previous image (red circle), zooming in on a magnesian-chromite overgrown by magnetite with small euhedral magnetite crystals nearby.*



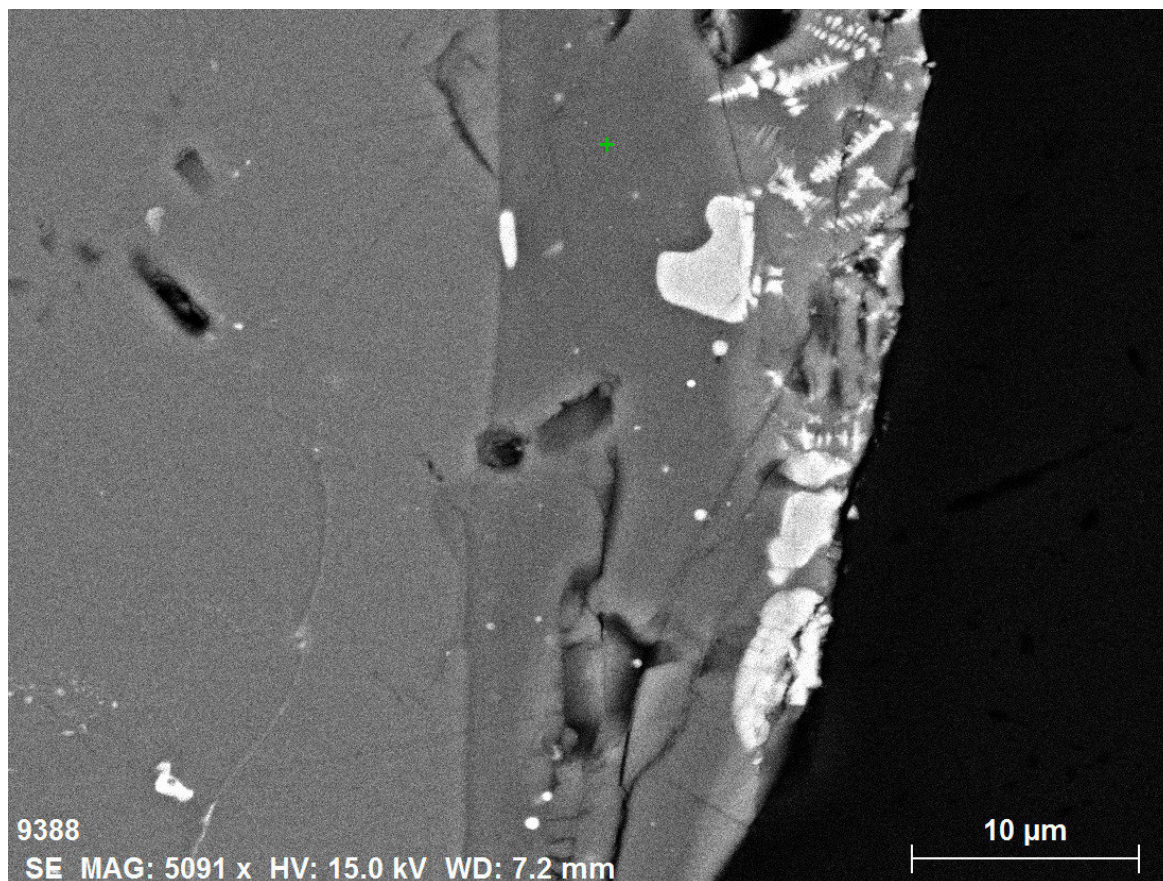


**Fig. 2.5.9.** – *Crustal zone. Crust chromites and dendritic magnetites are found on the border; the intermediate, darker area is plagioclase, while the innermost lighter zone is sub-calcic pyroxene.*

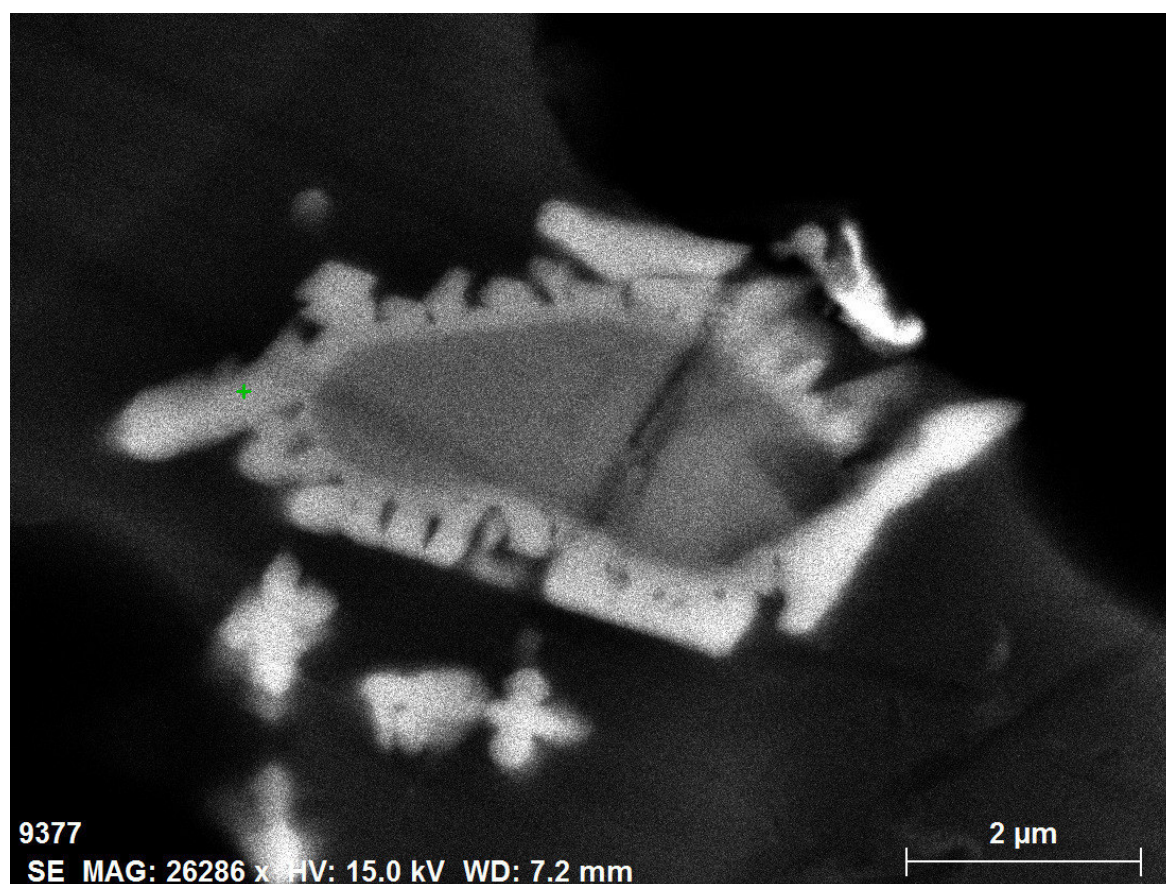


**Fig. 2.5.10.** – *An example of a crust chromite sheathed in magnetite overgrowth.*

We have found and classified 27 chromites – 13 from the bulk, 14 from the crust. The complete data record can be found in the appendix: here is the graph reporting Al# versus Mg# for the bulk chromites (blue crosses) and the crust chromites (red crosses). The error bars reported represent the standard deviation. The separation between bulk and crust is extremely neat, with crust chromites much more dispersed around the average value than bulk chromites.

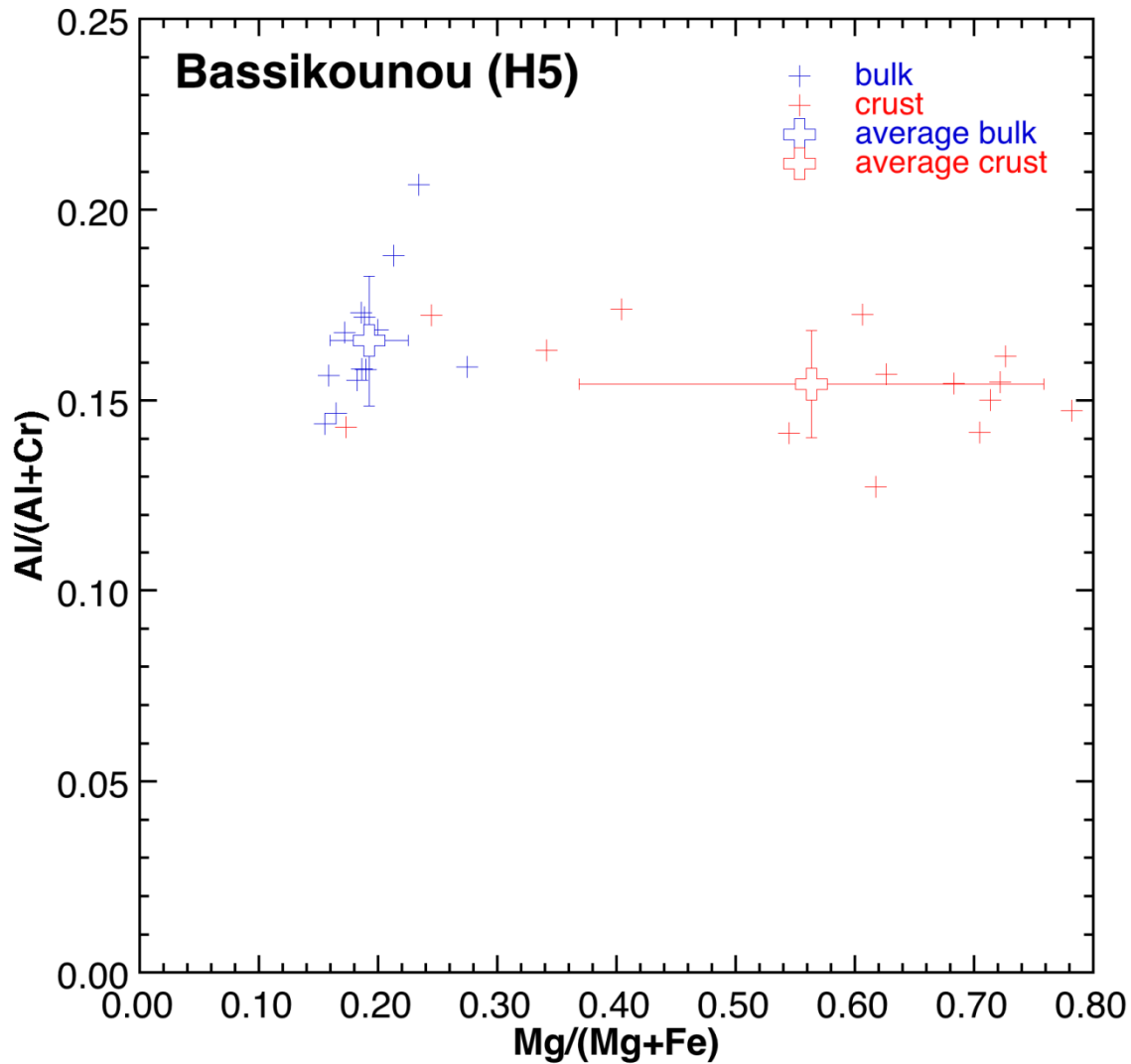


**Fig. 2.5.11.** – Plot of the Al# versus the Mg# for crust chromites (red) and bulk chromites (blue). The error bars represent the standard deviation.



## 2.6 Chelyabinsk (Russia)

**Fall. Ordinary chondrite, class LL, petrologic type 5, shock stage S4, weathering grade W0.**

The following is a citation extracted from the *Meteoritical Bulletin* (MB102):

**“History:** At 9:22 a.m. (local time) on February 15, 2013, a bright fireball was seen by numerous residents in parts of the Kurgan, Tyumen, Ekaterinburg and Chelyabinsk districts. Images of the fireball were captured by many video cameras, especially in Chelyabinsk. Residents of the Chelyabinsk district heard the sound of a large explosion. The impact wave destroyed many windows in Chelyabinsk and surrounding cities. Many people were wounded by glass fragments. A part of the roof and a wall of a zinc plant and a stadium in Chelyabinsk were also damaged. Numerous (thousands) stones fell as a shower around Pervomaiskoe, Deputatsky and Yemanzhelinka villages ~40 km S of Chelyabinsk. The meteorite pieces were recovered and collected out of snow by local people immediately after the explosion. The snow cover was about 0.7 m deep. The falling stones formed holes surrounded by firm snow. Largest stones reached the frozen soil. A stone may have broken the ice of Chebarkul Lake, located 70 km W of Chelyabinsk. Small meteorite fragments were found around the 8 m hole in the ice but divers did not find any stones on the lake bottom.

**Physical characteristics:** The meteorite stones and fragments are from <1 g to 1.8 kg in weight and from a few mm to 10 cm (mainly 3-6 cm) in size. The total mass collected by local people is certainly >100 kg and perhaps > 500 kg. Fusion crusted stones are common. **The fusion crust is black or brown and fresh.** Broken fragments are rare. The interior of the stones is fresh but in some pieces there is evidence for weak oxidation of metal grains.

**Petrography:** (D.D. Badyukov and M.A. Nazarov, Vernad). The majority (2/3) of the stones are composed of a light-colored lithology with a typical chondritic texture. Chondrules (~63%) are readily delineated and set within a fragmental matrix. The mean chondrule diameter is 0.93 mm. The chondrule glass is devitrified. The main phases are olivine and orthopyroxene. Olivine shows mosaicism and planar fractures. Rare grains of augite and clinobronzite are present. Small and rare feldspar grains show undulatory extinction, planar deformation features, and are partly isotropic. Troilite (4 vol.%) and FeNi metal (1.3 vol.%) occur as irregularly shaped grains. Accessory minerals are chromite, ilmenite, and Cl-apatite. A significant portion (1/3) of the stones consist of a dark, fine-grained impact melt containing mineral and chondrule fragments. Feldspar is well developed and practically isotropic. No high-pressure phases were found in the impact melt. There are black-colored thin shock veins in both light and dark lithologies.

**Geochemistry:** (M.A. Nazarov, N.N. Kononkova, and I.V. Kubrakova, Vernad). Mineral chemistry: Olivine  $Fa_{27.9\pm0.35}$ ,  $N=22$ ; orthopyroxene  $Fs_{22.8\pm0.8}Wo_{1.30\pm0.26}$ ,  $N=17$ ; feldspar  $Ab_{86}$ ; chromite  $Fe/Fe+Mg=0.90$ ,  $Cr/Cr+Al=0.85$  (at.%). Major element composition of the light lithology (XRF, ICP-AS, wt%): Si=18.3, Ti=0.053, Al=1.12, Cr=0.40, Fe=19.8, Mn=0.26, Ca=1.43, Na=0.74, K=0.11, P=0.10, Ni=1.06, Co=0.046, S=1.7. Atomic ratios of  $Zn/Mn \times 100=1.3$ ,  $Al/Mn=8.8$ . The impact melt lithology has almost the same composition but it is distinctly higher in Ni, Zn, Cu, Mo, Cd, W, Re, Pb, Bi (ICP-MS).

Si=18.3, Ti=0.053, Al=1.12, Cr=0.40, Fe=19.8, Mn=0.26, Ca=1.43, Na=0.74, K=0.11, P=0.10, Ni=1.06, Co=0.046, S=1.7. ”

A comprehensive description of the fall of this meteorite (which caused the most important airburst event since the Tunguska object in 1908) can be found in Popova *et al.* (2013).

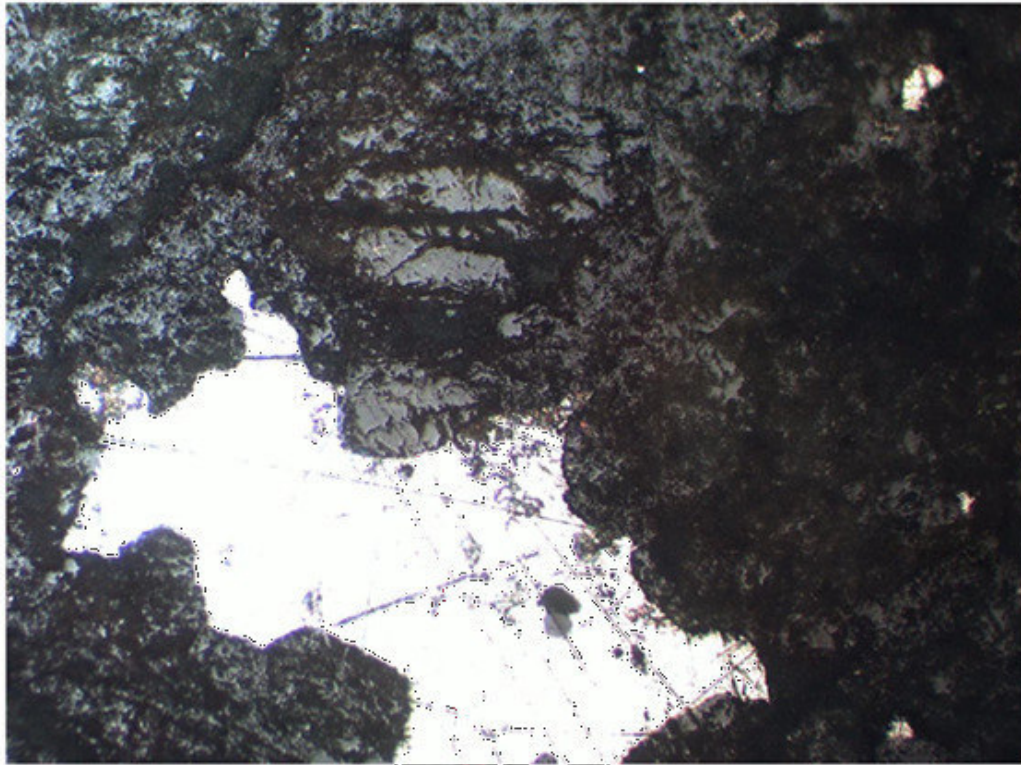


**Fig. 2.6.1.** – A chondrule (barred olivine) above a metallic (Fe-Ni) area. Image taken with the petrographic microscope, in reflected light.

The equilibrated petrologic type (5) ensures that olivines and pyroxenes have been metamorphosed enough to display a homogeneous chemical composition. We found an average Fe# of 35% for olivines and 30% for pyroxenes – hence confirming the LL classification. Pyroxenes are often sub-calcic – as in figure 2.6.2. Chondrules are still recognizable, like the barred olivine shown in fig. 2.6.1.

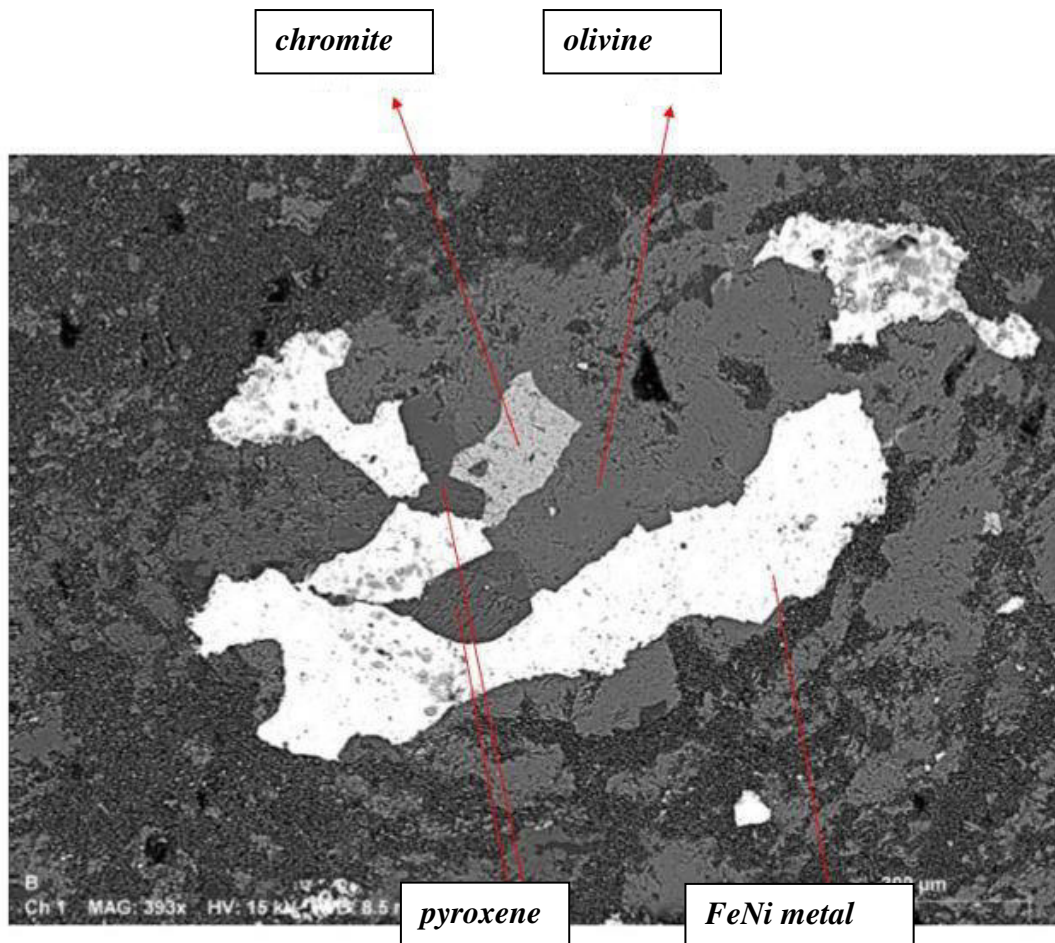


*Fig. 2.6.2. –Bulk chromite with olivine, pyroxene, and Fe-Ni metal nearby.*



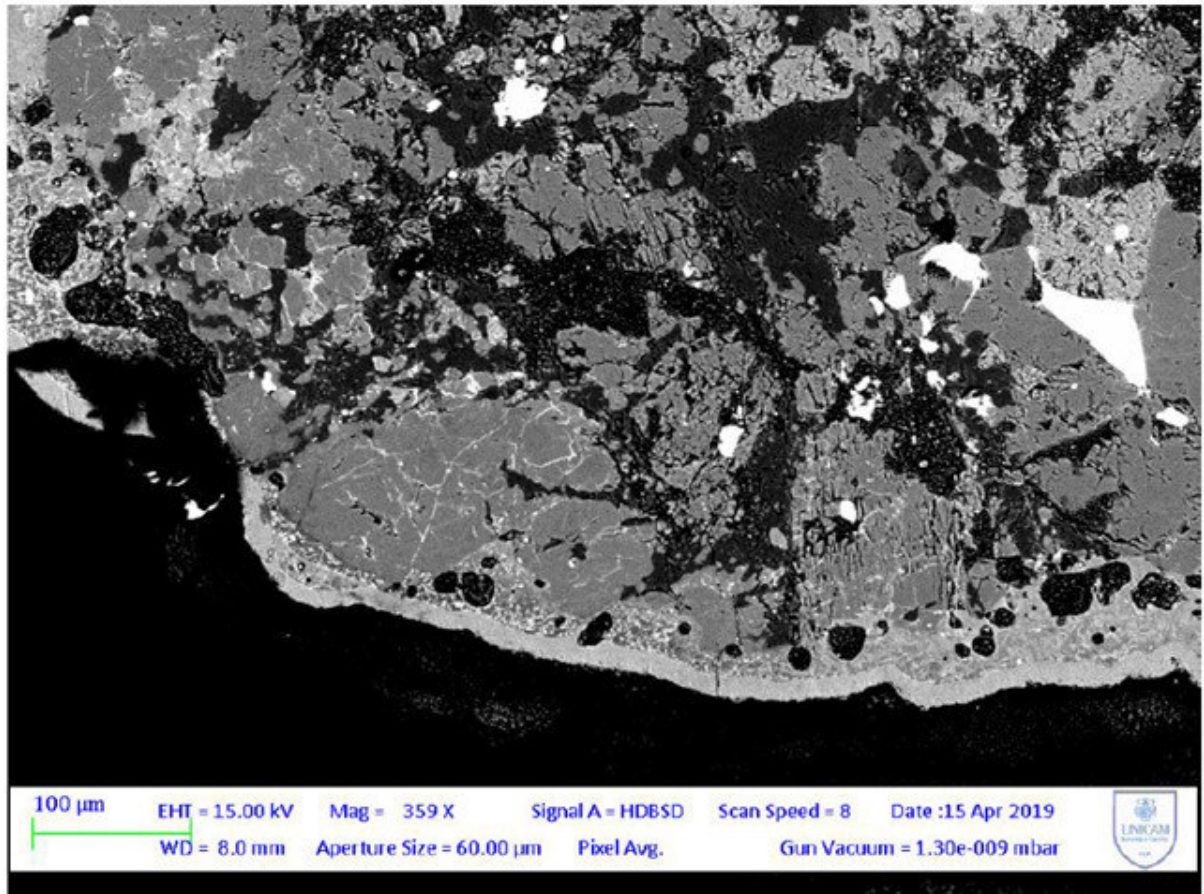


**Fig. 2.6.3.** – Fusion crust (imaged in back-scattered electrons).

Figure 2.6.3 clearly shows the transition between the outer fusion crust (composed mainly of magnetite dendrites) and the sub-crustal zone or inner crust, which features silicate glass, olivines and pyroxenes (relics from the original structure, before the crust formed) and iron sulfides like troilite.

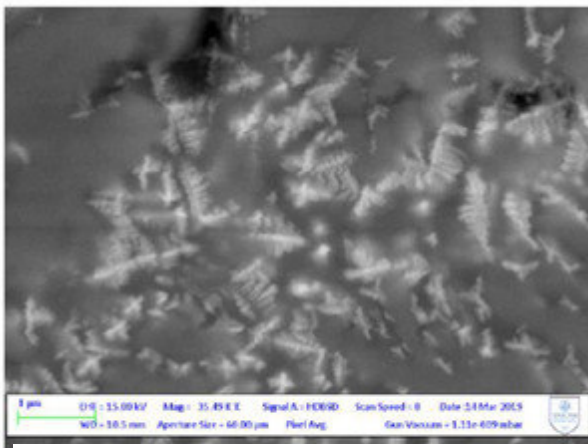


**Fig. 2.6.4.** – Crust chromite surrounded by dendritic magnetites.

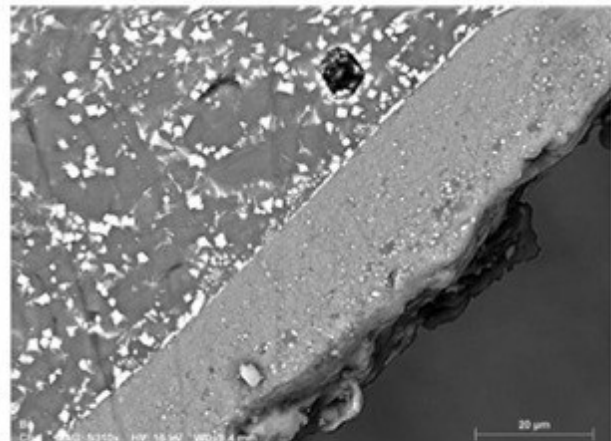


**Fig. 2.6.5.** – Euhedral crust chromites.

Like in other meteorites, several crust chromites are surrounded by magnetite with a dendritic morphology (figures 2.6.4 to 2.6.7). These chromites display a higher Mg# than chromites without magnetite.

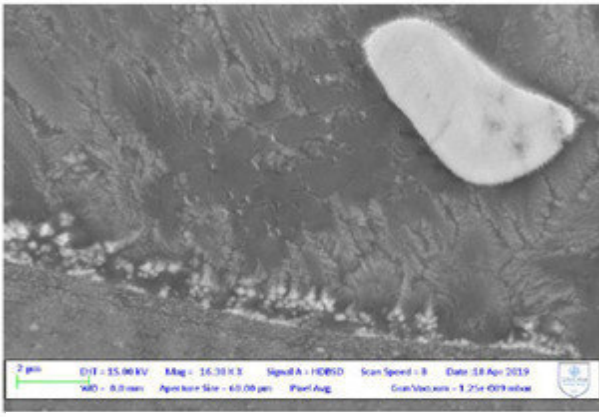


**Fig. 2.6.6.** – Crust chromite surrounded by dendritic magnetites

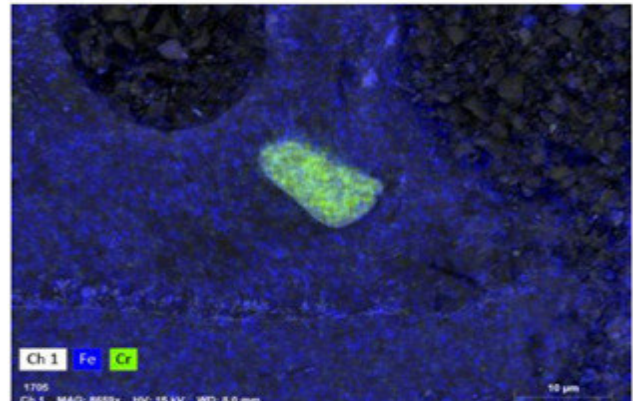


**Fig. 2.6.7.** – Map of element distribution (Fe and Cr)

We have found and classified 25 chromites – 11 from the bulk, 14 from the crust. The complete data record is available in the appendix: below is shown the graph reporting  $Al\#$  versus  $Mg\#$  for the bulk chromites (blue circles) and the crust chromites (red circles). The error bars reported represent the standard deviation. The separation between bulk and crust is evident; bulk chromites are more clustered around the average value than their crustal counterparts.

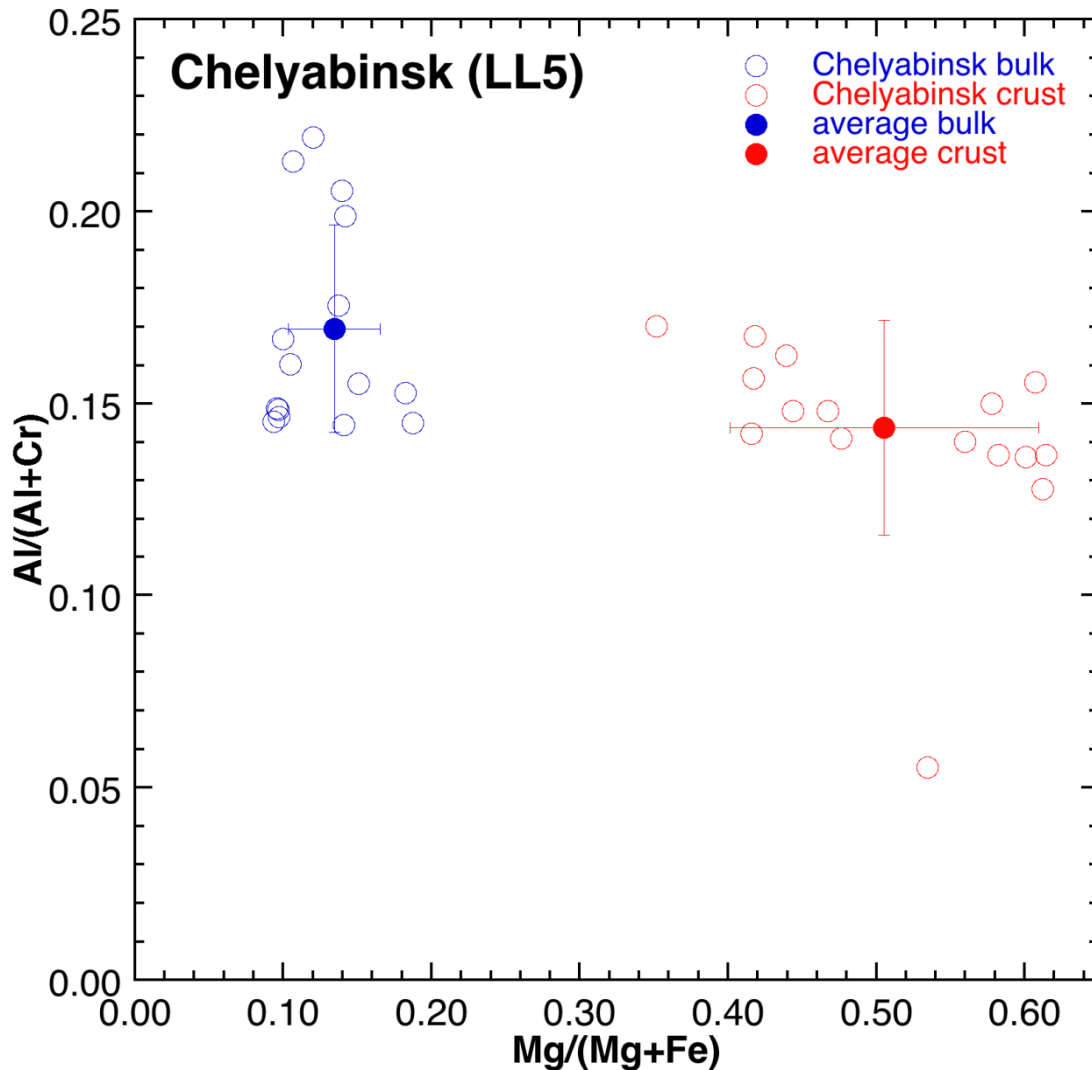


**Fig. 2.6.8.** – Plot of the  $Al\#$  versus the  $Mg\#$  for crust chromites (red) and bulk chromites (blue). The error bars represent the standard deviation.



## 2.7 Chergach (Mali)

**Fall. Ordinary chondrite, class H, petrologic type 5, shock stage S3, weathering grade W0.**

The following is a citation extracted from the *Meteoritical Bulletin* (MB94):

**“History:** In fall and winter, 2007 ~100 kg of meteorites were collected in the Erg Chech, north of Taoudenni. Nomads reported the stones fell after a smoke cloud was seen and several detonations were heard over a wide area during daytime in July 2007. The finder of the first meteorites was Mr Ouled Bleila, who died in a car accident on his way back from the trip to the Chergach strewn field in October 2007. According to the Tuareg people from Algeria who visited the fall site in September 2007, the elliptical strewn field stretches for more than 20 km in a northeasterly direction. No fireball was reported.

**Physical characteristics:** A large number of fusion-crust stones have been recovered, the largest ones are 17.8 and 13.9 kg, the smallest ones about 1.5 g. Total known weight ~100 kg.

**Petrography:** (E. Gnos, MHNGE; B. Hofmann, NMBE, M. Eggimann, UBE/NMBE) Mean chondrule size is 0.38 mm ( $n = 61$ ). Mean size of plagioclase grains is  $\sim 20 \mu\text{m}$ . Troilite is polycrystalline, rich in silicate inclusions, and shows diffuse boundaries to metal. Some metal is rich in silicate- and troilite inclusions. No Cu metal observed. Shock stage is S3, some shock veins are visible, no weathering (W0). In addition to this dominant lithology, a significant number of stones consist of chondritic clasts (H5 S3-4 W0, identical to the homogeneous lithology) set in a fine-grained, black, silicate impact melt matrix with abundant droplets of metal and metal-troilite. Shock stage of small clasts is up to S4.

**Mineral compositions and geochemistry:** Olivine  $\text{Fa}_{18.2}$  (chondrite fragments in impact melt are  $\text{Fa}_{18.4}$ ), pyroxene  $\text{Fs}_{15.5} \text{Wo}_{1.2}$  (fragments in impact melt are  $\text{Fs}_{16.0}$ ,  $\text{Wo}_{1.4}$ ).

**Cosmogenic radionuclides:** (Patrick Weber, Particle Physics Group, Institute of Physics, University of Neuchâtel) Gamma-spectroscopy performed in November, 2007 showed the presence of the following short-lived radionuclides:  $^{46}\text{Sc}$ ,  $^{56}\text{Co}$ ,  $^{54}\text{Mn}$ ,  $^{58}\text{Co}$ ,  $^7\text{Be}$ ,  $^{57}\text{Co}$ ,  $^{22}\text{Na}$ ,  $^{60}\text{Co}$ ,  $^{26}\text{Al}$ . Recalculated to July, 2007,  $^{22}\text{Na}$  was  $44.0 \pm 1.1 \text{ dpm/kg}$  and  $^{26}\text{Al}$   $20.8 \pm 0.8 \text{ dpm/kg}$ . The  $^{22}\text{Na}/^{26}\text{Al}$  activity ratio of 2.1 is consistent with a fall in July, 2007 and demonstrates that this material is not identical with Bassikounou.

**Classification:** Ordinary chondrite (H5), some stones suggest an H impact melt breccia. S3, W0.

**Type specimens and distribution:** 115 g at NMBE; 17.8 kg P. Hermann, Canada; 13.9 kg D. Gheesling, USA; 4.9 kg S. Buhl, Germany.”

A study of the metal-troilite textures in Chergach (and also in other meteorites) is available in Tomkins (2009); a recent paper by Łuszczek and Krzesińska (2020) focuses on the Cu content of this meteorite (along with others), in order to assess the resource potential of S-asteroids by analysing ordinary chondrites.

This sample shows the usual features of an ordinary H chondrite, with larger (40-50  $\mu\text{m}$  or more), mostly anhedral chromites in the bulk (figures 2.7.1 to 2.7.3) and smaller ( $\leq 15 \mu\text{m}$ ), subhedral to euhedral chromites present in the crust – often in association with dendritic magnetites and magnesiochromites (figures 2.7.4, 2.7.5, 2.7.6 and 2.7.8), and sometimes found encased in magnetite overgrowth (fig. 2.7.7). Chondrules are also present (fig. 2.7.9 features a radial pyroxene), with mixed sulfide/metal grains (fig. 2.7.10).

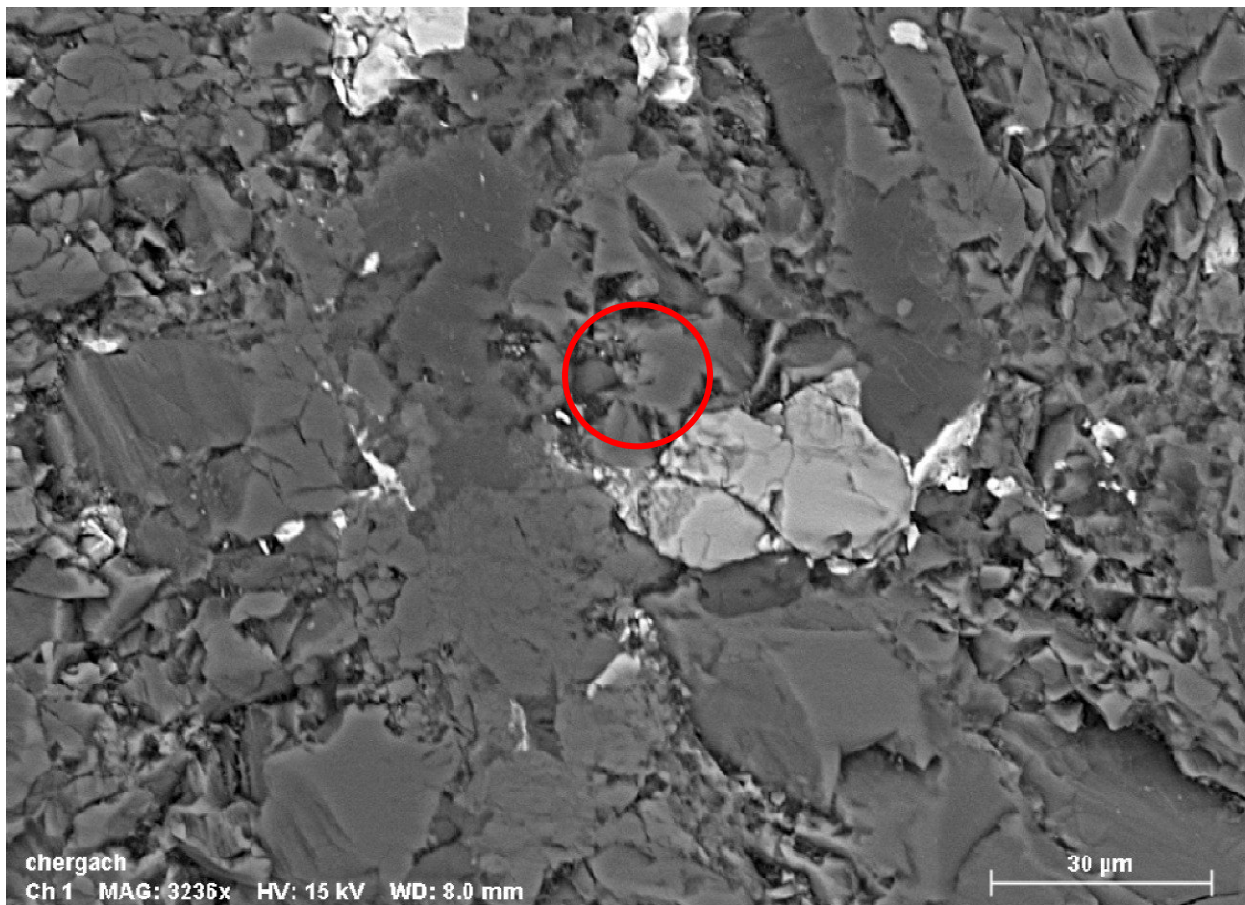


*Fig. 2.7.1. – Bulk chromite with apatite (red circle) and plagioclase nearby (darker grey) .*

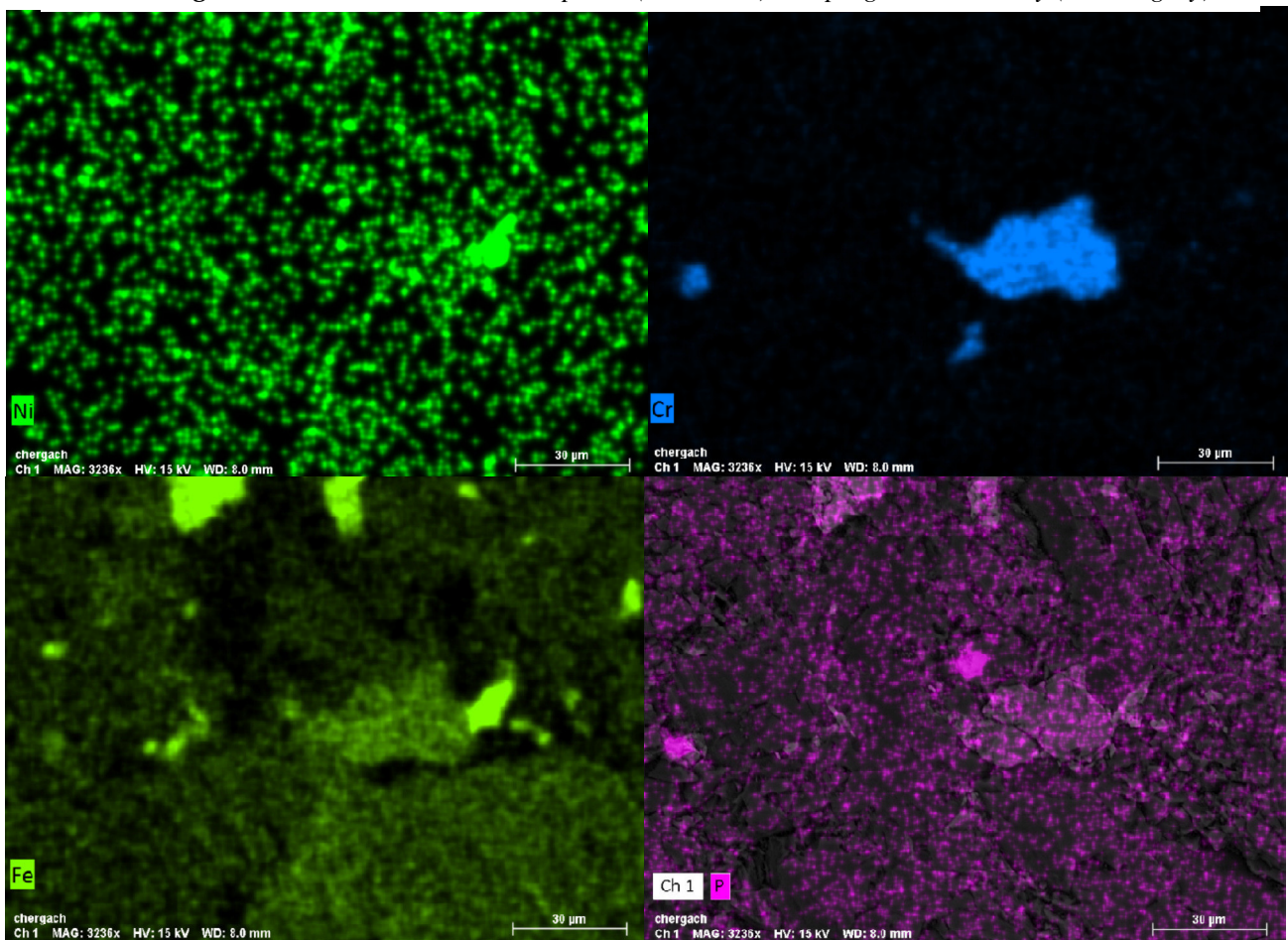


*Fig. 2.7.2. – Relative elemental abundances (Ni, Cr, Fe, and P) for the area represented in figure*



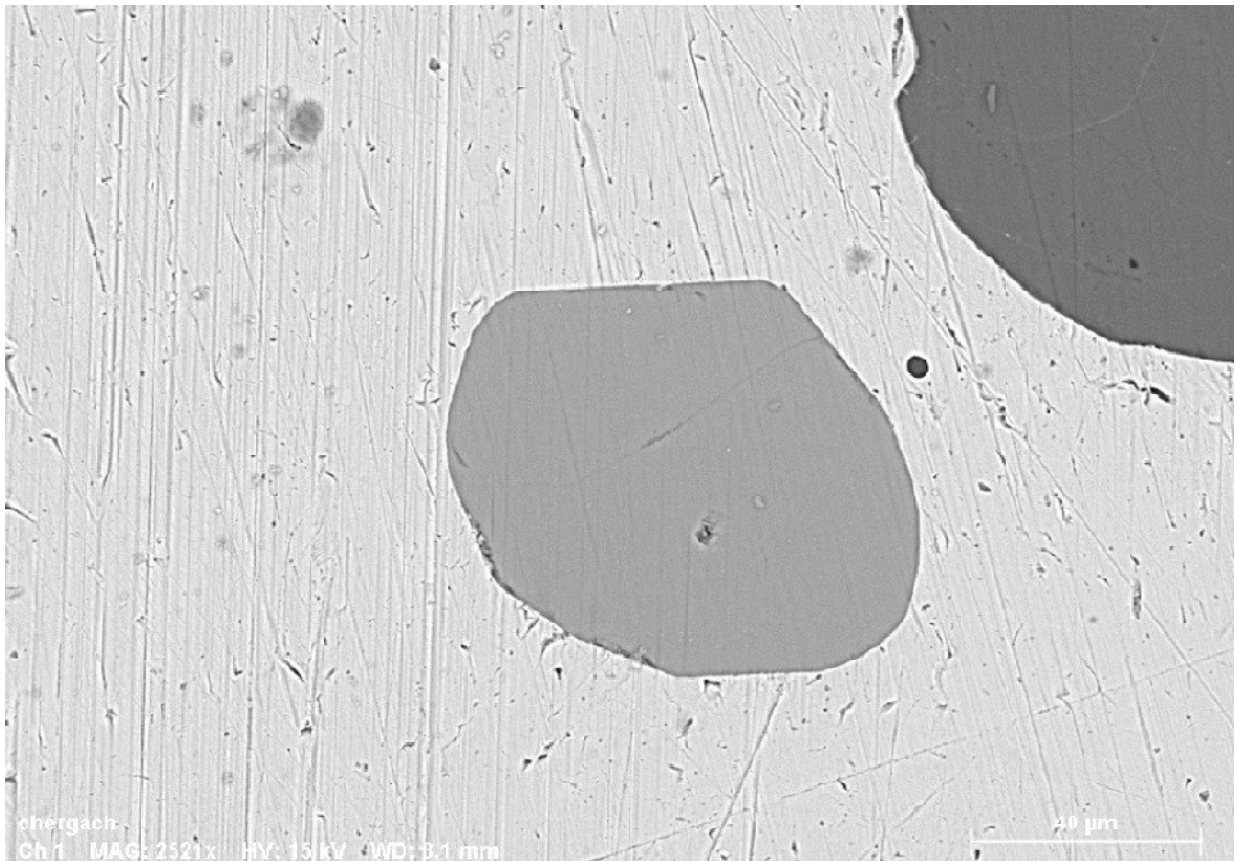


*Fig. 2.7.3. – Bulk chromite.*

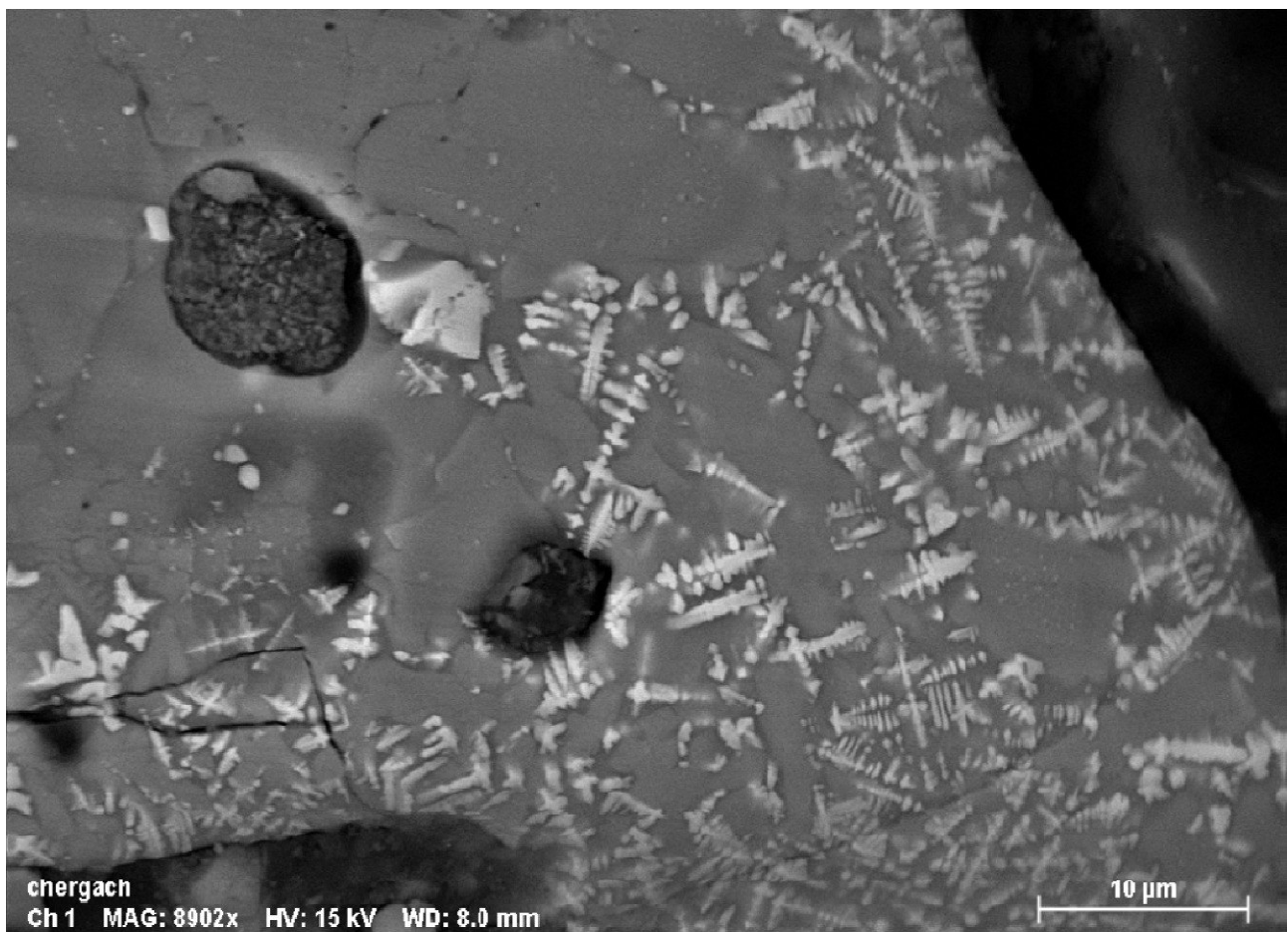


*Fig. 2.7.4. – Portion of the crust displaying crust chromites and dendritic magnetites.*



*Fig. 2.7.5. – Another crustal zone featuring crust chromites, dendritic magnetites and a magnesio-chromite (red circle).*



*Fig. 2.7.6. – Zooming in on the magnesio-chromite (green points). On the upper left (red circle) stands a magnesio-ferrite.*

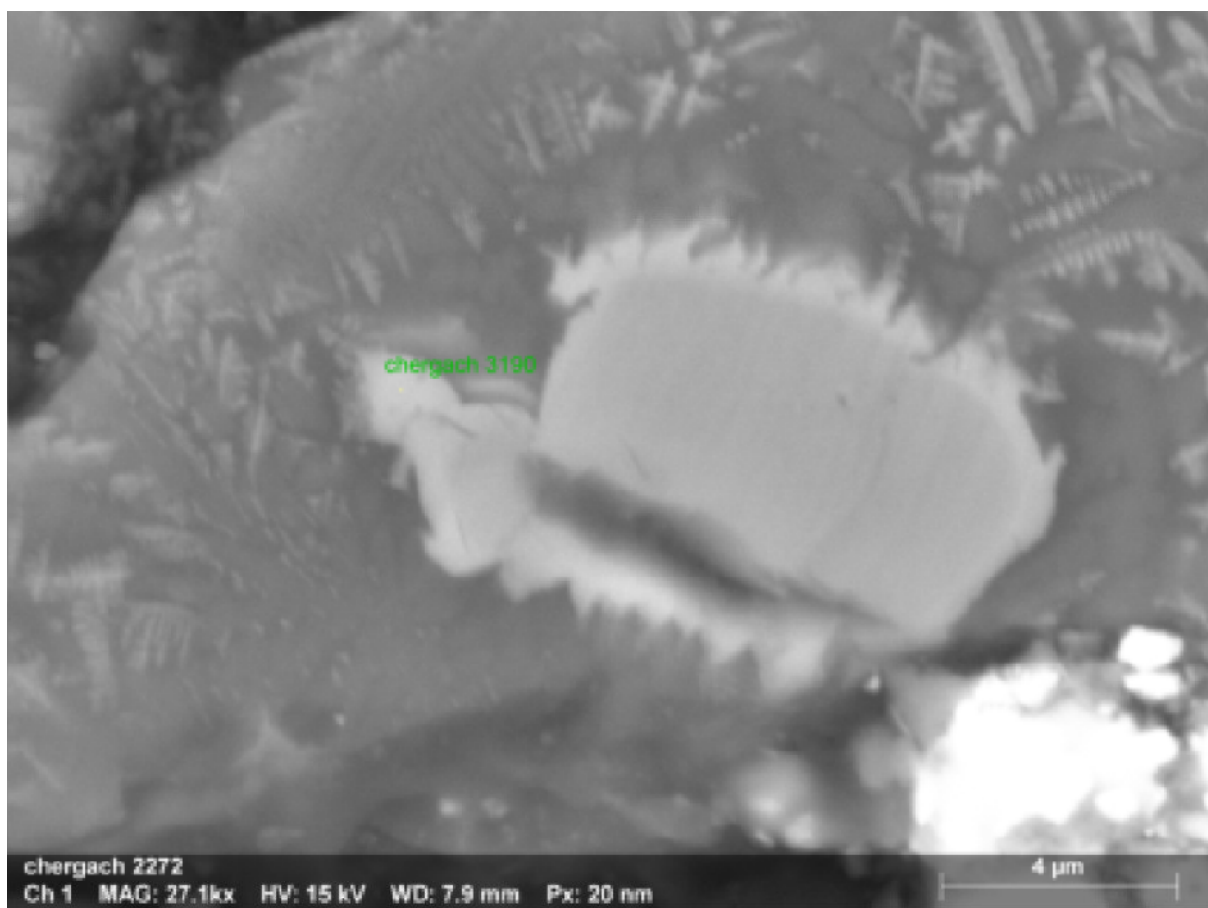


*Fig. 2.7.7. – A magnesio-chromite encased in magnetite overgrowth.*

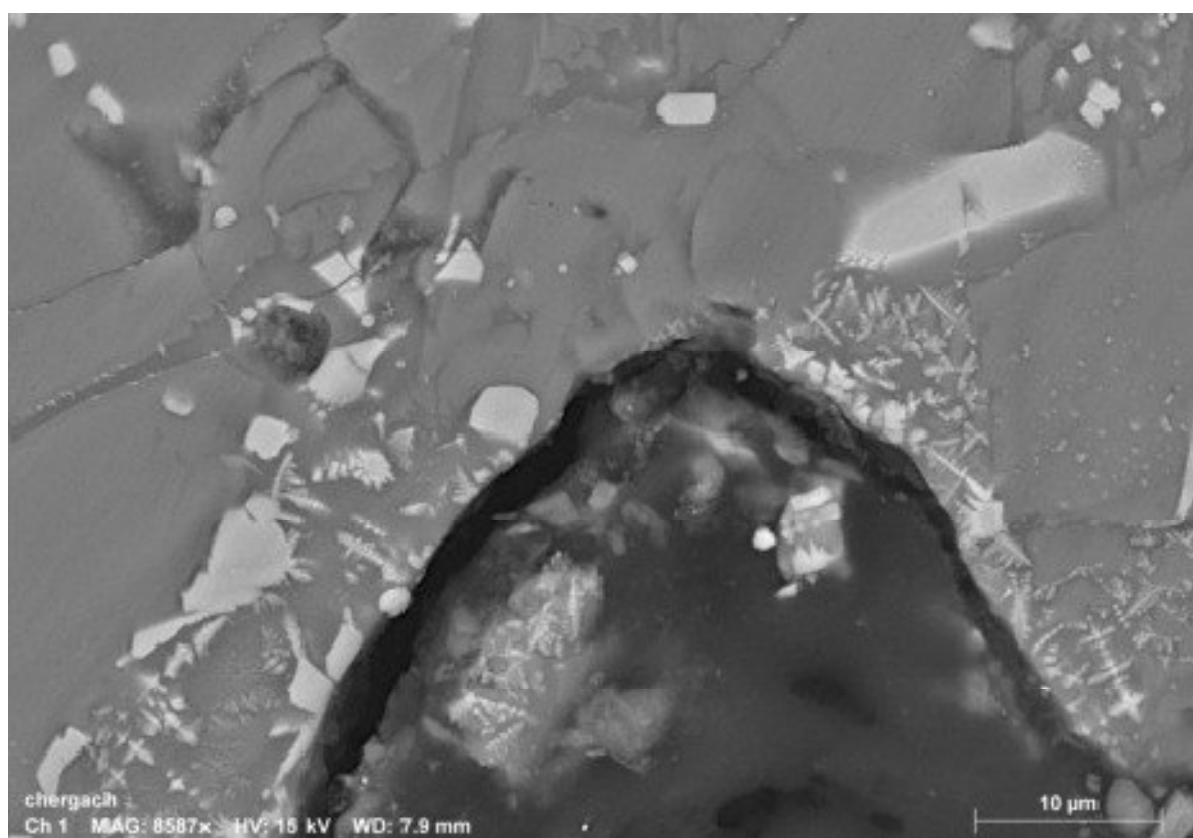


*Fig. 2.7.8. – Crustal zone with dendritic magnetites, chromites and magnesiochromites. Elemental abundance map also shows the presence of small amounts of Ti.*



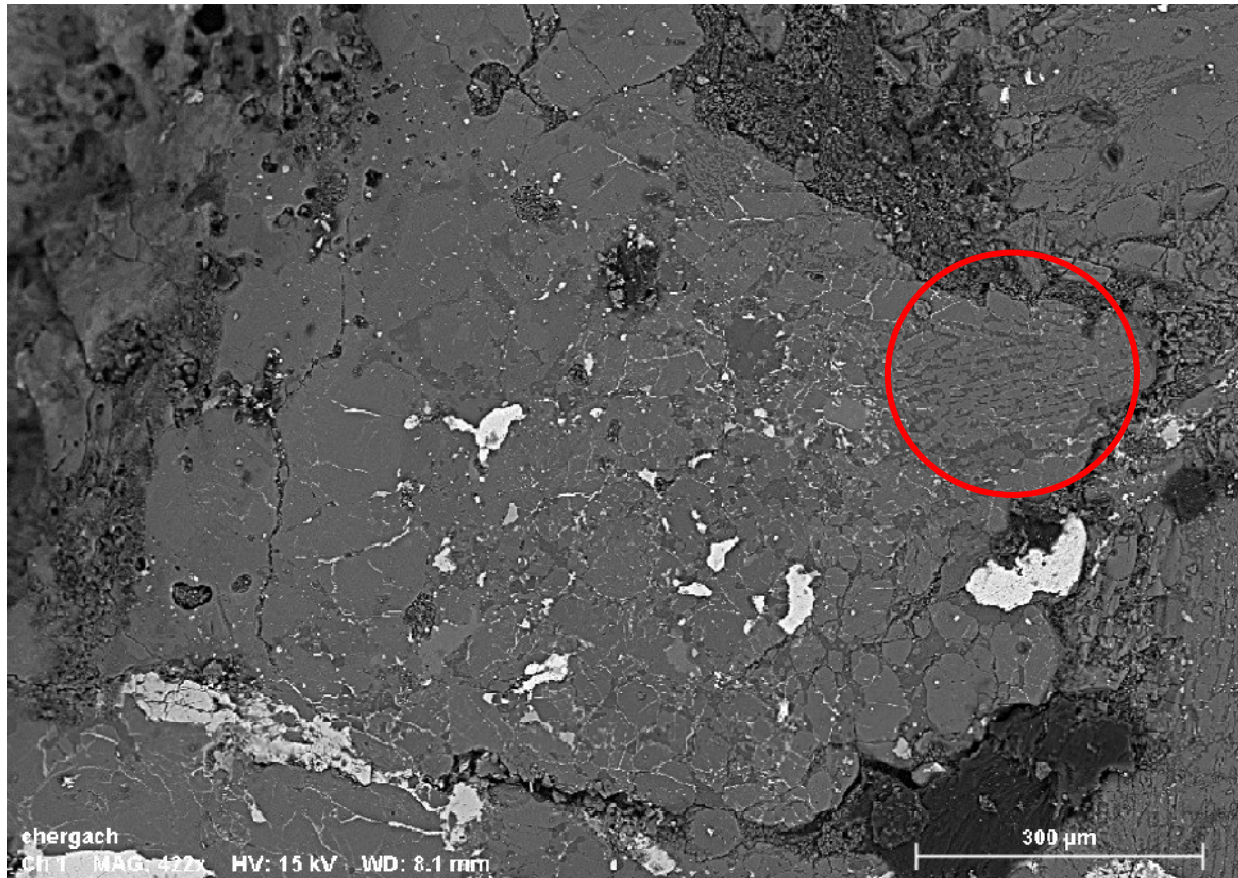
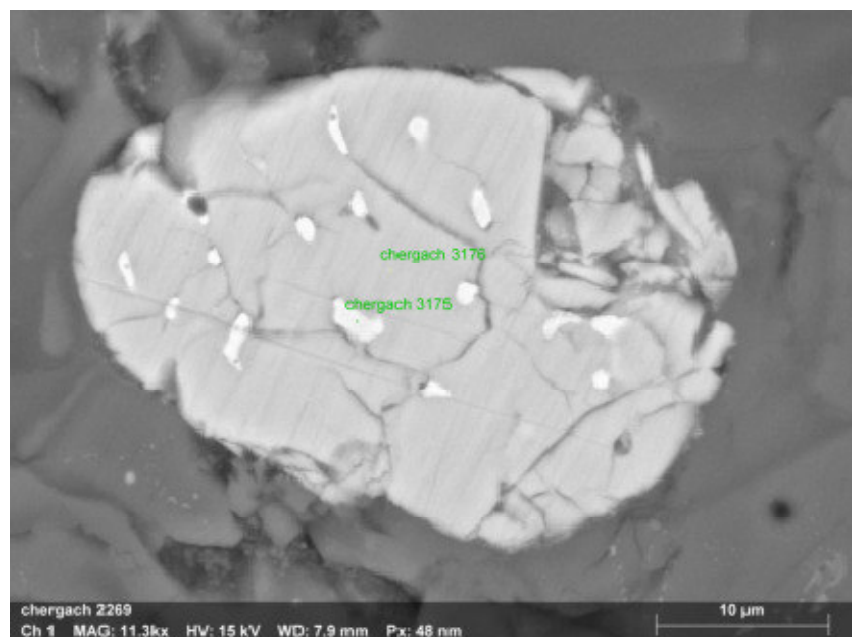


*Fig. 2.7.9. – A radial pyroxene.*

*Fig. 2.7.10. – A sulfide (troilite) grain, studded with small iron blebs. No nickel was found here.*



We have found and classified 31 chromites – 14 from the bulk, 17 from the crust. The complete data record is available in the appendix: below is shown the graph reporting Al# versus Mg# for the bulk chromites (blue circles) and the crust chromites (red circles). The error bars reported represent the standard deviation. The separation between bulk and crust is striking, as the great dispersion of the data for crust chromites; bulk chromites, on the other hand, are tightly clustered around the average value.

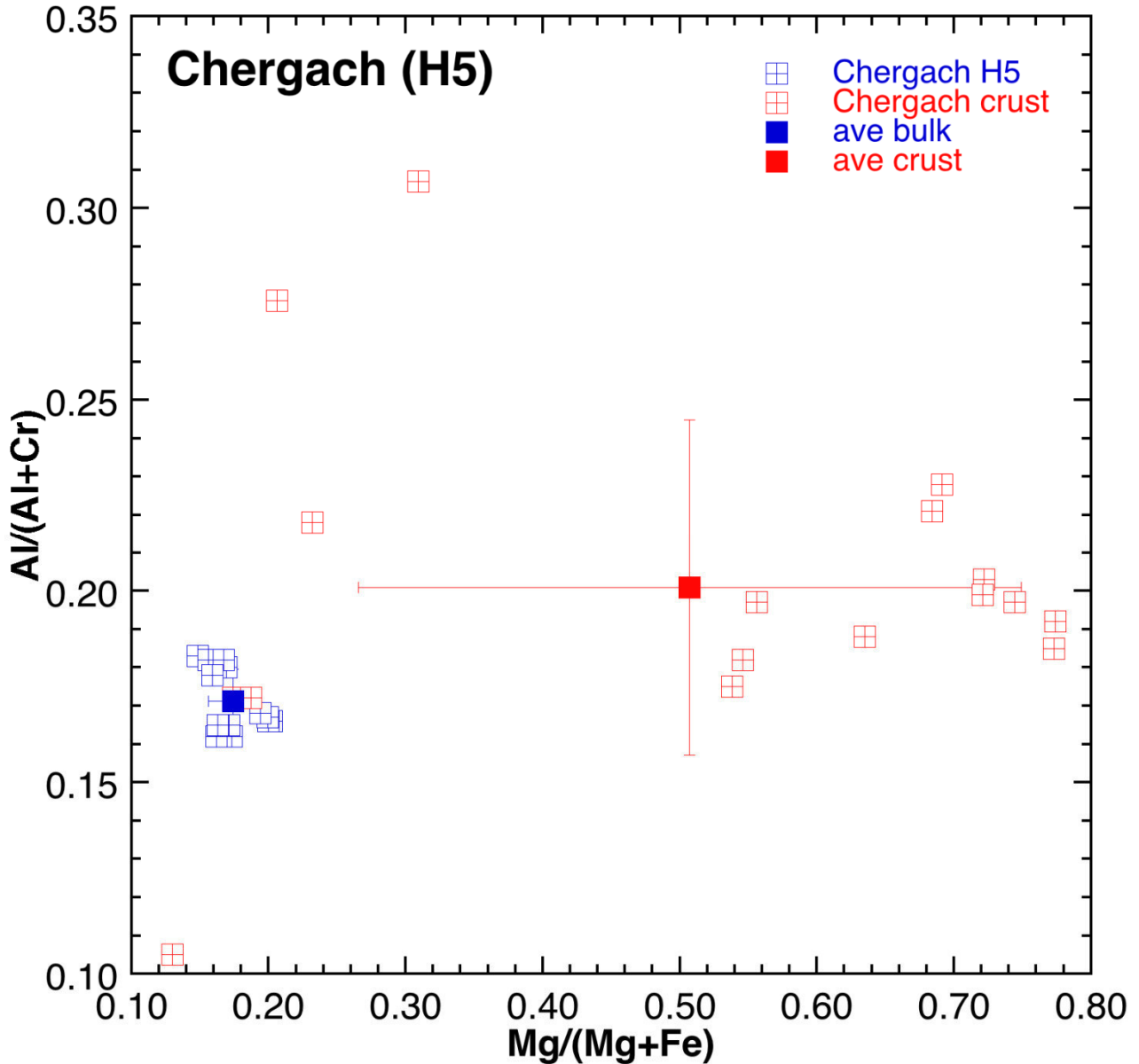


**Fig. 2.7.11.** Plot of the Al# versus the Mg# for crust chromites (red) and bulk chromites (blue). The error bars represent the standard deviation.

## 2.8 Kabo (Nigeria)

### ***Fall. Ordinary chondrite, class H, petrologic type 4.***

The following is a citation extracted from the *Meteoritical Bulletin* (MB51):

*“Kabo. Synonym: Gwarzo. Place of fall: Kabo, Gwarzo District, Kano State, Nigeria. 11° 50'N, 8° 09'E. Date of fall: April 25, 1971, about 4:30 p.m. local time (1530 GMT). Class and type: Stone. Olivine-bronzite chondrite (H5). Number of individual specimens:4. Total weight: More than 10 kg.*

*Circumstances of fall: The shower occurred on a Sunday afternoon while farmers were in their fields. Sound directions and crater asymmetry indicated that the meteorite approached from the west. "Thunder-like sounds were heard consecutively and these were followed by the inclined descent of a reddish object with trails of cloudy smoke following it". During the following week the District Head collected the specimens and forwarded them to the Emir of Kano. One specimen was recovered in two pieces of about 3 kg each, one stone weighed over 5 kg, one almost 3 kg, and the smallest 0.9 kg.*

*Sources: Report of a field investigation by T. A. Badejoko, Department of Geology, University of Ibadan, Nigeria, forwarded by Professor M. O. Oyawoye, Head of Department. Dr. Deborah E. Ajakaiye, Ahrnadu Bello University, Zaria, Nigeria. Report circulated by Smithsonian Institutions Center for Short-Lived Phenomena, Cambridge, Massachusetts (Event number 51-7, cards number 1218, 1236 and 1263 of May 24, June 9 and July 23, 1971).”*

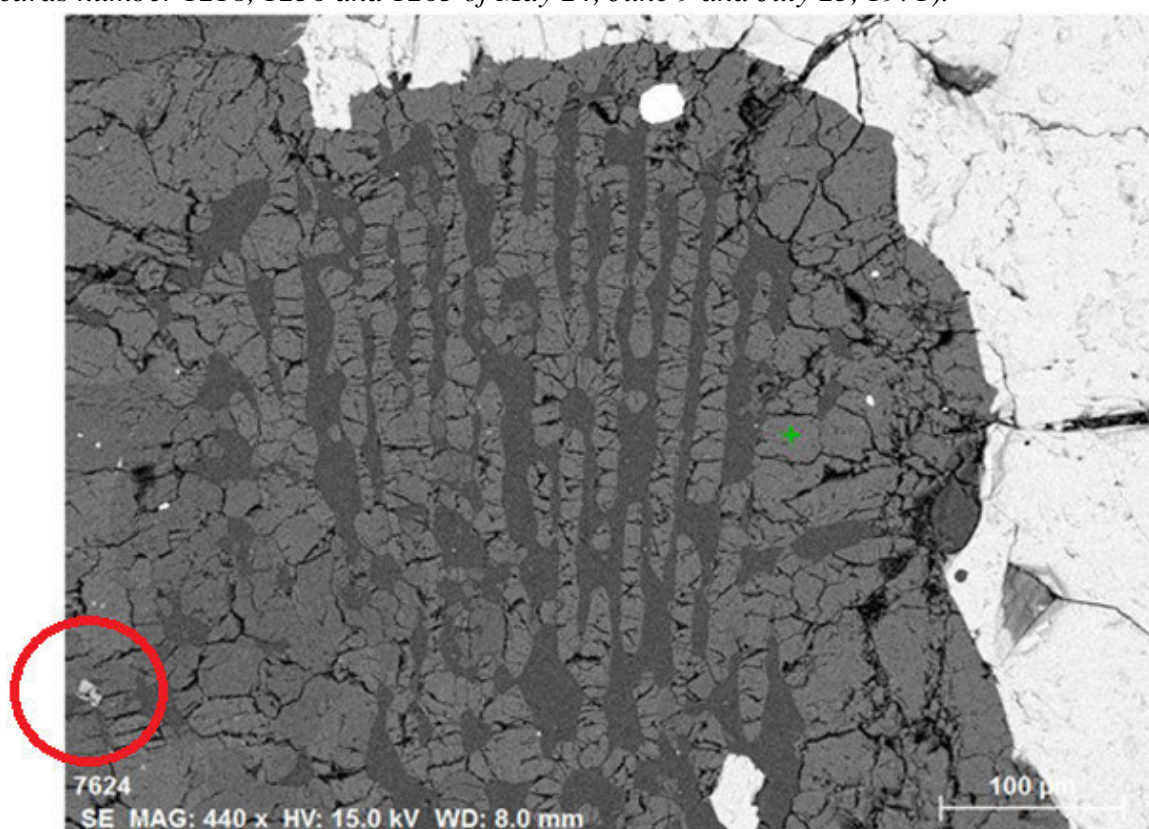


**Fig. 2.8.1. – Barred olivine chondrule**

Additional information about this fall can be found in Hutchison *et al.* (1973).

Like any ordinary H chondrite, Kabo displays a high content of siderophile elements. Given its petrologic type (4), it has numerous chondrules (~0,3 mm across) which have been



metamorphosed enough to homogenize olivine chemical composition and re-crystallise the fine-grained matrix.

The barred olivine chondrule portrayed in figure 2.8.1 exhibits a fayalite content of ~ 30% and a typical mesostasis with Na and K. To the left (bottom, red circle) an (almost) euhedral

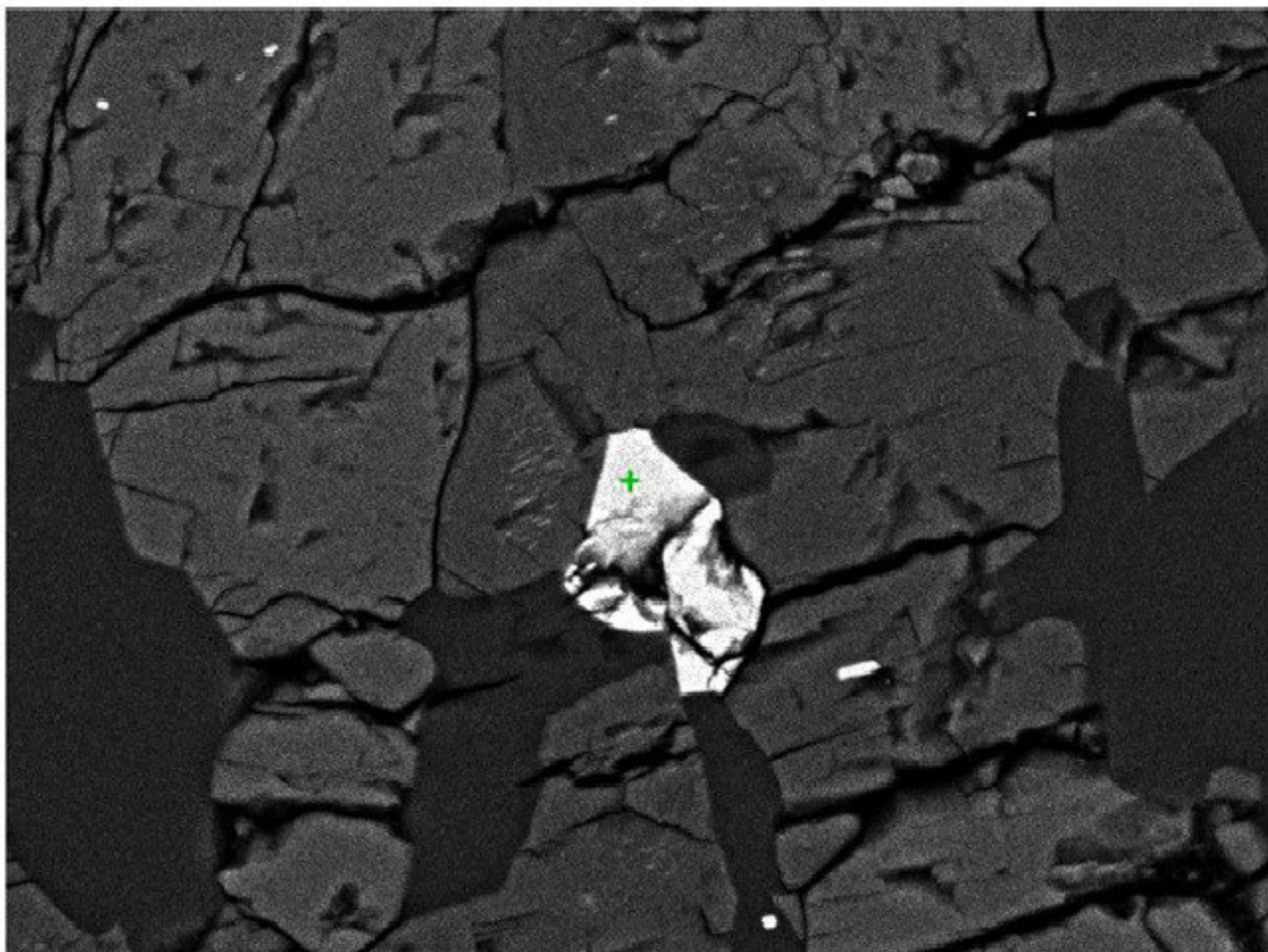


**Fig. 2.8.2.** – Euhedral chromite found at the boundary of the barred olivine chondrule.

chromite is visible, also magnified in figure 2.8.2; part of the octahedral structure is easily recognizable.

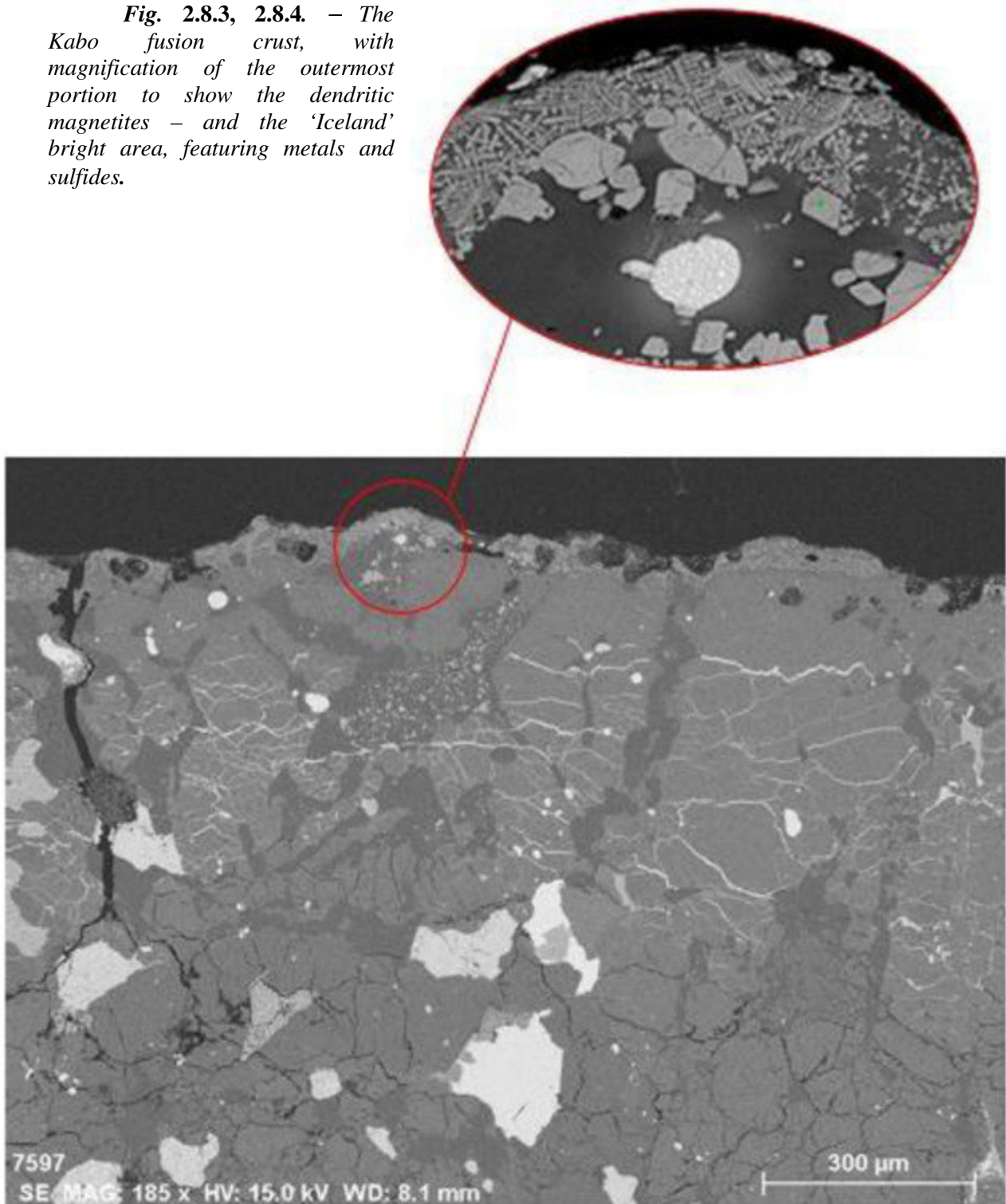
This BSE image also shows the various nuances of grey, generated by the different electronic density of pyroxene (darker) and olivine (lighter); the mesostasis is clearly visible among the olivine bars.

The fusion crust is well-developed in this meteorite (fig. 2.8.3 and 2.8.4 – with a zooming on the outer crust). Sulfide veins are evident in the sub-crustal area, whereas the outermost crust displays a host of dendritic magnetites; also very interesting looks the bright, roughly circular area (whose shape reminds of Iceland) in the bottom of the oval image. SEM analyses found a composition of sulfides studded with Fe-Ni metal grains; this feature will deserve further attention.

Figure 2.8.5 shows a chromite surrounded by magnetite – a feature also found in other meteorites examined in this work. Like in other similar structures, the  $Mg\#$  for the chromite is higher than the average value for chromites lacking a magnetite sheath; consequently, the Fe content is lower.



**Fig. 2.8.3, 2.8.4.** – *The Kabo fusion crust, with magnification of the outermost portion to show the dendritic magnetites – and the ‘Iceland’ bright area, featuring metals and sulfides.*



We have found and classified 21 chromites in this sample – 10 from the bulk, 11 from the crust. The complete data record is available in the appendix: we show below the graph reporting  $Al\#$  versus  $Mg\#$  for the bulk chromites (blue crosses) and the crust chromites (red crosses). The error bars reported represent the standard deviation. The dichotomy bulk/crust is evident, as is the much wider dispersion of the crust chromites around the average value.

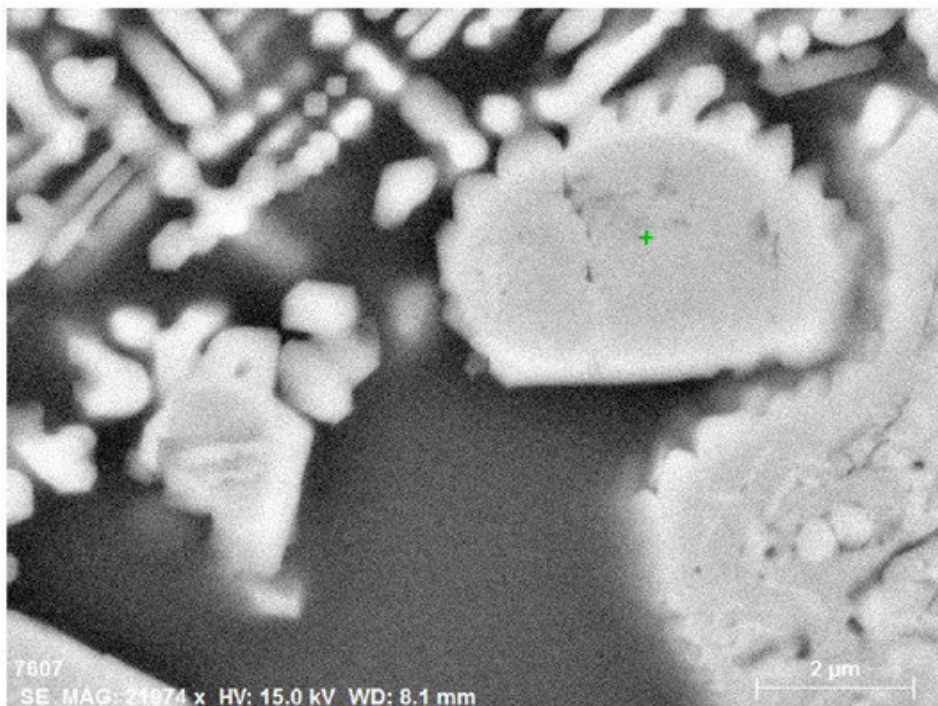


**Fig. 2.8.5.** – Chromite surrounded by dendritic magnetites

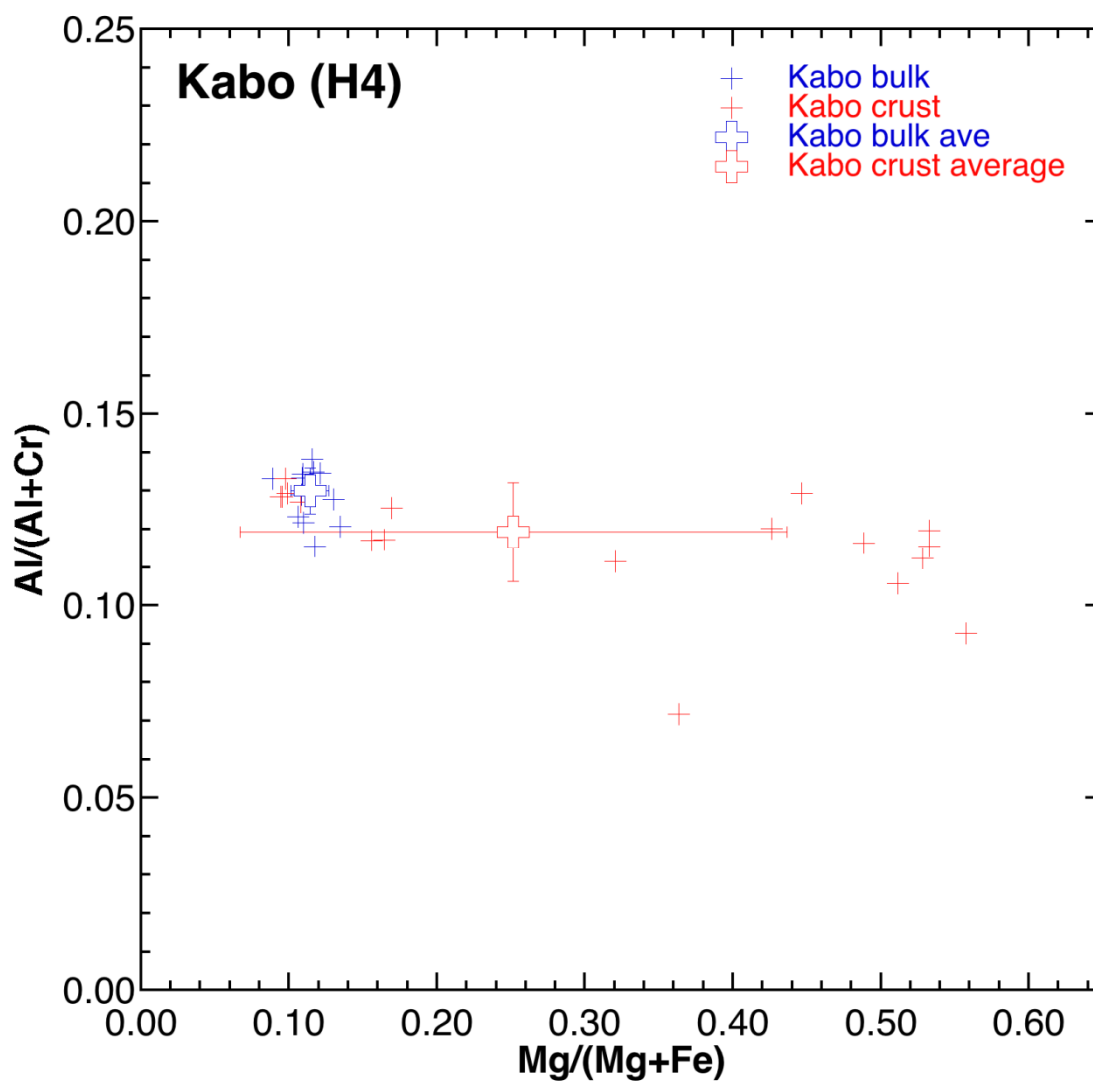


**Fig. 2.8.6.** Plot of the Al# versus the Mg# for crust chromites (red crosses) and bulk chromites (blue crosses). The error bars represent the standard deviation.

## 2.9 Kilabo (Nigeria)

**Fall. Ordinary chondrite, class LL, petrologic type 6, shock stage S3, weathering grade W0.**

The following is a citation extracted from the *Meteoritical Bulletin* (MB87):

“Kilabo 12°46'N, 9°48'E Nigeria Fell 2002 July 21, 19:30 hrs local time. Ordinary chondrite (LL6.) Mr. Mallam Yahava Muhammad of Hadejia, Nigeria, observed a brilliant fireball moving south to north. Two loud detonations were heard several minutes later. Mr. Mallam Audu and several neighbours in Kilabo heard the stone fall and later recovered it. The meteorite was found in the crater measuring 35 cm wide by 20 cm deep in sandy soil. The meteorite had fragmented on impact into many pieces, the largest of which was 2.2 kg. A total weight of ~19 kg was recovered. Stones were recovered in five villages in the region, with the largest piece in Kilabo. Classification (P. Sipiera, Harper; M. Zolensky, JSC): olivine, Fa31.1, CaO”

Several papers were written about Kilabo – such as Alexeev *et al.* (2008) (focusing upon luminescence, track and cosmogenic radionuclides), Cole *et al.* (2007) (on cosmic-ray exposure history), Yakame *et al.* (2012) (on shock textures) and Ustinova *et al.* (2008) (on the orbit and the possible parent body), to cite but a few.

This meteorite is a fall, fragmented on impact into many pieces. The largest was 2.2 kg, with a total weight of ~19 kg recovered. Stones were found five villages in the region, with the largest piece in Kilabo. Data for classification: olivine, Fa31.1, CaO <0.09, predominantly <0.05. Low Ca-pyroxene, Fs27.1 PMD = 0.02 (P. Sipiera, Harper; M. Zolensky, Johnson Space Center, in the Meteoritical Bulletin Database). Abundant

coarse-grained plagioclase, mainly An84Or5, ranges from An61Or25 to An86Or3. Coarse-grained diopside and troilite are abundant; pentlandite is a minor phase. The meteorite is brecciated, with thick black shock veins present.

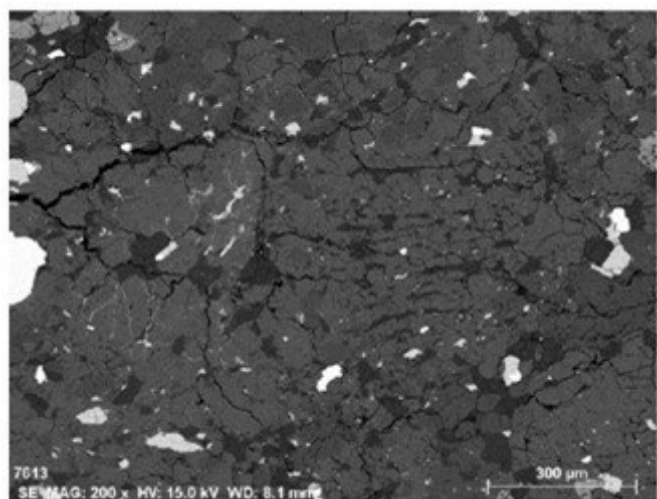
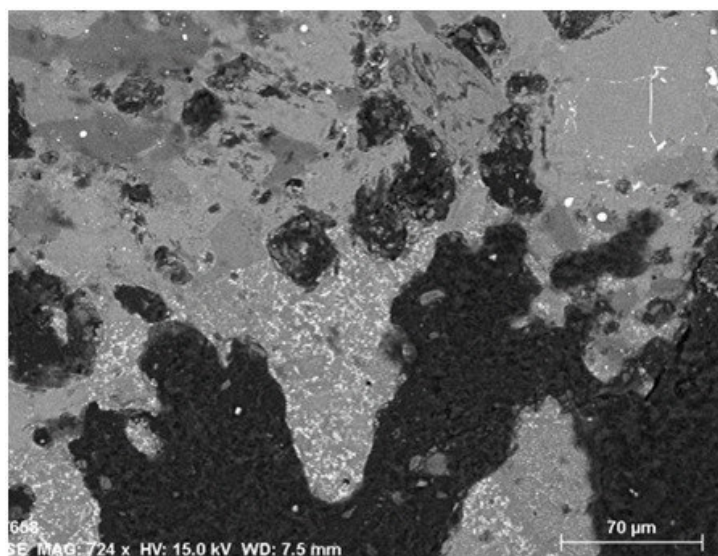


**Fig. 2.9.1.** A barred olivine



The advanced petrological type (6) speaks of a metamorphosed object with low-Ca pyroxenes converted to orthopyroxenes and coarse-grained secondary phases, like feldspar. Many chondrules of the sample have been obliterated, so that their characterisation by optical microscope was quite difficult. Only by SEM a barred olivine could be spotted and studied (fig. 2.9.1); its boundaries are ill-defined and the

**Fig. 2.9.2.** BSE image of Kilabo's fusion crust



mesostasis between the bars was predominantly plagioclase.

This sample displays a remarkably well-preserved fusion crust. Some areas of the outer crust host many dendritic magnetites, which is a tell-tale crustal signature; their peculiar comb-like morphology is the result of fast cooling (fig. 2.9.2).

At greater magnification magnetite crystals (about some hundred of nanometers to some microns across) exhibit an octahedral morphology.

Bulk chromites vary greatly in size, from a few microns up to 100  $\mu\text{m}$ . In figure 2.9.3, for instance, the largest chromite is about 90  $\mu\text{m}$  across, whereas the small crystal inside the olivine is barely above 3  $\mu\text{m}$ .

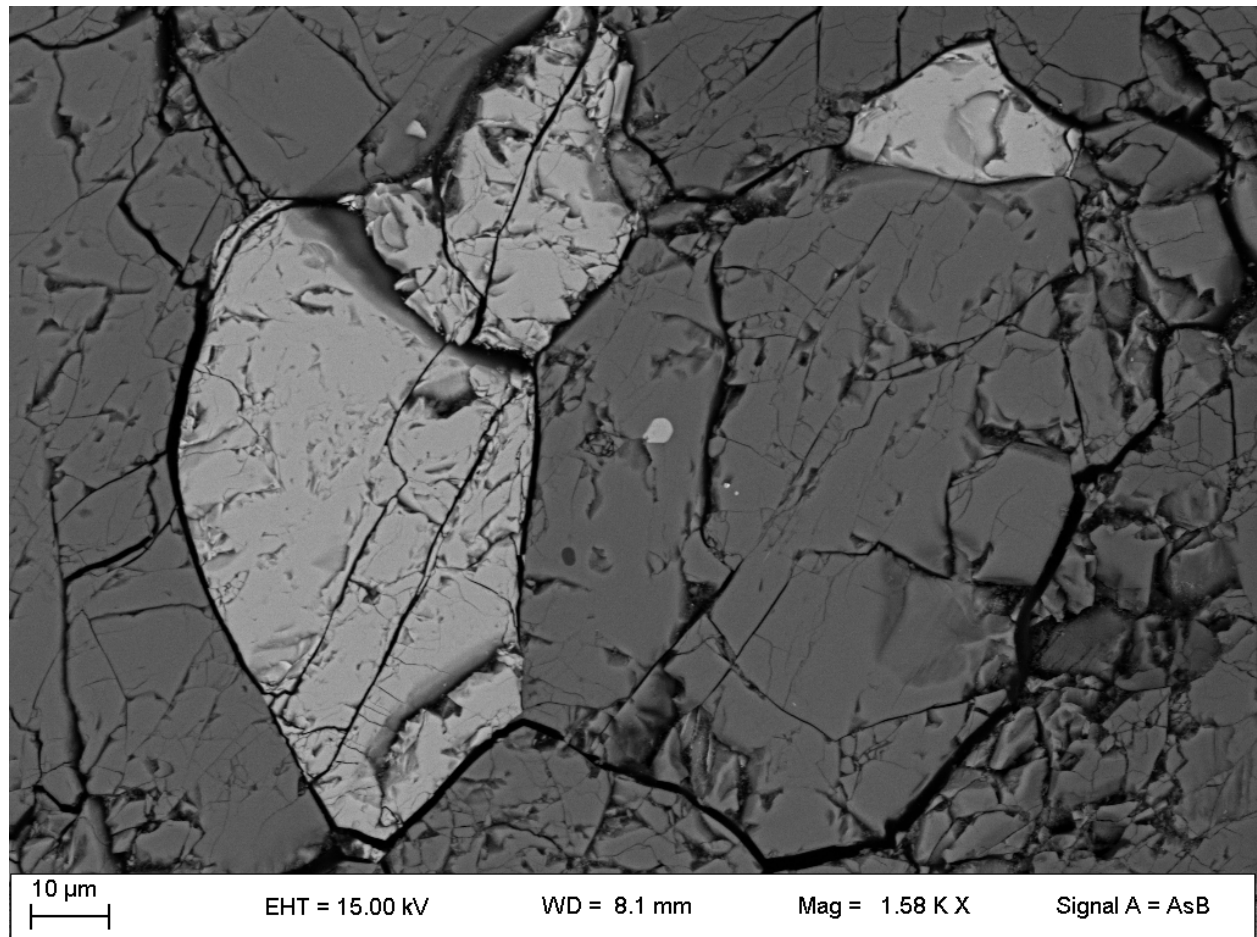


**Fig. 2.9.3.** *Chromites from the bulk of Kilabo*

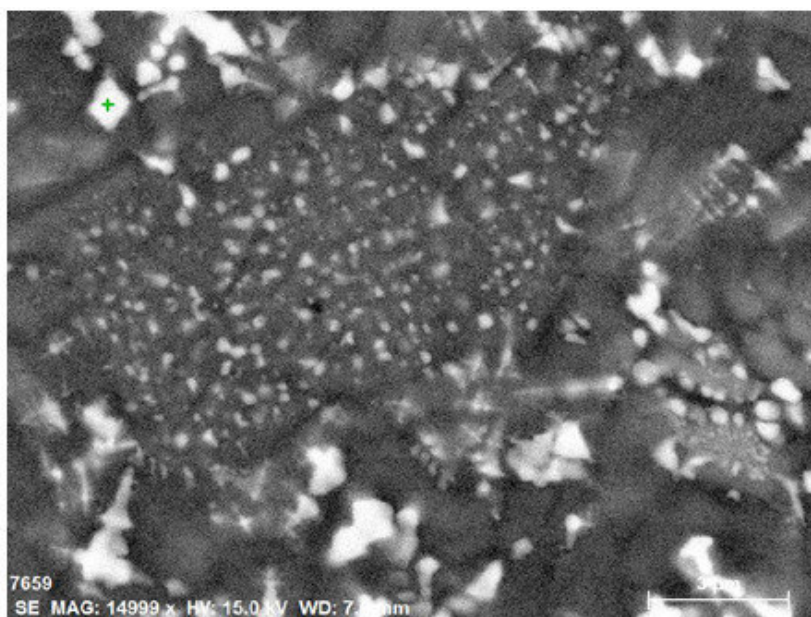


**Fig. 2.9.4.** *Dendritic magnetites have an octahedral structure which is clearly visible in the picture*



Like other samples examined in the present work, chromites found within the fusion crust are generally smaller than their bulk counterparts, varying in size from a few microns (sometimes even less) to tens of microns – often with dendritic magnetites nearby (figures 2.9.4 to 2.9.6).

In the outermost part of the crust we found a chromite surrounded by a ring of dendritic magnetites (figures 2.9.7 and 2.9.8). The SEM image clearly shows that iron from the magnetite forms a ring around the chromite, with a Mg-content higher with respect to other chromites.

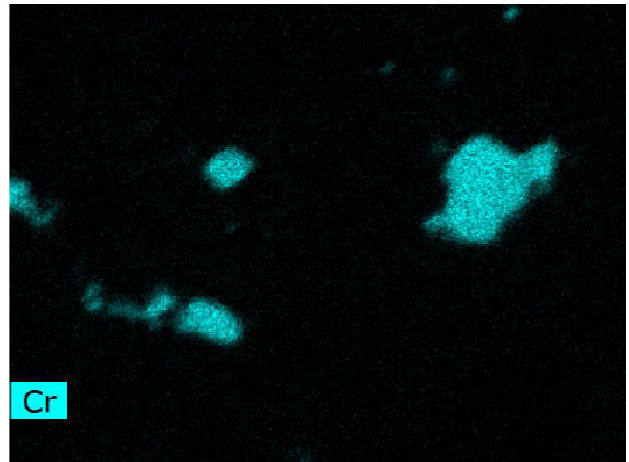
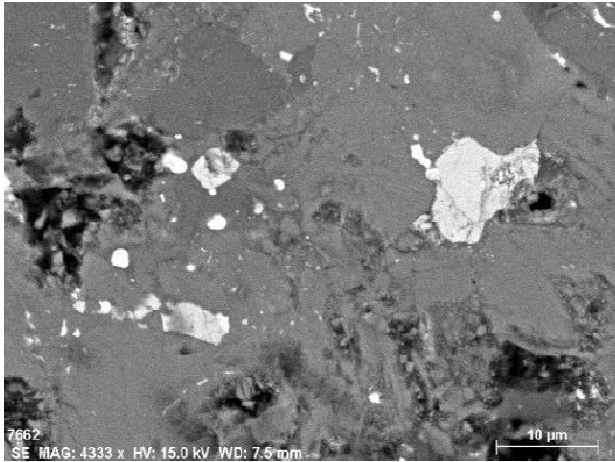


**Fig 2.9.5, 2.9.6.** *Chromites within the fusion*

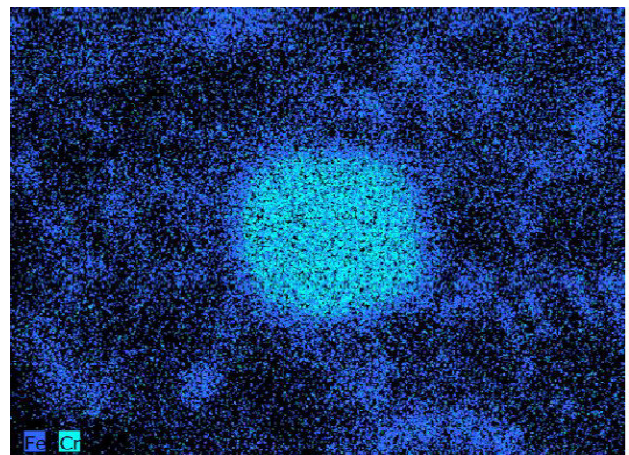
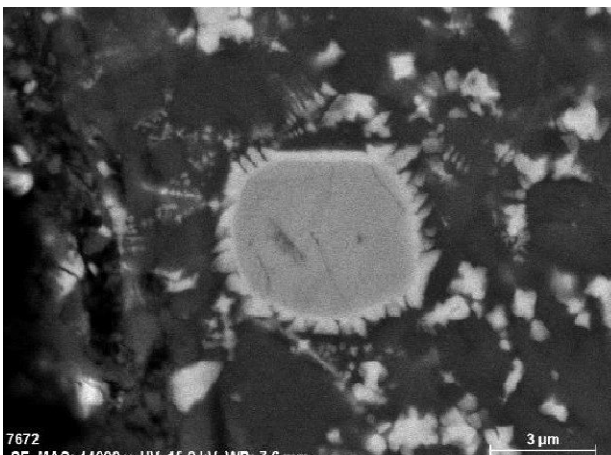


**Fig. 2.9.7, 2.9.8 .** *Chromite encased in dendritic magnetites and map of relative element abundance*

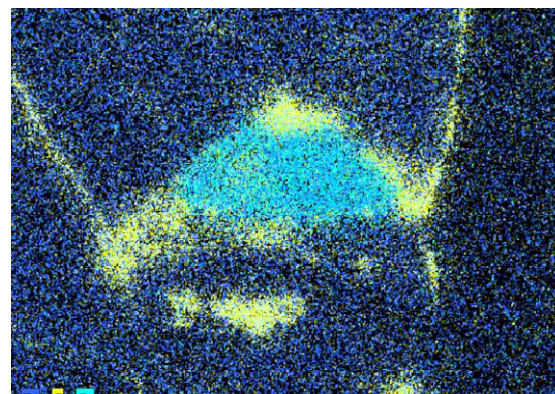
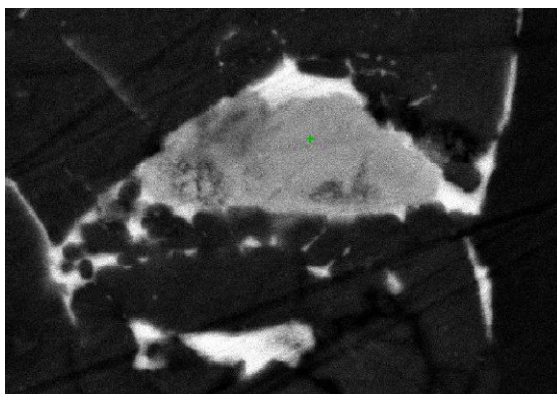


**Fig. 2.9.9, 2.9.10.** *Iron sulfide veins surrounding a crustal chromite and relative abundance map (Fe, S, Cr).*

This meteorite also displays sulfide veins surrounding or crossing many chromites (figures 2.9.9 and 2.9.10). Particularly interesting are the spherules of Fe/Ni sulfide found in the fusion crust, which are no doubt worth further analysis (fig. 2.9.11).

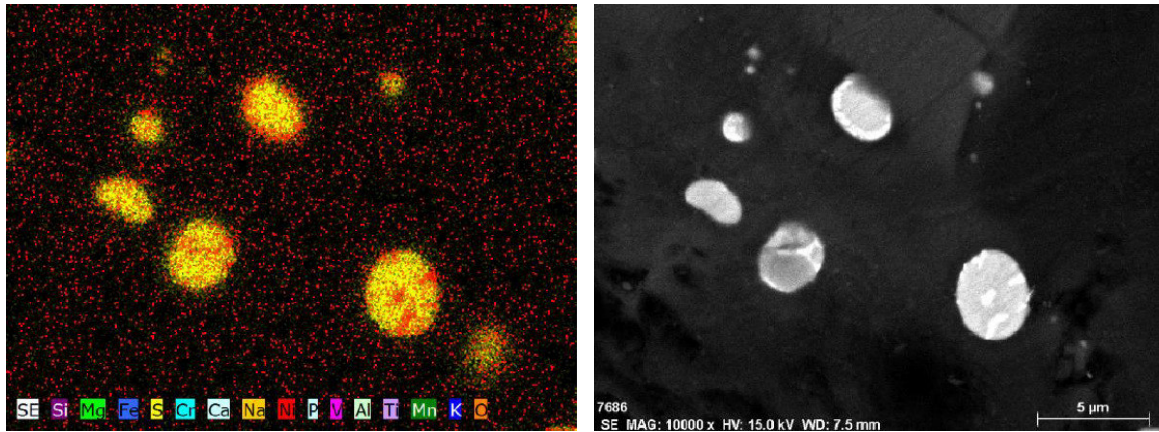


**Fig. 2.9.11.** Spherules of Ni sulfide and map of element distribution

We have found and classified 22 chromites – 13 from the bulk, 9 from the crust. The complete data record is available in the appendix: below is shown the graph reporting Al# versus Mg# for the bulk chromites (blue) and the crust chromites (red). The error bars reported represent the standard deviation. The separation between bulk and crust is clearly visible, with bulk chromites much more clustered around the average value than crust chromites – which, for their part, look also richer in magnesium than bulk chromites.

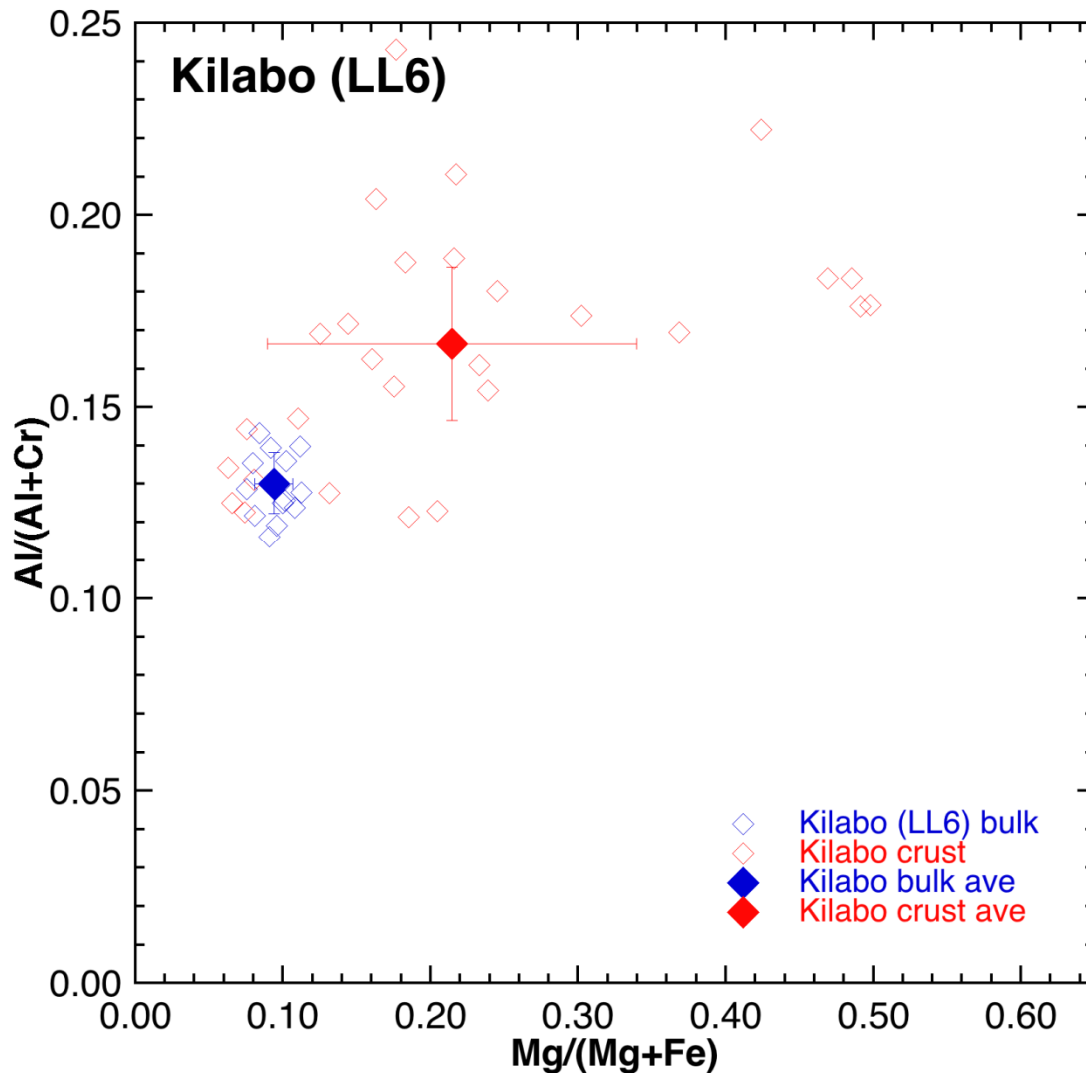


**Fig. 2.9.12.** Plot of the Al# versus the Mg# for crust chromites (red) and bulk chromites (blue). The error bars represent the standard deviation.



## 2.10 NWA869 (Northwestern Africa)

**Find.** Ordinary chondrite, breccia, type L3-6, shock stage S3, weathering grade W1. The precise location of the strewn field from where the specimen was collected is unknown.

This meteorite, initially L4-6 (breccia), was later revised to L3-6. The following is a citation extracted from the *Meteoritical Bulletin* (MB90):

*“Revised classification and description. Submitted by K. Metzler, IfP, with data from Metzler et al. (2011) and Welten et al. (2011).*

*Physical characteristics:* Most samples are individual meteorites but some fragments (mostly >1 kg) also occur. In most cases the fusion crust has been polished or ablated by wind erosion. Many samples are more severely affected and show faces with deep wind erosion features. Fracture faces, formed by ground collision, show a typical gray-green color and sometimes visible brecciation (light and/or dark clasts). Due to the coarseness of this breccia, there are some stones that consist of only a single lithology.

*Petrography:* This chondritic breccia consists of about 75 vol% matrix with unequilibrated and equilibrated L-chondrite clasts (up to 5.5 cm), some of which display shock-darkening. Impact melt-rock clasts, themselves either clast-free or clast-poor, also occur and are strongly depleted in Fe,Ni metal and sulfide.

*Geochemistry:* Northwest Africa 869 is a regolith breccia, containing solar noble gases and preirradiated lithologies. Olivine in lithic clasts:  $Fa_{0.2-49.2}$ ; olivine in matrix:  $Fa_{10.3-29.3}$ ; low-Ca pyroxene in lithic clasts:  $Fs_{2.1-35.9}$ ; low-Ca pyroxene in matrix:  $Fs_{7.0-23.9}$ . Bulk oxygen isotopes:  $\delta^{17}O = 3.52$ ;  $\delta^{18}O = 4.67$ ;  $\Delta^{17}O = 1.09$  per mil. Terrestrial age:  $4.4 \pm 0.7$  ka. Preatmospheric meteoroid size and mass:  $225 \pm 25$  cm, 120-230 T.

*Classification:* Because NWA 869 contains unequilibrated clasts, its classification is revised to L3-6.”

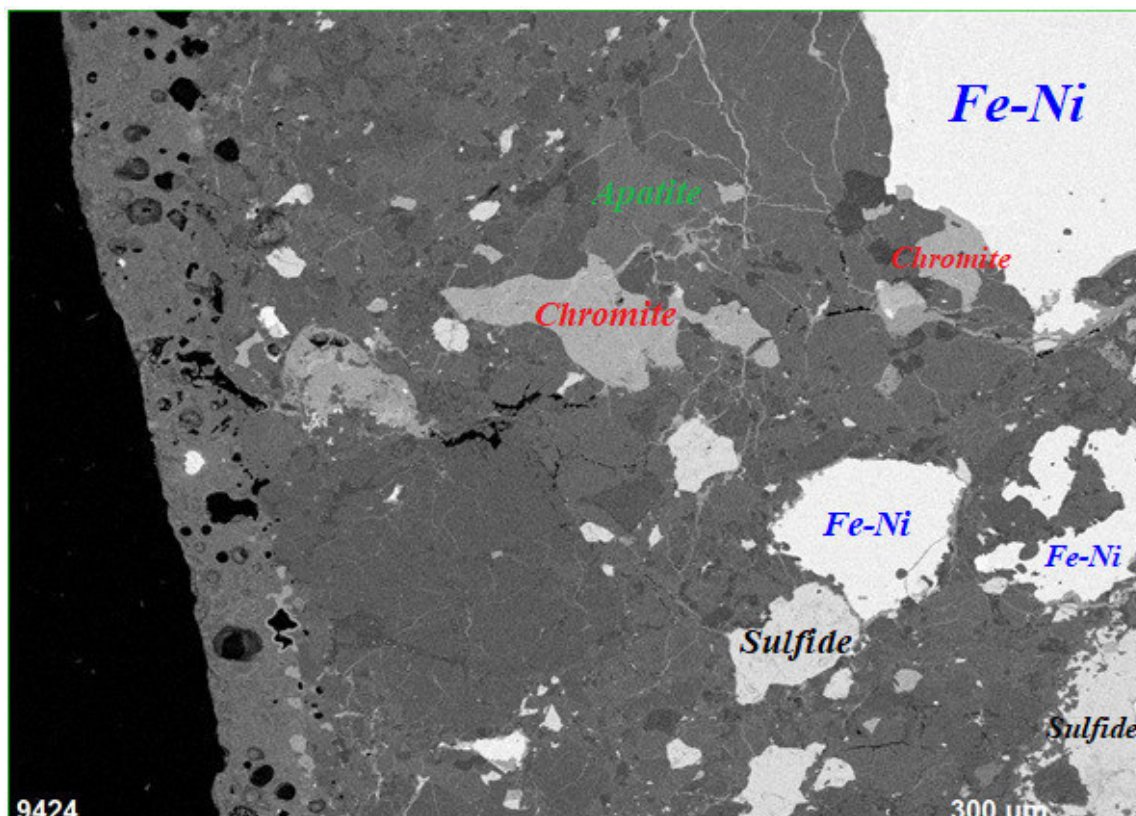


**Fig. 2.10.1.** View of the crust/sub-crustal zone/bulk. The crust is easily recognizable by the cavities left after degassing of volatiles; some of the most prominent minerals are reported.



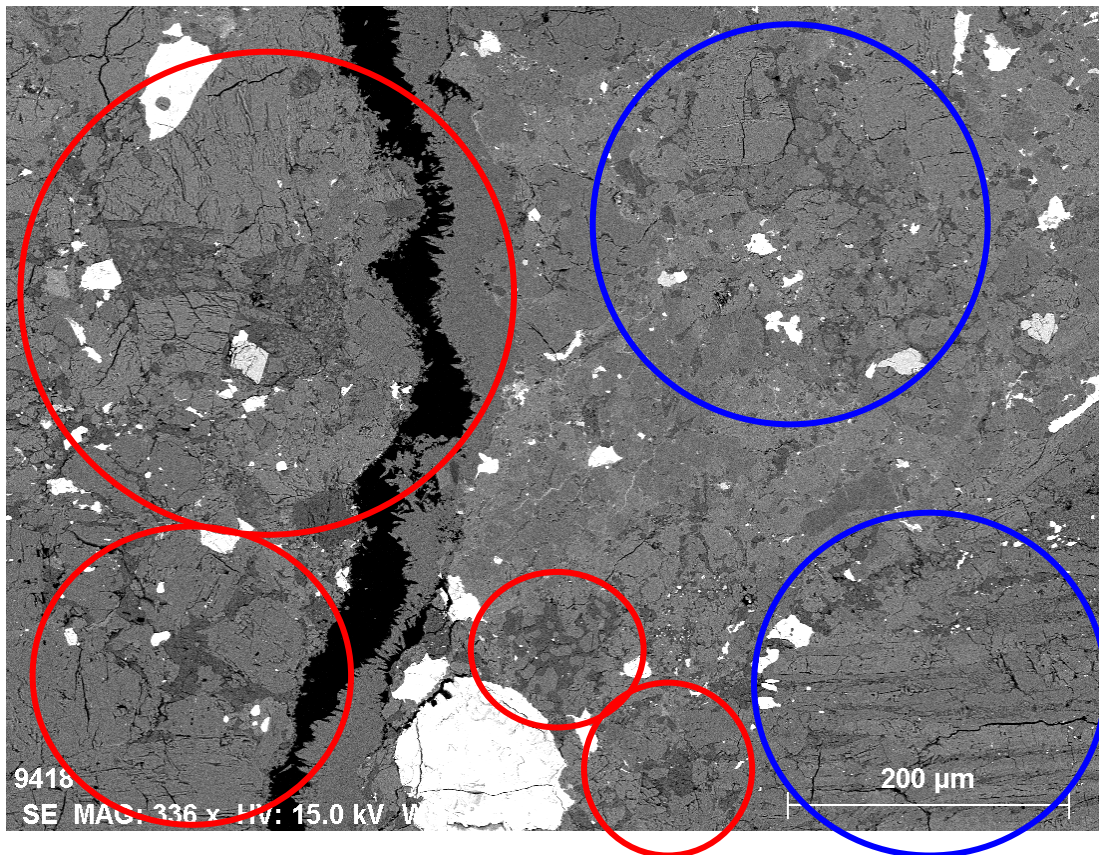


**Fig. 2.10.2.** Some chondrules are recognizable in this image: porphyritic ones (red circles) and a barred olivine (blue circle). The bright area below is troilite.

A detailed study of NWA869 (and its other fragments) can be found in Metzler *et al.* (2011); however, a number of papers in literature deal with this breccia.

The crust is characterized by cavities left after the degassing of some volatiles (fig. 2.10.1), while the bulk hosts some chondrules (fig. 2.10.2). Figure 2.10.3 displays a probable chromite-plagioclase assemblage (see Ch. 1, p. 21).

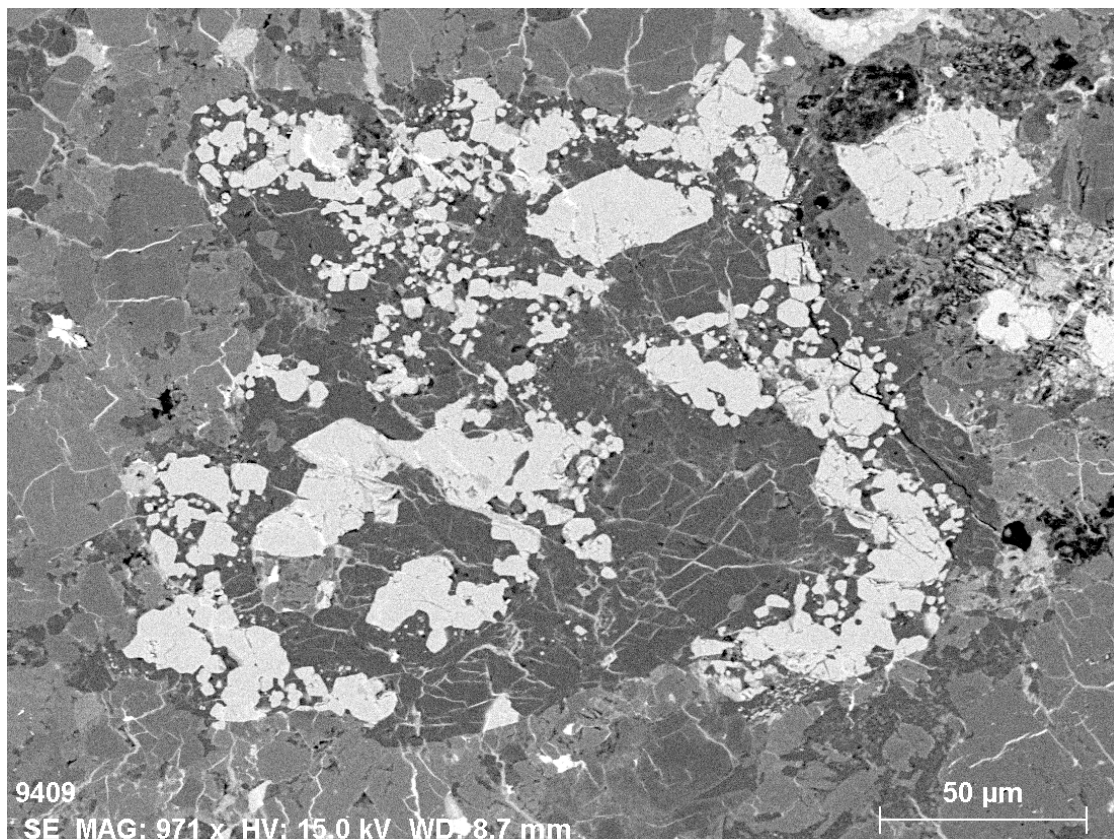


**Fig. 2.10.3.** An example of chromite-plagioclase assemblage.



We have found and classified 30 chromites – 10 from the bulk, 20 from the crust. The complete data record is available in the appendix: here is the graph reporting Al# versus Mg# for the bulk chromites (blue circles) and the crust chromites (red circles). The error bars reported represent the standard deviation. The separation between bulk and crust is less pronounced than in other meteorites of our set.

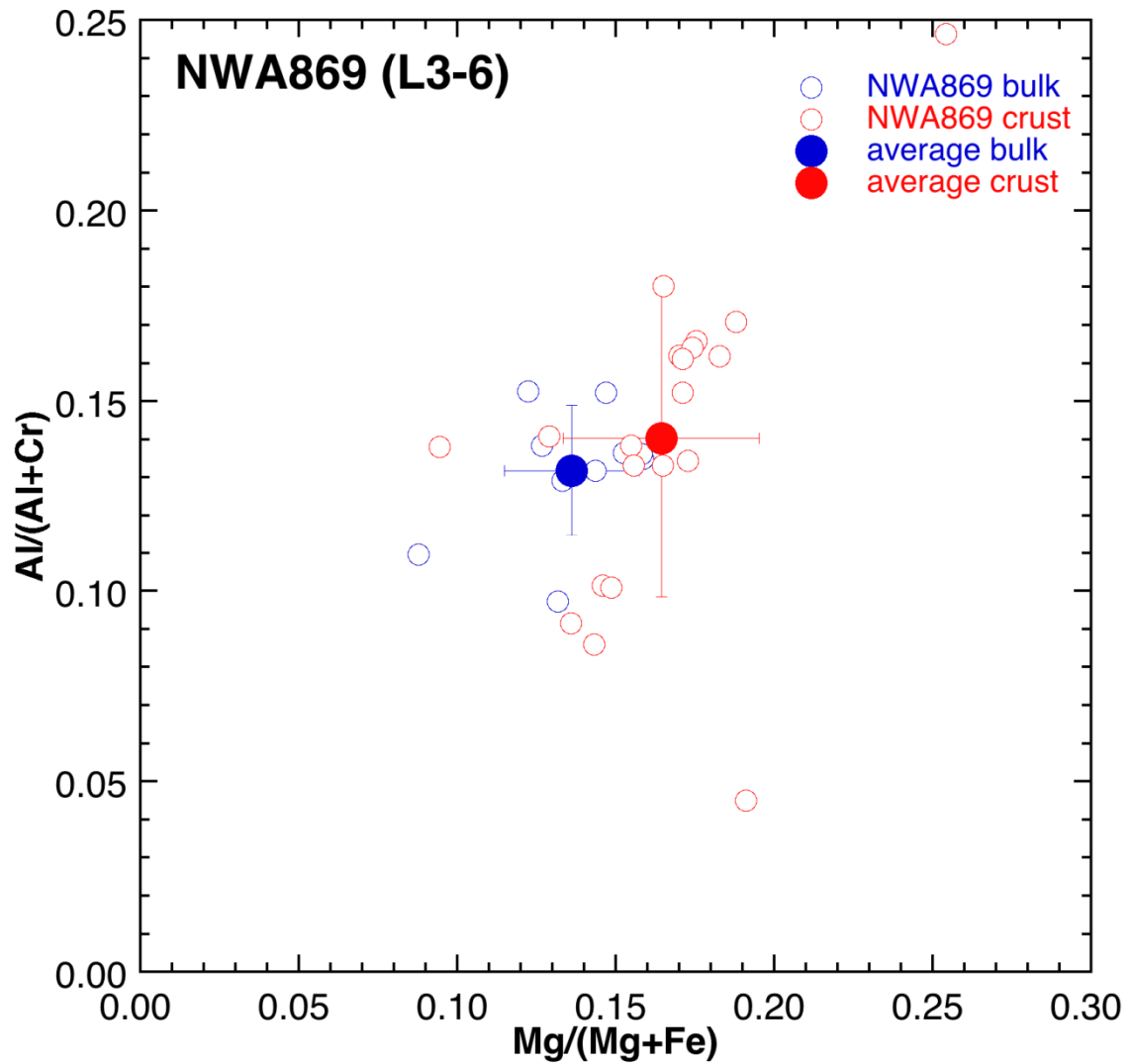


**Fig. 2.10.4.** Plot of the Al# versus the Mg# for crust chromites (red circles) and bulk chromites (blue circles). The error bars represent the standard deviation.

## 2.11 Tamdakht (Morocco)

**Fall. Ordinary chondrite, class H, petrologic type 5, shock stage S3, weathering grade W0.**

The following is a citation extracted from the *Meteoritical Bulletin* (MB95):

“Tamdakht 31°09.8', 7°00.9'W Tamdakht, (Ouarzazate) Morocco Fall: 20 December 2008, 22:37 hrs (local time; UT+00) Ordinary chondrite (H5) History (H. Chennaoui-Aoudjehane): On December 20, 2008, witnesses from a number of locations in Morocco (Agadir, Marrakesh, Ouarzazate) observed a meteor with a W to E trajectory. According to the local newspaper, *Al Massae* (of December 27th), people from the high Atlas Mountains (between Marrakesh and Ouarzazate) heard a sound and felt an aftershock. Due to the high relief in this mountain region, covered with snow at this time of the year, searching for the meteorite was a difficult task. The first reports on finding pieces of a meteorite came a couple of weeks later. The largest impact pit is located near Oued Achir (1.10 m diameter and 70 cm depth, 31°09.8'N, 7°00.9'W), with a stone exceeding 30 kg and many small fragments. A second one is smaller, (about 20 cm diameter and 10 cm depth; 31°09.9'N 07°02.3'W) located 2 km W from the first one; the main mass from the second impact was probably about 500 g. Nine new impacts coordinates have been reported by S. Buhl and M. Aid, and P. Thomas reported 3 other impacts. A strewn field of at least 25 km long and 2 km wide has been outlined. Physical characteristics: Total weight is presently estimated to be 100 kg. Pieces recovered as of February 15, 2009, are 30 kg, 1.5 kg, 3.8 kg, 3.69 kg, 2.4 kg, 1.5 kg, 1 kg, 800 g, and 399 g. One major fragment of 1.7 kg and many small pieces from the same stone (ranging 500 to below 1 g) were also recovered. The largest fragment shows a nearly complete dull gray fusion crust, other pieces are 90% crusted to free of crust, often broken along preexisting fractures. Thick fusion crust, locally more than 1 mm. Petrography (Albert Jambon, Omar Boudouma, D. Badia UPVI and M. Denise, MHP): Abundant chondrules with visible but not well-delimited outlines. Chondrule size is 0.1 to 1.5 mm. Dominant olivine and orthopyroxene. Abundant chromite, rare clinopyroxene and ilmenite. Numerous pockets with chromite, plagioclase and phosphate (merrillite and Cl-apatite). Kamacite, with deformed Neumann bands, and taenite, twinned troilite. Copper. Mode: metal+troilite 10%. Mineral compositions and geochemistry:  $\log \chi = 5.3$ . Olivine  $Fa_{18} \pm 0.5$  Opx =  $En_{83} Fs_{16} Wo_2$  Minor calcic pyroxene. Plagioclase is  $Ab_{83-86} An_{5-15} Or_{7-2}$ . Ca-phosphate (merrillite and Cl-apatite). Chromite: Cr# ( $100 \times \text{molar Cr}/[\text{Cr} + \text{Al}]$ ) = 82. Metal: kamacite with 5% Ni and taenite with 36–47% Ni. Oxygen isotopes (C. Suavet, J. Gattacecca CEREGE):  $\delta^{17}O = 3.26\text{‰}$ ,  $\delta^{18}O = 5.01\text{‰}$ , and  $\Delta^{17}O = 0.65\text{‰}$ . Magnetic susceptibility is  $\log \chi = 5.3 \times 10^{-9} \text{ m}^3/\text{kg}$ . Classification: Ordinary chondrite (H5), S3, W0. Type specimens: A mass of 21 g and one polished section provided by P. Thomas are on deposit at UPVI. 1 piece of 15.8 g provided by L. Labenne and small fragments totaling 20 g at UHAC. Two pieces 10.4 g and 8.6 g at MBE (B. Hoffman), Svend Buhl 2 kg; Meteoritica (PThomas) 2.65 kg; M. Zeroual 20 kg, main mass anonymous finder.”

Further information on this meteorite can be found in Chennaoui *et al.* (2017).

The crust of this meteorite looks richer in iron than the bulk. This looks rather odd, because plasmatron experiments seem to point to a quick evaporation of iron contained in a chondritic sample exposed to a plasma (Pittarello *et al.*, 2016 [seminar], 2019). Another feature deserving further analysis is the scarce correlation between Fe and Ni. In the following some images of the crust of the meteorite are shown. Fig 2.11.1 features a chromite at the boundary of the crust. Despite its small size (~10  $\mu\text{m}$ ), it looks a bulk chromite; its sulfide veinlets suggest it was already in place when the crust formed.

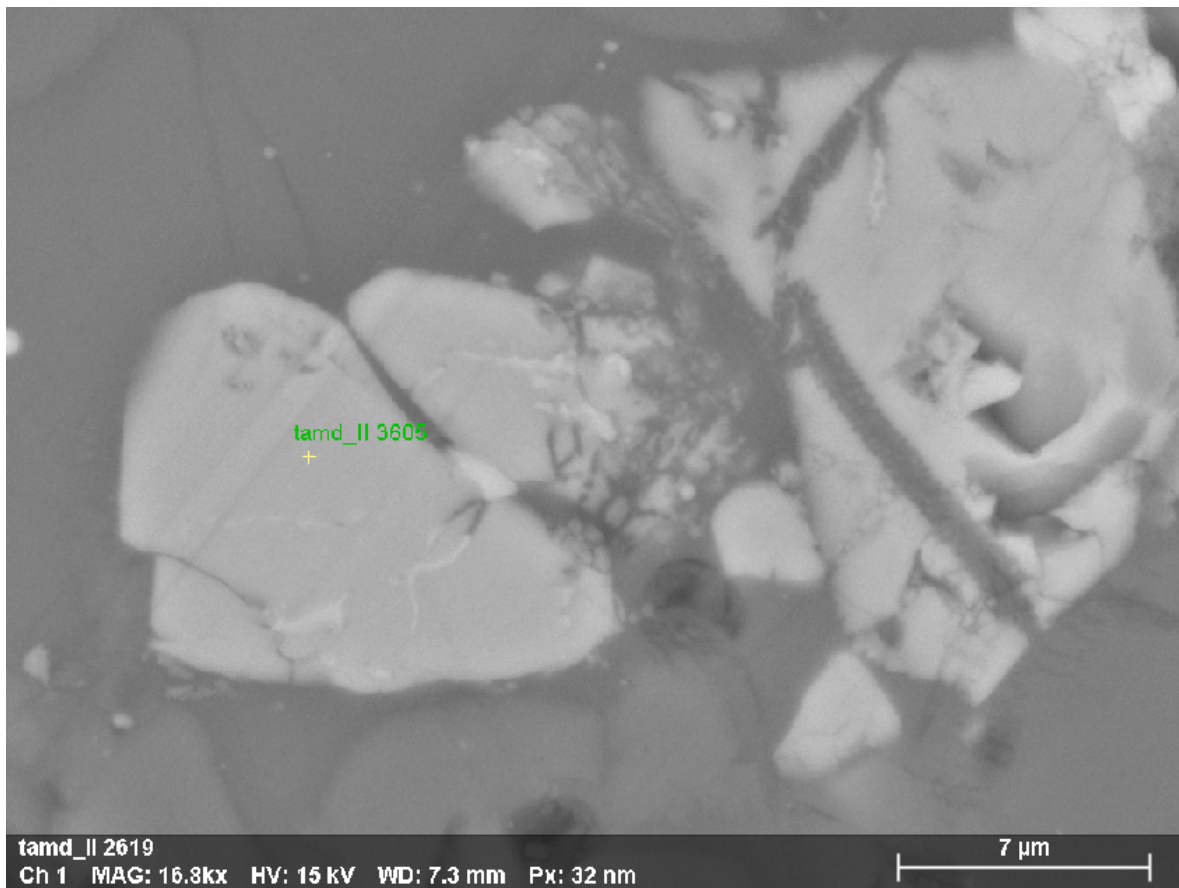


*Fig. 2.11.1. Bulk chromite pre-existing the formation of the crust.*



*Fig. 2.11.2. Chromite formed within the crust.*



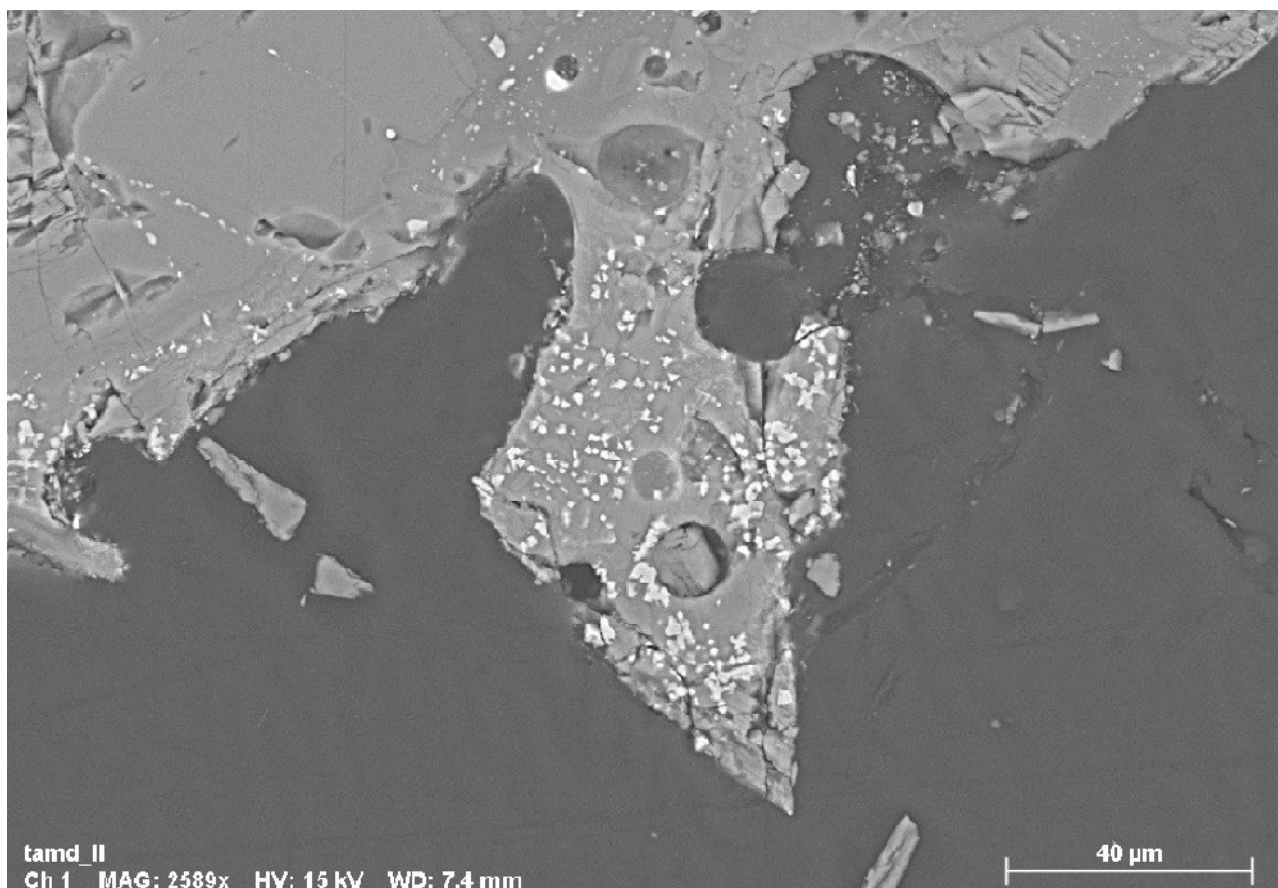


**Fig. 2.11.3.** Zone of the crust studded with small chromites. Unfortunately, they are too small to provide reliable, unbiased SEM data.

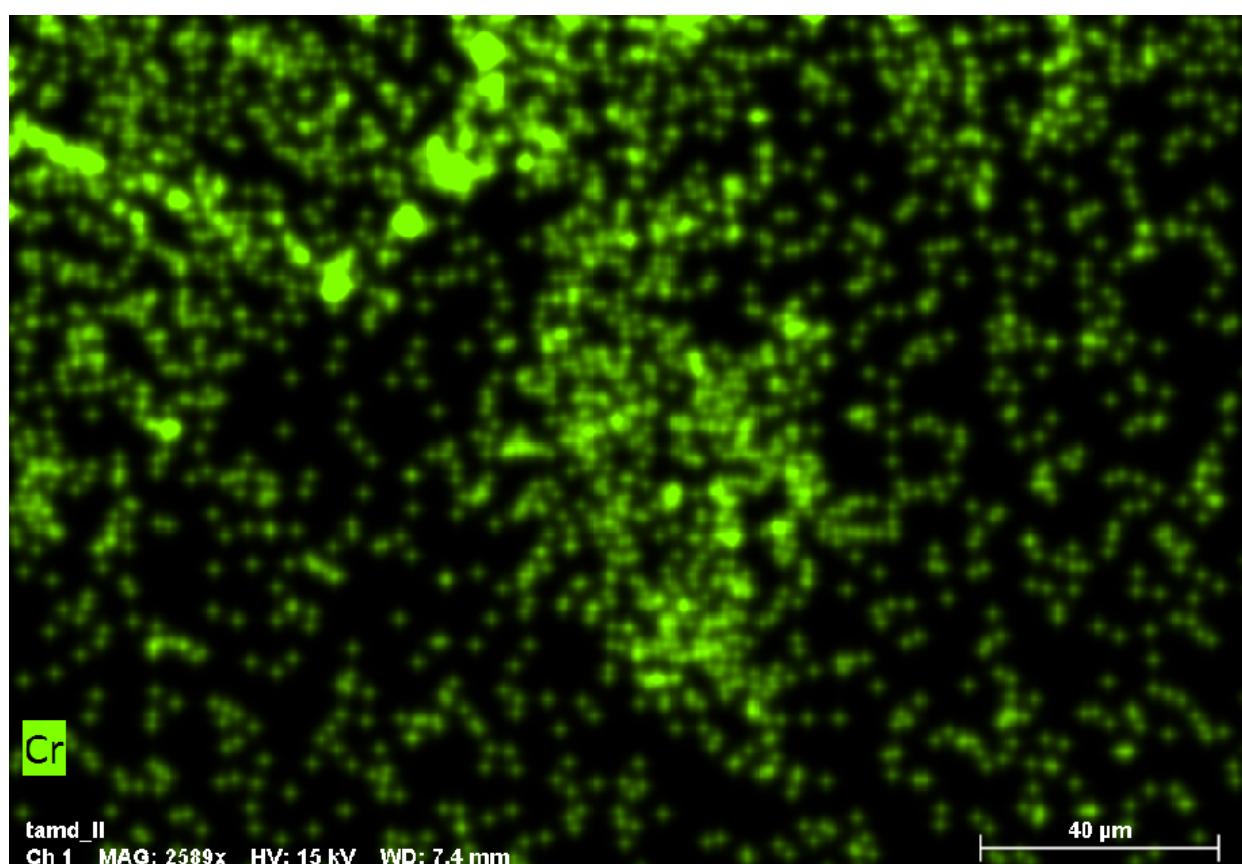


**Fig. 2.11.4.** Chromium relative abundance for the crustal zone represented in the previous figure



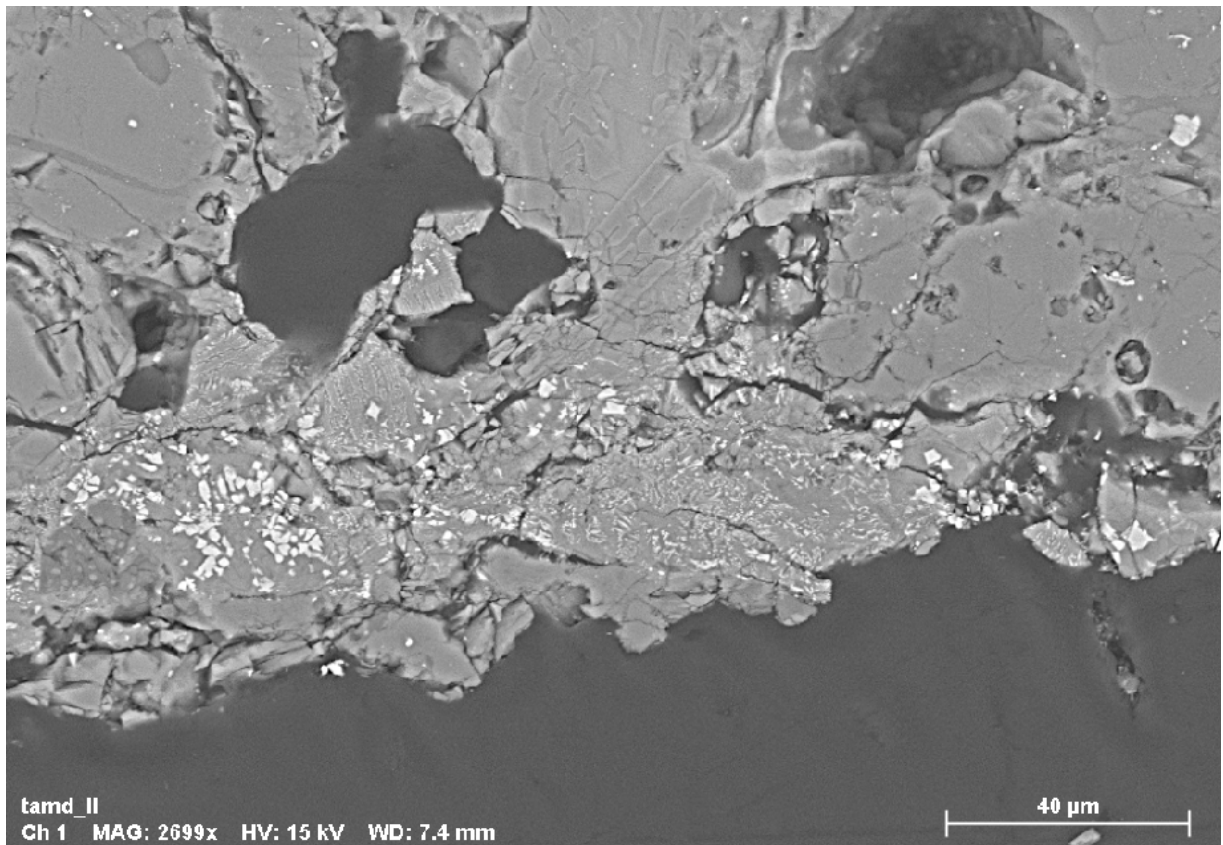


*Fig. 2.11.5. Typical crust features. The small bright spots are crust chromites.*

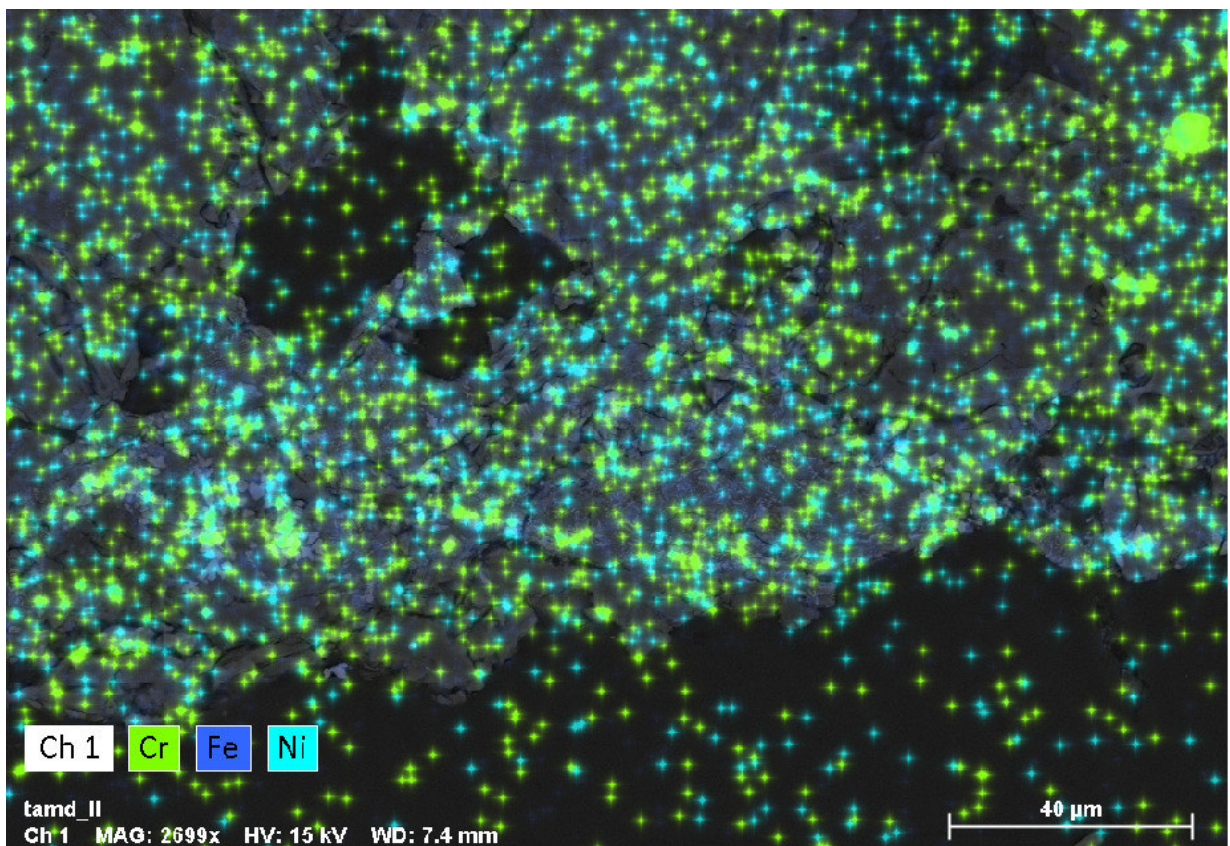


*Fig. 2.11.6. Elemental abundance map used to find crust chromites.*



**Fig. 2.11.7.** Crust chromite (~ 5 μm across).

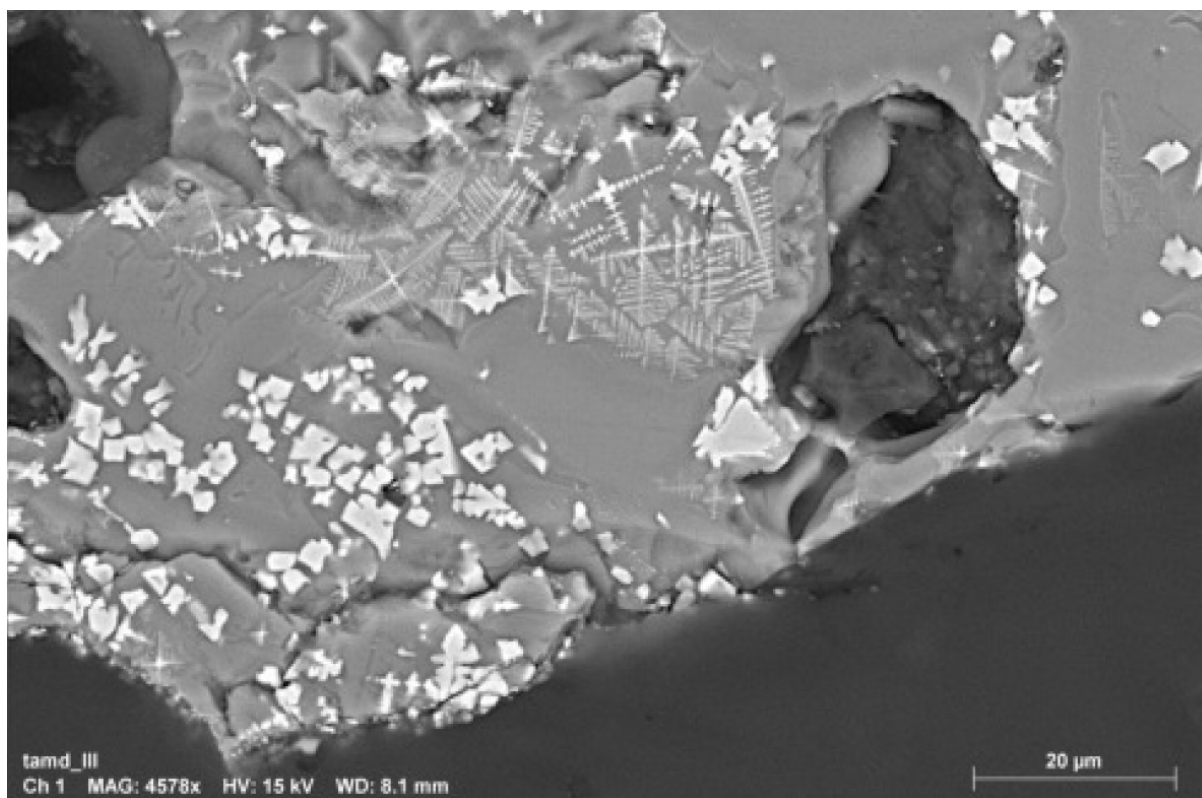


**Fig. 2.11.8.** Crustal zone featuring dendritic magnetites and euhedral crust chromites. The one at center right (near the dark hole), however, is the only one in this area to have provided valuable data.



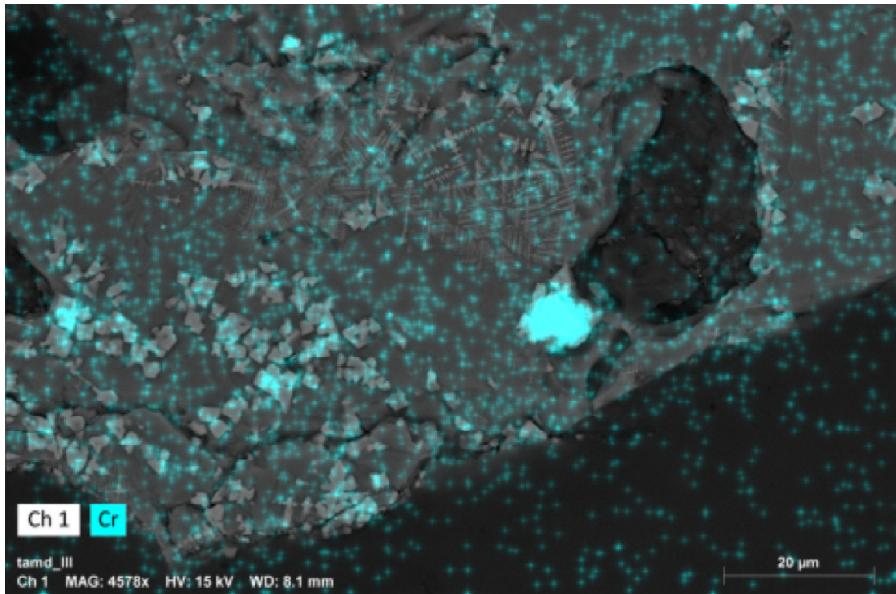


**Fig. 2.11.9.** The same area of the previous image, with superimposed the chromium relative abundance (light blue). Cr distribution map has been used to locate chromites in the crust.

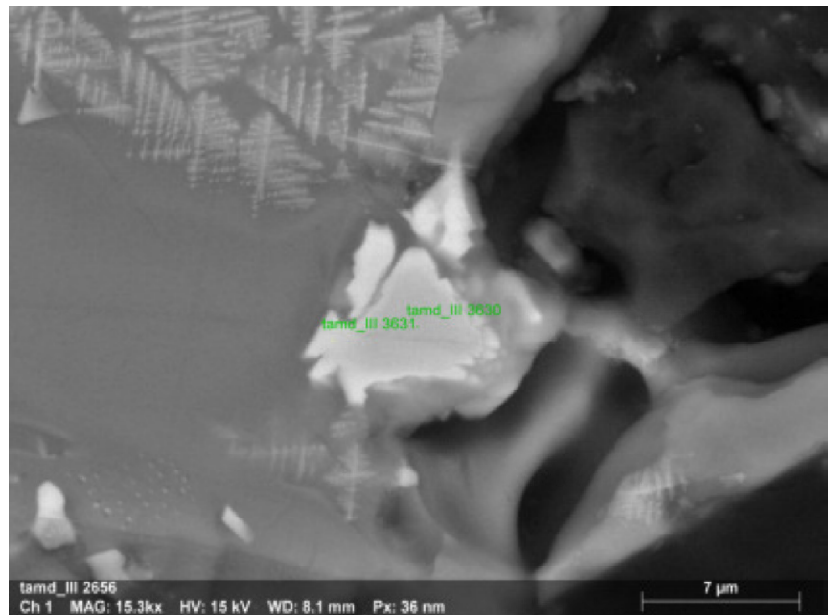


**Fig. 2.11.10.** Zooming in on the biggest chromite. Dendritic magnetites are visible on the upper left.

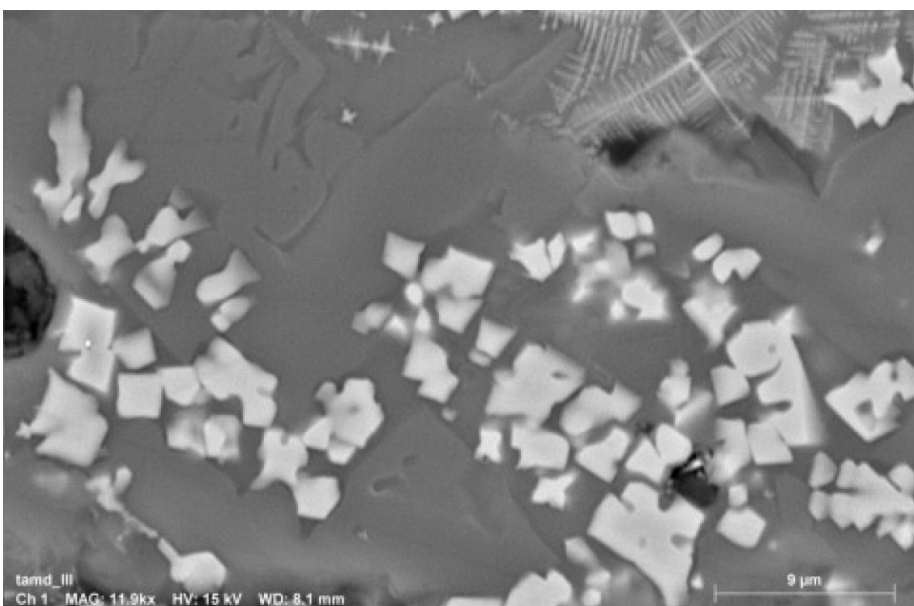
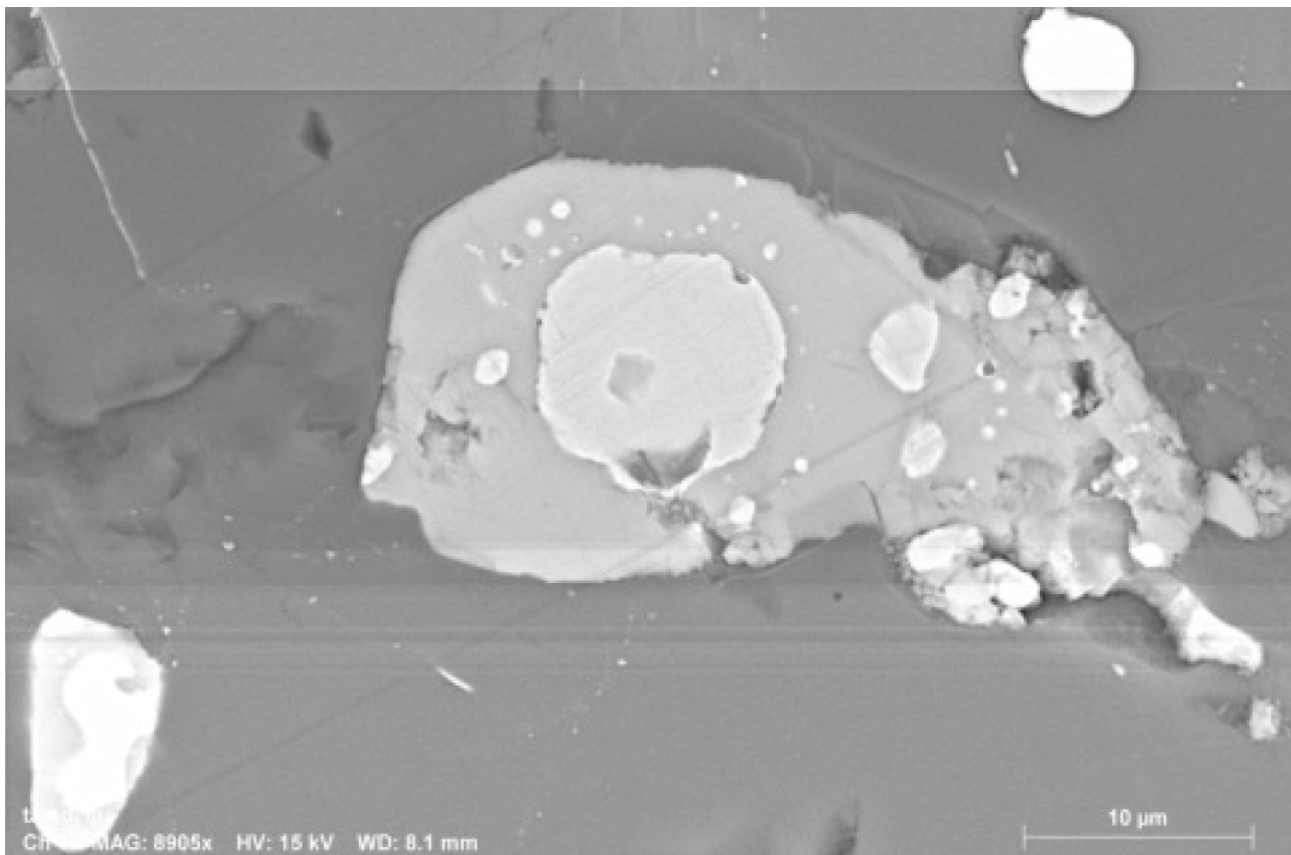


**Fig. 2.11.11.** Lower left portion of figure 2.11.8, displaying the small euhedral magnetites.



*Fe-Ni alloy within Fe sulphide. The chemical analysis shows a small quantity of P correlating with Ca, suggesting the presence of apatite around the sulphide. A significant amount of P is present also within the Fe-Ni alloy (ca. 1% P)*

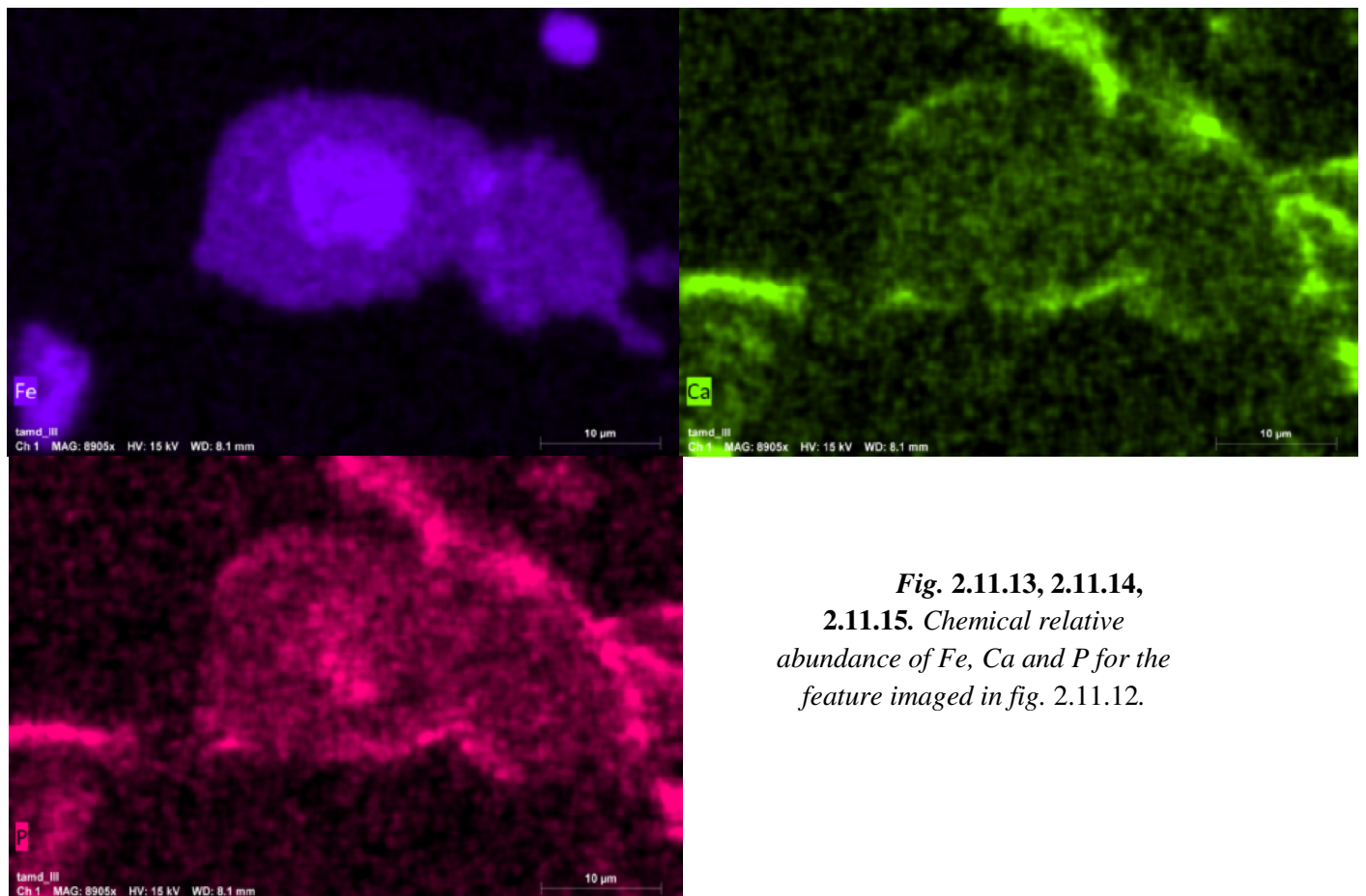


**Fig. 2.11.13, 2.11.14, 2.11.15.** Chemical relative abundance of Fe, Ca and P for the feature imaged in fig. 2.11.12.

We have found and classified 26 chromites in this meteorite – 13 from the bulk, the same number from the crust. The complete data record is available in the appendix: below is shown the graph reporting Al# versus Mg# for the bulk chromites (blue squares) and the crust chromites (red squares). The error bars reported represent the standard deviation. The separation between bulk and crust, though visible, is less pronounced than in other meteorites examined in this study. Crust chromites are much more dispersed around the average value than their bulk equivalents.

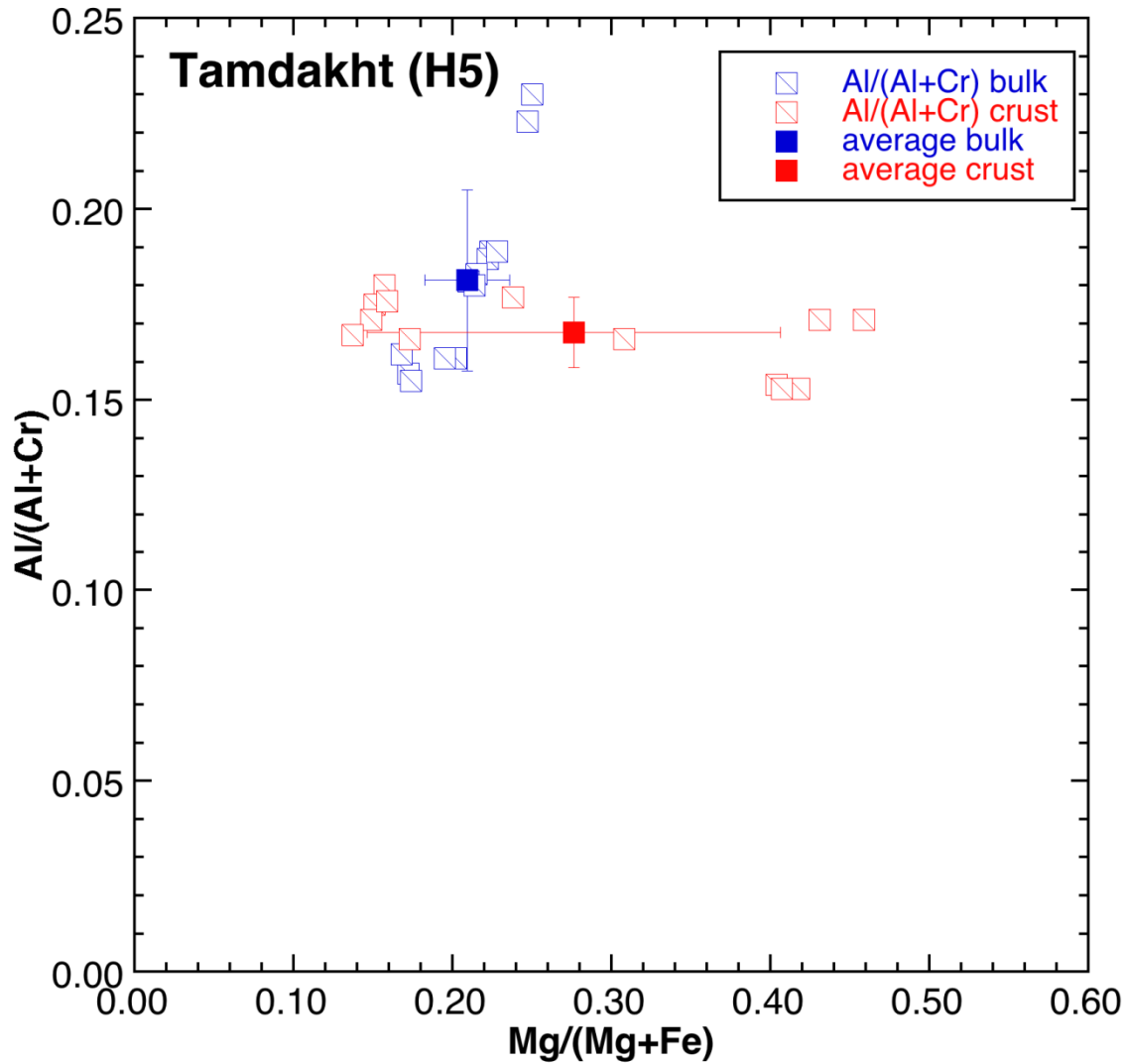


**Fig. 2.11.16.** Plot of the Al# versus the Mg# for crust chromites (red squares) and bulk chromites (blue squares). The error bars represent the standard deviation.



## 2.12 Viñales (Cuba)

**Fall (1 February 2019). Ordinary chondrite, type L6, shock stage S3, weathering grade W0.**

The following is an extract from the *Meteoritical Bulletin* (MB108):

*“22°37.17’N, 83°44.57’. Pinar del Rio, Cuba. Fall: 2019 Feb 0. Classification: Ordinary chondrite (L6).*

*A bright bolide accompanied by loud sonic booms flew across the province of Pinar Del Rio, Cuba, at 1:17 pm local time (18:17:10 UTC) on 1 February 2019. A long smoke trail was also observed. The residents thought a plane had crashed, as they heard explosions and then ground rumbling lasting 15 to 20 s. A meteorite shower fell on Viñales Valley, a national monument since 1978 and a UNESCO world heritage site. The area is covered by a forest and fields. The first and some of the largest stones were collected near the monument "Mural of Prehistory" by artist Leovigildo Gonzalez Morillo. Others were discovered in and around Viñales and throughout the Viñales Valley. Some of the meteorite individuals penetrated the ground, one of them broke through an asphalt road, and many were recovered from rooftops.*

*Hundreds of individual samples were collected by the local residents. The stones are covered by black fusion crust with reddish smears of a laterite clay. The substance of the meteorite of light gray color can be seen in small areas of the broken crust. The masses of stones are in a range 2 to 1100 g. In total, about 50-100 kg of the meteorite were collected.*

*The interior is light-colored; silicates are transected by dark, pseudotachylite-like shock veins. The rock is highly recrystallized; chondrule margins are difficult to discern. Recognizable chondrule types include POP, PO and BO, ranging up to ~1 mm in diameter. The meteorite samples contain the several vol% of black inclusions of melt rock. Metal grains range in size up to about 700  $\mu\text{m}$ . The rock exhibits moderate silicate darkening. Chromite grains are moderately to extensively fractured. Some troilite grains and some kamacite grains are polycrystalline. A few kamacite grains contain small rounded grains of troilite within them. Metallic Cu was not observed. There are several small chromite-plagioclase assemblages and some olivine grains contain small chromite veinlets. The shock veins range to more than 1 cm in length and are typically 20  $\mu\text{m}$  to 150  $\mu\text{m}$  wide. The veins contain major silicate and small blebs of metallic Fe-Ni, and to a lesser extent, troilite; these opaque blebs are typically 1-3  $\mu\text{m}$  in diameter. Also present in the veins are cellular metal-troilite veinlets 10-30  $\mu\text{m}$  in length. Elongated aggregates of chromite occur alongside portions of some shock veins. Slabs of Viñales show intersecting dark shock veins, anastomosing veins, and a few quasi-circular melt concentrations where veins intersect. Coarse metal grains are heterogeneously distributed in some samples – some regions of these samples have abundant coarse metal; other regions have none. Near the dark fusion crust, numerous thin veinlets of troilite surround and penetrate fractures within silicate grains. Magnetic susceptibility (J. Gattacceca, CEREGE):  $\log \chi (\times 10^{-9} \text{ m}^3/\text{kg}) = 4.93$  measured on a 18 g sample.*

*Mineral compositions and geochemistry: (Borisovsky S. E., IGM; A. Rubin, UCLA and L. Garvie, ASU) Olivine,  $\text{Fa}_{24.7 \pm 0.3}$  (N=15, IGM),  $\text{Fa}_{24.6 \pm 0.4}$  (n=23, UCLA); low-Ca pyroxene,  $\text{Fs}_{21.0 \pm 0.4}\text{Wo}_{1.5 \pm 0.3}$  (N=21, UCLA),  $\text{Fs}_{20.2 \pm 0.3}\text{Wo}_{1.6 \pm 0.2}$  (N=15, IGM); other minerals characterized by UCLA and ASU include diopside ( $\text{Fs}_{8.1 \pm 0.1}\text{Wo}_{44.8 \pm 0.6}$ ; n=5), plagioclase (which has an average size of ~80  $\mu\text{m}$ ;  $\text{Ab}_{90.0 \pm 0.5}\text{Or}_{1.8 \pm 1.2}$ ; n=14), chromite, kamacite ( $6.6 \pm 0.6$  wt.% Ni;  $0.89 \pm 0.12$  wt.% Co), troilite (containing 0.7-0.42 wt.% Ni), taenite, and accessory tetrataenite, merrillite and*

chlorapatite. Oxygen isotopes (K. Ziegler, UNM):  $\delta^{18}\text{O}$ =4.38, 4.55, 4.69;  $\delta^{17}\text{O}$ =3.39, 3.50, 3.57;  $\Delta^{17}\text{O}$ =1.08, 1.09, 1.09 (all ‰).

The individual sample of 148 g and one transparent-polished section are deposited in Vernad; 22 g, UCLA; 18 g, CEREGE; 8 individual samples of total mass 2.31 kg are on deposit in Institute of Geophysics and Astronomy (IGA), Havana, Cuba. Large specimen masses are also held by John Higgins, MFarmer, and DPitt.”

A detailed study of this meteorite can be found in a paper by Yin and Dai (2021).

The crust of this sample exhibits the familiar features of small crust chromites and sulfide veins (fig. 2.12.1). Bulk chromites are also typical in size and shape (fig. 2.12.2), as are crust chromites (smaller and euhedral); however, some of them are found included in plagioclase (figures 2.12.3 and 2.12.5), whereas others are crossed by sulfide veins (fig. 2.12.4).

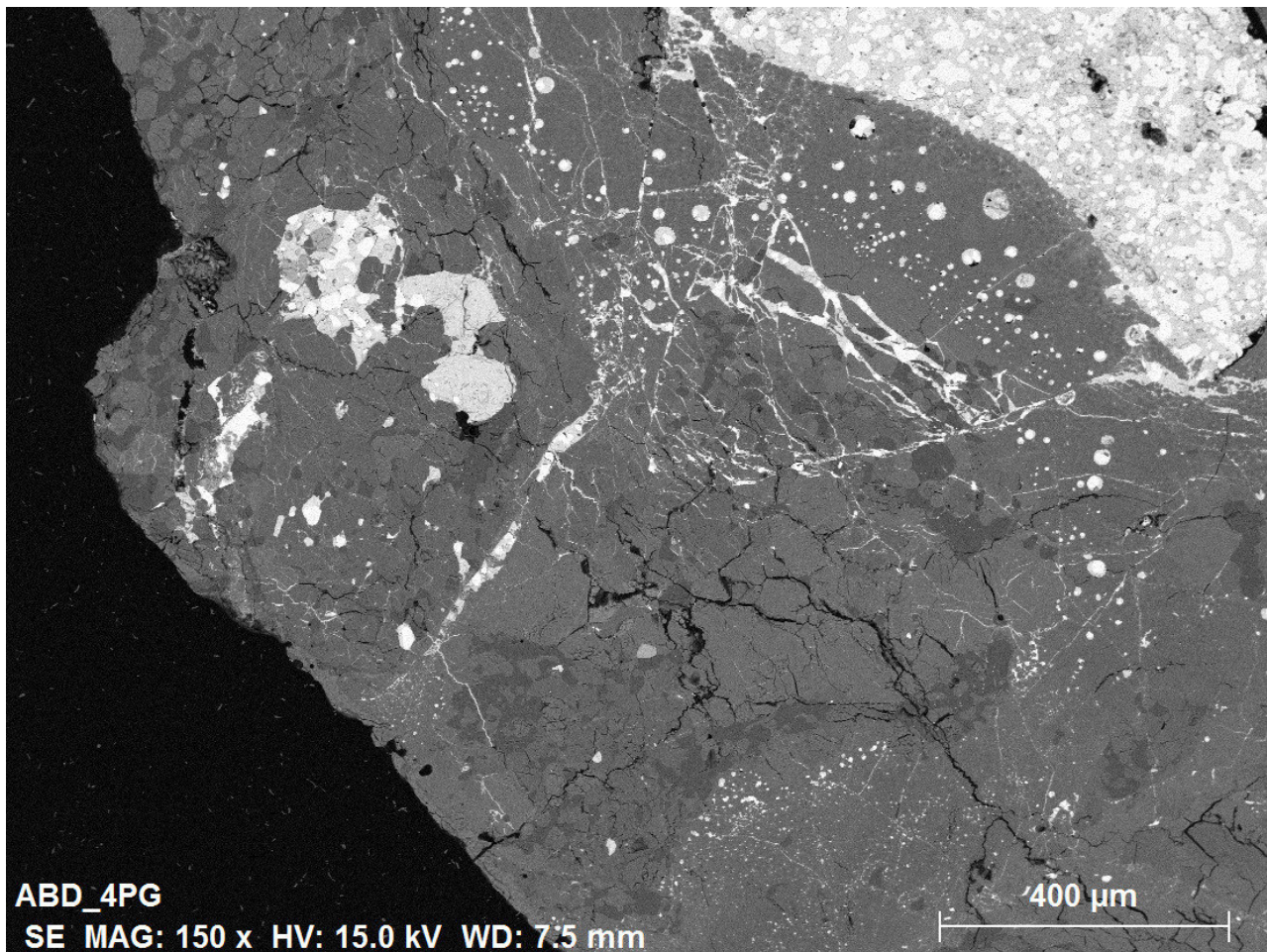


**Fig. 2.12.1.** Portion of Viñales crust, exhibiting small chromites and sulfide veins.



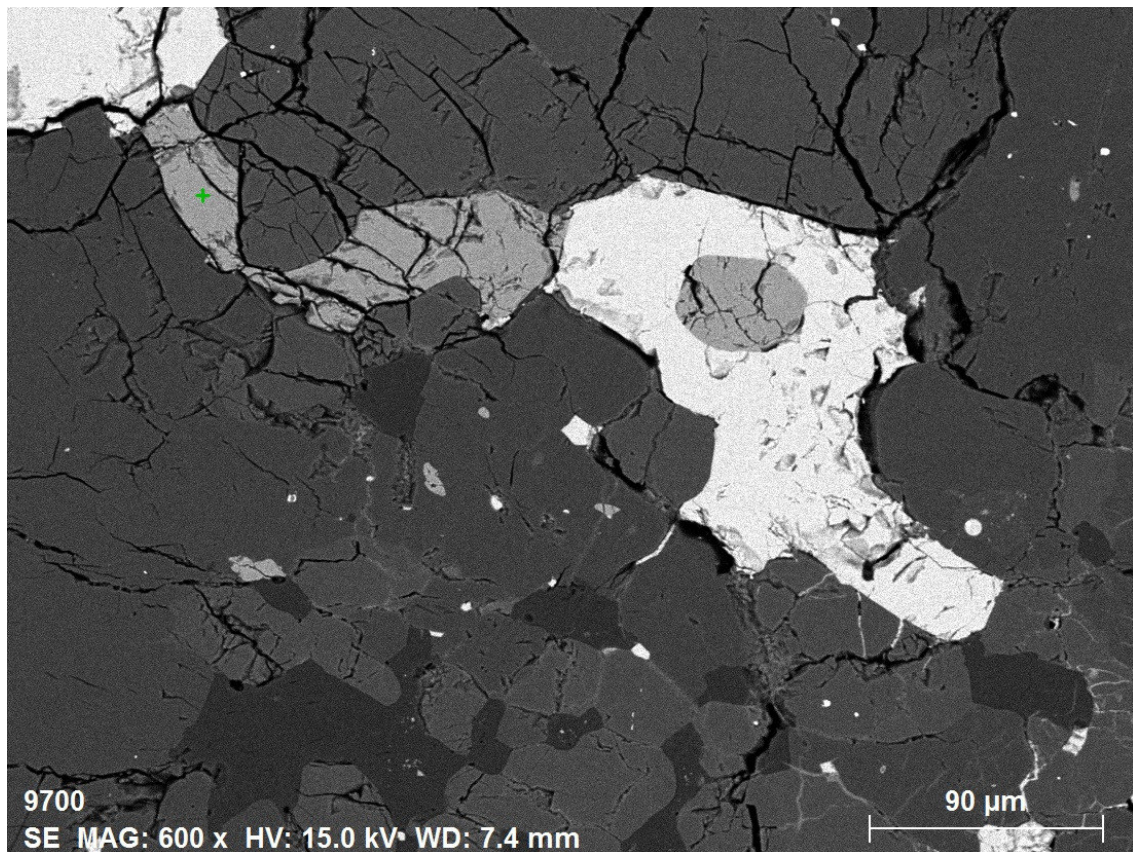


**Fig. 2.12.2.** Three bulk chromites – the third one surrounded by brighter troilite.

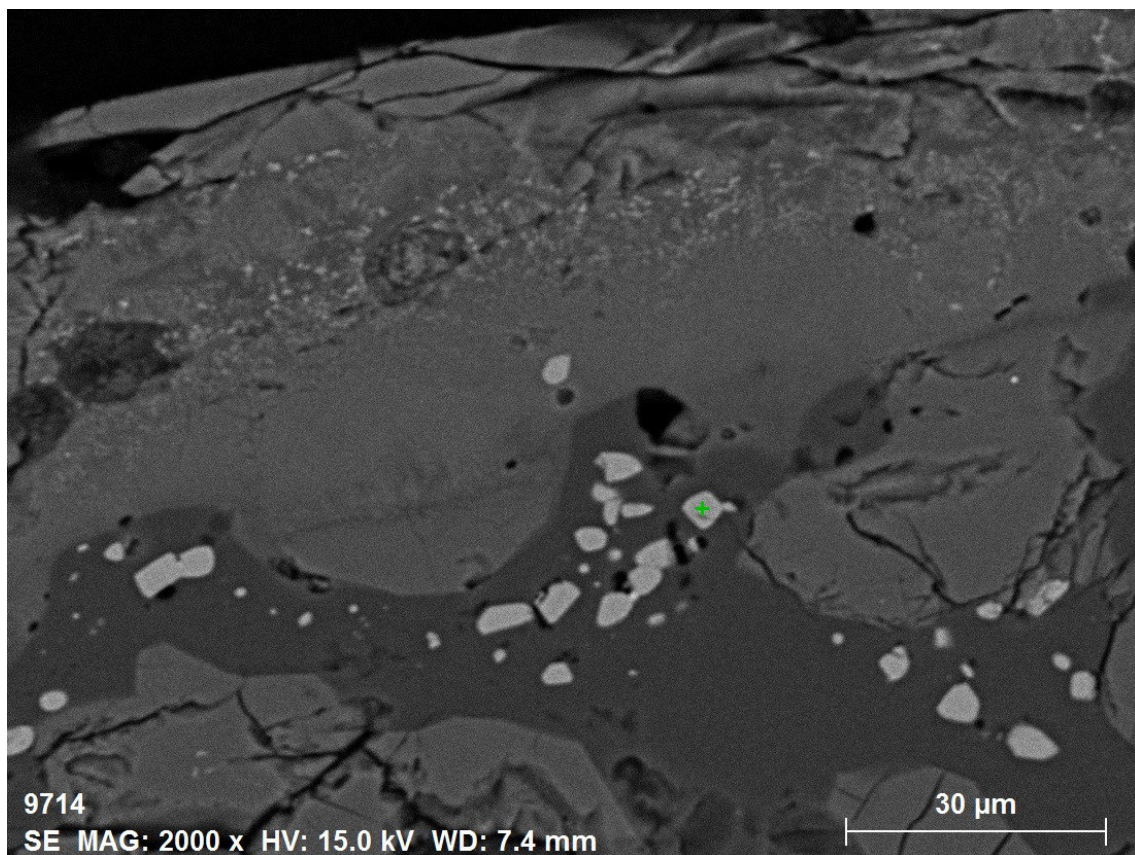


**Fig. 2.12.3.** Euhedral chromite in a chromite-plagioclase assemblage partially melted and extruded in the melted crust .



**Fig. 2.12.4.** Bulk chromite intersected by sulfide veins.

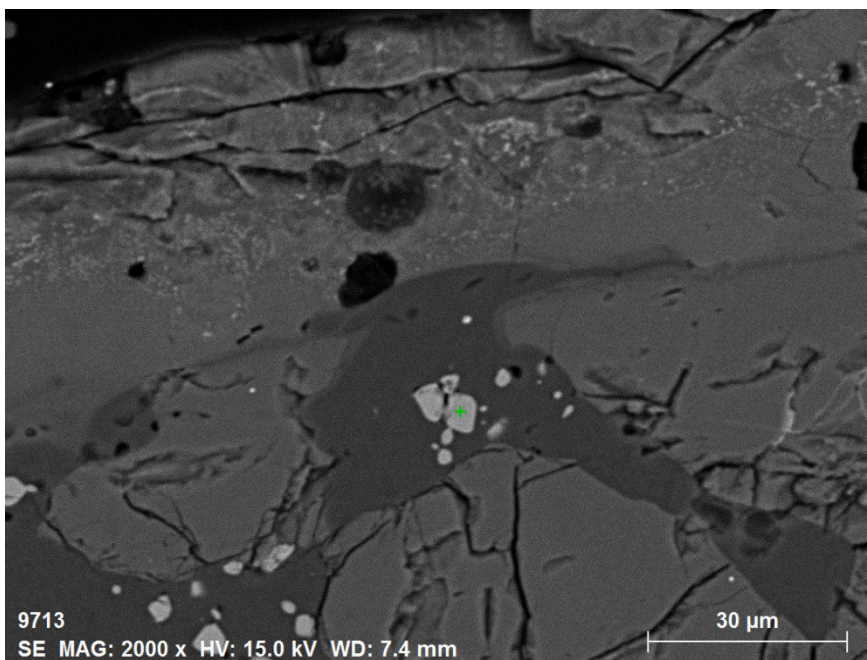
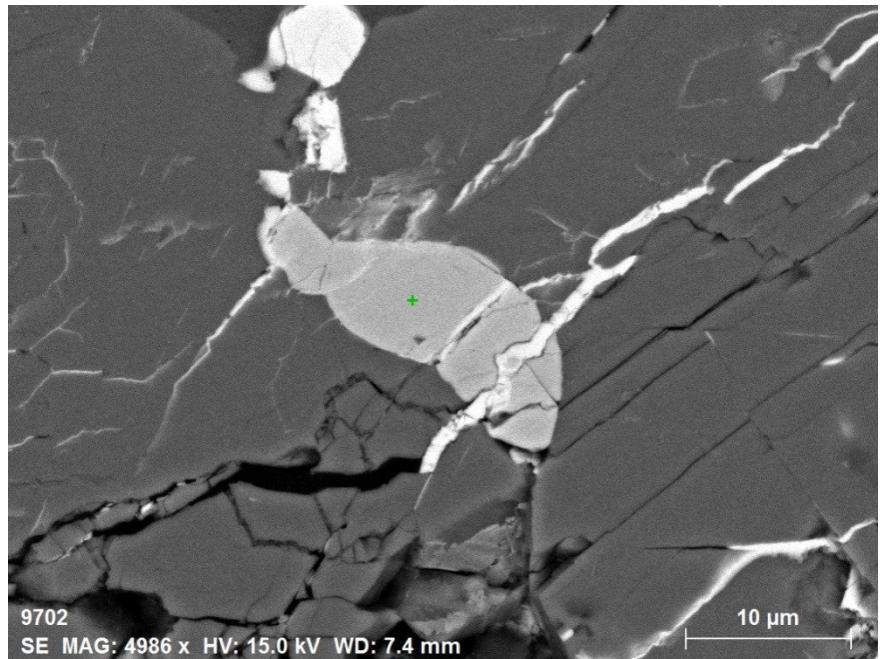


**Fig. 2.12.5.** Euhedral chromite in a chromite-plagioclase assemblage partially melted and extruded in the melted crust.

32 chromites were found and classified – 15 from the bulk, 17 from the crust. The complete data record can be found in the appendix: here is the graph reporting Al# versus Mg# for the bulk chromites (blue squares) and the crust chromites (red squares). The error bars reported represent the standard deviation. The separation between bulk and crust is surely less pronounced than in other meteorites of our set. Also much smaller is the dispersion of the points (bulk and crust alike) around the average value.

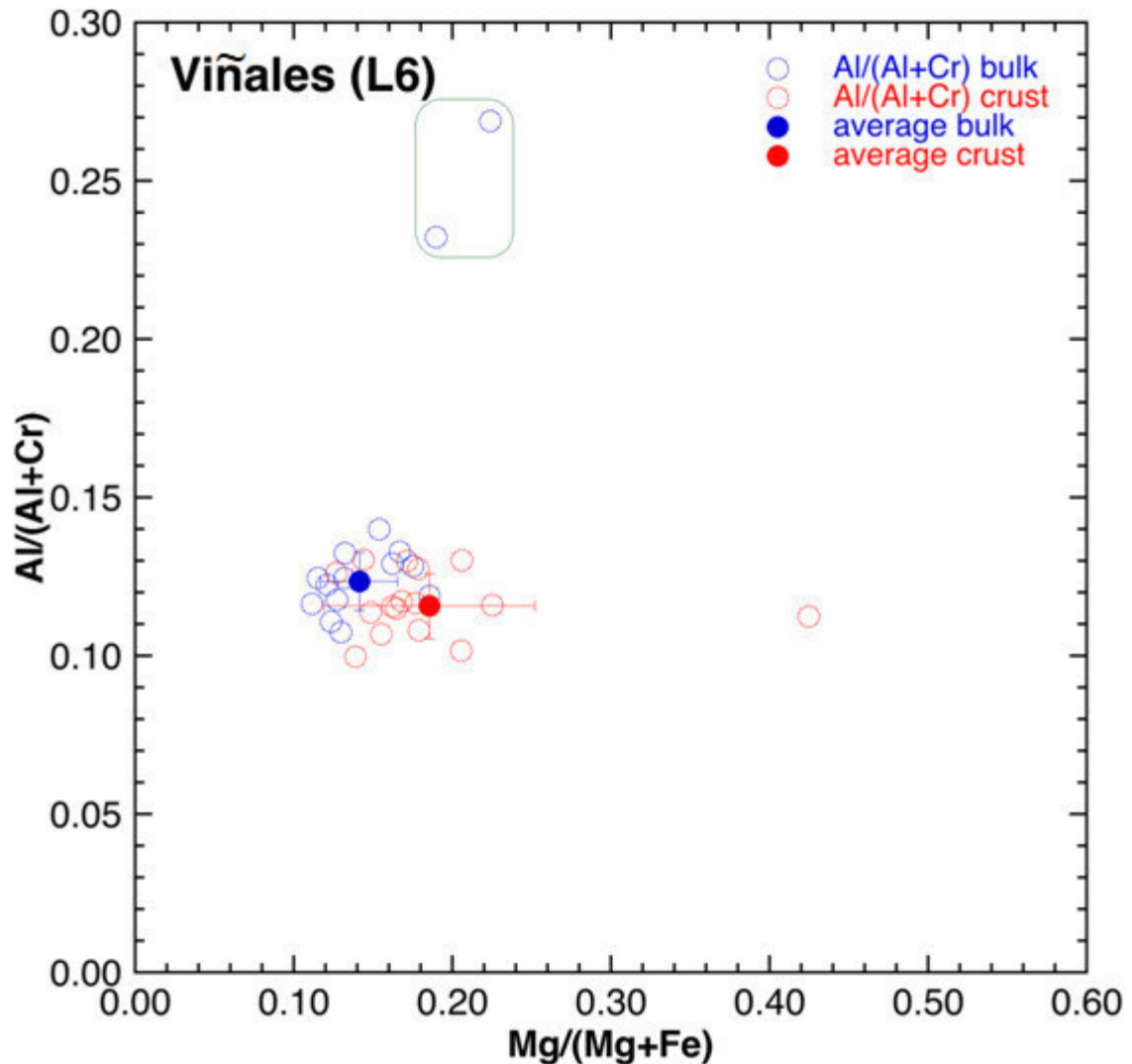


**Fig. 2.12.6.** Plot of the Al# versus the Mg# for crust chromites (red circles) and bulk chromites (blue circles). The error bars represent the standard deviation. Two outliers (upper part of the figure) have been excluded from the averages and standard deviations; these two points are related to chromite plagioclase assemblage which, sometimes, display much higher Al# than bulk chromites.

## 2.13 El Hammami (Mauritania)

### *Find. Ordinary chondrite, class H, petrologic type 5, shock stage S2.*

The following is a citation extracted from the *Meteoritical Bulletin* (MB92):

*“In 1997 January, an unknown mass of material, possibly broken apart from a single large stone, was sold to meteorite collectors by nomads near the town of Mhamid, Morocco; this material has since been resold under the names Mhamid and Hamada du Draa. The nomads claimed that this meteorite was found to the south, in Algeria (~29°50'N 5°50'W), in the direction of a fireball seen in 1995 January. In 1997 September, the same nomads shipped a fragment of a meteorite that they claimed was seen to fall on 1997 August 10 to Mr. Edwin Thompson. In 1997 November, Thompson traveled to Mauritania and collected six fresh-looking stones totaling ~200 kg (individual masses of 80, 51, 30, 26, 8, and 4 kg) at the base of the El Hammami Mountains in Mauritania (1000 km southwest of Mhamid, Morocco), probably in the place where they fell; fragments of these have been sold by Thompson and other dealers under the name El Hammami. Classification and mineralogy of El Hammami stones (A. Rubin, UCLA): olivine,  $Fa_{18.8}$ ; pyroxene  $Fs_{16.7}Wo_{1.4}$ ; shock stage S2; contains metal veins; petrologic type 5. Classification and mineralogy of Hamada du Draa stones (D. Weber, Mün): olivine,  $Fa_{19.2}$ ; pyroxene  $Fs_{17.4}$ ; shock stage S2; contains conspicuous metal-rich veins; petrologic type 5/6; some of the material appears weathered and rusts easily, but the bulk is quite fresh. Specimens from El Hammami stones: ~100 kg, Thompson; type specimen, UCLA. Specimens originally called Hamada du Draa are now scattered in private collections, and some may remain in Morocco; type specimen, ~1 kg, Mün.*

*Because all of the above-described material seems likely to represent a single fall, the name **El Hammami** shall be the official collective name. Mhamid and Hamada du Draa should be considered only as unofficial synonyms for El Hammami. The total known mass of material is probably ~240 kg.”*

Chips from El Hammami event have been used in the past for high speed friction (van der Bogert *et al.*, 2003) or weathering experiments in the laboratory (Schwenzer *et al.*, 2007). A sample has been also processed in the VKI (von Karman Institute) Plasmatron in Brussels, a facility that is commonly used for testing spacecraft heat shields; therefore, it should represent a good approximation of the conditions experienced by any material during the atmospheric entry. This complex process involves melting, evaporation and oxidation of the original material, inducing significant changes in chemistry and microstructures that may bias the study of meteorites recovered on the ground.

Mechanisms of heating and ablation are generally investigated by numerical simulations (for instance, Love and Brownlee, 1991) or by heating experiments – which, however, fall short of reproducing the real process in a satisfactory way. The plasmatron offers a viable alternative to the above approaches, even though it's very expensive and requires a number of preliminary tests in order to give reliable results.

The Plasmatron generates a plasma jet in a test chamber kept at sub-atmospheric pressure (between 5 and 200 mbar), by heating a gas (argon,  $N_2$ ,  $CO_2$ , air or any other gas mixture) to temperatures up to about 10000 K and with a potential heat flux of 16 MW/m<sup>2</sup>, using electrical current loops induced inside a plasma torch.

[Source: <https://www.vki.ac.be/index.php/50-research-and-consulting/facilities/plasma-facilities>; Pittarello *et al.*, 2016]



Conditions of the experiment were as follows (source: Pittarello, 2016 seminar):

Experiment name	Material	Sample holder	Heat flux (MW/m <sup>2</sup> )	Heat flux probe	Pressure (hPa)	Duration (s)
OC2.1	ordinary chondrite	cork	1.01	flat	200	21

The maximum measured temperature (of air) near the sample surface was 2360 K. Such conditions corresponded to a 3.8 m-sized bolide traveling at 6.5 km/s at an altitude of 55 km (Pittarello, same source).

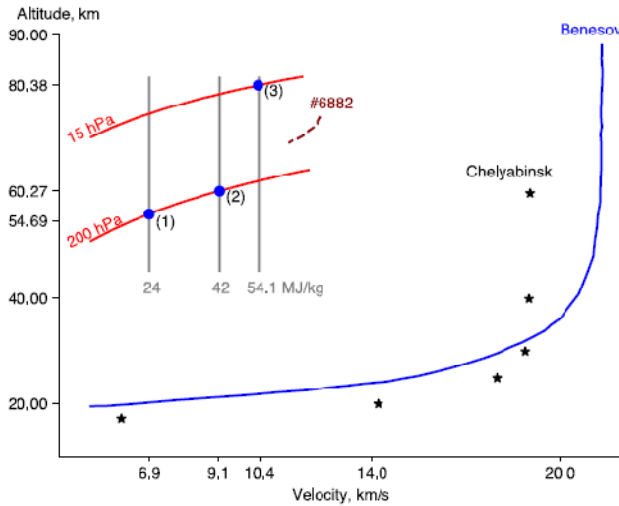
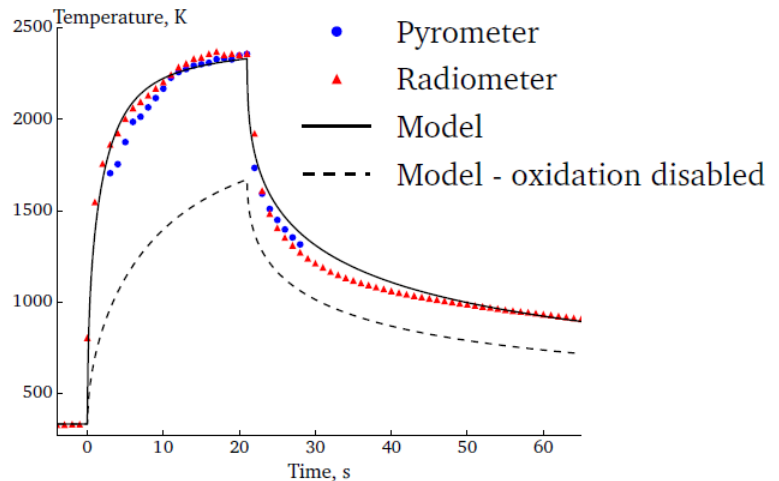


**Fig. 2.13.2.** – Comparison of the surface temperature measurements (blue bullets: pyrometer, red triangles: radiometer with estimated emissivity) with the numerical simulation of the thermal response of the sample. Exothermic heterogeneous reactions have a significant impact on the simulations (full lines: model including oxidation reaction, dashed lines: oxidation disabled). From Helber *et al.*, 2019

**Fig. 2.13.1.** – Duplication of the Plasmatron test conditions to flight conditions. The Benešov fireball reported by Borovička & Spurný (1996) has an estimated value of 2.3 m diameter body with 21.3 km/s velocity. The Chelyabinsk event (Borovička *et al.*, 2013) is estimated to be 18 m in size, with an entry velocity of 19 km/s. The trajectory #6882 is one of the 413 photographic meteors reported by Shepard *et al.* (1967) and Jacchia & Whipple (1961). The sizes of these bodies are not reported. From Helber *et al.*, 2019



Partial melting and boiling of the sample were reported at surface temperatures between 2280 and 2360 K; however, no substantial mass losses due to evaporation or mechanical removal were observed during the experiment.

Exothermic oxidation reactions of iron may play an important role in the surface chemistry, and this was first inferred from the change of colour of the sample after the experiment – and further supported by analysis of the recovered material. Ionized atoms (Ca II, Mg II, and Fe II) were identified by emission spectroscopy, with the lines of Ca II being the strongest in the range from 350 to 450 nm. In addition, recorded sodium and potassium emission signals could not be fully assigned to ablation of the test samples because of the use of a cork sample holder (fig. 3.10.3), which contaminated the boundary layer with those elements (Helber *et al.*, 2019).

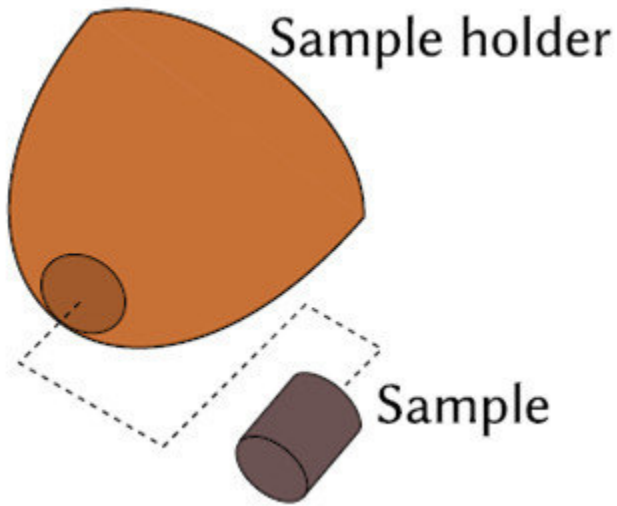


**Fig. 2.13.3.** The sample and its cork holder. The El Hammami sample, embedded in the holder, was 16 mm in diameter. Adapted from Helber et al., 2019

**Fig. 2.13.4.** The El Hammami sample, before (a) and after (b) the exposure. From Helber et al., 2019

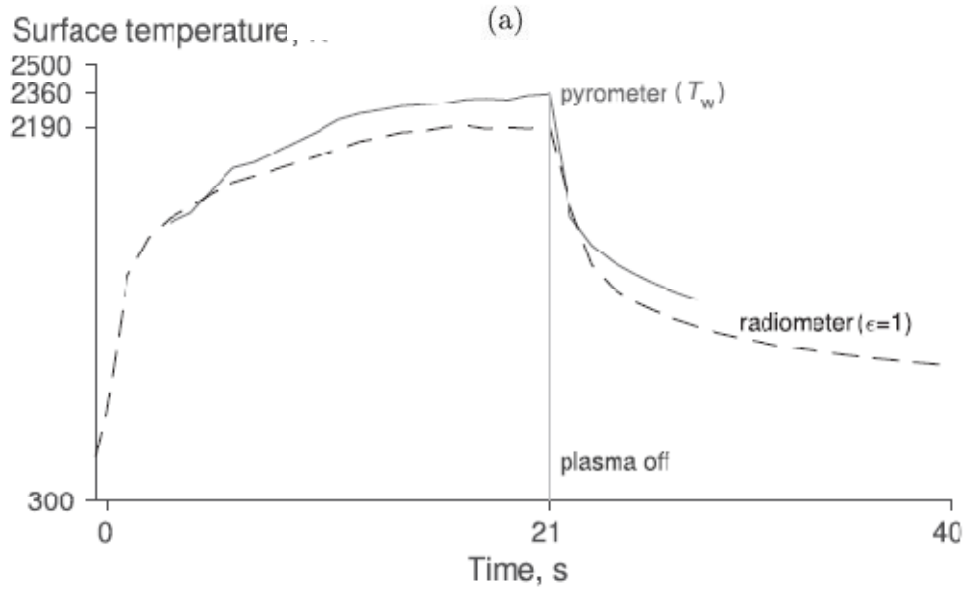
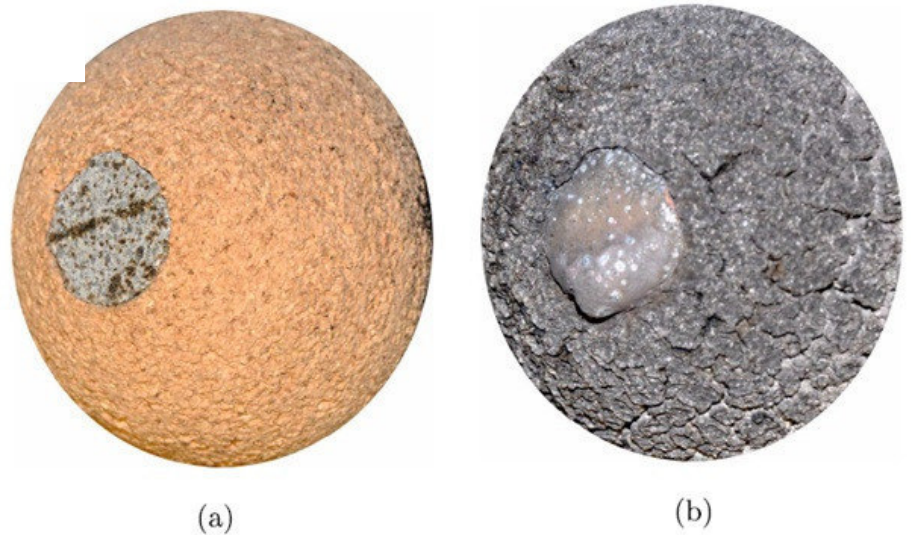


**Fig. 2.13.5.** Surface temperature of El Hammami sample (full line), measured with the pyrometer. Dashed lines are radiometer measurements. From Helber et al., 2019

The plasmatron treatment has surely affected the sample in various ways. A number of dendritic and cruciform magnetites can be found in the melted crust (figures 2.13.6, 2.13.7, 2.13.8 and 2.13.11), often with zoned, skeletal olivines nearby (figures 2.13.7., 2.13.8, 2.13.9, 2.13.11); zonation appears to be an almost ubiquitous feature, likely caused by fast cooling processes with variations in the Mg#. Magnetites are very symmetrical, often more than their natural counterparts.

Rather than merely confined in chromites, Cr is found often dispersed as a background element in the crust – which exhibits several bubbles and cavities, testifying a tormented history like it was expected to do (fig. 2.13.10). Some crust chromites appear weathered, even cleaved (fig. 2.13.12); sometimes even their bulk counterparts look fractured by lines which are not parallel to the surrounding sulfide veins (fig. 2.13.13).

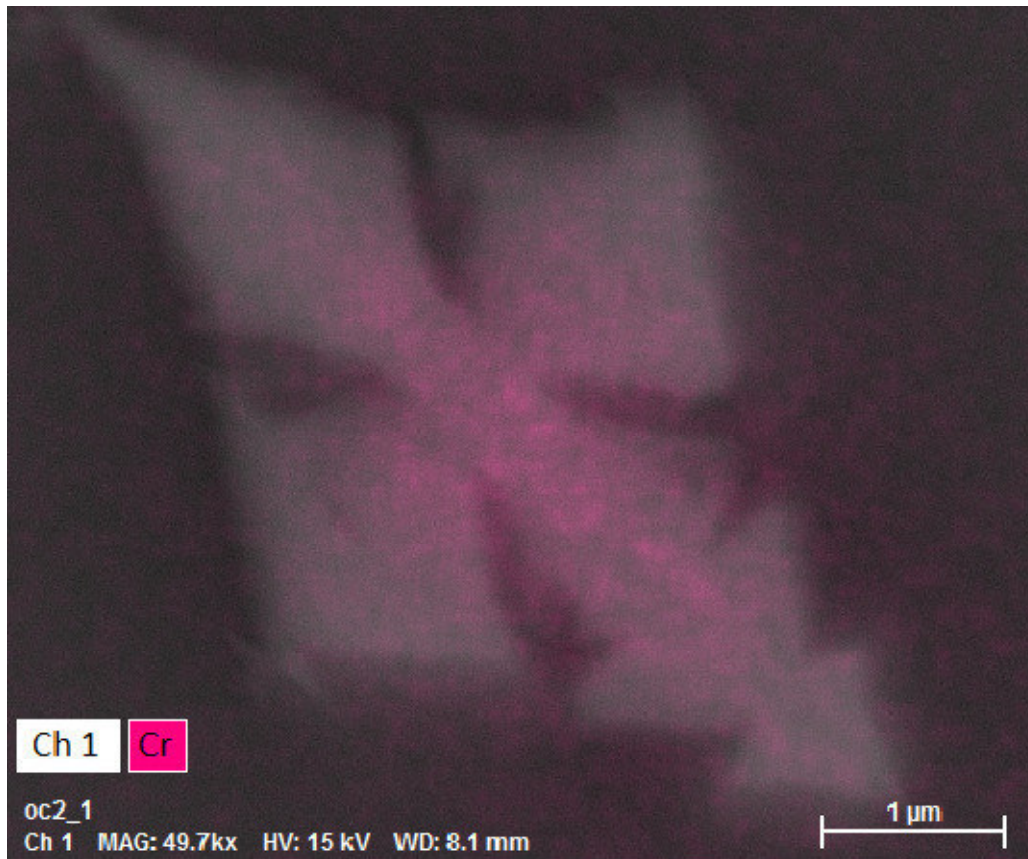


**Fig. 2.13.6.** Magnetite from the crust of El Hammami, which also exhibits some Cr.



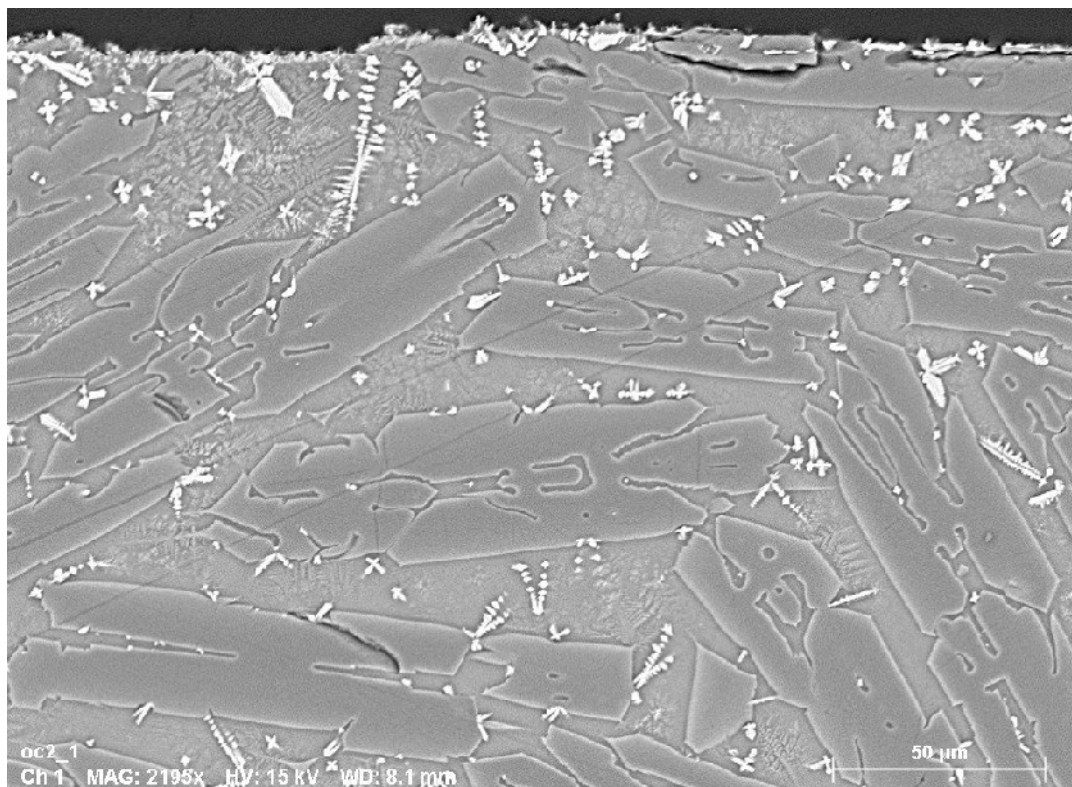


**Fig. 2.13.7.** *Portion of the crust, displaying magnetites and skeletal, zoned olivines.*

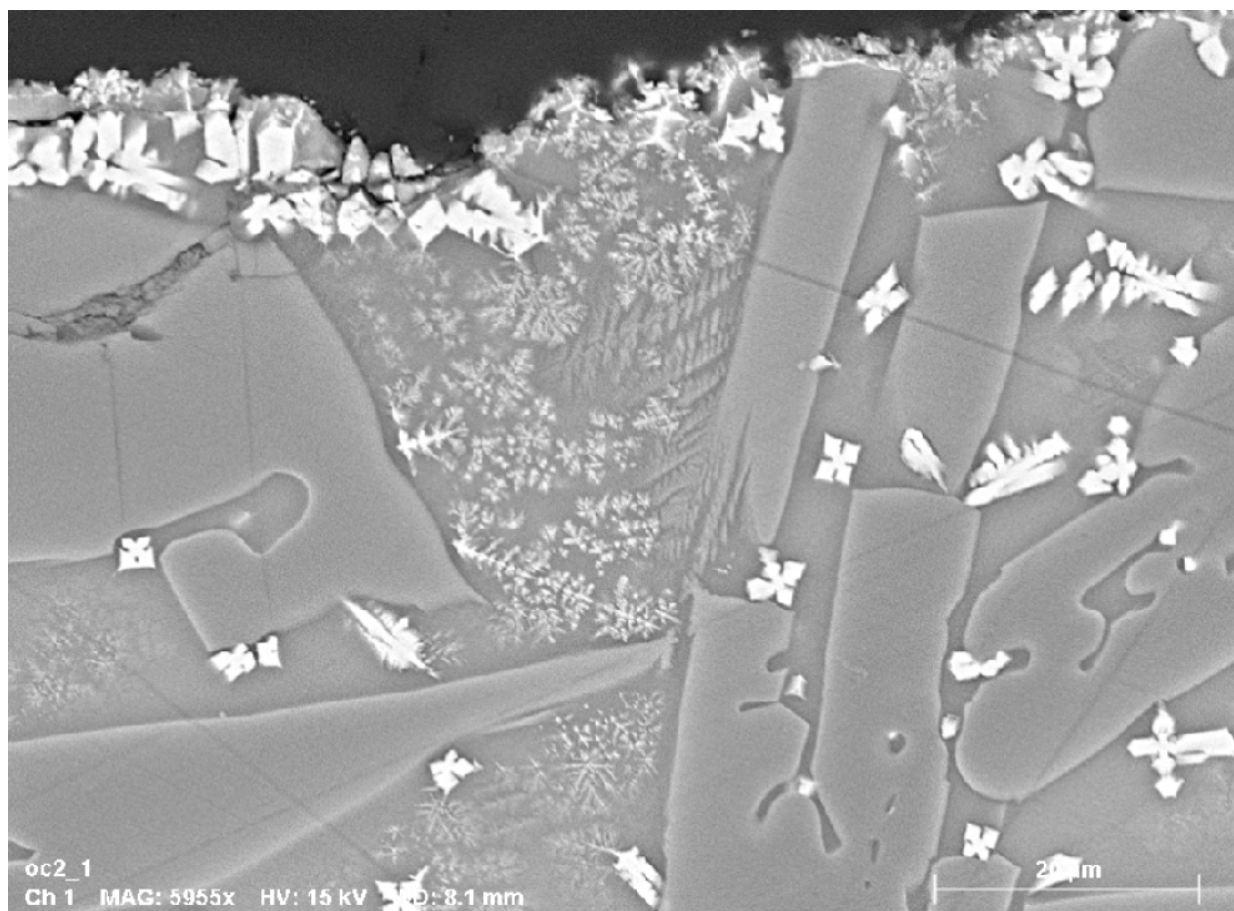


**Fig. 2.13.8.** *Portion of the crust studded with magnetites among skeletal, zoned olivines.*

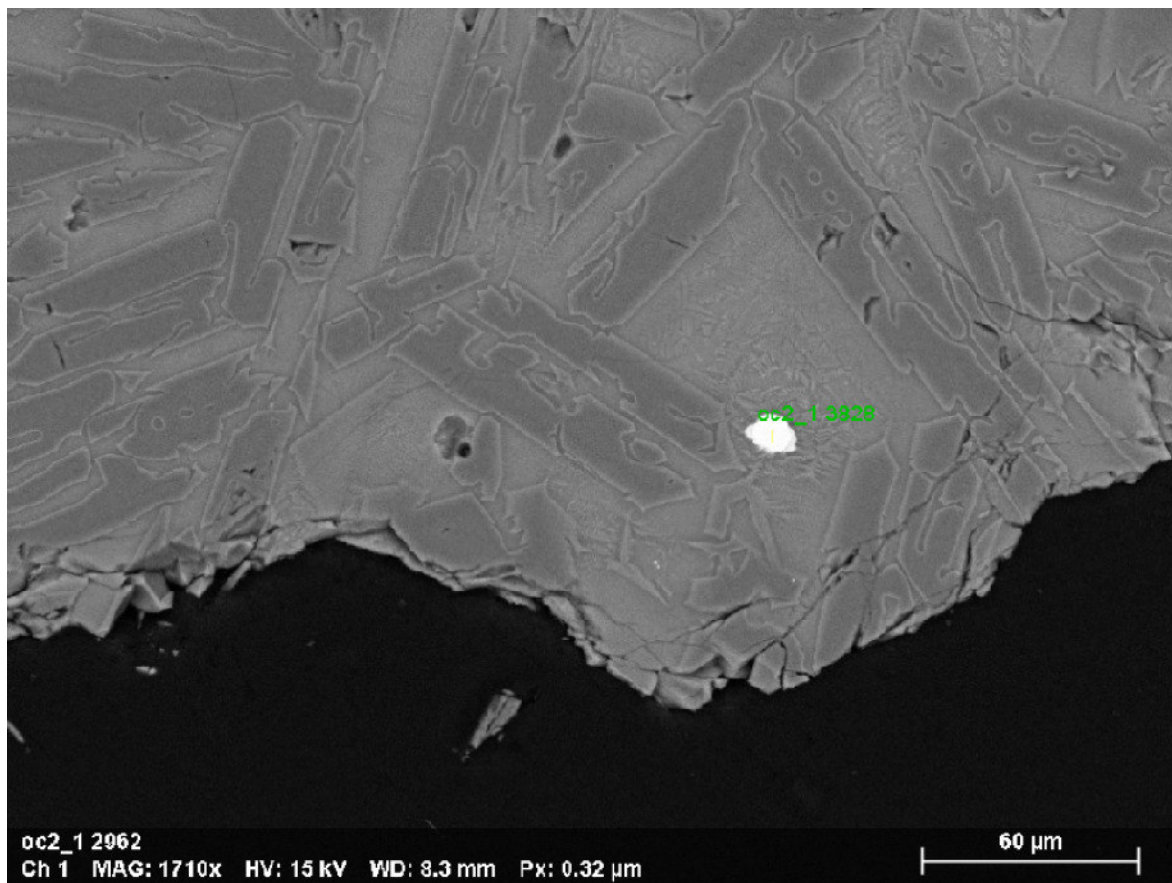


**Fig. 2.13.9.** Tetraetaenite (bright spot) surrounded by zoned olivines. Zonation likely due to fast cooling.

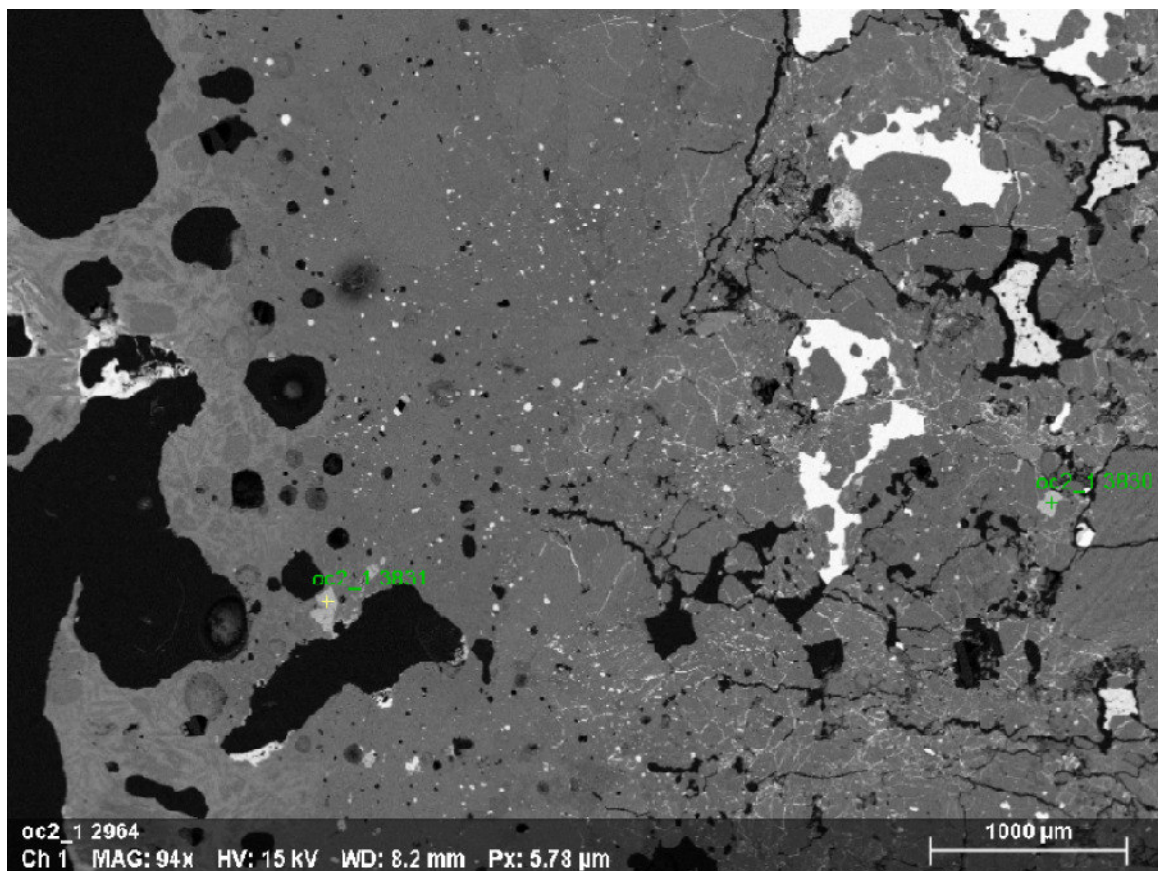


**Fig. 2.13.10.** Large-scale image of the sub-crustal zone, featuring veinlets of melted material. The green points are two chromites

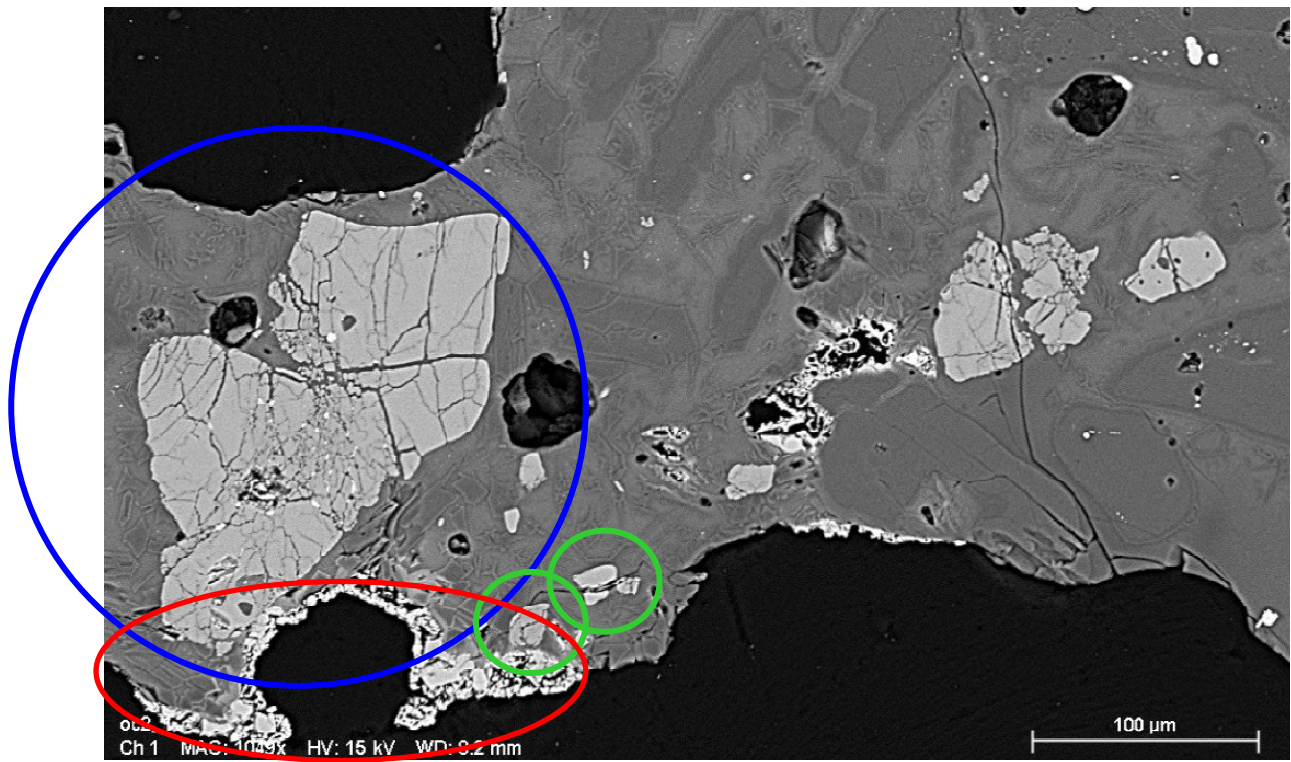


**Fig. 2.13.11.** Small magnetites (red oval) with a relic bulk chromite (blue circle), rather fractured. The green circles encompass crust chromites.



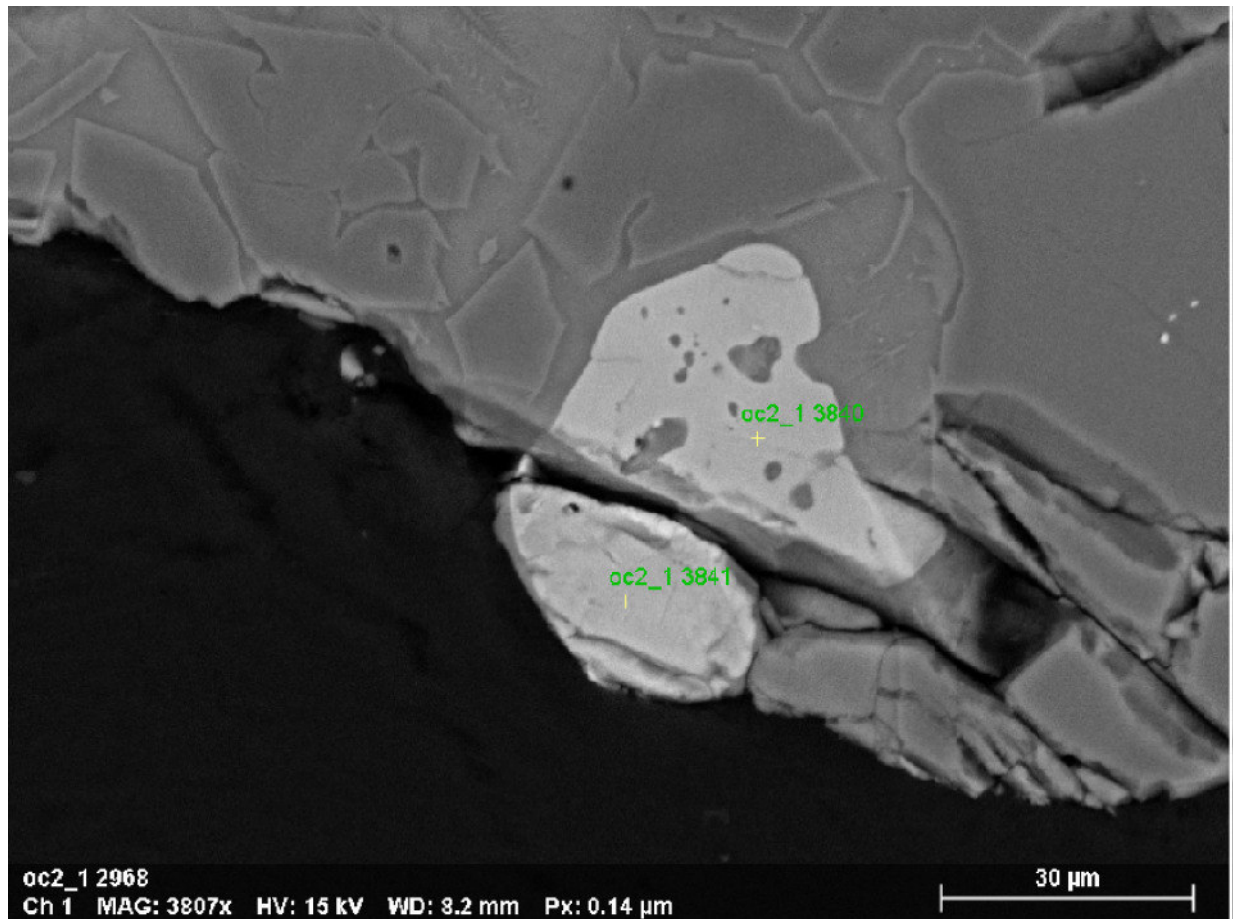


*Fig. 2.13.12. Two crust chromites.*

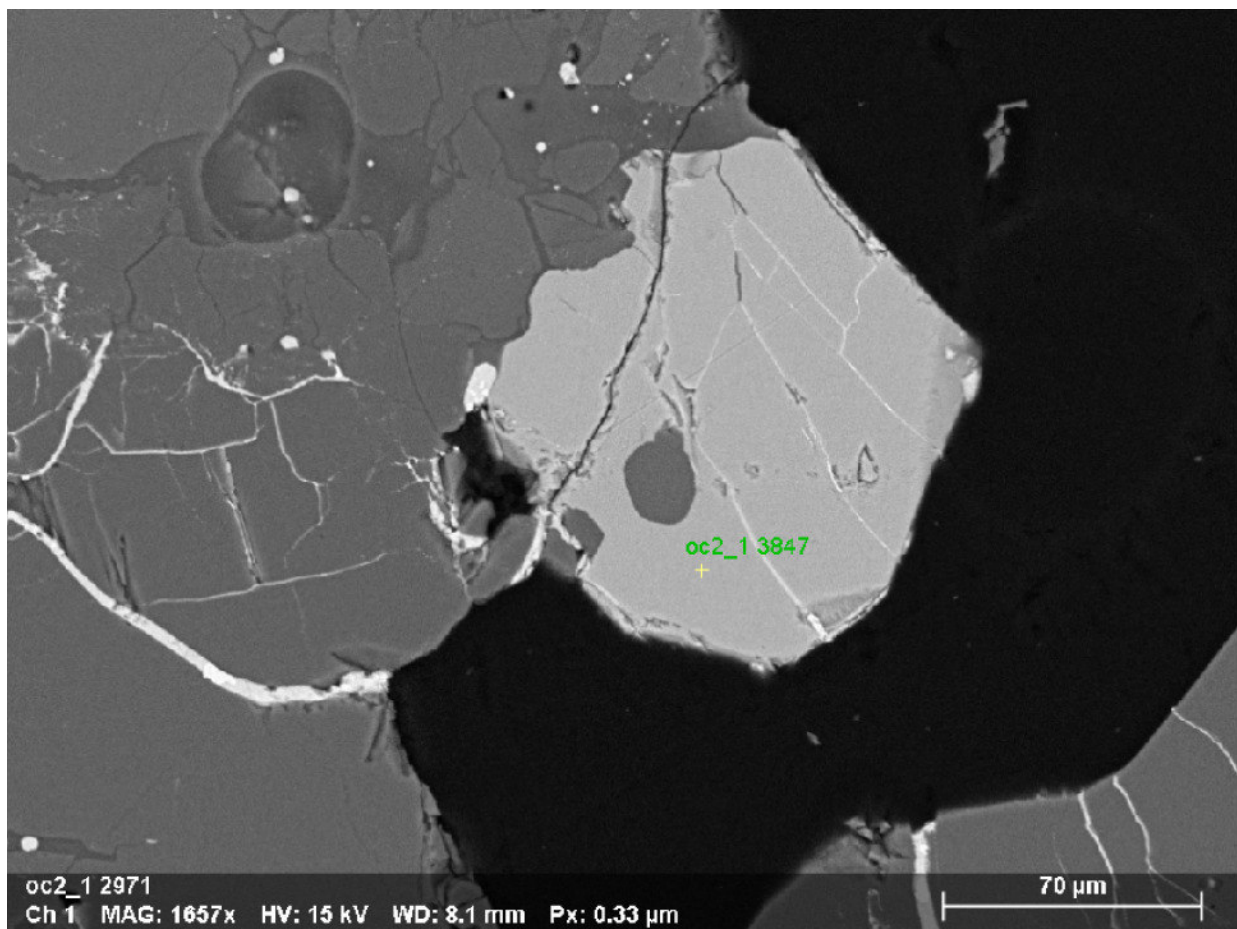


*Fig. 2.13.13. Fractured bulk chromite: fractures are not parallel to the veinlets surrounding the chromite.*

We have found and classified 25 chromites – 15 from the bulk, 10 from the crust. The complete data record is available in the appendix: below is shown the graph reporting  $Al\#$  versus  $Mg\#$  for the bulk chromites (blue circles) and the crust chromites (red circles). The error bars reported represent the standard deviation. The separation between bulk and crust is clear, though less evident than other meteorites studied in this work: bulk chromites are more tightly clustered around the average value.

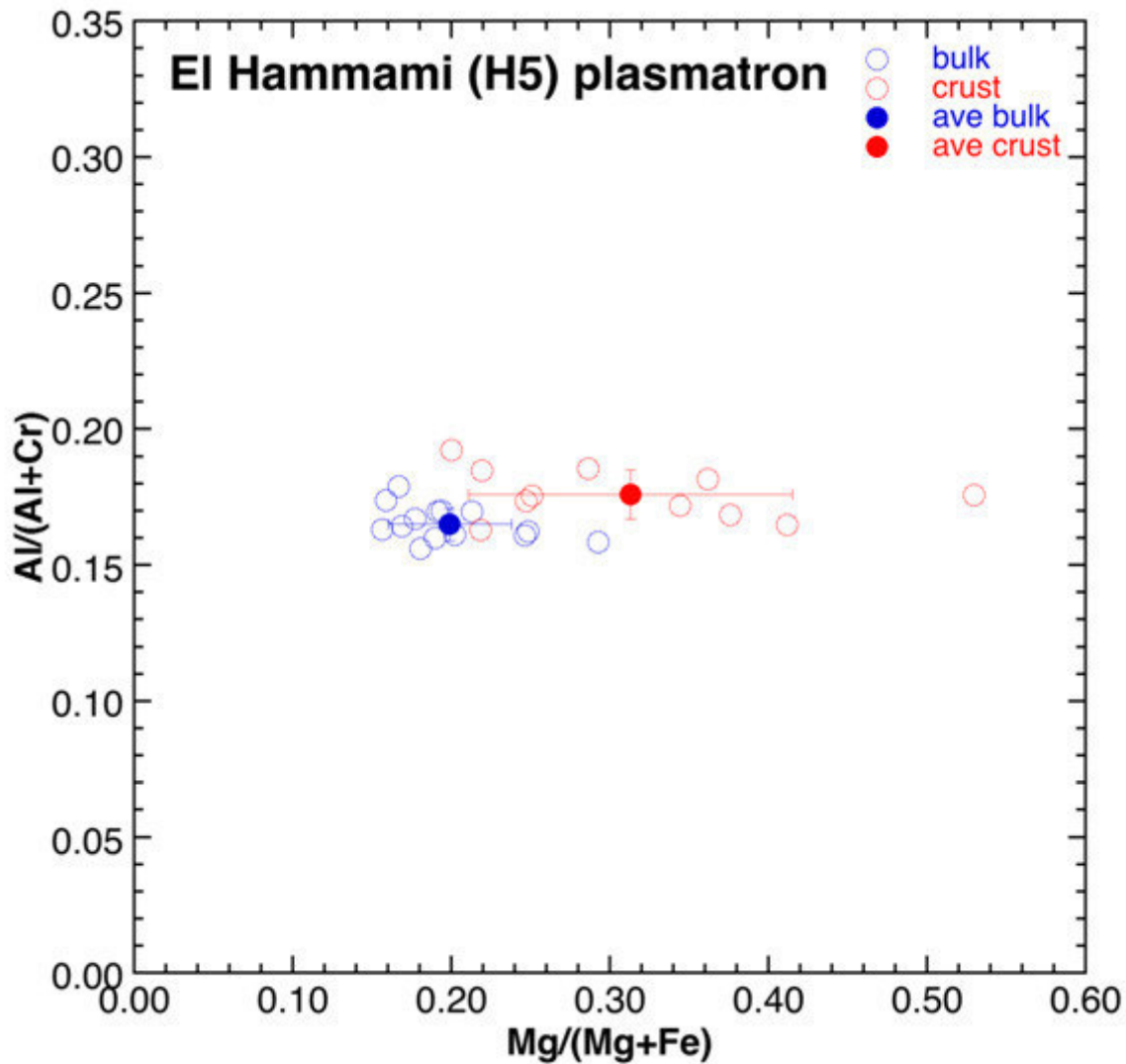


**Fig. 2.13.14.** Plot of the  $Al\#$  versus the  $Mg\#$  for crust chromites (red) and bulk chromites (blue). The error bars represent the standard deviation.

## 2.14 Discussion and conclusions

In this thesis we reported the microchemical characterization, by FE Scanning Electron Microscopy, of the chromites major and minor element composition in the fusion crusts of 10 ordinary chondrites and compared the resulting compositions with those of the chromites found in the bulk of the same meteorites. In order to minimise the possible effect of terrestrial alteration on the composition and texture of the chromites, we selected mostly “fall” meteorites (i.e., meteorites whose falls have been witnessed and that have been recovered soon after landing). In particular, the following meteorites were analysed:

- two from the LL group (Chelyabinsk LL5, Kilabo LL6)
- three from the L group (Aba Panu L3.6, Viñales L6, NWA869 L3-6)
- four from the H group: Bassikounou H5, Chergach H5, Kabo H4, Tamdakht H5.

Moreover, we also examined an H ordinary chondrite (El Hammami, H5) that has been experimentally melted (creating in laboratory a fusion crust in the process) by Plasmatron, at the von Karman Institute in Brussels, operated at known plasma temperature and velocity, and for which the surface temperature has been measured during the melting experiment. With the exceptions of El Hammami and NWA869, all the other meteorites are “falls”.

The compositions were calculated by normalising the sum of cations to three per formula units. Using this normalization, most compositions resulted in (Cr+Al+Ti+V) summing up to 2 cations per formula units, and in (Fe+Mg) summing up to 1 cation per formula units. The few exceptions (only for chromites within the crusts) will be discussed separately.

We plotted the chemical data in terms of the Mg# and the Al#. Most chromites, both in the bulk and in the fusion crusts, display minor but detectable amounts of Ti and V. Only a very minor number of chromites within the crusts display also small amounts of Ni.

Overall, we analysed 134 chromites in the bulk and 150 chromites in the crust.

In the bulk, we managed to analyse several kinds of chromites representative of a range of shock stages: from unfractured chromites, to fractured chromites, fractured chromites containing sulphide veins, and chromite-plagioclase assemblages. In the Chelyabinsk meteorite we also found a chromite vein within plagioclase. Most of these chromites display a subhedral to anhedral shape, and sizes up to several hundred micrometers across, whereas chromites in the plagioclase-chromite assemblages display smaller sizes (few micrometers) and a euhedral shape.

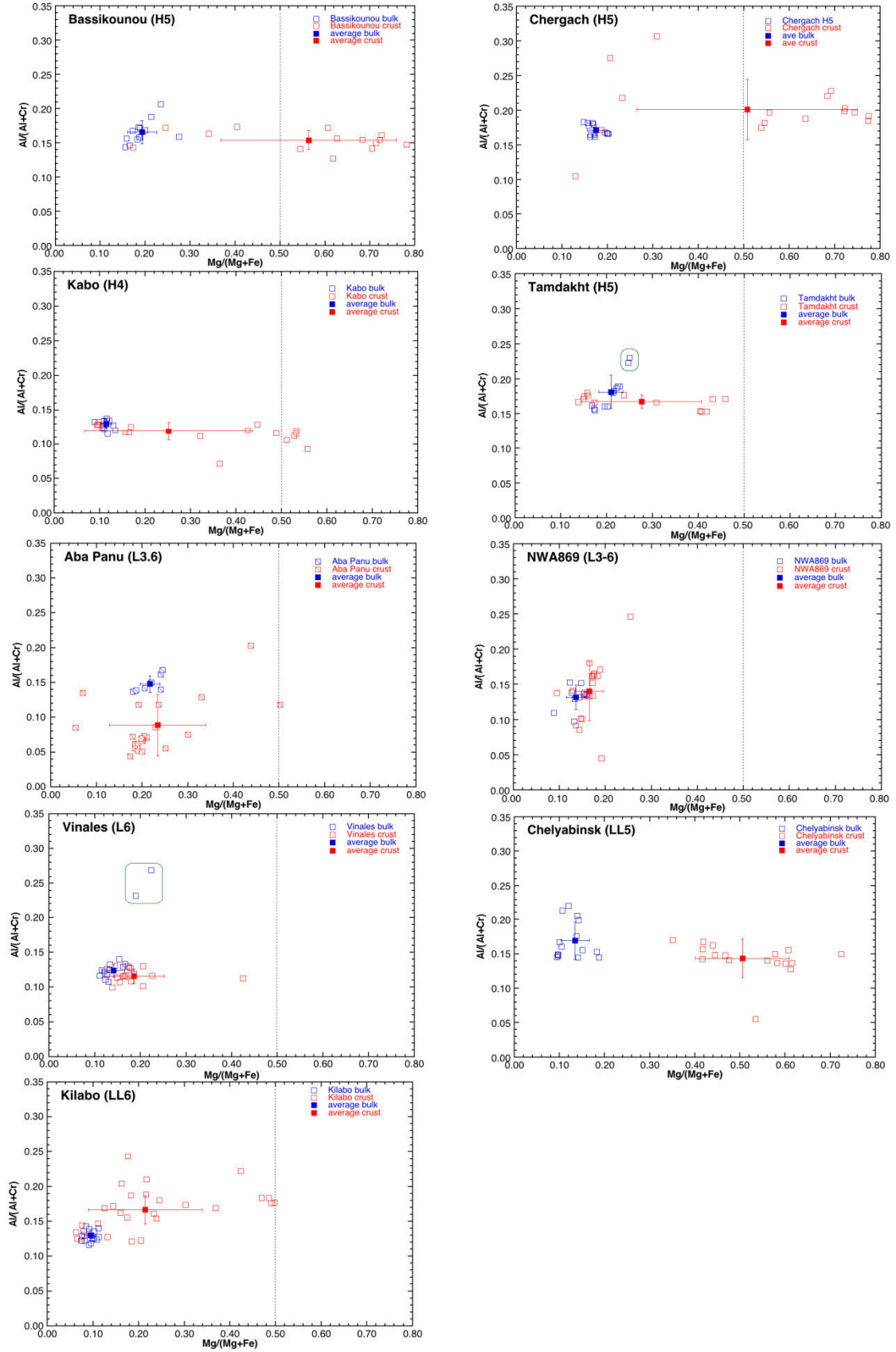
The vast majority of the chromites analysed display a very narrow range of the Al#, close to 0.14; only chromites within the plagioclase-chromite assemblages display higher values of Al# – a fact already observed by Rubin (2003). The Mg# of all the chromites analysed varies between 0.09 and 0.56, in agreement with major element compositional data already reported by Ramdohr (1967), Bunch *et al.* (1967), Schmitz *et al.* (2001), Rubin (2003), Wlotzka (2005), Heck *et al.* (2009), Thaisen *et al.* (2009), Schmitz (2013), and Lenaz *et al.* (2015); in particular, we noticed that LL ordinary chondrites exhibit slightly lower values of the Mg# compared to L and H ordinary chondrites. It is worth noticing that the standard deviations of both the Al# and the Mg# of the chromites in the bulk are generally quite low within each meteorite.

Chromites found within the fusion crusts display marked morphological differences, compared to those in the bulk: most of them are euhedral and display a much smaller size, from sub-micrometric to a few micrometers. Size is a limit to our study, as we found that only for chromites larger than 2-3 micrometers we managed to determine reliable compositions: in fact, for smaller crystal size, the interaction volume of the electrons exceeds that of the crystal and also



fluorescence emission from surrounding minerals (often olivine) markedly alters the Mg content of the analysed crystal. Despite this limitation, we managed to analyse a large number (150) of chromites, roughly equalling that of chromites in the bulk (134).

The composition of chromites in the fusion crusts can display minor to very large differences with respect to those in the bulk. While the Al# is comparable with that determined for the chromites in the bulk (between 0.09 and 0.17), the Mg# display much larger standard deviations compared to those in the bulk, and also higher values, sometimes falling within the field of magnesio-chromite composition (Mg#>0.5).



In few cases, we encountered normalised chromite compositions in the fusion crust in which the sum of Mg+Fe significantly exceeded 1 (and correspondingly, the sum of Al+Cr+Ti+V was significantly lower than 2). Our preliminary interpretation is that these compositions may result

from the presence of  $\text{Fe}^{3+}$  in the octahedral site of these crust chromites (thus introducing a magnetite component in the composition). From SEM data alone, we cannot confirm nor reject this hypothesis. It would be feasible, for future studies, to test this hypothesis by measuring Raman spectra of these unusually Fe-rich chromites, in order to confirm the presence of a significant  $\text{Fe}^{3+}$  component by comparing spectral data with those of Lenaz and Lughì (2013) and Kharbush (2018).

The presence of small but significant amounts of  $\text{Fe}^{3+}$  in the fusion crusts is compatible with experimental data on a basalt melted at the same conditions of a natural meteorite (discussed later) by means of a plasmatron at conditions tentatively mimicking those of an incoming meteoroid: in that experiment, the  $\text{Fe}^{3+}/(\text{Fe}^{2+}+\text{Fe}^{3+})$  ratio of the glass formed from the melted basalt ranged between 0.15 and 0.17. These values are consistent with the formation of small amounts of magnetite in the silicate melt, and also with a significant magnetite component in the chromite eventually formed within a melted portion of a meteorite. It is also worth remarking that a small but significant fraction (22 out of 150, or ~15%) of chromites grown in the fusion crust display a detectable Ni content, in marked contrast with those found in the bulk (only 3 out of 134, or ~2.2%).

As for the textural relationships between the minerals found within the fusion crust, we would like to remark that chromites have been always found in the mesostasis between the olivine crystals. Other spinel group minerals also have been found within the crust (namely, magnetite), always in the external portion of the melted crust layer. In several cases, chromite crystals have been found mantled by magnetite micro- to nano-crystals. While sometimes the chromite crystals were subhedral to anhedral (and interpreted as relicts from the bulk) we also observed cases where small euhedral to subhedral chromite crystals were mantled by magnetite or displayed magnetite dendrites from the vertices. Since the reverse case (i.e., magnetite mantled by chromite) has never occurred in this study, such findings may be interpreted as an indication of the crystallization sequence within the fusion crust: olivine, chromite, magnetite.

We also analysed the chromite compositions in a find meteorite (El Hammami) experimentally melted by means of a plasmatron at the Von Karman Institute (B), which has been already studied by Pittarello et al. (2019). During this experiment, both plasma temperature (10000 K) and surface temperature of the meteorite (ranging between 2400 and 2000 K) were measured. The experimentally formed fusion crust displays many features similar to those observed in the fusion crusts of many meteorites (i.e. skeletal olivines with a concentric zoning, dendritic olivines, euhedral chromites, skeletal magnetite, botroidal aggregates of Fe-FeS) and in the outer substrate (sulphide veins). When the compositions of chromites within the fusion crust were compared with those in the unmelted portion, the same pattern already observed in natural fusion crusts was evident: the average Mg# of crust chromites is significantly higher than that of bulk chromites (ca. 0.32 vs 0.20) and the standard deviation is much higher than that of bulk chromites.

These data clearly suggest that the Mg# of fusion crusts may be significantly different from that of bulk chromites. If this is the case, small size chromites in ablation spherules found in the sedimentary record – which are surely useful when attempting to trace the infall of extraterrestrial material back to the past history of Earth – may be biased and may not reflect the composition of the ordinary chondrite meteoroids from which the ablation spherules originated. For this reason, when using the chromite compositions to infer data on meteoroid composition, only chromites with a large size (possibly representative of bulk chromites) should be considered.



## Cited references

- Anders, E., and Grevesse, N. (1989). Abundances of the elements: Meteoritic and solar. *Geochimica et Cosmochimica Acta*, Vol. 53, Issue 1, pp. 197-214.
- Alexeev, V. A., Gorin, V. D., Ivliev, A. I., Kashkarov, L. L., and Ustinova, G. K. (2008). Recently fallen Bukhara (CV3) and Kilabo (LL6) chondrites: A parallel study of luminescence, tracks, and cosmogenic radionuclides. *Geochemistry International*, vol. 46, pp. 849–866, Springer.
- Beckett, J. R., Connolly, H. C., Ebel, D. S. (2006). Chemical Processes in Igneous Calcium-Aluminum-rich Inclusions: A Mostly CMAS View of Melting and Crystallization. In *Meteorites and the Early Solar System II* (D. S. Lauretta and H. Y. McSween Jr., eds.), Univ. of Arizona, Tucson.
- Biagioni, C., Pasero, M. (2014). The systematics of the spinel-type minerals: An overview. *American Mineralogist*, 99 (7), pp. 1254-1264.
- Bischoff, A., Scott, E. R. D., Metzler, K., and Goodrich C. A. (2006). Nature and origins of meteoritic breccias. *Meteorites and the Early Solar System II* (D. S. Lauretta and H. Y. McSween Jr., eds.). Univ. of Arizona, Tucson.
- Bland, P. A., Smith, T. B., Jull, J. T., Berry, F. J., Bevan, A. W. R., Cloudt, S., Pill, C. T. (1996). The flux of meteorites to the Earth over the last 50 000 years. *MNRAS*, Vol. 283. Issue 2, pp. 551-565.
- Brezina, A. (1904). The Arrangement of Collections of Meteorites. *Proceedings of the American Philosophical Society*, Vol. 43, No. 176, pp. 211-247. Published by: American Philosophical Society Stable URL: <https://www.jstor.org/stable/983506>
- Bronshten, V. A. (1983). Physics of Meteoric Phenomena. D. Reidel Publishing Company, Dordrecht, Holland. Translated from Russian edition, 1981 Nauka ed.
- Brownlee, D. E., Bates, B. and Beauchamp, R. H. (1983). Meteor Ablation Spherules as Chondrule Analogs. *Lunar and Planetary Science XIV*, 14-19 March, Lunar and Planetary Institute.
- Bunch, T. E., Keil, K. and Snetsinger, K. G. (1967). Chromite composition in relation to chemistry and texture of ordinary chondrites. *Geochimica et Cosmochimica Acta*, Vol. 31, pp. 1569-1582.
- Chennaoui, H. A., Mazurier, A., El Albani, A., Devouard, B., Rochette, P., Boudouma, Shisseh, T. (2017). Tamdakht meteorite (Morocco): an important fall with a rare fusion crust. *80th Annual Meeting of the Meteoritical Society, held July 23-28, 2017 in Santa Fe, New Mexico. LPI Contribution No., 1987, id.6140*

- Clayton, R. N. and Mayeda, T. K. (1996). Oxygen-isotope studies of achondrites. *Geochimica et Cosmochimica Acta*, Vol. 60, pp 1999–2018.
- Cole, K. J., Schultz, L., Sipiera, P. P., and Welten, K. C. (2007). Kilabo and Bensour, Two LL6 Chondrite Falls from Africa with Very Similar Mineralogical Compositions but Different Cosmic-Ray Exposure Histories. *38th Lunar and Planetary Science Conference, (Lunar and Planetary Science XXXVIII), held March 12-16, 2007 in League City, Texas. LPI Contribution No. 1338, p.1477*
- Cotto-Figueroa, D., Fazle Rabbi, Md, Rai, A., Chattopadhyay, A., Laurence A.J. Garvie A. A. L. and Asphaug, E. (2019). On the Strength of the Aba Panu (L3) Meteorite: Implications for Hazard Mitigation. *EPSC Abstracts Vol. 13, EPSC-DPS2019-1560-1*
- Ebel, D. S. (2006). Condensation of rocky material in astrophysical environments. In *Meteorites and the Early Solar System II, (D. S. Lauretta and H. Y. McSween Jr., eds.), Univ. of Arizona, Tucson.*
- Fedkin, A. V., and Grossman, L. (2006). The fayalite content of chondritic olivine: Obstacle to understanding the condensation of rocky material. In *Meteorites and the Early Solar System II, (D. S. Lauretta and H. Y. McSween Jr., eds.), Univ. of Arizona, Tucson.*
- Genge, M.J. and Grady, M.M. (1999). The fusion crusts of stony meteorites: Implications for the atmospheric reprocessing of extraterrestrial materials. *Meteoritics & Planetary Science*, 34, 341-356.
- Helber, B., Dias, B., Bariselli, F., Zavalan, L. F., Pittarello, L., Goderis, S., Soens, B., McKibbin, S. J., Claeys, P., and Magin, T. E., (2019). Analysis of Meteoroid Ablation Based on Plasma Wind-tunnel Experiments, Surface Characterization, and Numerical Simulations. *The Astrophysical Journal*, 876:120 (14pp).
- Huss, G. R., Rubin, A. E., and Grossman J. N. (2006). Thermal metamorphism in chondrites. In *Meteorites and the Early Solar System II (D. S. Lauretta and H. Y. McSween Jr., eds.). Univ. of Arizona, Tucson.*
- Hutchison, R., Ajakaiye, D. E., Elliott, C. J., and Fry, F. A. (1973). The Kabo, Nigeria, meteorite fall. *Mineralogical Magazine, Volume 39, Issue 303, pp. 340–345.*
- Hutchison, R. (2004). Meteorites: A Petrologic, Chemical and Isotopic Synthesis. *Cambridge Univ. Press, Cambridge.*
- Kallemeyn, G. W., Boynton, W. V., Willis, J., and Wasson, J. T. (1978). Formation of the Bencubbin polymict meteoritic breccia. *Geochimica et Cosmochimica Acta*, 42, pp. 507–515.
- Kallemeyn, G. W. and Wasson, J. T. (1981). The compositional classification of chondrites: I. The carbonaceous chondrite groups. *Geochimica et Cosmochimica Acta*, 45, pp. 1217–1230.

Kallemeyn, G. W., and Wasson, J. T. (1982). The compositional classification of chondrites: III. Ungrouped carbonaceous chondrites. *Geochimica et Cosmochimica Acta*, 46, pp. 2217–2228.

Kallemeyn, G. W., and Wasson J. T., (1985). The compositional classification of chondrites: IV. Ungrouped chondritic meteorites and clasts. *Geochimica et Cosmochimica Acta*, 49, pp. 261–270.

Kallemeyn, G. W., Rubin, A. E., Wang, D., and Wasson, J. T. (1989). Ordinary chondrites: Bulk compositions, classification, lithophile-element fractionations, and composition-petrographic type relationships. *Geochimica et Cosmochimica Acta*, 53, pp. 2747–2767.

Kallemeyn G. W., Rubin A. E., and Wasson J. T. (1991) The compositional classification of chondrites: V. The Karoonda (CK) group of carbonaceous chondrites. *Geochimica et Cosmochimica Acta*, 55, pp. 881–892.

Kallemeyn G. W., Rubin A. E., and Wasson J. T. (1994) The compositional classification of chondrites: VI. The CR carbonaceous chondrite group. *Geochimica et Cosmochimica Acta*, 58, pp. 2873–2888.

Kallemeyn, G. W., Rubin, A. E., and Wasson, J. T. (1996). The compositional classification of chondrites: VII. The R chondrite group. *Geochimica et Cosmochimica Acta*, 60, pp. 2243–2256.

Kerridge, J. F. (1985). Carbon, hydrogen, and nitrogen in carbonaceous chondrites: Abundances and isotopic compositions in bulk samples. *Geochimica et Cosmochimica Acta*, 49, pp. 1707–1714.

Kharbish, S. (2018). Raman spectroscopic features of Al- Fe<sup>3+</sup>- poor magnesiochromite and Fe<sup>2+</sup>- Fe<sup>3+</sup>- rich ferrian chromite solid solutions. *Mineralogy and Petrology*, 112 (2), pp. 245–256.

Krot, A. N., Keil, K., Goodrich, C. A., Scott, E. R. D., Weisberg, M. K. (2003). Classification of Meteorites. In *Treatise on Geochemistry*, vol. 1, cap. 1, H. D. Holland and K. K. Turekian (eds.), Elsevier.

Krot, A. N., Zolensky, M. E., Wasson, J. T., Scott, E. R. D., Keil, K., and Ohsumi, K. (1997). Carbide-magnetite assemblages in type-3 ordinary chondrites. *Geochimica et Cosmochimica Acta*, Vol. 61, No. 1, pp. 219–237.

Kung C. C., and Clayton, R. N. (1978). Nitrogen abundances and isotopic compositions in stony meteorites. *Earth and Planetary Sciences Letters*, 38, pp. 421–435.

Lenaz, D., Lughi, V. (2013) Raman study of MgCr<sub>2</sub>O<sub>4</sub>-Fe<sup>2+</sup>Cr<sub>2</sub>O<sub>4</sub> and MgCr<sub>2</sub>O<sub>4</sub>-MgFe<sup>3+</sup>O<sub>4</sub> synthetic series: The effects of Fe<sup>2+</sup> and Fe<sup>3+</sup> on Raman shifts. *Physics and Chemistry of Minerals*, 40 (6), pp. 491–498.

Love, S. G., Brownlee, D. E. (1991). Heating and thermal transformation of micro-meteoroids entering the Earth's atmosphere. *Icarus*, Vol. 89, Issue 1, pp. 26–43.



McSween, H. (1987). *Meteorites and Their Parent Planets. Cambridge University Press, Cambridge.*

Metzler, K., Bischoff, A., Greenwood, R., Palme, H., Gellissen, M., Hopp, J., Franchi, I. A., and Trieloff, M. (2011). The L3–6 chondritic regolith breccia Northwest Africa (NWA) 869: (I) Petrology, chemistry, oxygen isotopes, and Ar-Ar age determinations. *Meteoritics & Planetary Science*, Vol. 46, Nr 5, pp. 652–680 (2011).

Norton, R. O. (1994). *Rocks from Space. Mountain Press Publishing Company*

Norton, R. O. (2002). *The Cambridge Encyclopedia of Meteorites. Cambridge University Press, Cambridge.*

Pittarello, L., Goderis, S., Soens, B., McKibbin, S.J., Giuli, G., Bariselli, F., Dias, B., Helberg, B., Lepore, G.O., Vanhaecke, F., Koeberl, C., Magin, T. E., Claeys, P. (2019). Meteoroid atmospheric entry investigated with plasma flow experiments: Petrography and geochemistry of the recovered material. *Science Direct, Icarus 331*, pp. 170-178.

Popova, O. P., Jenniskens, P., Emel'yanenko, V., Kartashova, A., Biryukov, E., Khaibrakhmanov, S., Shuvalov, V., Rybnov, Y., Dudorov, A., Victor I. Grokhovsky, Badyukov, D. D., Yin, Q., Gural, P. S., Albers, J., Granvik, M., Evers, L. G., Kuiper, J., Kharlamov, V., Solovyov, A., Rusakov, Y. S., Korotkiy, S., Serdyuk, I., Korochantsev, A. V., Larionov, M. Yu., Glazachev, D., Mayer, A. E., Gisler, G., Gladkovsky, S. V., Wimpenny, J., Sanborn, M. E., Yamakawa, A., Verosub, K. L., Rowland, D. J., Roeske, S., Botto, N. W., Friedrich, J. M., Zolensky, M. E., Le, L., Ross, D., Ziegler, K., Nakamura, T., Ahn, I., Lee, J. I., Zhou, Q., Li, X., Li, Q., Liu, Y., Tang, G., Hiroi, T., Sears, D., Weinstein, I. A., Vokhmintsev, A. S., Ishchenko, A. V., Schmitt-Kopplin, P., Hertkorn, N., Nagao, K., Haba, M. K., Komatsu, M., Mikouchi, T. (2013). Chelyabinsk Airburst, Damage Assessment, Meteorite Recovery, and Characterization. *Science* 29, Vol. 342, Issue 6162, pp. 1069-1073.

Prior, G. T. (1916). On the genetic relationship and classification of meteorites. *Mineralogical Magazine*, 18 (83), pp.26–44.

Ramdohr, P. (1967). Chromite and chromite chondrules in meteorites-I. *Geochimica et Cosmochimica Acta*, 31 (10), pp. 1961-1962,IN59-IN69,1963-1967.

Rout, S.S., Heck, P.R., Zaluzec, N.J., Ishii, T., Wen, J., Miller, D.J., Schmitz, B. (2017). Shocked chromites in fossil L chondrites: A Raman spectroscopy and transmission electron microscopy study. *Meteoritics and Planetary Science*, 52 (9), pp. 1776-1796.

Rubin, A. E. (1990). Kamacite and olivine in ordinary chondrites: Intergroup and intragroup relationships. *Geochimica et Cosmochimica Acta*, 54, pp. 1217–1232.

Rubin, A.E. (1997). Mineralogy of meteorite groups. *Meteoritics and Planetary Science*, 32 (2), pp. 231-247.

Rubin, A.E. (2003). Chromite-plagioclase assemblages as a new shock indicator; Implications for the shock and thermal histories of ordinary chondrites. *Geochimica et Cosmochimica Acta*, Vol. 67 (14), pp. 2695-2709.

Sears, D. W. G., Grossman, J. N., Melcher, C. L., Ross, L. M., and Mills, A. A. (1980). Measuring the metamorphic history of unequilibrated ordinary chondrites. *Nature*, 287, pp. 791–795.

Sears, D. W. G., Kallemeyn, G. W., and Wasson, J. T. (1982) The compositional classification of chondrites: II. The enstatite chondrite groups. *Geochimica et Cosmochimica Acta*, 46, pp. 597–608.

Schmitz, B., and Tassinari, M. (2001). Fossil Meteorites. In Peucker-Ehrenbrink B., Schmitz B. (eds), *Accretion of Extraterrestrial Matter Throughout Earth's History*. Springer, Boston, MA., pp. 319-331.

Stennikov, A. V., Fedulov, V. S., Naimushin, S. G., Dushenko, N. V. and Voropaev, S. A. (2020). Study of the Composition of ABA Panu (L3) Meteorite Degassing Products. *Solar System Research*, 54, pp. 150–154.

Taylor, S., and Brownlee, D. E. (1991). Cosmic Spherules in the Geologic Record. *Meteoritics and Planetary Science*, 26 (3), pp. 203-211.

Taylor, S., Lever, J. H., and Harvey, R. P. (1998). Accretion rate of cosmic spherules measured at South Pole. *Nature*, Vol. 392, pp. 899-903.

Tomkins, A. G. (2009). What metal-troilite textures can tell us about post-impact metamorphism in chondrite meteorites. *Meteoritics & Planetary Science* 44, Nr. 8, pp. 1133–1149.

Ustinova, G. K., Alexeev, V. A., and Gorin, V. D. (2008). Orbits and Probable Parent Body of the Kilabo and Bensour LL6-Chondrites. In *39th Lunar and Planetary Science Conference, (Lunar and Planetary Science XXXIX), held March 10-14, 2008 in League City, Texas. LPI Contribution No. 1391., p.1011*

Van Schmus, W. R., Wood, J. A. (1967). A chemical-petrologic classification for the chondritic meteorites. *Geochimica et Cosmochimica Acta*, Vol. 31, Issue 5, pp. 747-754.

Vinnikov, V., Gritsevich, M., and Turchak, L. (2014). Shape estimation for Košice, Almahata Sitta and Bassikounou meteoroids. *Challenges in 21st Century Cosmology Proceedings IAU Symposium No. 306, A. F. Heavens, J.-L. Starck & A. Krone-Martins (eds)*.

Wasson, J. T., and Kallemeyn, G. W. (1988). Composition of chondrites. *Philos. Trans. R. Soc. London*, A325, pp. 535–544.

Weisberg M. K., Prinz M., Clayton R. N., Mayeda T. K., Grady M. M., and Pillinger C. T. (1995). The CR chondrite clan. *Proc. NIPR Symp. Antarct. Meteorites*, 8, pp. 11–32.

Weisberg, M. K., McCoy, T. J., and Krot, A. N. (2006). Systematics and Evaluation of Meteorite Classification. *Meteorites and the Early Solar System II (D. S. Lauretta and H. Y. McSween Jr., eds.)*. Univ. of Arizona, Tucson.

Wlotzka, F. (2005). Cr spinel and chromite as petrogenetic indicators in ordinary chondrites: Equilibration temperatures of petrologic types 3.7 to 6. *Meteoritics & Planetary Science*, 40, No. 11, pp. 1673–1702.

Yakame, S., Uesugi, M., Karouji, Y., Ishibashi, Y., Yada, T., Okada, T., Abe, M., Fujimura, A. (2012). Observation of Shock Textures in Fragments of Kilabo(LL6). In 75th Annual Meeting of the Meteoritical Society, held August 12-17, 2012 in Cairns, Australia. Published in *Meteoritics and Planetary Science Supplement*, id.5169

Yin, F., and Dai, D. (2021). Petrology and mineralogy of the Viñales meteorite, the latest fall in Cuba. *Science Progress*, Vol. 104(2), pp. 1–12.

Zolensky, M., Bland, P. A., Brown, P., Holliday, I. (2006). Flux of Extraterrestrial Materials. In *Meteorites and the Early Solar System II* (D. S. Lauretta and H. Y. McSween Jr., eds.). Univ. of Arizona, Tucson.



# ABA PANU L3.6

Name	Fe	Mg	Mn	Ni	Cr	Al	Ti	V	sum A	sum B	Mg#	Al#	Fe <sub>3+</sub> /Fe <sub>tot</sub>	TiO <sub>2</sub> wt%	Type	Num
2577	0,894	0,347			1,622	0,090	0,047		1,241	1,759	0,280	0,053	0,27	1,78	BULK	1
3405	0,397	0,239			2,167	0,004	0,098	0,095	0,636	2,364	0,376	0,002	0	3,60	BULK	2
3406	0,396	0,227			2,136	0,045	0,099	0,096	0,623	2,377	0,365	0,021	0	3,65	BULK	3
3407	0,403	0,233			2,121	0,049	0,110	0,084	0,636	2,364	0,366	0,023	0	4,04	BULK	4
3408	0,394	0,241			2,111	0,060	0,108	0,086	0,636	2,364	0,380	0,027	0	3,99	BULK	5
3409	0,400	0,263			2,013	0,088	0,143	0,092	0,664	2,336	0,397	0,042	0	5,32	BULK	6
3410	0,388	0,259			2,135	0,039	0,100	0,080	0,647	2,353	0,401	0,018	0	3,67	BULK	7
3411	0,392	0,253			2,128	0,051	0,098	0,078	0,645	2,355	0,393	0,024	0	3,60	BULK	8
3412	0,401	0,253			2,109	0,060	0,094	0,083	0,654	2,346	0,387	0,027	0	3,48	BULK	9
3494	0,746	0,285			1,600	0,324	0,031	0,015	1,031	1,969	0,276	0,168	0,04	1,18	BULK	10
3499	0,745	0,288			1,190	0,760	0,015	0,002	1,033	1,967	0,279	0,390	0,04	0,60	BULK	11
3500	0,715	0,264			1,278	0,715	0,018	0,011	0,979	2,021	0,270	0,359	0	0,73	BULK	12
3502	0,647	0,356			1,015	0,958	0,018	0,006	1,003	1,997	0,355	0,486	0,00	0,75	BULK	13
3504	0,783	0,249			1,607	0,311	0,045	0,005	1,031	1,969	0,241	0,162	0,04	1,73	BULK	14
3505	0,805	0,209			1,649	0,272	0,048	0,016	1,014	1,986	0,206	0,142	0,02	1,84	BULK	15
3506	0,793	0,251			1,635	0,266	0,049	0,006	1,044	1,956	0,241	0,140	0,06	1,86	BULK	16
3507	0,794	0,224			1,622	0,286	0,057	0,016	1,018	1,982	0,220	0,150	0,02	2,19	BULK	17
3508	0,779	0,253			1,578	0,319	0,056	0,015	1,032	1,968	0,245	0,168	0,04	2,17	BULK	18
3509	0,835	0,184			1,637	0,259	0,069	0,015	1,019	1,981	0,180	0,137	0,02	2,59	BULK	19
3510	0,826	0,190			1,647	0,265	0,056	0,016	1,016	1,984	0,187	0,139	0,02	2,12	BULK	20
3425	0,847	0,225			1,724	0,131	0,074		1,072	1,928	0,210	0,071	0,08	2,75	CRUST	21
3426	0,857	0,220			1,714	0,135	0,074		1,077	1,923	0,204	0,073	0,09	2,78	CRUST	22
3431	0,865	0,225			1,714	0,159	0,038		1,089	1,911	0,206	0,085	0,10	1,41	CRUST	23
3432	0,729	0,569			1,331	0,339	0,021	0,011	1,298	1,702	0,438	0,203	0,41	0,86	CRUST	24
3432 bis	0,730	0,569			1,331	0,339	0,020	0,011	1,298	1,702	0,438	0,203	0,41	0,83	CRUST	25
3434	0,833	0,247	0,018		1,697	0,160	0,035	0,010	1,098	1,902	0,229	0,086	0,12	1,31	CRUST	26
3436	0,871	0,190			1,762	0,136	0,037	0,005	1,060	1,940	0,179	0,072	0,07	1,36	CRUST	27
3438	0,848	0,362			1,622	0,132	0,032	0,004	1,210	1,790	0,299	0,075	0,25	1,22	CRUST	28
3448	0,840	0,282			1,754	0,102	0,022		1,122	1,878	0,251	0,055	0,14	0,84	CRUST	29
3448 bis	0,839	0,282			1,755	0,101	0,022		1,121	1,879	0,251	0,055	0,14	0,84	CRUST	30
3449	0,857	0,195			1,766	0,116	0,048	0,018	1,052	1,948	0,185	0,062	0,06	1,77	CRUST	31
3450	0,849	0,200			1,765	0,116	0,051	0,019	1,049	1,951	0,191	0,062	0,06	1,90	CRUST	32
3451	0,817	0,403			1,517	0,224	0,024	0,015	1,220	1,780	0,330	0,129	0,27	0,93	CRUST	33
3452	0,814	0,277			1,615	0,251	0,026	0,016	1,091	1,909	0,254	0,135	0,11	1,01	CRUST	34
3453	0,871	0,206			1,654	0,221	0,029	0,019	1,078	1,922	0,192	0,118	0,09	1,08	CRUST	35
3454	0,771	0,778			1,249	0,167	0,023	0,013	1,549	1,451	0,502	0,118	0,71	0,95	CRUST	36
3472-73-74	0,879	0,199			1,771	0,103	0,049		1,078	1,922	0,184	0,055	0,09	1,83	CRUST	37
3475	0,817	0,476			1,537	0,114	0,041	0,016	1,293	1,707	0,368	0,069	0,36	1,58	CRUST	38
3476-77	0,861	0,217			1,756	0,126	0,040		1,078	1,922	0,201	0,067	0,09	1,51	CRUST	39
3478-79	0,842	0,211			1,747	0,123	0,058	0,018	1,053	1,947	0,200	0,066	0,06	2,18	CRUST	40
3480-81	0,860	0,213			1,727	0,130	0,065	0,005	1,073	1,927	0,198	0,070	0,08	2,42	CRUST	41
3485	0,863	0,180			1,813	0,082	0,040	0,022	1,043	1,957	0,173	0,044	0,05	1,46	CRUST	42
3486	0,855	0,201			1,784	0,098	0,045	0,016	1,056	1,944	0,191	0,052	0,07	1,67	CRUST	43
3487	0,856	0,213			1,778	0,095	0,047	0,011	1,069	1,931	0,200	0,051	0,08	1,75	CRUST	44
3490	0,805	0,248			1,692	0,226	0,024	0,004	1,053	1,947	0,236	0,118	0,07	0,91	CRUST	45

# BASSIKONOU H5

Name	Fe	Mg	Mn	Ni	Cr	Al	Ti	V	sum A	sum B	Mg#	Al#	Fe <sub>3+</sub> /Fe <sub>tot</sub>	TiO <sub>2</sub> wt%	Type	Num
10755	0,865	0,193			1,572	0,289	0,056	0,025	1,058	1,942	0,182	0,155	0,07	2,13	BULK	1
10756	0,852	0,212			1,538	0,312	0,062	0,025	1,064	1,936	0,199	0,169	0,07	2,37	BULK	2
10757	0,867	0,202			1,555	0,292	0,058	0,025	1,069	1,931	0,189	0,158	0,08	2,21	BULK	3
10758	0,892	0,203			1,531	0,321	0,052		1,095	1,905	0,186	0,173	0,11	2,00	BULK	4
10759	0,795	0,301			1,534	0,290	0,057	0,024	1,096	1,904	0,274	0,159	0,12	2,20	BULK	5
10764	0,866	0,234			1,505	0,116	0,045		1,101	1,667	0,213	0,072	0,38	1,84	BULK	6
10765	0,911	0,167			1,601	0,269	0,051		1,078	1,922	0,155	0,144	0,09	1,94	BULK	7
10766	0,837	0,256			1,472	0,384	0,028	0,022	1,093	1,907	0,234	0,207	0,11	1,10	BULK	8
10767	0,945	0,186			1,428	0,246	0,195		1,131	1,869	0,165	0,147	0,14	7,35	BULK	9
10768	0,863	0,200			1,552	0,322	0,038	0,024	1,063	1,937	0,189	0,172	0,07	1,47	BULK	10
10807	0,890	0,185		0,045	1,502	0,303	0,050	0,025	1,120	1,880	0,172	0,168	0,13	1,90	BULK	11
10819	0,861	0,197			1,565	0,295	0,059	0,023	1,058	1,942	0,186	0,158	0,07	2,25	BULK	12
10820	0,887	0,167			1,582	0,294	0,044	0,027	1,054	1,946	0,158	0,157	0,06	1,66	BULK	13
10776	0,863	0,180			1,637	0,273	0,023	0,023	1,043	1,957	0,173	0,143	0,05	0,89	CRUST	14
10792	0,316	0,818		0,027	1,506	0,276	0,036	0,021	1,161	1,839	0,722	0,155	0,51	1,52	CRUST	15
10793	0,330	0,789		0,029	1,541	0,254	0,034	0,023	1,148	1,852	0,705	0,142	0,45	1,40	CRUST	16
10794	0,318	0,844		0,028	1,474	0,284	0,032	0,020	1,190	1,810	0,726	0,162	0,60	1,36	CRUST	17
10798	0,710	0,368			1,562	0,305	0,028	0,027	1,078	1,922	0,341	0,163	0,11	1,10	CRUST	18
10799	0,698	0,473			1,466	0,309	0,030	0,025	1,171	1,829	0,404	0,174	0,24	1,19	CRUST	19
10800	0,533	0,821			1,327	0,277	0,021	0,021	1,354	1,646	0,606	0,173	0,66	0,91	CRUST	20
10801	0,878	0,284			1,472	0,307	0,034	0,025	1,163	1,837	0,245	0,172	0,19	1,30	CRUST	21
10804	0,365	0,787		0,021	1,509	0,276	0,019	0,023	1,173	1,827	0,683	0,154	0,47	0,78	CRUST	22
10805	0,527	0,629		0,031	1,505	0,248	0,041	0,019	1,188	1,812	0,544	0,142	0,36	1,65	CRUST	23
10810	0,410	0,688		0,023	1,535	0,286	0,035	0,025	1,120	1,880	0,626	0,157	0,29	1,42	CRUST	24
10814	0,417	0,674		0,030	1,594	0,233	0,026	0,026	1,121	1,879	0,617	0,127	0,29	1,07	CRUST	25
10815	0,317	0,791		0,022	1,524	0,270	0,055	0,021	1,130	1,870	0,714	0,150	0,41	2,30	CRUST	26
10816	0,266	0,952		0,033	1,443	0,249	0,037	0,019	1,251	1,749	0,782	0,147	0,94	1,60	CRUST	27

# CHELYABINSK LL5

Name	Fe	Mg	Mn	Ni	Cr	Al	Ti	V	sum A	sum B	Mg#	Al#	Fe <sub>3+</sub> /Fe <sub>tot</sub>	TiO <sub>2</sub> wt%	Type	Num
2671-B2811-12-13	0,993	0,108			1,548	0,275	0,076		1,101	1,899	0,098	0,151	0,10	2,84	BULK	1
2720-21	0,942	0,132			1,481	0,392	0,052		1,074	1,926	0,123	0,209	0,08	2,00	BULK	2
2728	0,935	0,104	0,018		1,587	0,318	0,038		1,057	1,943	0,100	0,167	0,06	1,44	BULK	3
2729	0,993	0,107			1,547	0,266	0,087		1,100	1,900	0,097	0,147	0,10	3,27	BULK	4
2730	0,944	0,156			1,456	0,361	0,083		1,099	1,901	0,142	0,199	0,11	3,18	BULK	5
2731	0,949	0,130			1,441	0,405	0,076		1,079	1,921	0,120	0,219	0,08	2,89	BULK	6
3825	0,902	0,201			1,503	0,271	0,103	0,020	1,103	1,897	0,183	0,153	0,11	3,92	BULK	7
3826	0,909	0,161			1,540	0,283	0,087	0,020	1,070	1,930	0,151	0,155	0,08	3,30	BULK	8
3827	0,928	0,152			1,536	0,260	0,102	0,021	1,081	1,919	0,141	0,145	0,09	3,84	BULK	9
3828	0,896	0,142			1,564	0,333	0,041	0,023	1,039	1,961	0,137	0,176	0,04	1,54	BULK	10
3829	0,905	0,209			1,507	0,255	0,106	0,019	1,113	1,887	0,187	0,145	0,13	4,01	BULK	11
2722	0,610	0,478			1,564	0,254	0,078	0,015	1,088	1,913	0,439	0,140	0,14	3,09	CRUST	12
2723	0,697	0,497			1,536	0,255	0,015		1,194	1,806	0,244	0,142	0,13	0,61	CRUST	13
2724	0,623	0,566			1,497	0,246	0,068		1,189	1,811	0,476	0,141	0,30	2,71	CRUST	14
2724 BIS	0,372	0,428			1,859	0,109	0,161	0,071	0,800	2,200	0,535	0,055	0	6,16	CRUST	15
B2823-24-25-31	0,508	0,730			1,440	0,247	0,065		1,238	1,752	0,590	0,147	0,49	2,67	CRUST	16
B2826	0,508	0,802		0,015	1,423	0,209	0,043		1,326	1,674	0,612	0,128	0,64	1,78	CRUST	17
3833	0,722	0,391			1,508	0,309	0,069		1,113	1,887	0,351	0,170	0,16	2,70	CRUST	18
3834-35	0,349	0,919			1,420	0,250	0,046	0,016	1,268	1,732	0,725	0,150	0,77	1,95	CRUST	19
3836-37	0,504	0,690			1,435	0,253	0,098	0,020	1,193	1,807	0,578	0,150	0,38	4,02	CRUST	20
3838-39	0,619	0,494			1,529	0,266	0,081	0,012	1,112	1,888	0,444	0,148	0,18	3,21	CRUST	21
3840	0,607	0,533			1,461	0,254	0,126	0,019	1,140	1,860	0,467	0,148	0,23	5,02	CRUST	22
3841	0,659	0,471			1,517	0,282	0,097	0,020	1,130	1,916	0,417	0,157	0,13	3,78	CRUST	23
3842	0,674	0,484			1,447	0,291	0,082	0,021	1,158	1,842	0,418	0,168	0,23	3,28	CRUST	24
3844	0,474	0,734			1,428	0,263	0,085	0,016	1,208	1,792	0,607	0,156	0,44	3,49	CRUST	25



# CHERGACH H5

Name	Fe	Mg	Mn	Ni	Cr	Al	Ti	V	sum A	sum B	Mg#	Al#	Fe <sub>3+</sub> /Fe <sub>tot</sub>	TiO <sub>2</sub> wt%	Type	Num
3154	0,859	0,149	0,024		1,571	0,353	0,045		1,032	1,968	0,148	0,183	0,04	1,70	BULK	1
3155	0,870	0,161			1,570	0,349	0,050		1,031	1,969	0,156	0,182	0,04	1,89	BULK	2
3177	0,807	0,204	0,022		1,595	0,318	0,053		1,033	1,967	0,202	0,166	0,04	2,03	BULK	3
3178	0,808	0,202	0,020		1,596	0,318	0,056		1,031	1,969	0,200	0,166	0,04	2,12	BULK	4
3179	0,824	0,205	0,023		1,578	0,316	0,054		1,052	1,948	0,199	0,167	0,06	2,04	BULK	5
3180	0,865	0,181	0,020		1,577	0,304	0,054		1,066	1,934	0,173	0,162	0,08	2,04	BULK	6
3181	0,828	0,169	0,024		1,586	0,349	0,044		1,021	1,979	0,169	0,180	0,02	1,68	BULK	7
3182	0,852	0,170	0,029		1,555	0,346	0,048		1,051	1,949	0,167	0,182	0,06	1,84	BULK	8
3183	0,885	0,168	0,034		1,534	0,332	0,048		1,087	1,913	0,159	0,178	0,10	1,81	BULK	9
3205	0,835	0,161	0,029		1,616	0,312	0,047		1,026	1,974	0,162	0,162	0,03	1,78	BULK	10
3206	0,826	0,170	0,026		1,609	0,319	0,051		1,022	1,978	0,171	0,165	0,03	1,94	BULK	11
3207	0,839	0,163	0,028		1,609	0,319	0,043		1,030	1,970	0,163	0,165	0,04	1,61	BULK	12
3216	0,855	0,205	0,026		1,548	0,313	0,053		1,087	1,913	0,194	0,168	0,10	2,01	BULK	13
3218	0,258	0,614			1,110	1,017	0,000		0,873	2,127	0,704	0,478	0	0,00	BULK	14
3158	0,398	1,034		0,015	1,214	0,309	0,030		1,448	1,552	0,722	0,203	1,12	1,30	CRUST	15
3159	0,395	1,023	0,013	0,016	1,217	0,303	0,032		1,448	1,552	0,721	0,199	1,13	1,39	CRUST	16
3186	0,527	0,615			1,501	0,319	0,038		1,142	1,858	0,538	0,175	0,27	1,56	CRUST	17
3187	0,471	0,591	0,020		1,505	0,369	0,044		1,082	1,918	0,556	0,197	0,17	1,80	CRUST	18
3188	0,493	0,593	0,023		1,511	0,336	0,043		1,109	1,891	0,546	0,182	0,22	1,76	CRUST	19
3199	0,463	0,806			1,389	0,322	0,021		1,268	1,732	0,635	0,188	0,58	0,88	CRUST	20
3200	0,446	0,966	0,019		1,197	0,339	0,033		1,430	1,570	0,684	0,221	0,97	1,44	CRUST	21
3201	0,302	1,027			1,362	0,309			1,329	1,671	0,773	0,185	1,09	0,00	CRUST	22
3202	0,326	0,947			1,361	0,335	0,031		1,273	1,727	0,744	0,197	0,84	1,36	CRUST	23
3203	0,449	1,002			1,175	0,348	0,027		1,450	1,550	0,691	0,228	1,00	1,20	CRUST	24
3204	0,293	1,003	0,019		1,332	0,316	0,037		1,315	1,685	0,774	0,192	1,08	1,62	CRUST	25
3226	0,849	0,179	0,025		1,577	0,328	0,042		1,053	1,947	0,174	0,172	0,06	1,61	CRUST	26
3227	0,805	0,120	0,025		1,793	0,211	0,045		0,951	2,049	0,130	0,105	0	1,69	CRUST	27
3228	0,881	0,203	0,024		1,541	0,320	0,031		1,108	1,892	0,187	0,172	0,12	1,19	CRUST	28
3229	0,866	0,262			1,444	0,402	0,026		1,128	1,872	0,232	0,218	0,15	1,02	CRUST	29
3230	0,691	0,309	0,018		1,340	0,595	0,047		1,019	1,981	0,309	0,307	0,03	1,89	CRUST	30
3231	0,840	0,218			1,562	0,333	0,048		1,058	1,942	0,206	0,176	0,07	1,83	CRUST	31

# KABO H4

Name	Fe	Mg	Mn	Ni	Cr	Al	Ti	V	sum A	sum B	Mg#	Al#	Fe <sub>3+</sub> /Fe <sub>tot</sub>	TiO <sub>2</sub> wt%	Type	Num
8653-54-55	0,975	0,123			1,592	0,225	0,085		1,098	1,902	0,112	0,124	0,10	3,17	BULK	1
8656	0,985	0,117			1,595	0,224	0,078		1,102	1,898	0,106	0,123	0,10	2,90	BULK	2
8689	1,007	0,132			1,531	0,246	0,084		1,139	1,861	0,116	0,138	0,14	3,15	BULK	3
8690	1,010	0,099			1,568	0,241	0,082		1,109	1,891	0,089	0,133	0,11	3,05	BULK	4
8691	1,014	0,124			1,543	0,239	0,080		1,138	1,862	0,109	0,134	0,14	2,99	BULK	5
8696	1,019	0,134			1,518	0,237	0,092		1,153	1,847	0,116	0,135	0,15	3,43	BULK	6
8697	1,014	0,140			1,530	0,238	0,077		1,154	1,846	0,121	0,135	0,15	2,90	BULK	7
8712	0,967	0,150			1,587	0,218	0,078		1,117	1,883	0,135	0,121	0,12	2,91	BULK	8
8713	0,968	0,144			1,587	0,233	0,067		1,113	3,407	0,130	0,128	0	2,52	BULK	9
8717	1,000	0,121			1,573	0,233	0,072		1,122	1,878	0,108	0,129	0,12	2,70	BULK	10
8657	0,942	0,192			1,561	0,224	0,081		1,134	1,866	0,169	0,125	0,14	3,06	CRUST	11
8659	0,931	0,183			1,584	0,210	0,091		1,115	1,885	0,164	0,117	0,12	3,42	CRUST	12
8660	0,989	0,120			1,590	0,231	0,070		1,109	1,891	0,108	0,127	0,11	2,60	CRUST	13
8661	0,950	0,175			1,576	0,209	0,090		1,125	1,875	0,156	0,117	0,13	3,37	CRUST	14
8662	1,015	0,106			1,581	0,233	0,065		1,121	1,879	0,094	0,128	0,12	2,43	CRUST	15
8663	1,012	0,110			1,567	0,241	0,070		1,122	1,878	0,098	0,133	0,12	2,62	CRUST	16
8665-67	1,010	0,109			1,579	0,234	0,069		1,119	1,881	0,097	0,129	0,12	2,56	CRUST	17
8669	0,594	0,281			1,800	0,226	0,099		0,875	2,125	0,321	0,112	0	3,78	CRUST	18
8673	0,548	0,691		0,052	1,524	0,156	0,019		1,291	1,699	0,558	0,093	0,55	0,77	CRUST	19
8675	0,669	0,763		0,052	1,335	0,181			1,484	1,516	0,533	0,120	0,72	0	CRUST	20
8676-7-8-9-80-81-82	0,582	0,512		0,009	1,623	0,200	0,073		1,103	1,897	0,468	0,110	0,18	2,89	CRUST	21

# KILABO LL6

Name	Fe	Mg	Mn	Ni	Cr	Al	Ti	V	sum A	sum B	Mg#	Al#	Fe <sub>3+</sub> /Fe <sub>tot</sub>	TiO <sub>2</sub> wt%	Type	Num
8655-56	1,043	0,101			1,530	0,220	0,107		1,143	1,857	0,088	0,126	0,14	3,96	BULK	1
8652-57-58-59	1,026	0,109			1,536	0,220	0,109		1,136	1,864	0,096	0,125	0,13	4,05	BULK	2
8660	1,079	0,093			1,503	0,235	0,090		1,172	1,828	0,079	0,135	0,16	3,36	BULK	3
8680	1,017	0,123			1,532	0,217	0,111		1,141	1,859	0,108	0,124	0,14	4,13	BULK	4
8681	1,008	0,128			1,531	0,224	0,109		1,136	1,864	0,112	0,128	0,13	4,07	BULK	5
8682	1,033	0,110			1,540	0,208	0,109		1,143	1,857	0,096	0,119	0,14	4,04	BULK	6
8683	0,994	0,125			1,538	0,250	0,093		1,120	1,880	0,112	0,140	0,12	3,47	BULK	7
8686	1,015	0,116			1,531	0,241	0,098		1,131	1,869	0,102	0,136	0,13	3,66	BULK	8
8687	1,018	0,113			1,536	0,219	0,114		1,131	1,869	0,100	0,125	0,13	4,25	BULK	9
8693	1,062	0,097			1,516	0,253	0,072		1,159	1,841	0,084	0,143	0,15	2,67	BULK	10
8700	1,068	0,108			1,493	0,242	0,089		1,176	1,824	0,092	0,139	0,16	3,33	BULK	11
8701	1,093	0,089			1,491	0,220	0,107		1,182	1,818	0,075	0,129	0,17	3,96	BULK	12
8702	1,089	0,087			1,507	0,211	0,106		1,176	1,824	0,074	0,123	0,16	3,95	BULK	13
8812-13-14-16-17	1,045	0,175		0,007	1,384	0,305	0,084		1,227	1,773	0,143	0,180	0,22	3,18	CRUST	14
8818	1,444	0,096		0,059	1,147	0,178	0,076		1,600	1,400	0,063	0,134	0,42	2,82	CRUST	15
8819-20	0,950	0,263			1,341	0,358	0,088		1,213	1,787	0,217	0,211	0,22	3,42	CRUST	16
8823	0,979	0,297			1,369	0,263	0,092		1,276	1,724	0,233	0,161	0,28	3,55	CRUST	17
8824-25-26-27-28-29-30-31	0,988	0,342			1,337	0,240	0,093		1,330	1,670	0,257	0,152	0,33	3,60	CRUST	18
8832-33-35-36	0,639	0,603			1,390	0,313	0,054		1,242	1,758	0,486	0,184	0,38	2,21	CRUST	19
8838-40	1,092	0,147		0,030	1,416	0,230	0,086		1,269	1,731	0,118	0,140	0,25	3,21	CRUST	20
8846-47	0,983	0,214			1,429	0,313	0,061		1,197	1,803	0,179	0,180	0,20	2,35	CRUST	21
8850-51-52	1,055	0,098			1,504	0,244	0,098		1,153	1,847	0,085	0,140	0,14	3,66	CRUST	22



## NWA 869 L3-6

Name	Fe	Mg	Mn	Ni	Cr	Al	Ti	V	sum A	sum B	Mg#	Al#	Fe <sub>3+</sub> /Fe <sub>tot</sub>	TiO <sub>2</sub> wt%	Type	Num
10862	1.007	0.140		0,022	1,461	0,263	0,085	0,022	1,169	1,831	0,122	0,153	0,17	3,20	BULK	1
10863	0.941	0.143			1,654	0,178	0,059	0,025	1,084	1,916	0,132	0,097	0,09	2,20	BULK	2
10866	0.970	0.141			1,554	0,250	0,062	0,024	1,110	1,890	0,127	0,138	0,11	2,33	BULK	3
10867	0.961	0.165			1,519	0,273	0,059	0,023	1,126	1,874	0,147	0,152	0,13	2,23	BULK	4
10869	0.987	0.095			1,611	0,198	0,077	0,031	1,082	1,918	0,088	0,110	0,08	2,84	BULK	5
10870	1.036	0.159		0,027	1,458	0,216	0,080	0,023	1,222	1,778	0,133	0,129	0,21	3,02	BULK	6
10871	0.937	0.169			1,540	0,244	0,090	0,020	1,106	1,894	0,153	0,137	0,11	3,39	BULK	7
10872	0.926	0.174			1,544	0,241	0,095	0,020	1,100	1,900	0,159	0,135	0,11	3,56	BULK	8
10876	0.927	0.174			1,544	0,244	0,087	0,025	1,101	1,899	0,158	0,136	0,11	3,27	BULK	9
10877	0.951	0.159			1,541	0,234	0,092	0,024	1,110	1,890	0,144	0,132	0,12	3,45	BULK	10
10825	0.945	0.173			1,534	0,247	0,079	0,022	1,118	1,882	0,155	0,139	0,13	2,99	CRUST	11
10826	0.892	0.211			1,736	0,082	0,049	0,030	1,103	1,897	0,191	0,045	0,12	1,83	CRUST	12
10830	0.921	0.192			1,552	0,241	0,069	0,025	1,113	1,887	0,173	0,134	0,12	2,62	CRUST	13
10831	1.001	0.185			1,507	0,232	0,075		1,186	1,814	0,156	0,133	0,19	2,84	CRUST	14
10832	1.009	0.105		0,009	1,538	0,246	0,069	0,023	1,123	1,877	0,095	0,138	0,12	2,58	CRUST	15
10837	0.943	0.161			1,617	0,183	0,071	0,025	1,104	1,896	0,146	0,101	0,11	2,65	CRUST	16
10838	0.944	0.165			1,615	0,181	0,068	0,027	1,109	1,891	0,149	0,101	0,12	2,54	CRUST	17
10839	0.944	0.186			1,535	0,236	0,077	0,021	1,131	1,869	0,165	0,133	0,14	2,91	CRUST	18
10844	0.896	0.207			1,483	0,306	0,089	0,018	1,104	1,896	0,188	0,171	0,12	3,40	CRUST	19
10845	0.928	0.197			1,480	0,294	0,083	0,017	1,126	1,874	0,175	0,166	0,14	3,17	CRUST	20
10846	0.926	0.191			1,511	0,272	0,082	0,018	1,117	1,883	0,171	0,152	0,13	3,12	CRUST	21
10847	0.943	0.193			1,478	0,286	0,081	0,020	1,136	1,864	0,170	0,162	0,14	3,06	CRUST	22
10848	0.928	0.196			1,484	0,291	0,081	0,020	1,123	1,877	0,174	0,164	0,13	3,09	CRUST	23
10849	0.923	0.191			1,500	0,288	0,079	0,019	1,114	1,886	0,171	0,161	0,12	2,99	CRUST	24
10850	0.905	0.202			1,497	0,289	0,087	0,019	1,108	1,892	0,183	0,162	0,12	3,32	CRUST	25
10854	0.946	0.158			1,666	0,156	0,047	0,027	1,104	1,896	0,143	0,086	0,11	1,74	CRUST	26
10855	0.957	0.150			1,656	0,167	0,041	0,029	1,108	1,892	0,136	0,092	0,11	1,51	CRUST	27
10859	0.818	0.279			1,409	0,460	0,035		1,096	1,904	0,254	0,246	0,12	1,36	CRUST	28
10860	0.892	0.176			1,538	0,338	0,037	0,019	1,068	1,932	0,165	0,180	0,08	1,43	CRUST	29
10864	0.940	0.139			1,579	0,259	0,058	0,026	1,079	1,921	0,129	0,141	0,08	2,16	CRUST	30

# TAMDAKHT H5

Name	Fe	Mg	Mn	Ni	Cr	Al	Ti	V	sum A	sum B	Mg#	Al#	Fe <sub>3+</sub> /Fe <sub>tot</sub>	TiO <sub>2</sub> wt%	Type	Num
3595	0,779	0,225			1,569	0,366	0,050	0,012	1,004	1,996	0,224	0,189	0,00	1,92	BULK	1
3596	0,765	0,218	0,020		1,575	0,362	0,047	0,013	1,003	1,997	0,222	0,187	0,00	1,81	BULK	2
3597	0,768	0,211	0,025		1,577	0,352	0,054	0,013	1,003	1,997	0,215	0,183	0,00	2,07	BULK	3
3598	0,770	0,205	0,019		1,591	0,352	0,050	0,014	0,993	2,007	0,210	0,181	0	1,90	BULK	4
3599	0,773	0,211	0,022		1,585	0,349	0,049	0,011	1,005	1,995	0,214	0,180	0,01	1,89	BULK	5
3604	0,766	0,226	0,023		1,560	0,364	0,048	0,013	1,015	1,985	0,228	0,189	0,02	1,85	BULK	6
3606	0,806	0,167	0,029		1,626	0,302	0,056	0,014	1,002	1,998	0,172	0,157	0,00	2,13	BULK	7
3607	0,806	0,169	0,027		1,641	0,302	0,055		1,002	1,998	0,174	0,155	0,00	2,08	BULK	8
3614	0,780	0,197	0,029		1,623	0,312	0,051	0,008	1,006	1,994	0,202	0,161	0,01	1,94	BULK	9
3615	0,790	0,191	0,027		1,616	0,309	0,052	0,014	1,008	1,992	0,195	0,161	0,01	1,99	BULK	10
3623	0,818	0,165	0,027		1,614	0,313	0,048	0,015	1,010	1,990	0,168	0,162	0,01	1,82	BULK	11
3624	0,732	0,244	0,026		1,496	0,446	0,046	0,010	1,002	1,998	0,250	0,230	0,00	1,78	BULK	12
3625	0,735	0,241	0,020		1,514	0,434	0,044	0,012	0,996	2,004	0,247	0,223	0	1,73	BULK	13
3629	0,834	0,156	0,027		1,590	0,348	0,036	0,009	1,017	1,983	0,157	0,180	0,02	1,35	CRUST	14
3605 bis	0,831	0,148	0,028		1,613	0,343	0,022	0,016	1,006	1,994	0,151	0,175	0,01	0,84	CRUST	15
3612 bis	0,586	0,444	0,027	0,005	1,567	0,323	0,032	0,015	1,063	1,937	0,431	0,171	0,11	1,27	CRUST	16
3613 bis	0,549	0,466	0,023		1,595	0,329	0,025	0,014	1,038	1,962	0,459	0,171	0,07	0,98	CRUST	17
3618 bis	0,800	0,249	0,022		1,546	0,333	0,034	0,016	1,072	1,928	0,238	0,177	0,09	1,31	CRUST	18
3630	0,641	0,434		0,017	1,586	0,288	0,018	0,016	1,092	1,908	0,404	0,154	0,14	0,69	CRUST	19
3633	0,697	0,500	0,021	0,009	1,477	0,266	0,030		1,227	1,773	0,418	0,153	0,33	1,20	CRUST	20
3634	0,698	0,479	0,016		1,495	0,270	0,031	0,011	1,192	1,808	0,407	0,153	0,28	1,21	CRUST	21
3636	0,860	0,151			1,608	0,331	0,035	0,016	1,010	1,990	0,149	0,171	0,01	1,31	CRUST	22
3637	0,838	0,175			1,606	0,320	0,047	0,014	1,013	1,987	0,173	0,166	0,02	1,77	CRUST	23
3638	0,850	0,160			1,605	0,344	0,026	0,014	1,011	1,989	0,159	0,176	0,01	1,00	CRUST	24
3639	0,756	0,337			1,559	0,311	0,020	0,016	1,094	1,906	0,308	0,166	0,12	0,77	CRUST	25
3641	0,871	0,138	0,027		1,607	0,323	0,024	0,009	1,036	1,964	0,137	0,167	0,04	0,92	CRUST	26

# VIÑALES L6

Name	Fe	Mg	Mn	Ni	Cr	Al	Ti	V	sum A	sum B	Mg#	Al#	Fe <sub>3+</sub> /Fe <sub>tot</sub>	TiO <sub>2</sub> wt%	Type	Num
11103	0,877	0,186			1,606	0,236	0,071	0,024	1,063	1,937	0,175	0,128	0,07	2,68	BULK	1
11104	0,918	0,167			1,562	0,254	0,076	0,022	1,085	1,915	0,154	0,140	0,09	2,87	BULK	2
11105	0,927	0,141			1,595	0,244	0,069	0,024	1,068	1,932	0,132	0,133	0,07	2,59	BULK	3
11106	0,933	0,121			1,631	0,232	0,058	0,025	1,054	1,946	0,115	0,125	0,06	2,17	BULK	4
11107	0,879	0,176			1,629	0,250	0,042	0,024	1,055	1,945	0,167	0,133	0,06	1,56	BULK	5
11108	0,900	0,205			1,580	0,213	0,081	0,021	1,105	1,895	0,185	0,119	0,12	3,04	BULK	6
11110	0,914	0,177			1,581	0,235	0,070	0,024	1,091	1,909	0,162	0,129	0,10	2,62	BULK	7
11134	0,950	0,131			1,591	0,222	0,084	0,023	1,080	1,920	0,121	0,122	0,08	3,15	BULK	8
11135	0,937	0,136			1,616	0,216	0,071	0,024	1,074	1,926	0,127	0,118	0,08	2,65	BULK	9
11136	0,938	0,140			1,627	0,196	0,075	0,025	1,078	1,922	0,130	0,107	0,08	2,79	BULK	10
11137	0,830	0,239			1,372	0,505	0,054		1,069	1,931	0,224	0,269	0,08	2,13	BULK	11
11138	0,918	0,215			1,350	0,408	0,097	0,011	1,133	1,867	0,190	0,232	0,15	3,76	BULK	12
11146	0,953	0,134			1,624	0,202	0,086		1,087	1,913	0,124	0,111	0,09	3,22	BULK	13
11147	0,965	0,121			1,596	0,211	0,084	0,023	1,086	1,914	0,111	0,117	0,09	3,12	BULK	14
11148	0,948	0,144			1,606	0,229	0,074		1,092	1,908	0,132	0,125	0,10	2,75	BULK	15
11100	0,945	0,137			1,602	0,232	0,058	0,026	1,082	1,918	0,127	0,126	0,09	2,16	CRUST	16
11101	0,901	0,151			1,608	0,241	0,074	0,026	1,052	1,948	0,144	0,130	0,06	2,77	CRUST	17
11114	0,634	0,468			1,587	0,201	0,088	0,023	1,101	1,899	0,425	0,112	0,16	3,44	CRUST	18
11115	0,914	0,236			1,590	0,180	0,058	0,022	1,150	1,850	0,206	0,102	0,16	2,19	CRUST	19
11116	0,900	0,234			1,553	0,233	0,060	0,020	1,134	1,866	0,206	0,130	0,15	2,28	CRUST	20
11120	0,921	0,201			1,609	0,179	0,066	0,024	1,122	1,878	0,179	0,100	0,13	2,49	CRUST	21
11121	0,903	0,197			1,608	0,195	0,075	0,022	1,099	1,901	0,179	0,108	0,11	2,81	CRUST	22
11122	0,867	0,188			1,619	0,237	0,064	0,024	1,056	1,944	0,178	0,127	0,06	2,41	CRUST	23
11123	0,900	0,186			1,596	0,238	0,056	0,024	1,086	1,914	0,171	0,130	0,10	2,13	CRUST	24
11124	0,927	0,183			1,577	0,205	0,086	0,022	1,110	1,890	0,165	0,115	0,12	3,23	CRUST	25
11125	0,920	0,186			1,580	0,210	0,084	0,021	1,106	1,894	0,168	0,117	0,11	3,16	CRUST	26
11126	0,946	0,165			1,583	0,203	0,084	0,019	1,111	1,889	0,148	0,114	0,12	3,14	CRUST	27
11127	0,852	0,248			1,597	0,210	0,073	0,020	1,100	1,900	0,225	0,116	0,12	2,76	CRUST	28
11128	0,933	0,171			1,598	0,191	0,086	0,021	1,104	1,896	0,155	0,107	0,11	3,20	CRUST	29
11129	0,913	0,177	0,016		1,581	0,207	0,086	0,021	1,106	1,894	0,162	0,116	0,12	3,21	CRUST	30
11130	0,944	0,152			1,615	0,179	0,087	0,023	1,096	1,904	0,139	0,100	0,10	3,25	CRUST	31
11131	0,919	0,197			1,571	0,208	0,086	0,020	1,116	1,884	0,177	0,117	0,13	3,22	CRUST	32



## EL HAMMAMI H5

Name	Fe	Mg	Mn	Ni	Cr	Al	Ti	V	sum A	sum B	Mg#	Al#	Fe <sub>3+</sub> /Fe <sub>tot</sub>	TiO <sub>2</sub> wt%	Type	Num
3830	0,786	0,220	0,027		1,563	0,304	0,077	0,022	1,033	1,967	0,218	0,163	0,04	2,93	BULK	1
3847	0,829	0,153	0,030		1,613	0,314	0,045	0,045	1,012	2,018	0,156	0,163	0	1,70	BULK	2
3848	0,809	0,189	0,023		1,598	0,304	0,060	0,016	1,022	1,978	0,190	0,160	0,03	2,29	BULK	3
3849	0,808	0,161	0,032		1,615	0,352	0,022	0,010	1,000	2,000	0,167	0,179	0,00	0,85	BULK	4
3850	0,817	0,166	0,024		1,613	0,317	0,049	0,015	1,007	1,993	0,169	0,164	0,01	1,85	BULK	5
3851	0,748	0,310			1,576	0,297	0,055	0,014	1,058	1,942	0,293	0,158	0,08	2,13	BULK	6
3852	0,791	0,262			1,569	0,304	0,061	0,014	1,053	1,947	0,248	0,162	0,07	2,33	BULK	7
3854	0,845	0,159	0,018		1,593	0,335	0,039	0,010	1,023	1,977	0,159	0,174	0,03	1,48	BULK	8
3855	0,804	0,203			1,603	0,308	0,060	0,021	1,007	1,993	0,202	0,161	0,01	2,29	BULK	9
3856	0,811	0,195	0,021		1,586	0,325	0,047	0,015	1,027	1,973	0,194	0,170	0,03	1,80	BULK	10
3857	0,815	0,201			1,592	0,305	0,066	0,021	1,016	1,984	0,198	0,161	0,02	2,51	BULK	11
3858	0,807	0,218			1,574	0,322	0,058	0,020	1,025	1,975	0,213	0,170	0,03	2,23	BULK	12
3859	0,820	0,180	0,022		1,609	0,298	0,063	0,008	1,022	1,978	0,180	0,156	0,03	2,37	BULK	13
3860	0,835	0,197			1,571	0,321	0,055	0,021	1,032	1,968	0,191	0,170	0,04	2,08	BULK	14
3861	0,831	0,179	0,022		1,587	0,318	0,048	0,014	1,032	1,968	0,177	0,167	0,04	1,84	BULK	15
3831	0,761	0,255	0,054		1,527	0,325	0,057	0,021	1,070	1,930	0,251	0,176	0,09	2,21	CRUST	16
3833	0,815	0,204	0,055		1,514	0,360	0,034	0,018	1,074	1,926	0,200	0,192	0,09	1,29	CRUST	17
3834	0,737	0,295	0,050		1,513	0,344	0,042	0,019	1,082	1,918	0,286	0,185	0,11	1,62	CRUST	18
3835	0,792	0,222	0,059		1,526	0,346	0,033	0,022	1,073	1,927	0,219	0,185	0,09	1,27	CRUST	19
3836	0,646	0,389	0,020		1,566	0,318	0,052	0,009	1,055	1,945	0,376	0,169	0,09	2,03	CRUST	20
3837	0,626	0,438			1,566	0,309	0,046	0,015	1,064	1,936	0,412	0,165	0,10	1,82	CRUST	21
3840	0,689	0,361			1,569	0,326	0,039	0,016	1,050	1,950	0,344	0,172	0,07	1,54	CRUST	22
3841	0,757	0,249	0,022		1,589	0,334	0,035		1,028	1,957	0,247	0,174	0,06	1,34	CRUST	23
3843	0,683	0,387			1,545	0,343	0,027	0,016	1,070	1,930	0,362	0,182	0,10	1,06	CRUST	24
3844	0,569	0,640			1,442	0,308	0,027	0,014	1,209	1,791	0,530	0,176	0,37	1,12	CRUST	25

# SUMMARY OF RESULTS

NAME	TYPE	SHOCK	W Grade	Mg# bulk ave	Mg# bulk sdv	Mg# crust ave	Mg# crust sdv	Al# bulk ave	Al# bulk sdv	Al# crust ave	Al# crust sdv	TiO <sub>2</sub> wt% bulk ave	TiO <sub>2</sub> wt% bulk sdv	TiO <sub>2</sub> wt% crust ave	TiO <sub>2</sub> wt% crust sdv
<i>BASSIKOUNOU</i>	H5	S4	W0	0,192	0,033	0,563	0,195	0,157	0,030	0,154	0,014	2,34	1,55	1,32	0,39
<i>CHERGACH</i>	H5	S3	W0	0,212	0,143	0,507	0,242	0,193	0,082	0,195	0,040	1,75	0,53	1,38	0,46
<i>KABO</i>	H4	—	—	0,114	0,013	0,251	0,185	0,130	0,006	0,119	0,012	2,97	0,25	2,50	1,14
<i>TAMDAKHT</i>	H5	S3	W0	0,209	0,027	0,247	0,098	0,181	0,024	0,175	0,019	1,92	0,12	1,54	0,45
<i>ABA PANU</i>	L3.6	S4	W0	0,302	0,077	0,252	0,092	0,134	0,136	0,088	0,043	2,54	1,31	1,49	0,59
<i>NWA 869</i>	L3-6	S3	W1	0,136	0,021	0,164	0,031	0,132	0,017	0,140	0,042	2,95	0,52	2,57	0,66
<i>VIÑALES</i>	L6	S3	W0	0,150	0,033	0,185	0,067	0,140	0,046	0,116	0,010	2,74	0,52	2,82	0,45
<i>CHELYABINSK</i>	LL5	S4	W0	0,134	0,031	0,493	0,124	0,170	0,027	0,143	0,027	2,93	0,91	3,18	1,36
<i>KILABO</i>	LL6	S3	W0	0,094	0,013	0,198	0,127	0,130	0,008	0,165	0,026	3,76	0,44	3,11	0,54
<i>EL HAMMAMI</i>	H5	S2	—	0,197	0,036	0,323	0,102	0,165	0,006	0,177	0,008	2,05	0,49	1,53	0,39